1-1-1991

A morphological, mechanical and thermodynamic investigation of the isotactic polyvinylmethylether/ polystyrene polymer blend/

Gregory, Beaucage
University of Massachusetts Amherst

A MORPHOLOGICAL, MECHANICAL AND THERMODYNAMIC INVESTIGATION OF THE ISOTACTIC POLYVINYLMETHYLETHER/POLYSTYRENE POLYMER BLEND

A Dissertation Presented

by

GREGORY BEAUCAGE

Submitted to the Graduate School of the
University of Massachusetts in partial fulfillment
of the requirements for the degree of

DOCTOR OF PHILOSOPHY

May 1991

Department of Polymer Science and Engineering

A MORPHOLOGICAL, MECHANICAL AND THERMODYNAMIC INVESTIGATION OF THE ISOTACTIC POLYVINYLMETHYLETHER/POLYSTYRENE POLYMER BLEND

A Dissertation Presented

by

GREGORY BEAUCAGE

Approved as to style and content by:

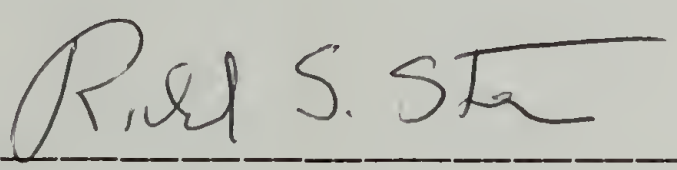

Richard S. Stein, Chairman of Committee

Richard J. Farris, Member

Larry Lo, Member

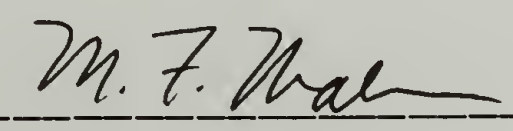

Michael F. Malone, Member

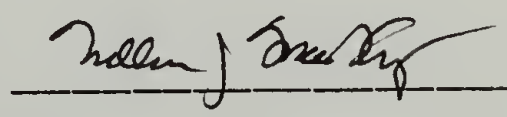

William J. MacKnight, Department Head and Member

Department of Polymer Science and Engineering

ACKNOWLEDGEMENTS

It is a great pleasure to express my gratitude for the continued support and encouragement of my parents, sister and brother. They will never fully appreciate the degree to which their presence has shaped my life and lead me to a deeper understanding of my purpose. My deepest appreciation goes to my companion in life Jean Holsinger who I married during my residence at UMASS. Although a scientist in her own right she has taught me to never overlook the miracle of our being.

In the same light as my family I am indebted to Richard S. Stein. As all great teachers he serves as a model for his students. In retrospect it is clear that he pushed when a push was needed and waited patiently while his students grew. The greatest gift a teacher can give is to encourage a student to explore.

I wish to acknowledge my committee members: Prof. MacKnight for his Polymer Science Course, the visiting scientists he brought to the department and his encouragement especially at the end of my stay at UMASS; Prof. Farris for introducing me to Continuum Mechanics and his advice concerning the mechanics sections of the thesis; Prof. Malone for his interest and encouragement; and Larry Lo who found time in his work schedule to help me with many aspects of

the project including but not limited to the financial support of NOVA Corporation.

I also acknowledge Dr. J. Hoffmann, Dr. E. DiMarzio and Dr. C. Guttman for introducing me to Polymer Science while a part-time student at the University of Maryland. I am indebted to Jim Lunt, A. Osman and S. Kirby of Polysar (now NOVA) Corporation's Sarnia Ontario plant for their assistance in the synthesis of isotactic PVME.

I acknowledge my collaborators, T. Hashimoto, R. Konigsveld, R. Prud'homme, H. Hasegawa, Peterman, M. Berard and W. Cheung. The neutron scattering experiments were conducted at Los Alamos National Lab's LANSCE facility (Department of Energy) under the guidance of Dr. P. Seeger and Dr. R. Hjelm without whom the work would have been impossible. The ellipsometer experiment was conducted using the equipment of Prof. Hoagland with the assistance of S. Chen.

Finally I would like to express my sincerest gratitude to my coworkers and friends at UMASS: M. Satkowski, S. Roystatzer, S. Roy, M. Berard, S. Anarudha, J. P. Autran, O. Aoki, P. Bhowmik, H. Schild, H. Marand, W. Herman, S. Ottino, Kita, Shiro, K. Tashiro, A. Hanyu, R. Composto, T. Mansfield, K. Bhatia, D. Golbran, R. Saraf, the technicians Norm and John, and the secretarial staff especially Jan, Eleanor and Sophie.

ABSTRACT

A MORPHOLOGICAL, MECHANICAL AND THERMODYNAMIC INVESTIGATION OF THE ISOTACTIC POLYVINYLMETHYLETHER/POLYSTYRENE POLYMER BLEND

May 1991

GREGORY BEAUCAGE,

B. S., ZOOLOGY, UNIVERSITY OF RHODE ISLAND

B. S., CHEMICAL ENGINEERING, UNIVERSITY OF RHODE ISLAND

Ph. D., UNIVERSITY OF MASSACHUSETTS

Directed by: Professor Richard S. Stein

A novel technique for the production of toughened polymers using LCST behavior as a mechanism for the production of rubbery domains is discussed. The polymer blend of isotactic polyvinylmethylether (PVME) with polystyrene (PS) is used. Synthesis, fractionation and characterization of isotactic PVME is reviewed. Thermodynamic effects of tacticity on miscibility are extensively investigated using light and neutron scattering. A simple critical point analysis is presented which indicates an entropic nature to the tacticity effect in this blend. Flory-Huggins-Staverman (F-H-S) theory is next applied to the tacticity effect. This more elaborate analysis also indicates an entropic nature to the tacticity effect.

Accounting for polydispersity results in a predicted fractionation in the phase separated blends which is supported by mechanical data.

F-H-S theory was used to generate a functional form for the interaction parameter in terms of the temperature and composition dependence of miscibility. From these functions a dramatic shift in the kinetics of phase separation with tacticity is predicted. Experimental data affirms this prediction. A novel, modified Cahn-Hillard analysis is presented for analysis of intermediate stages.

Neutron scattering data yields the composition and temperature dependence of the statistical segment length, b, of tactic PVME. A functional form for b is derived which predicts the equilibrium melting point and melting point depression behavior for the blends. A relationship between b and thermodynamic miscibility from a geometric perspective is discussed. The tacticity effect can be described in terms of an interaction parameter whose change with tacticity in terms of entropy is functionally related to the volume of an interacting group and in terms of enthalpy is functionally related to the surface area of an interacting group.

Two related studies are presented. The first pertains to a shift in glass transition of thin PS films with thickness as investigated using ellipsometry. The second study used neutron reflection data to disprove the supporting argument for a minus two thirds dependence of surface tension with molecular weight. An alternative theory for the molecular weight dependence of surface tension is presented.

TABLE OF CONTENTS

LIST OF TABLES

LIST OF FIGURES

CHAPTER 1

INTRODUCTION

A. A Review of Toughening In Styrenic Systems

The production of an impact resistant glassy polymer through the addition of an elastomer has been approached through a myriad of techniques. Bucknall[1] discusses the details of this technology extensively. The most direct approach to the production of a high impact material would seem to be the bulk mixing of the rubbery and glassy polymers. In general, this results in a composite material of drastically reduced modulus, strength and impact properties. The rubber particles in such a bulk mixture separate easily from the glassy matrix, producing voids which lead to failure at low stresses. Thus, one is incipiently faced with the problem of interfacial adhesion between the elastomer and glass. For styreneic polymer mixtures this has been commercially circumvented through the chemical grafting of the glassy component to the rubbery component of an immiscible mixture. High impact polystyrene (HIPS), for example, is industrially produced from a solution of butadiene rubber in styrene monomer. Polymerization of styrene results in phase separation of the two immiscible polymers. When the polystyrene volume percent exceeds the volume percent of polybutadiene, phase inversion occurs, wherein the matrix phase shifts from polybutadiene to polystyrene. Phase inversion does not occur in this system when the rubber content

exceeds twenty percent. The rubbery domains consist of roughly spherical particles with diameters greater than two microns. A distribution of rubber particle sizes is observed. Ardent mixing of the ternary mixture during phase inversion results in polystyrene inclusions in the rubbery domains. This serves to further improve the impact properties by increasing the volume of the suspended rubbery domains, the surfaces of which act to initiate and terminate stress relieving crazes.

Crazes are the predominant mechanism of stress abatement in HIPS. Elastic deformation of the rubber may also be a factor. In other toughened styrenics such as PS/Poly(phenylene oxide) and PS block-copolymers with butadiene shear bands may occur together with crazes. Generally it is observed that the presence of shear bands tends to inhibit the formation and growth of crazes[1]. Shear bands appear to be a more important mechanism of stress relief in systems where the matrix component is less brittle such as toughened poly(vinyl chloride) (PVC) and Poly(carbonate).

In the manufacture of toughened PVC a rubber with a solubility parameter close to that of PVC such as nitrile rubber (Poly(butadiene-co-acrylonitrile)) is mixed with the glassy polymer[2]. The rubber is partially compatible with PVC and a fine dispersion of the rubber in the glassy matrix with good interfacial properties results. Similarly, toughened polypropylene can be made by direct mechanical blending (in the melt) of polypropylene with ethylene-propylene-diene rubber (EPR). Irregularly shaped rubber particles result from such mechanical blending. Such irregular particles are less effective

toughening agents in comparison with spherical particles of similar average volume.

Another approach to the reinforcement of glassy polymers involves the use of block copolymers (SBS block copolymers for example) resulting in intimately bound rubbery domains. Durst and coworkers[3] found that a maximum in impact strength occurred in these systems when the fraction of butadiene in the block copolymers approached fifty percent.

In the present study, it was desired to produce a rubber modified glassy polymer through the phase separation of a miscible rubbery/glassy blend at elevated temperatures followed by quenching of the glassy phase below T_g[4]. Under ideal thermal cycling conditions, rubber particles of optimal size, intimately interfaced with the glassy matrix will be produced. The domain size and composition of the rubbery and glassy phases are under experimental control.

In order to manipulate the morphology of a simple binary polymer blend a phase diagram of the type shown in Figure 1.1 is desired.For such an ideal system, the phase separated morphology can be controlled, and to some extent predicted, by the careful manipulation of processing conditions. Following the dashed line in Figure 1.1 the temperature of the blend is raised above the glass transition temperature of both components and is processed as a miscible melt (A). After the first phase of processing is complete, the product can be thermally cycled above the binodal and, optionally, above the spinodal temperature (B) in order to effect a partial degree

of phase separation. Rapid quenching of a stoichiometrically optimal blend results in a glassy matrix (C) with an intimately interfaced rubbery suspension (C'). The extent of interaction at the interface could be controlled through the manipulation of the residence time above the binodal and/or spinodal temperatures. Other morphological characteristics of the product such as the crystallinity of the glassy and rubbery components could also be controlled in more complicated

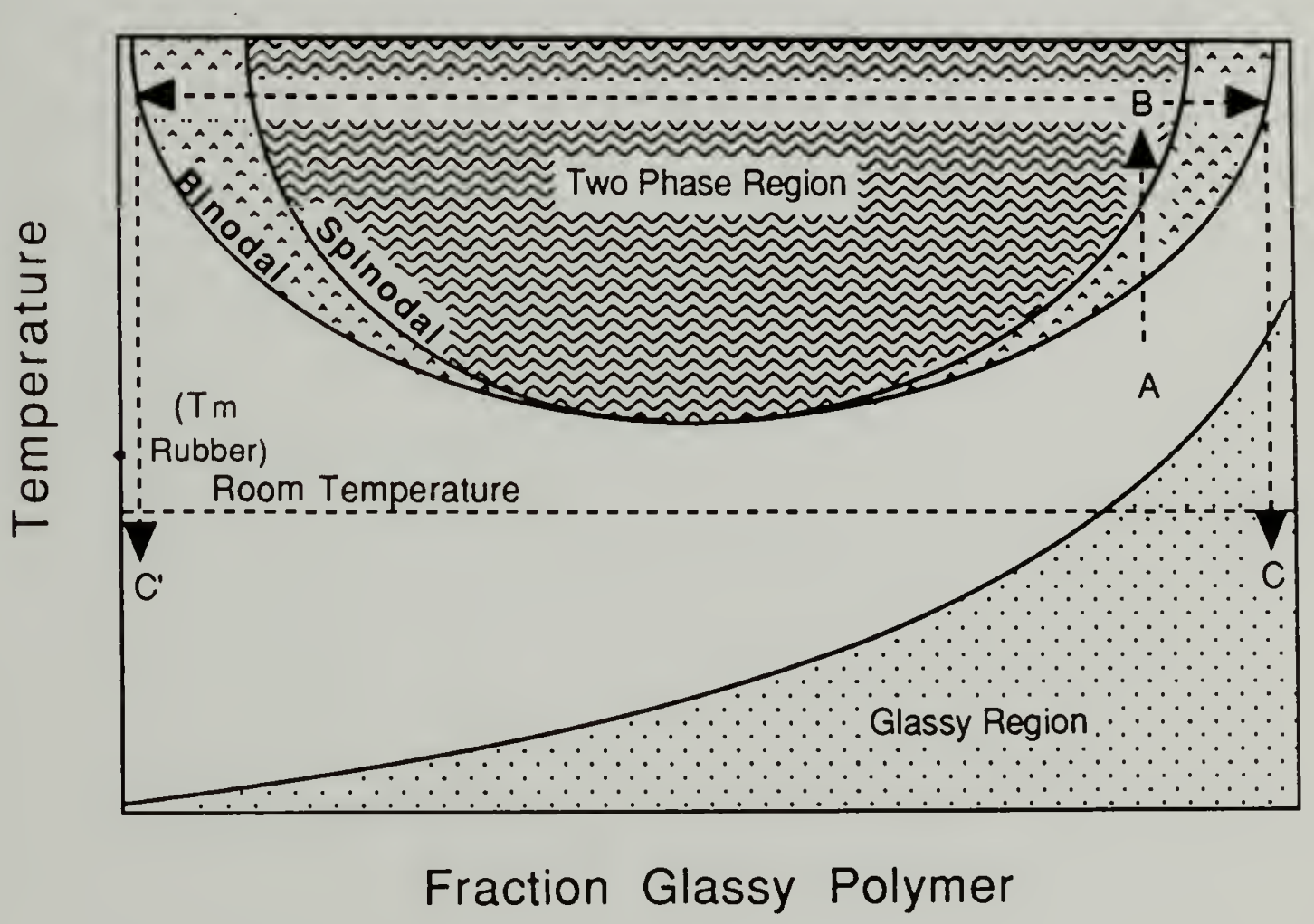

Figure 1.1 Ideal phase diagram for production of a rubber toughened glassy polymer through controlled phase separation.

phase diagrams. The mechanical properties of blends phase separated in the binodal may differ from those separated in the spinodal due to differences in the resulting morphology. (It should be noted that the

border between the spinodal and the binodal regions defined by Flory-Huggins (F-H) theory is not well defined in practice.)

A rubbery phase in the above scheme could be produced by chemically crosslinking the rubbery phase after phase separation. Alternatively, physical crosslinks could be induced in the rubbery phase. A high molecular weight rubbery material may exhibit entanglements which could act as physical crosslinks at the high strain rates present in localized fracture phenomenon. Physical crosslinks can also be produced in chemically tailored block copolymers. Such use of physical crosslinks in rubbery-glassy block-coploymers has lead to the production of thermoplastic elastomers. An alternative to these two schemes is the use of a limited degree of crystallinity (about 10%) in the rubbery phase as physical crosslinks (note T_m on y-axis of Figure 1.1). The latter route to physical crosslinks was chosen in this work since it was deemed difficult to control side reactions in a chemical crosslinking reaction, very high molecular weight PVME's were not available and were difficult to produce and the complexity of phase behavior in block-copolymer blends would make an academic study of such a system difficult. In the case of a partially crystalline rubbery phase, physical crosslinks are introduced in the rubber through thermal control of the degree of crystallinity. Deformation of the crystallites may act to further relieve stress in the composite material.

The system PVME/PS (polystyrene/poly(vinyl methyl ether)) was chosen as an ideal system which could produce the salient behavior of Figure 1.1. This system was chosen because its phase behavior is well

characterized, polystyrene is of commercial importance and is commercially available as monodisperse or bulk polydisperse samples allowing for both the study of the phase behavior and for sufficient quantities in order to conduct mechanical tests. Finally, the large index of refraction difference between the two polymers allowed for optical determination of the phase diagram and the availability of deuterated PS allowed for more elaborate studies of the miscibility involving neutron scattering and reflection. i-PVME (isotactic PVME), which is not commercially available, shows a partial degree of crystallinity (usually less than 10% as polymerized). The material forms imperfect crystallites which are detectable by X-ray diffraction, DSC analysis and other more obscure techniques such as measurement of the index of refraction. i-PVME with about 10% crystallinity is a rubbery material with a T_g of about -30°C, making it less than optimal for a commercial rubber but sufficiently rubbery for the purposes of an academic study.

A preliminary study of the miscibility of the i-PVME/polystyrene(PS) system was undertaken by Bank and coworkers.[4] Bank studied high molecular-weight i-PVME (650kg/mole) which had a relatively low degree of isotacticity. They found that this material showed some (unspecified) degree of miscibility with polystyrene. (In blends of atactic PVME with PS molecular weights for atactic PVME above 300kg/mole blended with PS in the 100kg/mole range would be expected to be immiscible above the glass transition due to a strong molecular weight effect in this system.) Generally, the phase behavior of the atactic system

exhibits an LCST (similar to Figure 1.1). The phase diagrams for the low molecular weight isotactic and heterotactic materials occur at convenient temperatures for study and well within the temperature range scheme specified in Figure 1.1.

In this study a moderate molecular weight PVME (ca. 99kg/mole) was used in order to widen the miscibility window. The polymer used has a much higher degree of isotacticity than that of Banks (70% isotactic triads) so that a higher density of physical crosslinks occurs, making the material more resilient. The atactic material is a viscous liquid. In contrast, the crystalline isotactic material is a rubber with thermally removable physical crosslinks (crystallites). Above the crystalline melting point isotactic and atactic PVME are visually and mechanically indistinguishable. The two tactic forms have identical glass transitions.

B. Energy Absorption in Toughened Polymers

Three mechanisms for the absorption of energy in rubber toughened materials have been suggested. Energy absorption due to deformation of the rubber particles in front of crack tips, enhancement of shear banding due to the presence of rubber particles and enhancement of crazing due to the presence of rubber particles. The first of these mechanisms has been shown to be insignificant[1]. The enhancement of shear banding and crazing have been observed in the literature[1] and in the toughened polymers studied in this project. (An example of this is the dramatic increase in stress whitening of

commercial high impact polystyrene when compared with virgin polystyrene.) In general, crazing and shear banding deformation mechanisms also occur in untoughened glassy polymers. The effect on the deformation mechanisms of adding a rubbery phase to a glassy polymer is one of quantity and not quality. Bucknall[1] notes that the rubber domains can be considered catalysts to stress relieving deformations.

Several postulates as to how rubber particles enhance the density of crazes (or shear bands) present in glassy polymers have been presented. First, amplification of the stress field in the vicinity of rubbery inclusions may lead to enhancement of crazing (or shear banding) mechanisms through a local shift in the glass transition of the polymer induced by the stress[1]. The rubber particles may also act as sites for craze initiation. Finally, the rubber particles may act as termination sites for crazes, reducing the size of individual crazes while increasing the total number of crazes. In recent years[1,5] it has been noted that cavitation of rubbery domains may precede craze formation in styrenic systems. Thus, it would appear that crosslinking of the rubbery phase may be required in order to control the degree of cavitation in the rubbery phase. Shear banding and crazing will be discussed in more detail below.

Shear bands are areas of concentrated deformation due to imperfections in the material on a local level. Shear bands form at 45° to the direction of strain. Shear bands differ from crazes in that little volume change occurs in the local region of a shear band. The kinetics

of shear band formation follows an Eyring-type rate law in that the logarithm of shear band velocity is linear in time, thus,

$$\frac{d\varepsilon}{dt} = 2\,A \exp\left(\frac{-\Delta H^*}{kT}\right) \sinh\left(\frac{gV^*\sigma}{4kT}\right) \qquad (1.1),$$

where, g, is the stress concentration factor[6]. The shear band activation enthalpy, ΔH^* and activation volume, gV^* are parameters which can be determined and used to predict deformation behavior. It should be noted that in the scheme of Figure 1.1, the matrix material is no longer pure glassy polymer. There is expected to be a slight degree of plasticization of the matrix due to a finite miscibility of the lower T_g material even in the phase separated blend. The barrier to achieving the activation volume would be expected to be strongly influenced by the glass transition of the matrix material in the system of Figure 1.1. Thus, reduction in the glass transition of the matrix material would directly effect ΔH^*, reducing the barrier to shear band formation and increasing the rate of shear band formation. Additionally, g, the stress concentration factor, will be dramatically altered in the region of a rubbery domain. g and ΔH in the presence of an uncrosslinked melt phase might not be expected to be drastically different from that of a rubbery phase.

One difference between a rubbery phase inclusion and a melt phase inclusion (i. e. phase separated isotactic and atactic PVME in a PS matrix) might be the degree of inherent strain in the highly plasticized glassy phase neighboring the inclusion. Chapter 8 discusses shifts in the glass transition of virgin polystyrene at the

interface with a resilient phase. Briefly, strains may be induced at such interfaces, whether by differences in thermal expansion, contraction due to crystallization, or other physical effects. In Chapter 7 these strains have been shown to induce significant shifts in the glass transition of PS. Similar behavior may occur in plasticized PS (requiring much less resilience in the neighboring phase). It is possible that local shifts in the glass transition occur due to strains induced in the matrix phase by the more resilient rubbery phase (at least locally to the interface).

As will be discussed in Chapter 6, shear banding is observed in the phase separated isotactic PVME blends. Since shear banding does not generally occur in virgin PS, a yield criterion for shear banding must be considered. Various yield criteria have been applied to shear band formation in rubber reinforced polymers. The von Mises yield criterion, modified for the effects of hydrostatic pressure(free volume effect) on the yield criteria has been successfully applied to shear banding in glassy polymers, following Sternstein and Ongchin[6],

$$\tau_{oct} = \frac{1}{3}[(\sigma_{11} - \sigma_{22})^2 + (\sigma_{22} - \sigma_{33})^2 + (\sigma_{33} - \sigma_{11})^2]^{1/2}$$
$$= \tau_0 - \mu_m P \qquad (1.2)$$

where, τ_{oct} is the stress acting on a plane having a normal which makes the same angle with all three principle directions (octahedral shear stress) ,τ_0 and μ_m are material constants, μ_m accounting for the effect of pressure on the state of the material. Clearly, μ_m will be strongly effected by plasticization of the matrix material in Figure 1.1

(and by strain induced shifts in T_g local to the interface of the rubbery material) thereby reducing the requisite σ_0 for the initiation of shear banding.

Crazes are the second major mechanism for stress relief in a glassy polymer. Crazes occur only under conditions of hydrostatic tension (a dilatational process) when the molecular weight is greater than the critical molecular weight for entanglements[1]. Crazes form at 90° to the tensile axis. A craze is a localized yield zone. It is the first stage of fracture. Crazes are stabilized by fibers of oriented polymer which span the craze gap creating a network of voids and polymer. Kramer[7] notes that crazes grow by a meniscus instability mechanism, and that the fibrils contain highly oriented polymer with the chain axis parallel to the fibril axis.

The kinetics of craze formation can be broken down into three stages,

(A) Initiation (void formation in regions of high stress concentration)

$$\text{Number of crazes} = N = k_i\, t \qquad (1.3)$$

The rate is not time dependent.

$$dN/dt = k_i \qquad (1.4)$$

(B) Propagation (craze generates a stress concentration at the craze tip which produces voids, incorporation of material from the yield zone occurs)

-Stress relaxation within the craze

-Time-dependent modulus of the bulk polymer[6]

$$dr/dt = k_p \qquad (1.5)$$

(C) Termination occurs when the stress concentration at the tip of the craze falls below the critical value for propagation.

Failure occurs when the craze length, r, grows beyond a critical value r* which is unique for each material.

The effect of temperature (T) on crazing behavior can be expressed in terms of a stress bias, σ_b[9],

$$\sigma_b = |\sigma_{11} - \sigma_{22}| = A(T) + \frac{B(T)}{(\sigma_{11}+\sigma_{22})} \qquad (1.6)$$

where A and B are temperature dependent material parameters. A and B depend on shifts in T_g of the matrix material of Figure 1.1 .

Catastrophic failure for crazes occurs when the craze fibrils fail. This has been related to a critical craze length r*. When the number of crazes increase, in a toughened material for instance, the average size of a craze is reduced. Thus, the attainment of crazes of size r* is more difficult and failure is avoided.

Pure PS exhibits pure crazing under tension (PS will display shear banding under a compressive load). Shear bands and crazes occur simultaneously in some of the materials studied in this project. The interaction between these two deformation mechanisms involve restriction of craze propagation by shear bands, the crazes being restricted to a size, r', which is the distance between shear bands. In the toughened materials discussed r' is smaller than r* and failure of the material is avoided.

Commercially toughened polymers display varying degrees of crazing and shear banding depending on the nature of the matrix polymer[1]. HIPS displays about 95% crazing, toughened PVC on the other hand shows about 8% crazing and about 92% shear band deformation. ABS toughened PS shows about 50% crazing and 50% shear band deformation.

The difference in mechanical properties between HIPS and PS are shown in the constant strain rate, engineering stress/strain plot and the true stress/strain plot of Figure 1.2 below[8] (engineering stress is the force per unit initial area, true stress is the force per unit actual area during the experiment).

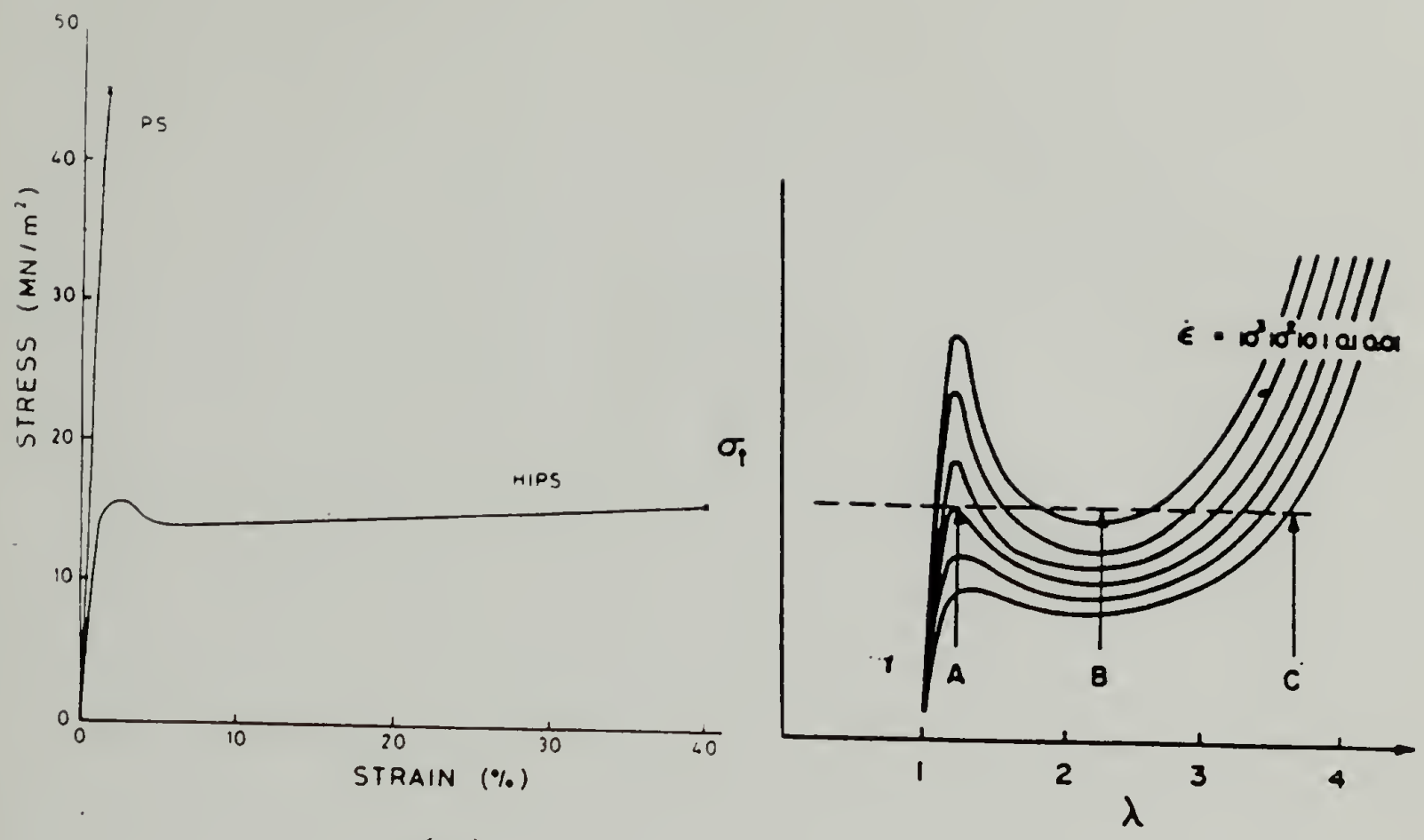

FIGURE 1.2 (a) Constant strain rate experiment for PS and HIPS[1] (engineering stress), (b) true stress vs. strain plot for HIPS[10].

In FIGURE 1.2(b) (true stress vs. strain) note that strain hardening occurs at high strains caused by stretching of chains and that upper and lower yield points occur even in the true stress vs. strain plot in contrast to deformation by necking. The upper and lower yield points indicate a strain softening effect due to structural changes. HIPS shows,

(A) An initial elastic response (identical to that of PS)

(B) Yielding and energy absorption at small strains, leading to an upper yield point (also observed with glass bead filled PS)

This corresponds to the induction period for crazes.

σ_y increases linearly with $\log(d\varepsilon/dt)$

(C) A lower yield point separated from the upper yield point by the yield gap.

The yield gap being due to strain softening during craze formation.

A yield drop is not seen in strain hardening materials (materials in which significant shear banding occurs).

(D) Fracture at high elongation (a large degree of elongation is not observed for glass bead filled PS).

The effect of the added rubber can take two forms in impact modified materials which deform by crazing,

(A) The rubber phase encourages a large number of small crazes to be formed, rather than a small number of large crazes which produce cracks in PS (dominant in more brittle matrix phase polymers such as PS).

(B) Rubber phase causes a local octahedral stress concentration which encourages the production of stress relieving shear bands (dominant in less brittle matrix phase toughened polymers such as PVC).

In general, we can categorize deformation behavior as viscoelastic (recoverable) or plastic (non-recoverable). Pure polystyrene under strains of < 0.2% is viscoelastic. Under strains of > 0.2% it is plastic. However, some of the deformation above 0.2% strain is recoverable. Crazes form by a cavitation mechanism resulting in the loss of local, intermolecular cohesion, and a decrease in density. Shear bands are known to relax to some extent. Under shear yielding there is little change in density and the material retains intermolecular cohesion.

Kramer[7] gives the bulk strain, ε , in terms of number of shear bands, N, shear strain in a shear band, *V*, shear band thickness, t, and growth distance of a shear band, l,

$$\varepsilon_s = N_s V t l^2 \qquad (1.7)$$

For crazing, Kramer gives,

$$\varepsilon_c = N_c a (1 - \lambda^{-1}) l^3 \qquad (1.8)$$

where a is the wedge angle. The term [a $(1 - \lambda^{-1})$ l] in equation 1.8 is derived from the average Burges vector , <b>,

$$\langle b \rangle = a\,(1 - \lambda^{-1})\,l \qquad (1.9)$$

N_c is the number density of crazes, l is the dimension of crazes in the plane. It should be noted that ε_c is proportional to l^3, thus if the crazes grow linearly, ε_c will increase in a cubic manner.

In the blend system under study, several material parameters are under experimental control,

(A) Physical crosslinks in the rubbery phase can be melted below the T_g of the matrix phase so that the effects of crosslinks on the mechanical properties can be investigated.

(B) The composition of the matrix phase can be varied through controlled phase separation to investigate the mechanism of stress relief for different degrees of matrix brittleness.

(C) The size of the rubber phase can be controlled through controlled phase separation.

In addition to the effect of the rubber particles on the energy absorption mechanism, the matrix phase will, to some extent, be plasticized by the i-PVME. Thus, the brittle to ductile failure envelope will shift. A reduction in the initial elastic modulus under constant strain rate (Chapter 3) shows this plasticizing effect. Finally, the effect of a resilient suspended phase may be to induce strains in the matrix local to the interface, leading to a reduction in the glass transition temperature of the matrix at the interface.

C. The Interface Between Phases

Interfacial properties between the disperse rubbery phase and the matrix glassy phase will dominate the degree of toughening once crosslinks are induced. This has been demonstrated for the case of the addition of an immiscible rubbery polymer to PS[1]. Thermodynamics can describe the degree to which an equilibrium mixture of two polymers will mix. Such an analysis is useful in describing the tendencies of a real toughen blend, although translational properties and kinetic behavior will modify this idealized equilibrium state. The thermodynamics of polymer blends has been adequately described using the lattice model of Flory. The well known Flory-Huggins equation for the Gibbs free energy change on mixing, ΔG, is given by,

$$\frac{\Delta G}{RT} = \frac{\phi_1}{m_1} \ln \phi_1 + \frac{\phi_2}{m_2} \ln \phi_2 + \chi \phi_1 \phi_2 \qquad (1.10),$$

where ϕ_i and m_i are the volume fraction and the number of lattice sites occupied (degree of polymerization) for the i'th component and R and T have their usual meaning. χ has been termed the interaction parameter and in its original form as used by Flory and derived by Hildebrand reflected the enthalpic component of the free energy of mixing. Since the m_i's are very large for high polymers the entropic component of equation 1.10 is very small. Consequently, the miscibility of a polymer blend is dominated by the interaction

parameter. Generally, a negative χ will indicate equilibrium miscibility (a lowering of the free energy on mixing).

Interfacial broadening in miscible phase separated polymer blends has been extensively studied using such techniques as neutron reflection[9] and Rutherford back scattering[10]. For example, two thin layers of differing PVME/PS composition will diffuse into each other above their glass transitions and below the LSCT for the system. It is expected that this type of mixing will improve interfacial adhesion between the disperse rubbery and the matrix glassy phase in this work. An investigation of the interaction parameter for the isotactic PVME/PS blend is appropriate in order to gain insight into the interfacial adhesion.

Factors other than the interaction energy between phases may be of importance to interfacial adhesion. For instance segregation of chain ends may weaken the interface. de Gennes has noted[11] that the surface tension of linear polymers is reduced at lower molecular weights (from a limiting value reached at high molecular weights). This has been interpreted as indicating a segregation of chain ends to the surface. Similar chain end segregation may play an important role in interfacial adhesion in phase separated blends. An investigation of chain end segregation for polystyrene was conducted using neutron reflection (Chapter 9). (Other factors such as a densification of polymer at the interface may account for the dependence of surface tension on molecular weight.)

D. Stress Distribution and Shifts in T_g

It has been noted above that disperse domains in a glassy matrix may lead to stress concentrations. Bucknall[1] among others has indicated that large volumetric strains induced in the matrix phase may cause a local increase in the free volume of the polymer, thereby causing a reduction in the glass transition temperature (at the craze tip for instance). Such a shifting of the glass transition would be of great importance in understanding the nature of the toughening effects of suspended domains. A study of such shifts in the glass transition of polystyrene due to strains was conducted using the ellipsometer (Chapter 8). Differences in the thermal expansion coefficients of the two phases present in the phase separated blends and/or crystallization of the i-PVME phase may induce strains in the toughened materials discussed in Chapter 3.

References

1. C. B. Bucknall, *Toughened Plastics*, Applied Science Publishers LTD, London, 1977, Chapter 1.

2. C. B. Bucknall, *Toughened Plastics*, Applied Science Publishers LTD, London, 1977, p. 100.

3. R. R. Durst, R. M. Griffith, A. J. Urbanic and W. J. van Essen, *ACS Div. Org. Coat. Plast. Prepr.*, **34**(2), 320 (1974).

4. G. Beaucage, R. S. Stein, U.S. Patent Application Filed 9/1989.

5. G. S. Y. Yeh, personnel communication.

6. C. B. Bucknall, *Toughened Plastics*, Applied Science Publishers LTD, London, 1977, Chapter 6.

7. E. J. Kramer, *J. Poly. Sci. (Phys.)*, **13**, 509 (1975).

8. C. B. Bucknall, *Toughened Plastics*, Applied Science Publishers LTD, London, 1977, p. 254.

9. J. Korberstein, personnel communication.

10. R. Composto, personnel communication.

11. P. de Gennes, *C. R. Acad. Sci. Paris, t. 307, Serie II*, 1841, (1988).

CHAPTER 2

SYNTHESIS, CHARACTERIZATION AND FRACTIONATION OF ISOTACTIC PVME

A. Synthesis

Isotatic poly(vinyl methyl ether) is not commercially available. The synthesis is, however, well understood. Lenz[1], discusses the preparation of crystalline PVME by homogeneous cationic polymerization using $BF_3.O(C_2H_5)_2$ catalyst. The polarity of the solvent is used to manipulate the tacticity via the degree of association of the reactive ionic end groups. Polar solvents favor the formation of isotactic polymer (crystallizable) through the formation of more intimate ion pairs. Higashimura and coworkers[2] noted that the presence of a chlorinated solvent (chloroform) was required for the synthesis of crystalline PVME using $BF_3.O(C_2H_5)_2$.

A typical synthetic scheme for the production of i-PVME involves cationic polymerization of vinyl methyl ether (Matheson Gas) at -78 °C under nitrogen using a 43:57 hexane to chloroform mixture as solvent (solvents were distilled over Ca_2H_2, monomer was dried over Ca_2H_2 and distilled into the reaction vessel). The concentration of $BF_3O(Et)_2$ was 7.7 mmol/l. Polymerization proceeded for two hours by which time gelation had occurred. The reaction was terminated using ammoniated methanol. (Atactic PVME was purchased from

Scientific Polymer Products Inc. and fractionated as described below. This treatment removed the heat stabilizer present in the commercial material.)

The product of this reaction procedure is a visco-elastic opaque solid (commercial, atactic PVME is a viscous liquid). Both the commercial, atactic PVME (a-PVME) and the synthesized i-PVME degrade in air at about 200 °C after about one minute in the absence of stabilizers (the PVME becomes yellow to brown). PVME of relatively high molecular weight (both a-PVME and i-PVME) have an LCST (phase separation on heating) with water. This phenomenon was used to purify the product of our synthesis. The PVME was purified by phase separation in hot water followed by hot filtration. Secondly, a solvent/non-solvent fractionation using benzene/heptane was performed on the PVME's. The combination of these two fractionation techniques could reduce the polydispersity from about 2.2 to about 1.5. Purification of PVME using membrane filtration (in aqueous solutions) was explored and seemed promising, however a large scale apparatus was not available.

Several PVME's synthesized in Kyoto by T. Hashimoto, H. Hasegawa[3] are also included in this thesis. They were prepared by cationic polymerization at -78 °C under high vacuum using toluene as a solvent. The solvent was washed with concentrated H_2SO_4, a 10% aqueous solution of NaOH and with distilled water in that order, dried with Ca_2H_2, distilled under atmospheric pressure, and sealed in vacuum. The concentration of $BF_3O(Et)_2$ was 10 mmol/l for i32 and 2 mmol/l for i40 (i32 refers to an isotactic sample of weight average

molecular weight 32kg/gmmole). Gellation of the polymerization mixture was observed for i32 and i40. The polymerization reaction was terminated with NH_3/MeOH. The polymerized products were precipitated by pouring the polymerization mixtures into a large quantity of petroleum ether. The precipitated polymers were vacuum dried. The dried polymer samples were slightly turbid solids for the isotactic PVME.

Table 2.1 summarizes the effects of reaction conditions on tacticity and molecular weight of PVME.

Alternative synthetic schemes for the synthesis of i-PVME include the use of other metal halide catalysts such as $SnCl_4.CCl_3CO_2H$ [4]. The use of a Sulfuric Acid-Aluminum Sulfate Complex[5,6,7] has also been suggested by Higashimura and coworkers. Higashimura reports that highly crystalline PVME can be obtained at -10°C using this system. DSC of the dried, as-polymerized PVME produced in our lab following the Higashimura technique showed a crystalline endotherm at 51.7°C and a glass transition at -28.1°C. The product retained traces of the catalyst which could not be removed by the purification technique used for the i-PVME produced via $BF_3O(Et)_2$ catalyst. Further, the factors influencing the $BF_3O(Et)_2$ procedure are better understood, leading to a greater control over the tacticity. Finally, the commercially available PVME used in this study was synthesized using $BF_3O(Et)_2$. Thus, the $BF_3O(Et)_2$ synthesis was chosen for use in this study

Table 2.1 Variables* controlling tacticity and molecular weight of PVME[8].

-Polarity of Solvent +	MW +	Isotacticity +
-Temperature +	MW -	Isotacticity -
-Low Catalyst Concentration (2.4×10^{-3}M)	MW +	Isotacticity +
-High Catalyst Concentration (4.0×10^{-3}M)	MW -	Atactic

* "+" = increases; "-" = decreases

More recently Higashimura[9,10] among others, has investigated living cationic polymerizations of poly(vinyl ethers) using the hydrogen iodide/iodine (HI/I_2) catalyst system. Although this technique produces very low polydispersities, the yield and molecular weights presently obtainable are not sufficient for our purposes. R. Faust and J. P. Kennedy[11] have recently written a series of articles concerning the mechanisms of such living carbocationic polymerizations.

Ketley[12] has extensively reviewed the synthesis and characterization of stereospecific vinyl ethers in Chapter 2 of his text, *The Stereochemistry of Macromolecules, Volume 2.*

B. Characterization of i-PVME

Three ^{13}C NMR scans are shown in Figure 2.1 below. Note that PVME 11 shows a sharper isotactic peak, 'i', while PVME 10 shows a broader peak. The broader the distribution (i.e. the wider the peak) the more 'blocky' is the polymer. The less 'blocky' i-PVME (number 11) shows a higher percentage crystallinity when annealed at room temperature indicating inclusion of amorphous segments into the imperfect i-PVME crystallites.

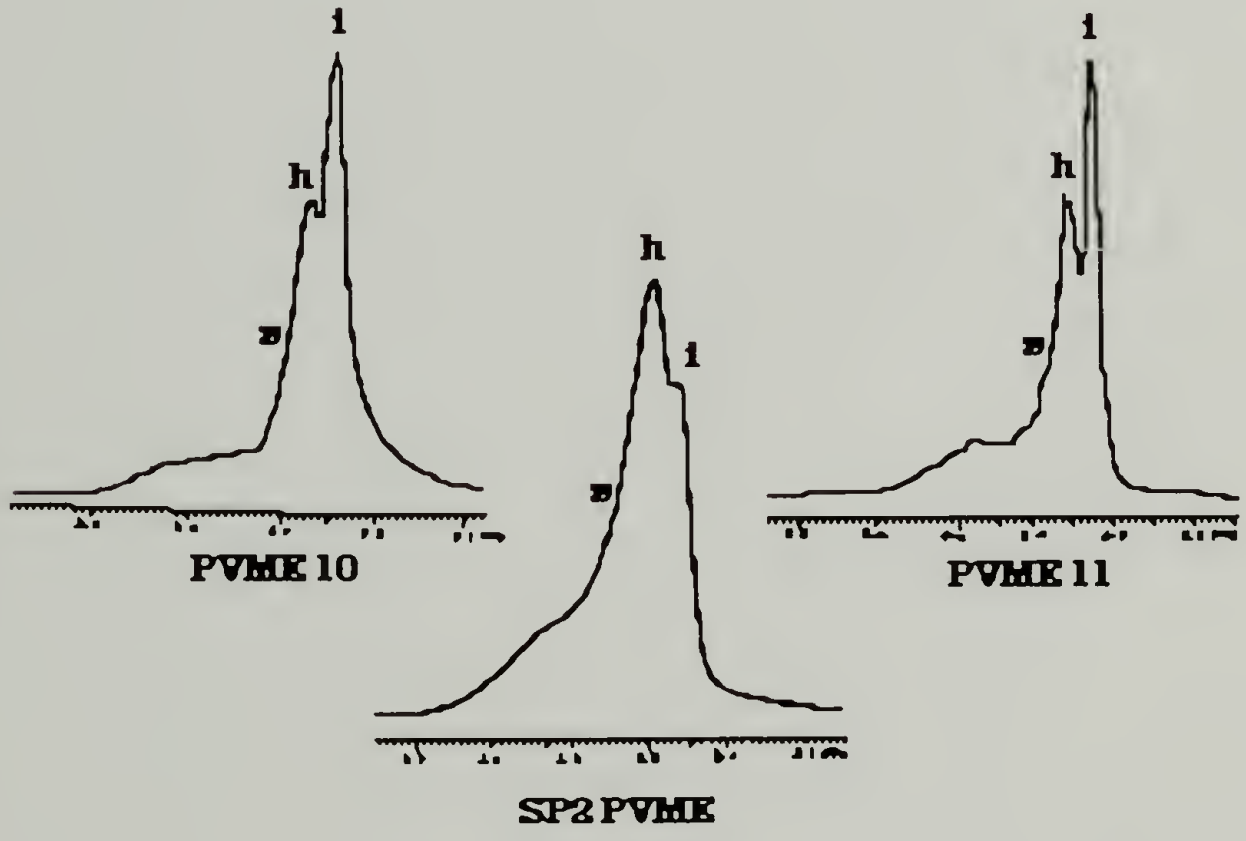

Figure 2.1 ^{1}H NMR of predominantly isotactic (i-PVME 10 and i-PVME 11) and atactic (SP_2) PVME.

Triad tacticities were determined by proton NMR following the procedure of Dombroski[13]. The triad tacticities of the synthesized

i-PVME samples and of the commercially purchased heterotactic PVME are presented in Table 2.2 below. (The triad tacticity of PVME obtained from Aldrich Chemical (hAld) which was not used in this study due to its high polydispersity, is also included for comparison.) The NMR experiments were run at least three times for each sample. The reported tacticities were reproducible to ±1 of the indicated percentages.

Table 2.2 Triad tacticities of the synthesized i-PVME samples and of commercially purchased heterotactic PVME's.

		PERCENT TRIAD TACTICITES		
		ISOTACTIC	HETERO-TACTIC	SYNDIO-TACTIC
PREDOMINANTLY HETEROTACTIC (AMORPHOUS)	hAld	34	55	11
	h99	31	69	0
PREDOMINANTLY ISOTACTIC (CRYSTALLINE)	i89	55	40	5
	i40	64	32	3
	i32	59	38	3

FIGURE 2.2 shows X-ray two theta scans for isotactic (i89) and atactic (a99) PVME samples. Corradini and Bassi[14] have analyzed the rhombohedral crystalline structure of *i*-PVME using X-ray diffraction.

The three strong crystalline peaks at 2θ= 10.84, 18.92 and 21.66 degrees shown in Figure 2.2 correspond to diffraction layer spacings of 2.05, 2.35 and 4.08 Angstroms, agreeing well with Corradini and Bassi's analysis.

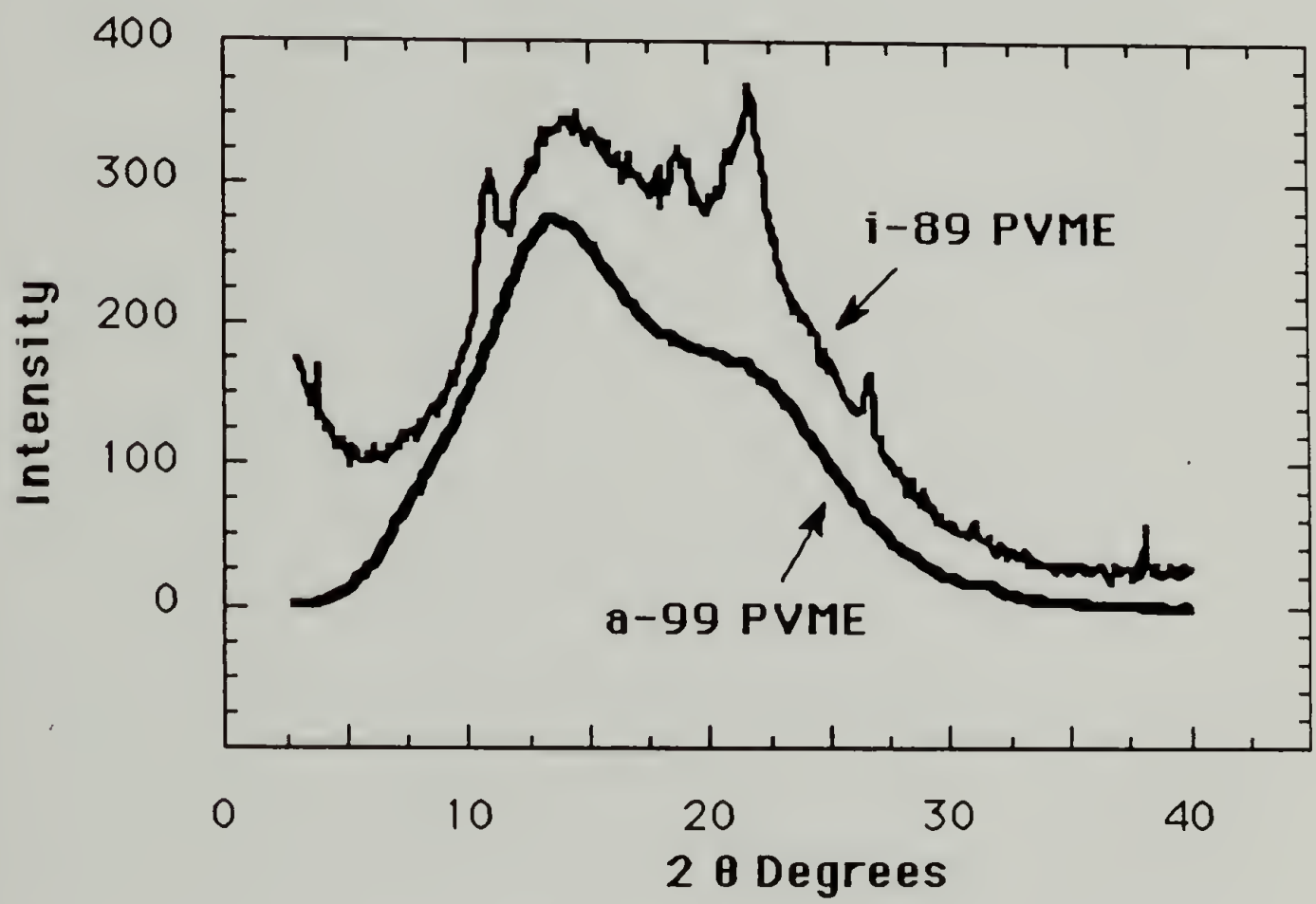

Figure 2.2 X-ray two theta scans for isotactic (i89) and atactic (a99) PVME samples.

Differential scanning calorimetry measurements were also made on several of the above samples. The corresponding glass transition and melting point data as well as the degree of crystallinity in the isotactic samples are presented in Table 2.3. It is of note that T_g is not significantly effected by the tacticity of the PVME sample in accord with the findings of Karasz and MacKnight[15].

Table 2.3 Characterization of PVME samples. (*As polymerized, **not measured, ***precipitated from toluene by addition of n-hexane and dried.)

		MW kg/mole	$\frac{M_w}{M_n}$	T_g(°C)	T_m(°C)	Percent Crystallinity (by X-ray)
Atactic	h99	99	3	-28.3	----	0
	hAld	NM*	NM*	NM*	----	0
Isotatic	i89	89	1.8	-28.3	35.5*	3.0*
	i40	40.2	1.6	-26.1***	54.3***	56.4***
	i32	31.9	1.6	-31.3	49.7	NM

The literature gives contradictory values for the melting point of i-PVME. A value of 140 to 144°C (determined by loss of birefringence) is reported by Vandenberg.[9]. (This technique for determination of the presence of crystallinity is highly inaccurate due to the possibility of orientation in the sample.) Vandenberg[10] later showed DTA plots which indicate multiple melting points for i-PVME, the highest of which occurs at about 56°C. Bank[4] reports an equilibrium melting point for i-PVME (6.50×10^5 molecular weight and a low degree of isotacticity) at 63°C. The observed melting points for the pure i-PVME studied here occurred between 35 and 70°C depending on the crystallization conditions. The highest melting point obtainable for the isotactic PVME synthesized in this project is about 70°C. In

Chapter 7 an equilibrium melting point of about 72°C was established on the basis of the temperature and composition dependence of the statistical segment length as determined using small angle neutron scattering. In samples obtained from the melt and annealed at room temperature the melting point was consistently about 40°C. The lack of spherulitic or other microscopic sized structures under the optical microscope (using crossed polars) indicate that imperfect crystallites are probably present in these materials.

C. Scale-up of i-PVME Synthesis

i-PVME used in the melt-blending experiments was synthesized in Sarnia Ontario at Polysar LTD's butyl rubber pilot plant (butyl rubber is also produced by a low temperature cationic polymerization) by the author under the direction of Dr. J. Lunt and Dr. A. Osman with the assistance of S. Kirby. A 3.5 liter Teflon coated Waring® blender cooled by thermostated liquid nitrogen jets was used, Figure 2.3. After cooling the solvent and monomer to -80°C under nitrogen, catalyst was injected and the reaction proceeded. Reaction temperature versus time data was used to monitor the reaction (Figure 2.4). It was found that the reaction would not proceed at temperatures below about -80°C (note PVME III in Figure 2.4). The highest molecular weight and highest degree of tacticity were produced in reactions

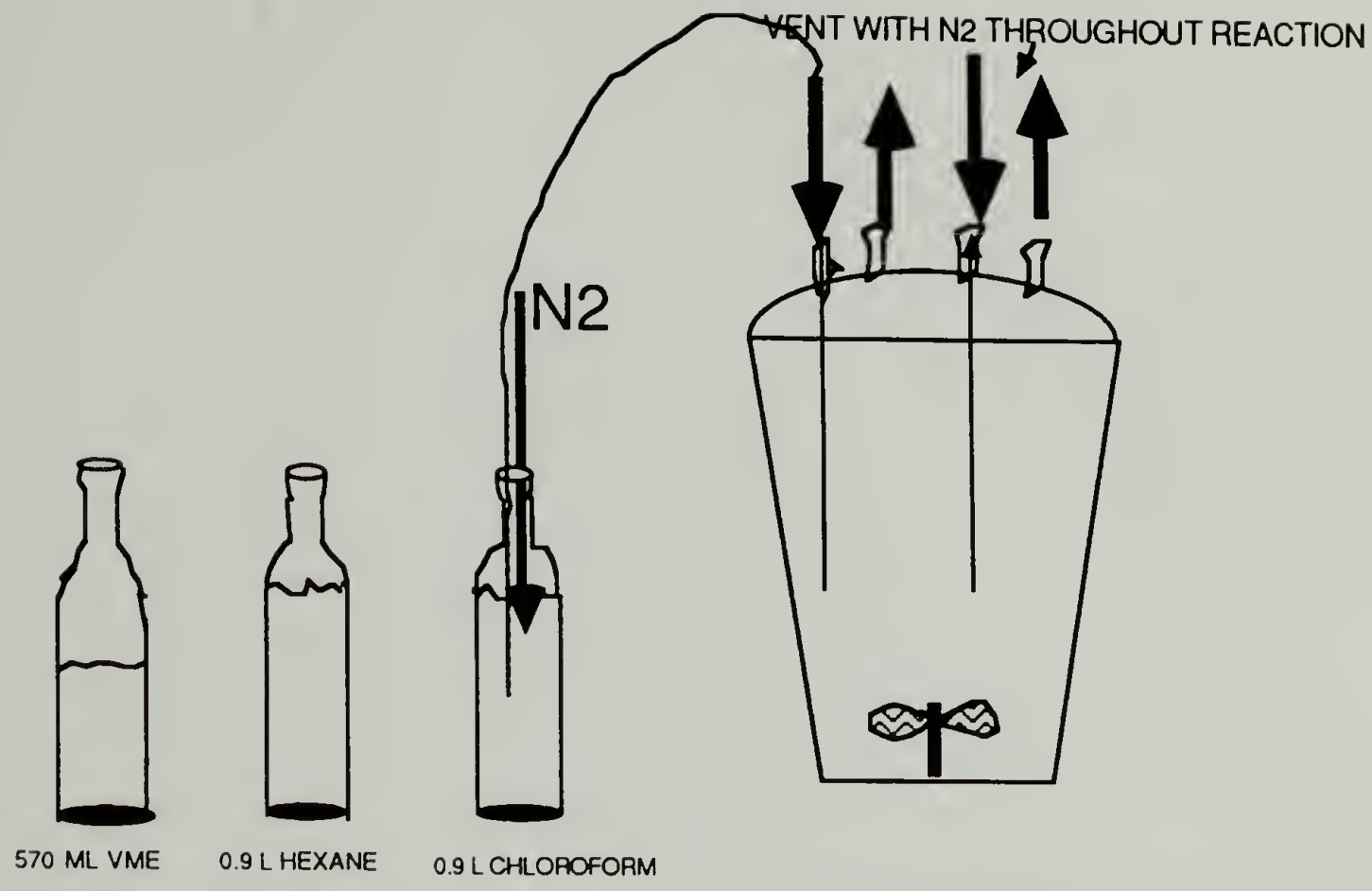

Figure 2.3 Experimental setup for large scale synthesis of i-PVME.

where the reaction temperature did not exceed 0°C). Thermal control better than that shown in Figure 2.4 would be impossible in practice for the large scale reaction (50 liters of liquid nitrogen were used per reaction in Figure 2.4). About ten pounds of i-PVME were produced in this way for use in melt blending experiments. About 1% Santonox White (antioxidant) was added to these PVME's in order to prevent degradation.

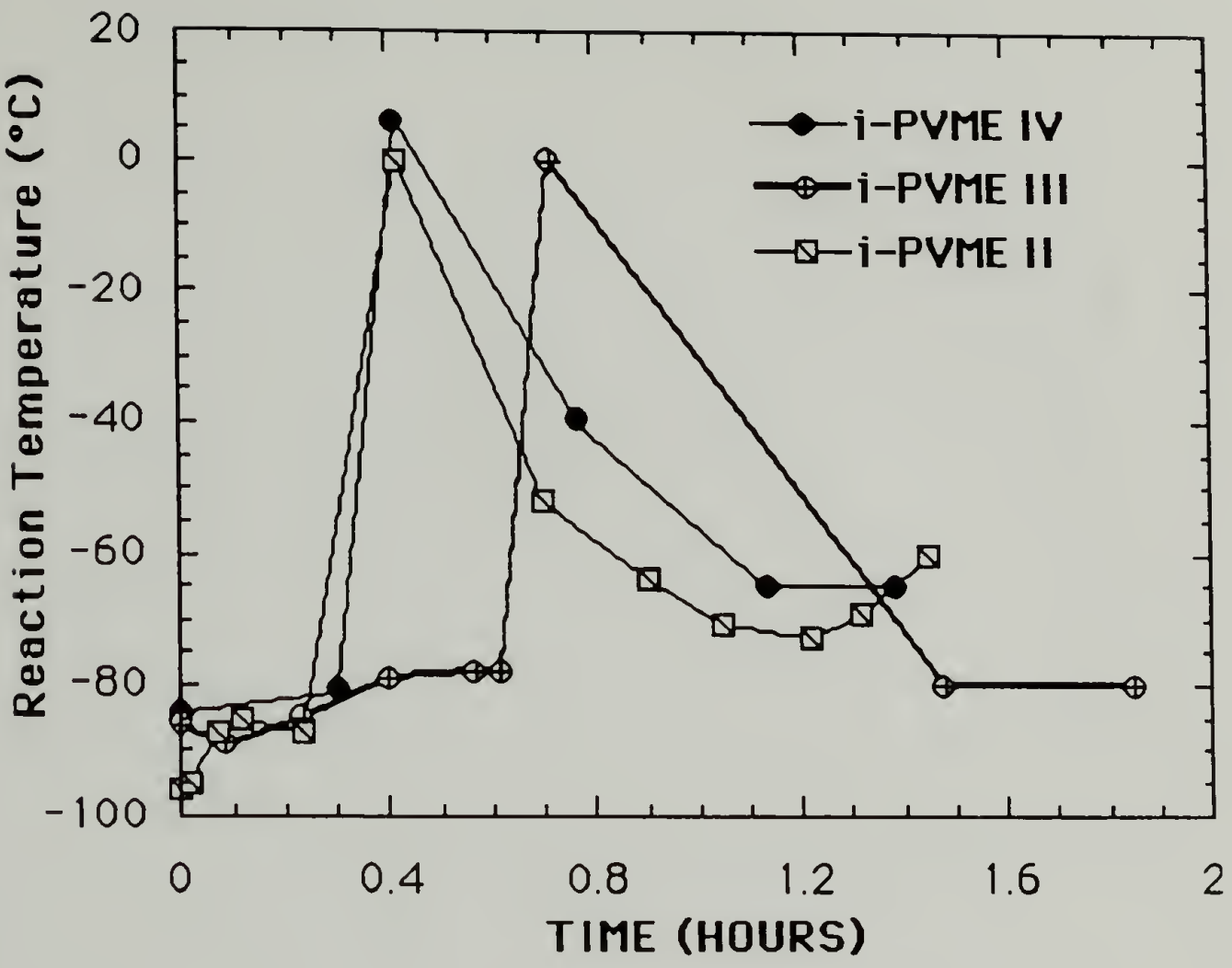

Figure 2.4 Reaction temperature versus time for a typical synthesis of isotactic PVME using the five liter reactor at Polysar's Sarnia Ontario pilot plant.

References

1. R. W. Lenz, *Organic Chemistry of Synthetic High Polymers*, Interscience Publishers, New York, 1967, p. 524.

2. S. Okamura, T. Higashimura and H. Yamamoto, *J. Polymer Sci.*, **33**, 510 (1958).

3. G. Beaucage, R. S. Stein, T. Hashimoto, H. Hasagawa, *Macromolecules* (in press).

4. Y, Ihsumi, T. Higashimura, and S. Okamura, *J. Polymer Sci.,Pt. A1*, **5**, 849 (1967).

5. T. Higashimura, Y. Ohsumi, K Kuroda, and S. Okamura, *J. Polymer Sci.,Pt. A1*, **5**, 863 (1967).

6. T. Higashimura, Y. Ohsumi, K Kuroda, and S. Okamura, *Makromol. Chem.*, **50**, 137 (1961).

7. T. Higashimura, Y. Ohsumi, K Kuroda, and S. Okamura, *J. Polymer Sci. A*, **2**, 3369 (1964).

8. S. Okamura, T. Higashimura and I. Sakurada, *J. Polymer Sci.*, **39**, 507 (1959).

9. M. Sawamoto, T. Enoki and T. Higashimura, *Macromolecules*, **20**(1), 1 (1987).

10. S. Aoshima, K. Ebara, and T. Higashimura, *Polymer Bulletin*, **14**, 425 (1985).

11. R. Faust and J. P. Kennedy, *J. Polymer Sci.: Part A: Poly. Chem.*, **25**, 1847 (1987).

12. A. D. Ketley, *The Stereochemistry of Macromolecules, Volume 2*, Marcel Dekker, New York, 1967, Chapter 2.

13. R. Bank, *Polymer Preprints*, **10**(2), 622 (1969).

14. J. W. Schurer, A. de Boer and G. Challa, *Polymer*, **16**, 201 (1975).

15. F. E. Karasz, W. J. MacKnight, *Macromolecules*, **1**(6), 229 (1963).

CHAPTER 3

PHASE DIAGRAMS FOR ISOTACTIC PVME/PS BLENDS AND QUALITATIVE ANALYSIS OF THE TACTICITY EFFECT

A. Background

In order to control the morphology of the i-PVME/PS blends the phase diagram and the thermal transitions (melting points and glass transitions) must be determined. The system polystyrene/poly(vinyl methyl ether) exhibits a lower critical solution temperature (LCST), i.e. it phase separates with increase in temperature. This behavior is probably due to a reduction in the strength of intermolecular interactions with an increase in temperature, specifically the aromatic (PS) methoxy group (PVME) interactions. Flory-Huggins theory relates the molar Gibbs free energy of isothermal mixing (ΔG_m),

$$\Delta G_m = - T \Delta S_m + \Delta H_m \qquad (3.1)$$

to the interaction parameter, χ. Thus,

$$\frac{\Delta G_m}{RT} = \frac{\phi_1}{m_1} \ln \phi_1 + \frac{\phi_2}{m_2} \ln \phi_2 + \chi \phi_1 \phi_2 \qquad (3.2)$$

where the parameters in 3.2 were described in Chapter 1. χ in the classic Hildebrand analysis as followed by Flory and Huggins would

follow a functional form of B/T. Such a functional form for χ predicts a UCST behavior (phase separation on cooling) but can not explain LCST behavior (phase separation on heating) as is observed in the PS/PVME blends. This is a direct result of the combinatorial entropy terms in equation 3.2 (first two terms) always being positive. A negative ΔG_m is a necessary but not a sufficient condition for complete mixing.

For a system with an attractive interaction (i.e. a miscible system), the interaction parameter, χ, is negative. In order to explain LCST behavior, Koningsveld, Kleintjens and Schultz[1] have suggested that χ has both an enthalpic and an entropic nature. This leads to a χ which varies with temperature as,

$$\chi = A + \frac{B}{T} \qquad (3.3),$$

where A and B are constants. This attractive interaction is proportional to the inverse of temperature as in the Hildebrand theory. For the system PVME/PS, χ becomes positive with increasing temperature and reaches a critical value at which phase separation occurs. This behavior is related to a positive value for "a" in equation 3.3 which is larger than the combinatorial entropy terms in equation 3.2. LCST behavior has also been speculated to occur through several postulated mechanisms, for instance differences in the thermal expansion coefficient for the two component lattices (equation of state theory).

B. Previous Work Involving Tactic Blends

Although tactic blends of PVME with PS have not been comprehensively studied previous to this work, other work involving blends of polymers having differing tacticities have been conducted. Previous work has concentrated on the acrylates due to the commercial availability of tactic forms in these systems. Challa and coworkers in the Netherlands have studied various blends involving poly(vinylidene flouride) (PVF_2). In a paper by E. Roerdink and G. Challa[2] the complete phase diagram for the system PVF_2/i-PEMA (isotactic poly(ethyl methacrylate) is presented. Cloud points were determined using an optical microscope in conjunction with a light dependent resistance device. DSC techniques were used to determine the melting, crystallization and glass transition temperatures.

A related system, PVF_2/i-PMMA (poly(methyl methacrylate) has been the subject of work by W. S. Herman and R. S. Stein at the University of Massachusetts[3]. Schurer, de Boar and Challa[4] have studied blends of PVC/i-PMMA and PVC/s-PMMA and found a single T_g for s-PMMA blends of less than 60%. i-PMMA was miscible over the entire composition range.

It has been shown by Challa and coworkers[5] that tacticity can have an effect on the phase diagram of a binary mixture. In work on poly(methyl methacrylate) (PMMA) of varying tacticities blended with poly(vinylidene fluoride) (PVF_2) it was concluded that the 5_1 helical form of i-PMMA interfered with specific interactions between the two blend components. s-PMMA has a planar zigzag conformation.

Prud'homme and coworkers[2] have also observed substantial tacticity effects in the system PMMA/poly(vinyl chloride) (PVC). In disubstituted vinyl polymers, such as PMMA, tacticity also has a large effect on the glass transition temperature (T_g). i-PMMA has a T_g of about 50°C whereas s-PMMA has a T_g of about 130°C[4]. For monosubstituted vinyl polymers such as PVME, tacticity does not significantly effect T_g[6]. Previous work involving stereoregularity in vinyl polymers has been analyzed in terms of tacticity effecting the local conformation which, in turn, affects specific group interactions with other constituent polymers and hence the miscibility. It is of interest to study systems of varying tacticity with similar thermal behavior (i.e. T_g) in order to distinguish the effect of tacticity on conformation and intermolecular interaction from that on segmental mobility (related to T_g).

C. Experimental Apparatus

The large differences in index of refraction for PS and PVME make possible an optical determination of the phase separation point. When an initially clear film of a PS/PVME blend is heated to the phase separation point the film becomes opaque. This is termed the cloud point for the blend and has been related to the binodal line on the phase diagram. (That is to say, the binodal and the cloud point curve are expected to follow similar behavior in composition and temperature although having slightly different values due to kinetics.) The location of the cloud point curve is dependent on such factors as the molecular weight, the tacticity of the components and the heating

rate of the experiment as well as the film thickness[7]. The latter two dependences are not expected for the equilibrium coexistence curve (the binodal). Figure 3.1 is a diagram of the cloud point apparatus (CPA) used to determine the phase diagram for the PS/PVME blends. In the experiment the blend is cast between glass cover slips (5-10 μ thick). A laser beam passes through the film. If the blend is miscible the light beam passes through the sample resulting in a very low background reading from the CPA detector (fiber optic line to photomultiplier tube (PMT) in Figure 3.1).

When the blend phase separates, domains of differing composition (and index of refraction) form. Figure 3.2 is a typical light scattering pattern of a phase separated, equi-weight PS/i-PVME blend at 156°C. The main beam is seen in the center. The ring which appears around the main beam is due to the presence of phase separated domains. The characteristic size of these domains is related inversely to the radius of the ring. At early stages of phase separation the domains are small and the ring is large (for the spinodal regime this corresponds to $q_{max} = \frac{4\pi}{\lambda} \sin\frac{\theta_{max}}{2}$). As phase ripening occurs, the domains become larger and the ring radius decreases. The cloud point pertains to early stages of phase separation and is thus studied at wide angles. In the CPA shown in Figure 3.3 critical reflection from the glass/air interface is used to collect light scattered over a wide angular range corresponding to $\theta = 90 \pm 50°$ (or $q = 6.8$ to $14\ \mu^{-1}$). q_{max} for PVME/PS is generally around $8\ \mu^{-1}$.

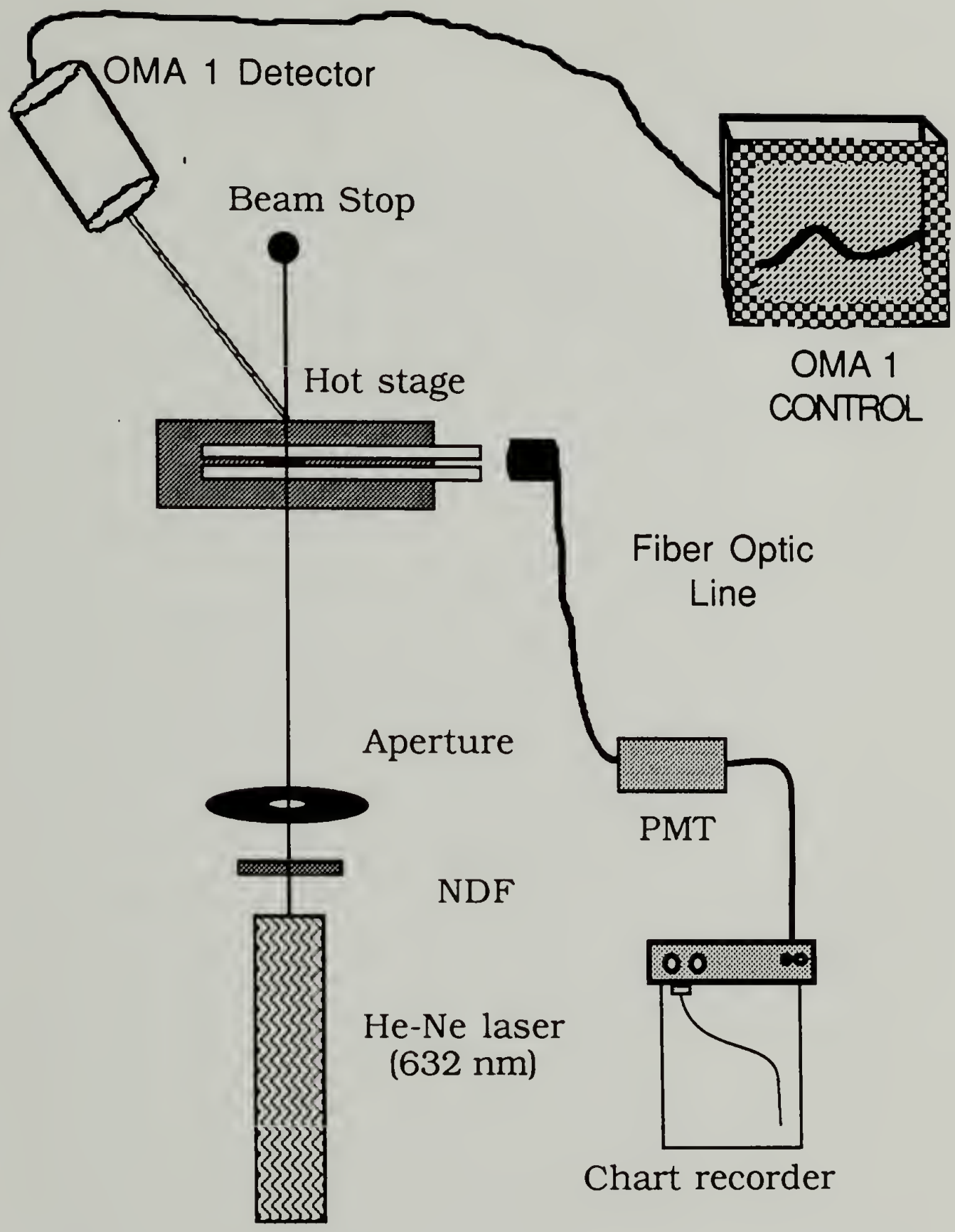

Figure 3.1 The cloud point apparatus (CPA) used to determine cloud point temperatures for PVME/PS blends.

Integration of wide angle data from the multichannel analyzer (OMA 1) shown in Figure 3.2 (6.8 to about 9 μ^{-1}) yields an integrated intensity which mimics the data obtained from the CPA (Figure 3.4).

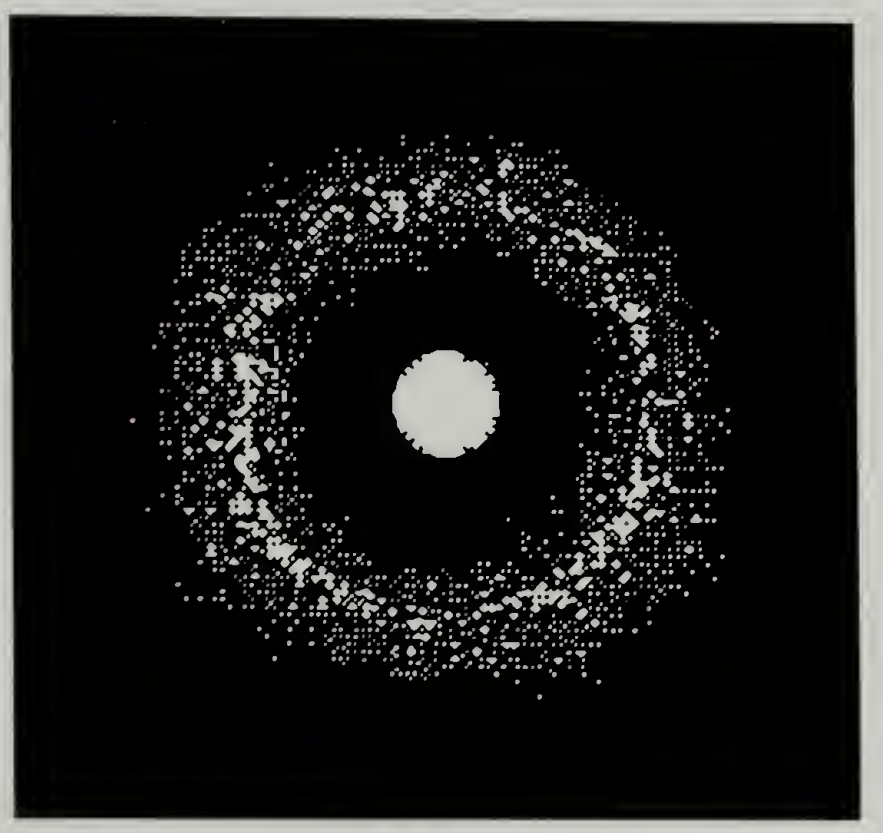

Figure 3.2 Typical light scattering pattern from a phase separated isotactic PVME/PS blend. (50% i-PVME 156°C computer enhanced digitized photograph).

The CPA, although very simple, represents an advancement in the detection of cloud points over the conventional turbidity measurement. In a turbidity measurement the detector is placed in the main beam. Initially, a large signal (full beam) is measured. This high intensity is slightly decreased at the phase separation point due to spinodal scattering (q_{max}). The signal to noise ratio in this case is poor. Using the CPA, cloud points have been determined for blends

with very small index of refraction differences such as poly(α-methyl styrene)/PS blends[8]. Additionally, thermal transitions such as

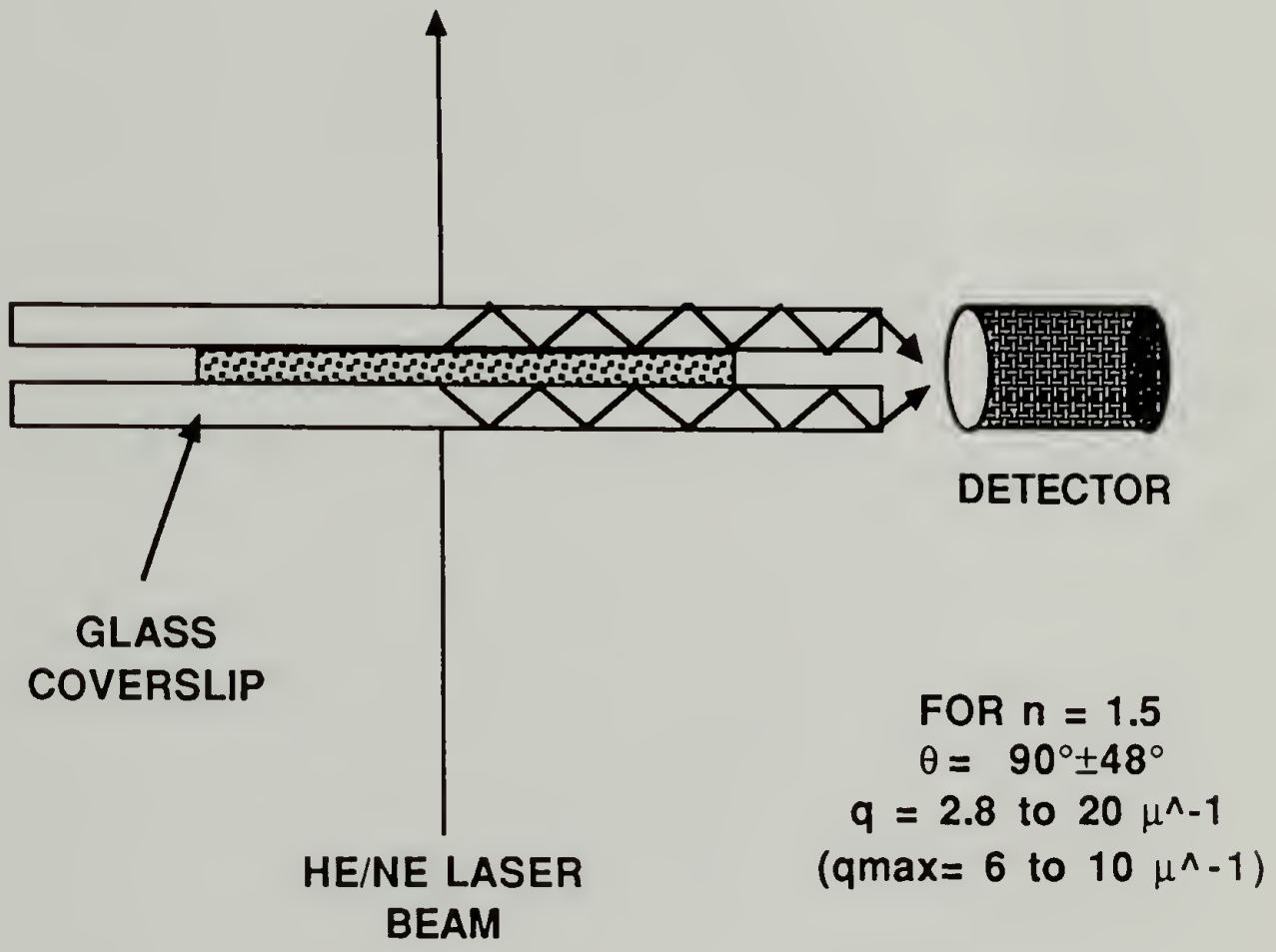

Figure 3.3 Cloud point apparatus showing the use of internal reflection to collect a wide range of scattering angles at the high angular range important to phase separation in polymer blends.

crystalline melting points, glass transitions and liquid crystalline transitions can be easily observed. Use of the CPA in conjunction with DSC data has proven to be very useful in semi-crystalline blend studies

(poly(carbonate)/polyester blends)[9] and in crosslinked-PS/PVME blend studies[10].

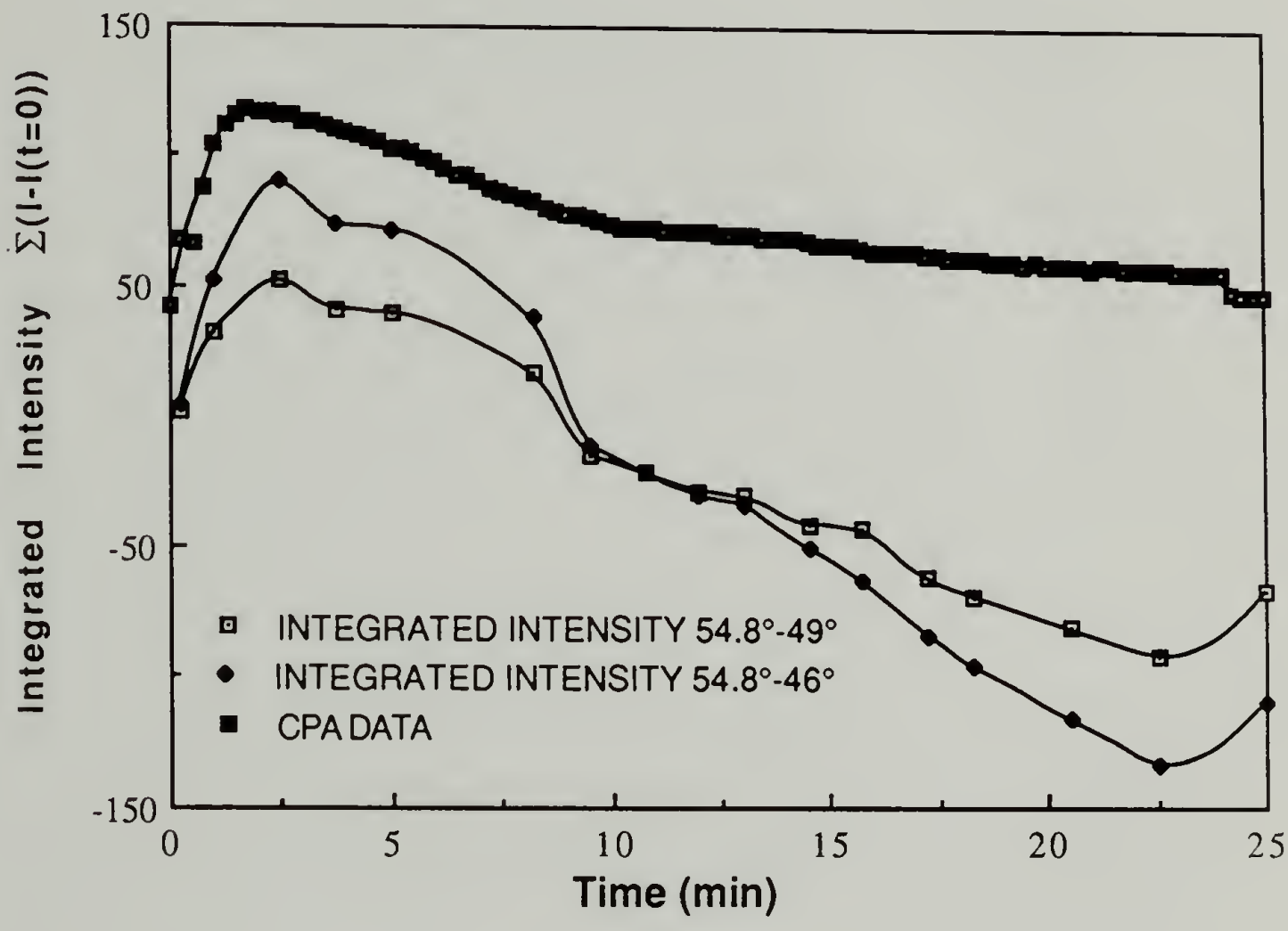

Figure 3.4 Integrated intensity from the OMA 1 compared with data from the CPA.

In determination of the cloud points for PVME/PS blends heating rates of 10, 2 and 0.2 °C/min were used and the cloud point at zero heating rate, T_{CP}, was estimated from a plot of these three points. Similar measurements made at Kyoto by Hashimoto and Hasegawa[11] determined T_{CP} by measuring the scattering intensity I(q,T) at $q=5.0x10^{-3}$ nm^{-1} with a photometer as a function of temperature. For this purpose the temperature was raised at a rate of

0.1 °C/min from a temperature well below T_{CP} to that above T_{CP}. At $T=T_{CP}$, $dI(q,T)/dT$ changes from approximately zero to a constant positive value. T_{CP} was determined as a temperature at which the two straight lines of I(q,t) vs. T for $T<T_{CP}$ and $T>T_{CP}$ intersect. The results of the two technique's are compared in Figure 3.5. The results

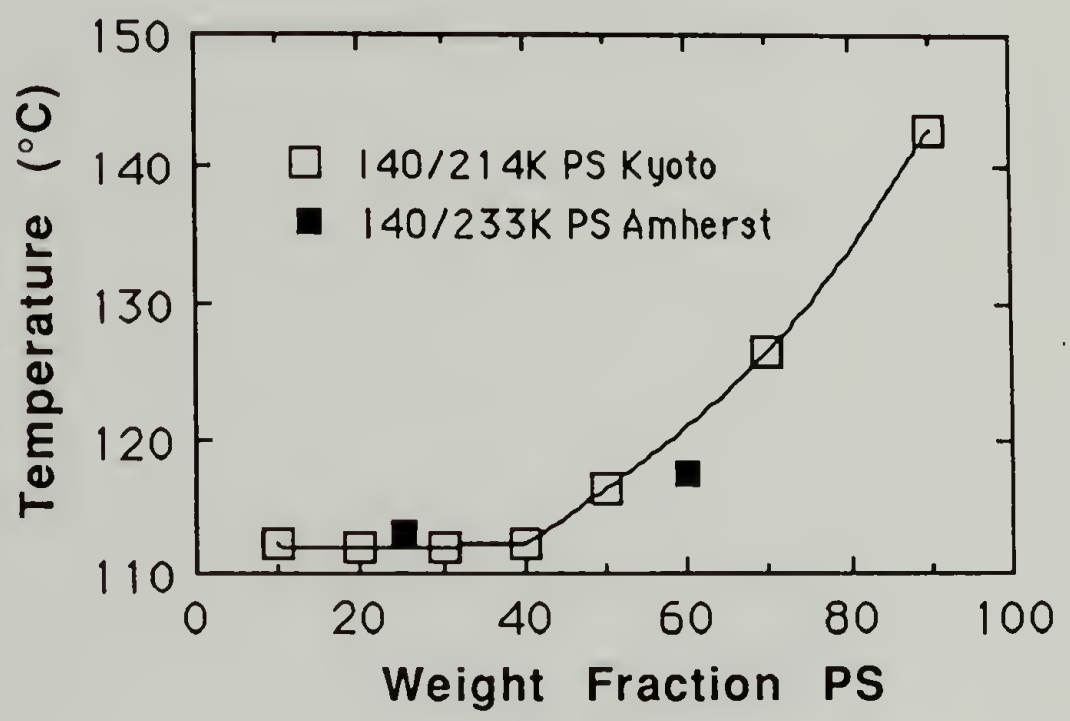

Figure 3.5 Comparison of two cloud point techniques discussed in text.

of the two techniques are essentially the same for the PVME/PS blends (taking into account the differences in the molecular weight of the PS).

D. Phase Diagram Polystyrene/Poly(vinyl methyl ether).

PVME samples are identified by "i" or "a" followed by the molecular weight in thousands, e.g. i40 is a predominantly isotactic

PVME of weight average molecular weight 40 kg/mole, and a99 refers to a predominantly atactic PVME of 99 kg/mole molecular weight. Blends are identified by the PVME component followed by the PS molecular weight, e.g. i40/214 is a blend of i40 with PS of molecular weight 214 kg/mole. Molecular weights of all polymers are reported as measured by GPC in terms of polystyrene standards. A Mark-Houwink analysis of the isotactic and atactic PVME indicated that this lead to errors in the molecular weight of less than 5% which is within the accuracy of the measured values.

Test specimens of the PVME/PS mixtures were cast from toluene solutions (10% polymer) at 30 °C, and dried further in a vacuum oven at room temperature. The as-cast films from toluene solutions showed two general types of behavior.

(I) The blends with no crystallinity (atactic PVME) were homogeneous as cast (transparent) and became turbid as their temperature was raised through the cloud point (this behavior was reversible).

(II) For the blends of higher crystallinity (i32 and i40) the as-cast samples were turbid. Figure 3.6a shows the change in turbidity as observed upon heating the as-cast film. Figure 3.6b presents a possible structural model for the turbidity behavior. In these cases the

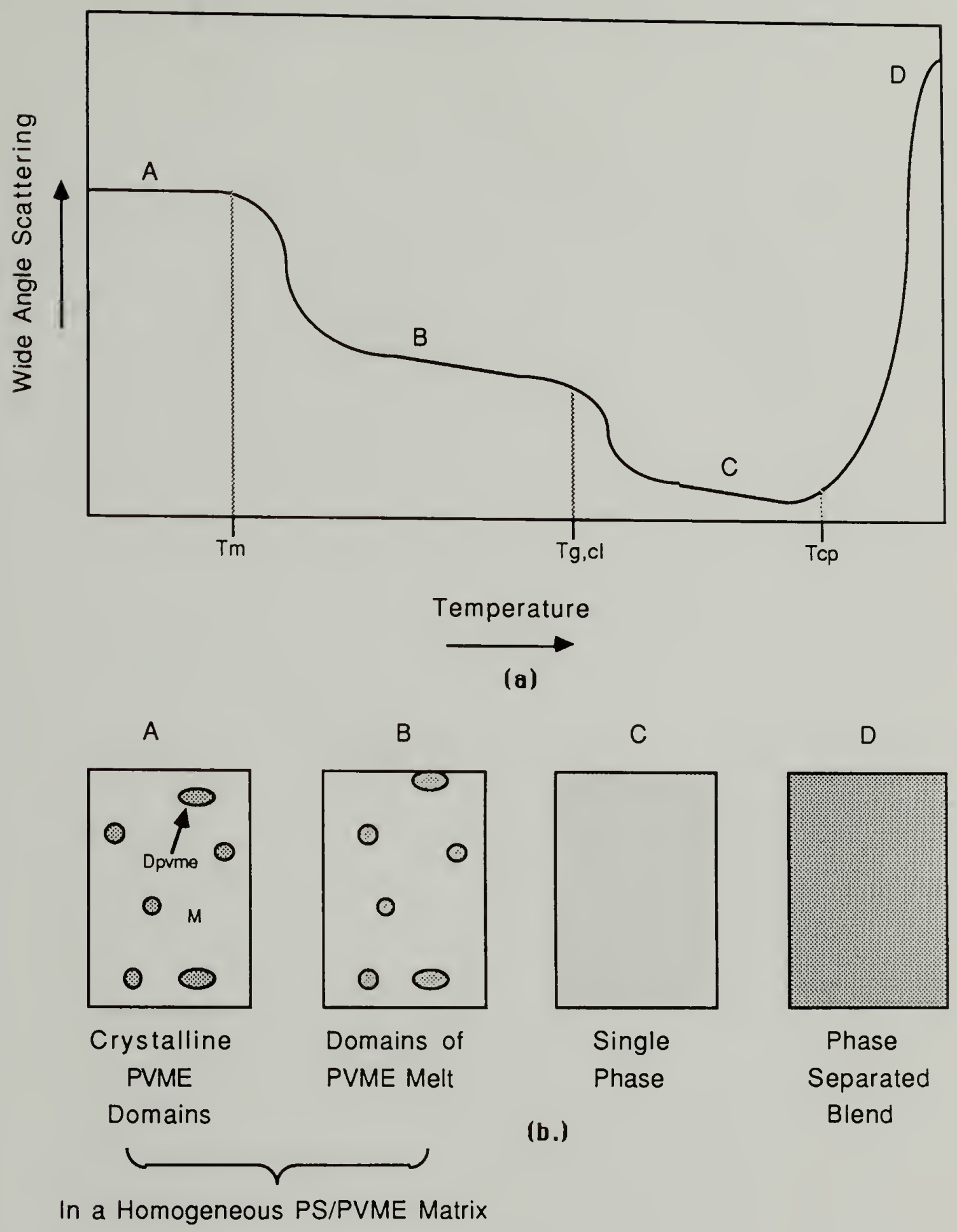

Figure 3.6 Clearing behavior of higher crystallinity blends. (a) Schematic representation of changes in the integrated wide angle scattering. (b) Schematic phase behavior.

turbidity was observed to decrease initially with heating (Figure 3.6a). Initially the blends display crystallization induced phase separation (A of Figure 3.6a and 3.6b), the phase separated regions comprising crystalline PVME domains (D_{PVME})in a homogeneous matrix of PS/PVME (M). At the melting point of the i-PVME the turbidity first decreases (B), followed by complete clearing (clearing temperature) at the glass transition temperature, $T_{g,cl}$ of the homogeneous matrix of PS/PVME. This is because above $T_{g,cl}$ the blends can achieve thermodynamic equilibrium and can become truly homogeneous.

An example of type (II) blend behavior is shown in Figure 3.7. The clearing temperatures, $T_{g,cl}$, and T_{CP}'s for i40 are given as a function of the weight fraction polystyrene. $T_{g,cl}$ for the mixture with ϕ_{PS}=0 corresponds to the melting temperature of pure PVME (i40).

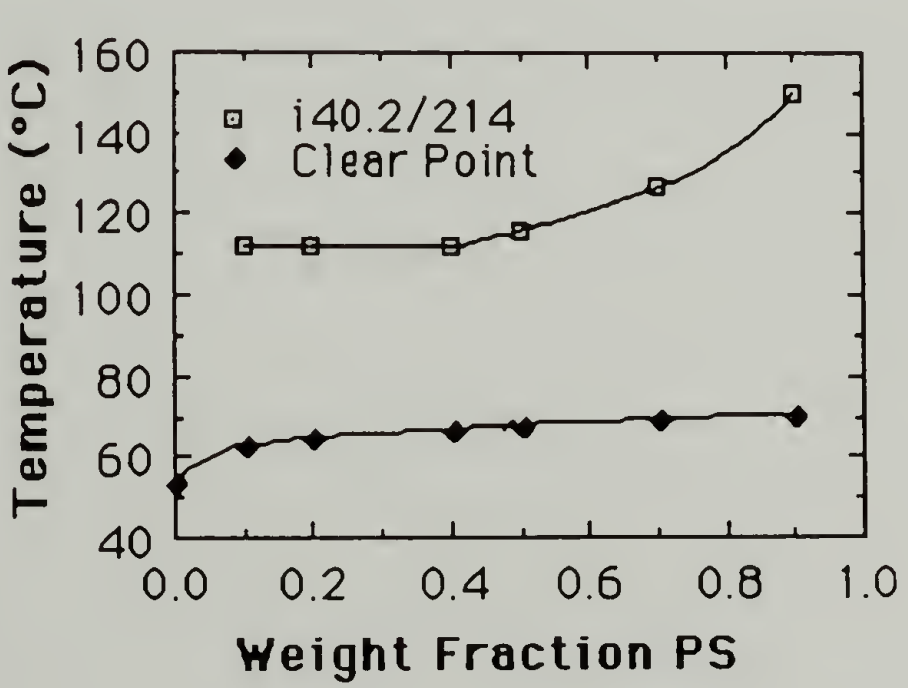

Figure 3.7 Type II behavior with clearing point and cloud point indicated. Data is for i40/214.

It should be noted that this $T_{g,cl}$ depends on the crystallization conditions and therefore on the thermal history of the test specimens. The $T_{g,cl}$ should correspond to the glass transition temperature of the matrix phase, in the structure shown as B in Figure 3.6 b, and should be different from T_g observed by lowering the temperature from the single-phase state below T_{CP} (C in Figure 3.6) because of the difference in composition. A reversible change in the turbidity associated with the cloud point, T_{CP}, was observed above $T_{g,cl}$ and is associated with the change of the structures between C and D of Figure 3.6. Upon rapidly lowering the temperature from the temperature below but close to T_{CP}, the miscible blend structure could be locked in below T_g without further crystallization. The T_g for the i89/120 blend has a T_g similar to a99/120 (note Table I of reference 12). Figure 3.8 shows a relationship between Yang`s T_g for

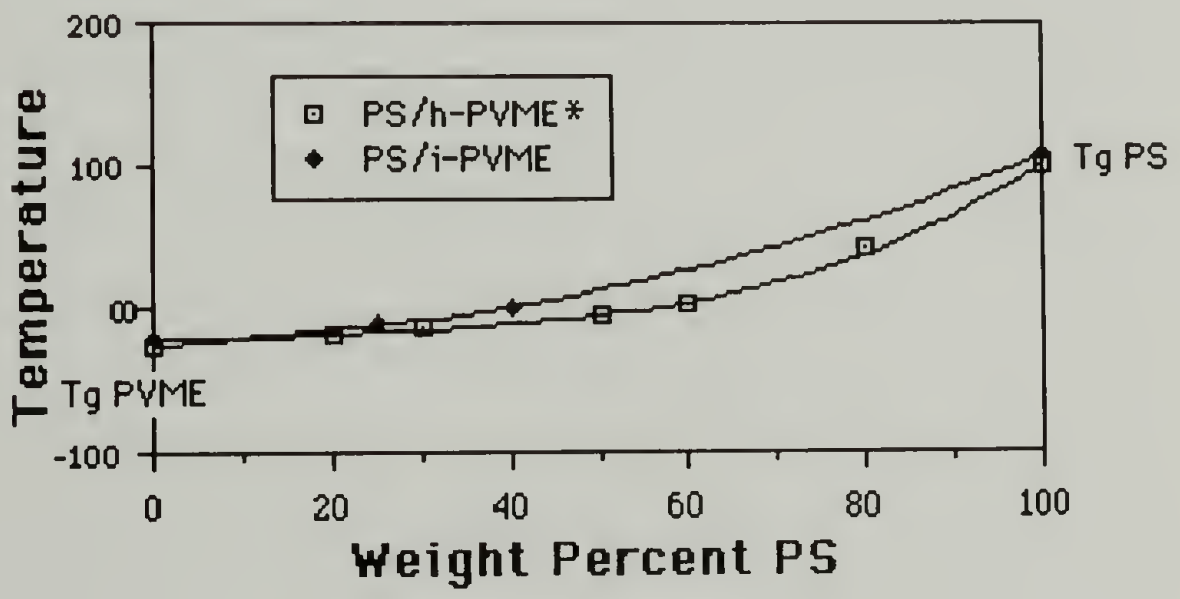

Figure 3.8 Comparison of the glass transition temperatures for isotactic and atactic PVME/PS blends. (data for atactic blends is from Yang reference 13).

the atactic blend (a99/120) and the T_g for the isotactic blend (i89/120).

Figure 3.9 is the cloud point curve (CPC) for the i89/120 and a99/120 blends. Both blends contain the same molecular weight PS, but different M_W for the two PVME's. In spite of the fact that the molecular weight of the PVME in a99/120 is higher than that for i89/120, the cloud point curve for a99/120 is higher than that for i89/120, implying a tacticity effect. Thus the isotactic PVME is less miscible with PS than the atactic PVME.

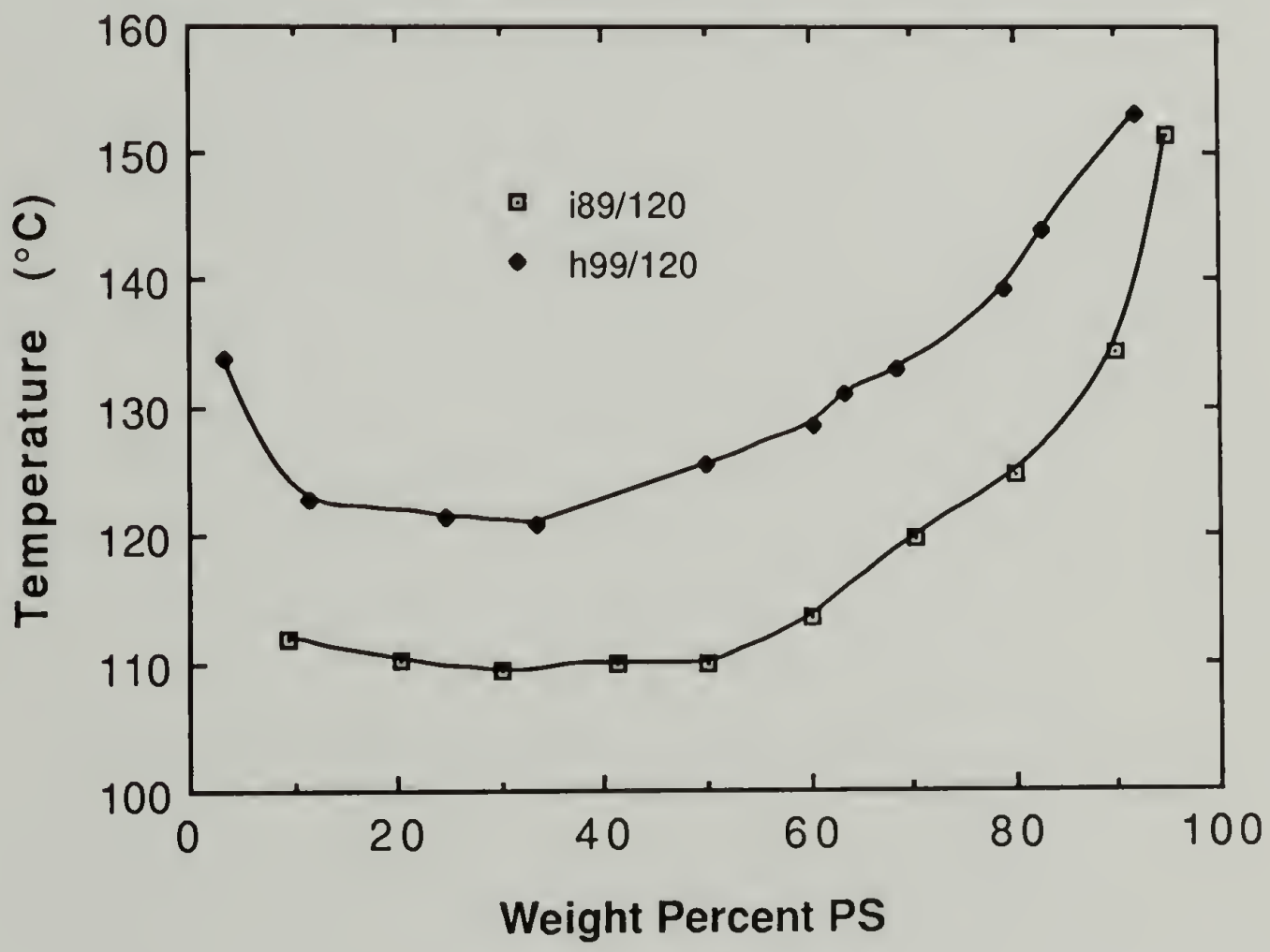

Figure 3.9 Cloud point curves for i89/120 and h99/120 blends.

Figure 3.10 is the CPC for i40/214, i32/214 and a99/233 blends. The relation between the cloud point curves for i32/214 and i40/214 may be explainable in terms of a combination of the molecular weight effect and the tacticity effect, since i32 and i40 have isotactic triad contents of 59 and 64 % respectively. If one considers purely molecular weight effects, a99/233 should be less miscible than i40/214. The opposite is observed, implying a tacticity effect.

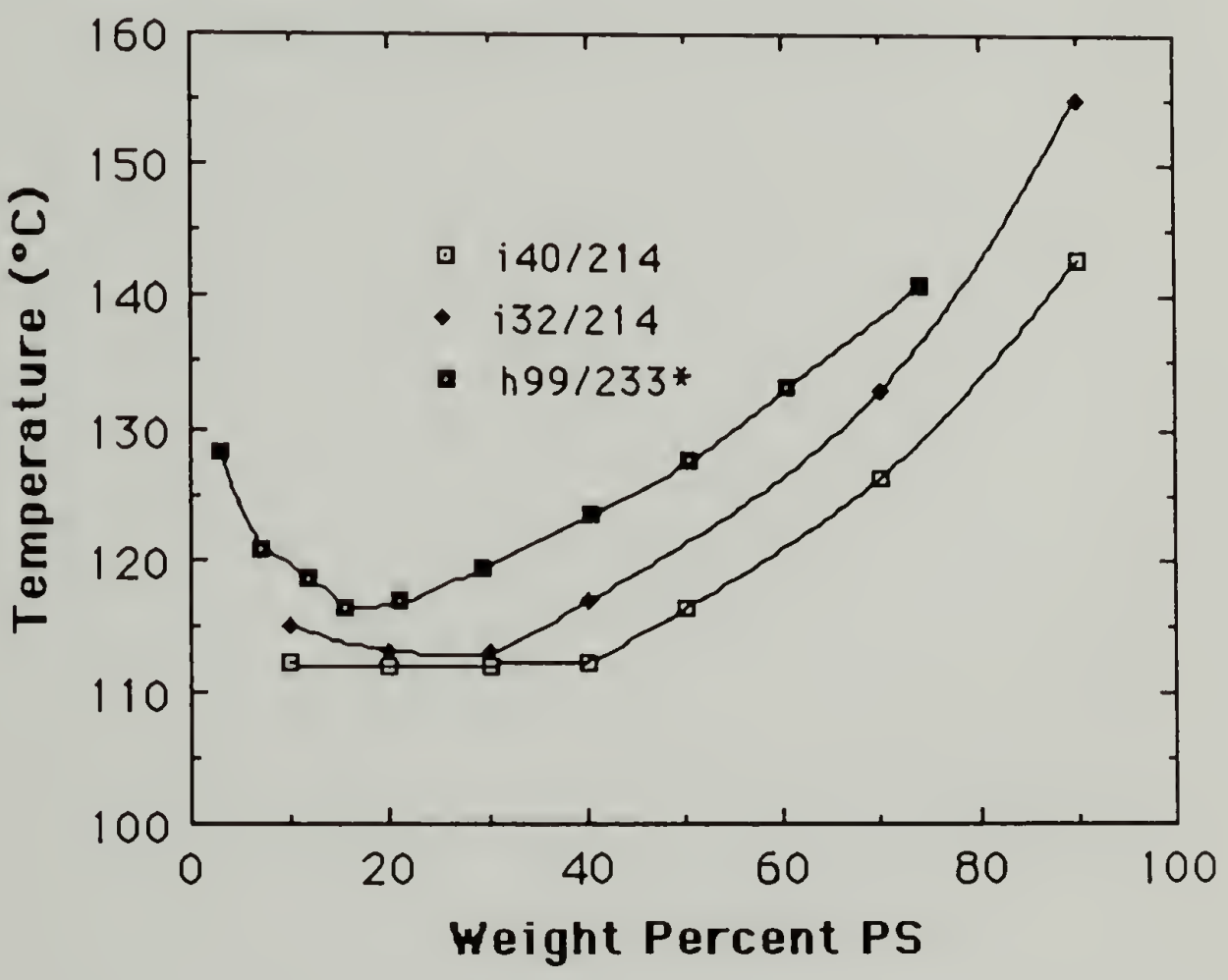

Figure 3.10 Cloud point curves for i40/214, i32/214 and h99/233 (the h99/233 data is from Yang reference 13).

In all of the cases the CPC of the blend is lower than expected in the isotactic PVME samples. This conclusion becomes somewhat

clearer after separating the molecular weight effect and the tacticity effect (see the analysis given in Figure 3.11 below).

E. Qualitative Analysis of the Tacticity Effect

In this section a qualitative separation of the tacticity effect and the molecular weight effect on the cloud point curves is attempted. The analysis is based on the following assumptions,

(i) The lowest cloud point temperature gives the critical temperature, T_c.

(ii) Flory-Huggins mean-field approximation will be used, i.e. the following equation for chi parameter at the critical point, χ_c, is used

$$2\chi_c = \frac{1}{(N_{w1}\,\phi_{1c})} + \frac{1}{(N_{w2}(1-\phi_{1c}))} \qquad (3.4)$$

where N_{w1} is the weight average polymerization index for component 1 (PVME in this case) and ϕ_{1c} is the volume fraction of component 1 for the critical mixture. Here, the correction for the difference in molar volumes of 1 and 2 was ignored in order to pursue qualitative analyses.

(iii) ϕ_{1c} can not be evaluated by Flory-Huggins theory since the composition dependence of χ for i-PVME/hydrogenous PS is not known (this dependence is determined for i-PVME/dPS in Chapter 7) ϕ_{1c} is taken as the value at which the cloud point becomes minimum, Thus, ϕ_{1c} is taken to have a value of 0.75 for all of the blends.

Table 3.1 gives the calculated χ_c values for the 11 blends studied, derived using equation 1. The weight average degree of polymerizations are obtained by dividing the molecular weights by the corresponding monomer molecular weight, i.e. 58.08 for PVME and 104.16 for PS. The T_c values are the cloud point temperatures at 0.75 weight fraction PVME (i.e. $T_c = T_{critical}$).

Table 3.1 Calculated χ_c values (derived using equation 1), T_c (measured), $1/T_c$ (measured), and % isotactic triad content for the 11 blends studied.

BLEND COMPOSITION	χ_c (calculated) ±0.00005	T_c (measured °C) ±0.1	$1/T_c$ (measured $(°K)^{-1}$) ±.000001	PERCENT ISOTACTIC TRIAD CONTENT
i32/214	0.00219	112.4	0.002593	59
i40/214	0.00194	111.4	0.002600	64
i40/233	0.00186	113.1	0.002589	64
i40/120	0.00270	117.2	0.002562	64
i89/120	0.00217	109.9	0.002610	55
h99/100	0.00247	123.4	0.002521	31
h99/120	0.00213	122.4	0.002528	31
h99/233	0.00129	117.9	0.002527	31

Figure 3.11 gives a plot of the calculated χ_c values versus the measured values of $1/T_c$ ($1/T_{cp}$ at 0.75 weight fraction PVME). Blends of a99 (isotactic triad percentage,I.T., of 31%) and i40 (I.T. = 64%) showed the expected decrease in χ_c with $1/T_{cp}$ (Figure 3.12). Blend i89 had insufficient data to determine this plot. Using

the estimated values for χ_c and the values of T_c obtained from the CPCs

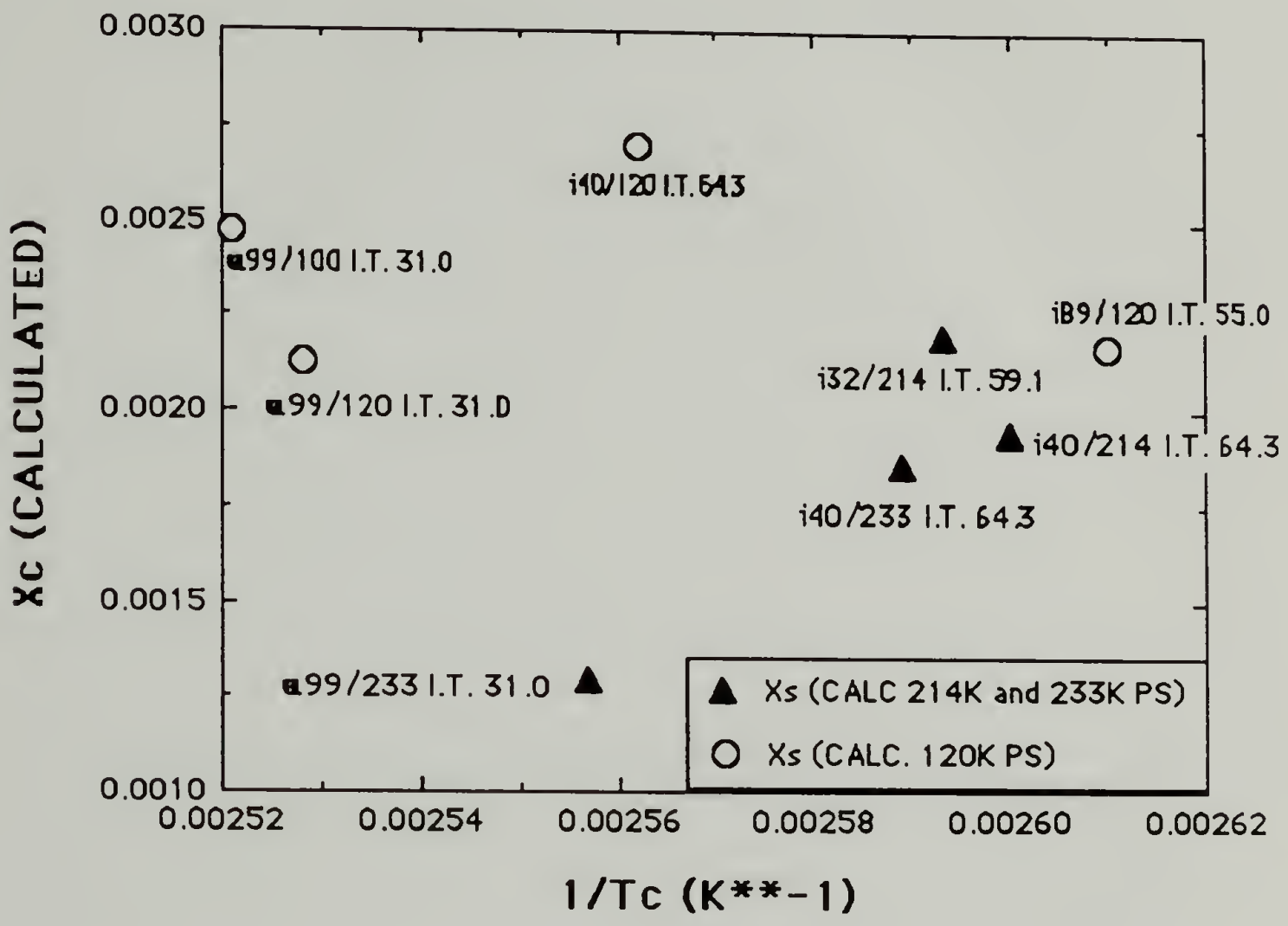

Figure 3.11 Calculated χ_c vs. $1/T_c$ ($T_c = T_{cp}$ at $\phi_{PVME}=\phi_1=0.75$) for various molecular weight blends. Isotactic PVME triad tacticities are indicated by I.T. followed by a percentage.

the values of the constants A and B in the empirical equation describing the temperature dependence of the Flory interaction parameter χ per monomer unit,

$$\chi_c = A + B / T_c \qquad (3.5)$$

can be estimated for the isotactic (i40) and atactic (a99) PVME blends. For the isotactic blends, i40, the estimated values are A ≅ 0.080 and B ≅ -30. For the atactic blends, a99, these parameters have estimated values A ≅ 0.078 and B ≅ -30 (see Figure 3.12). The slope of χ_c versus $1/T_c$, B, did not appear to significantly change within the accuracy of the calculation with a change in tacticity of 31 to 64%. The intercept appeared to show a significant shift.

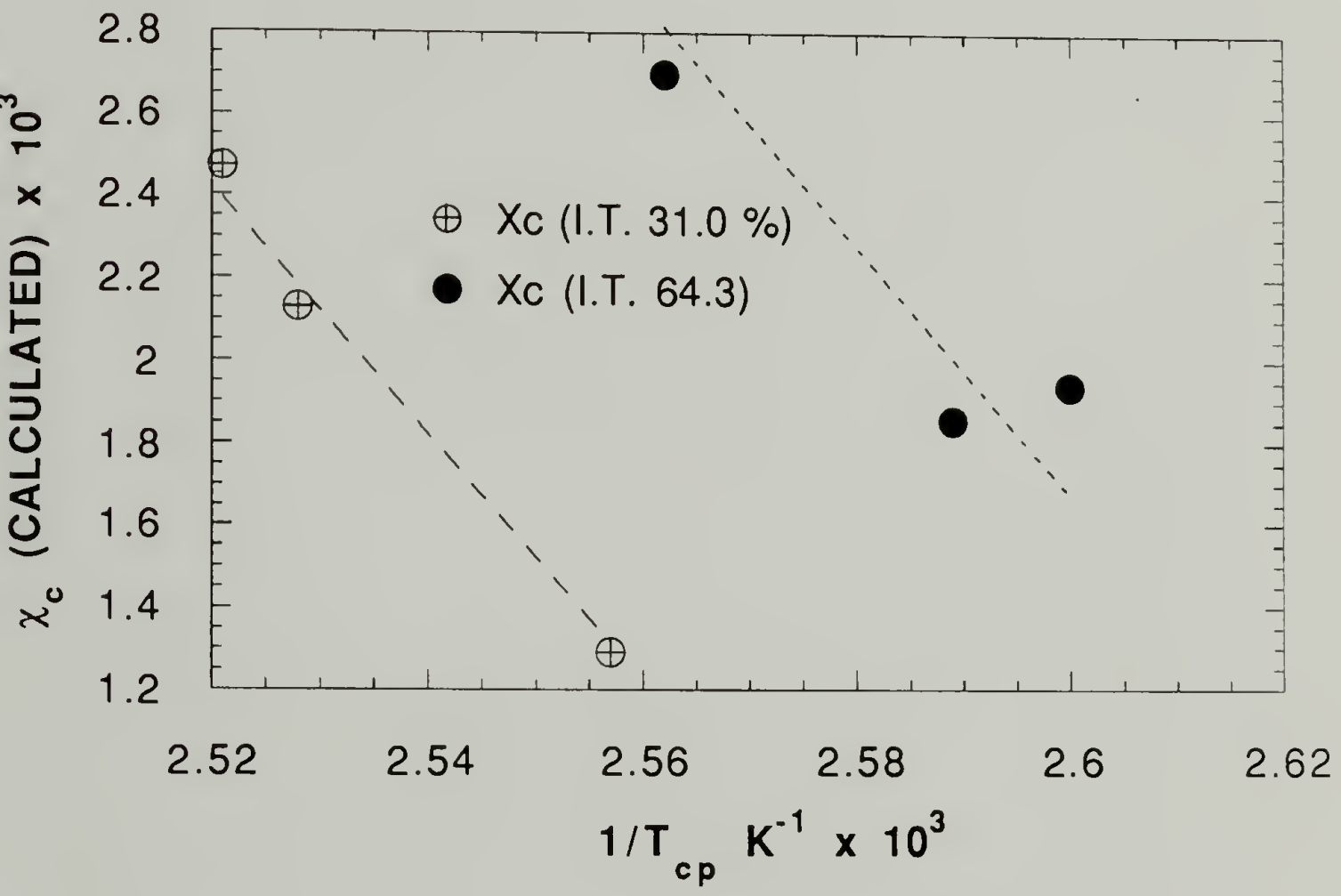

Figure 3.12 χ_c versus $1/T_{cp}$ (measured at 25% PS) for isotactic triad percentages (I.T.) of 31 (a99) and 64 (i40).

The data supports the view that increasing isotacticity increases the χ values at a given temperature. Hence at a given χ_s value, i.e. at a given set of molecular weights, the critical temperatures drop with increasing isotacticity. (An increased χ value decreases the miscibility and lowers the LCST curve.)

The tacticity effects are most clearly demonstrated by comparison of the T_c values between the a99/120 and i89/120 points of Figure 3.11, as they have about equal χ_c values. The molecular weight effects are most clearly demonstrated by comparison of the i40/120 and i40/214 (or i40/233) points for the isotactic material and the a99/100, a99/120, and a99/233 points for the atactic material.

Figures 3.13 and 3.14 show the effect of tacticity on the cloud point at 25% PS (approximately the critical composition) for blends of $\chi_{c,calculated} = 2.05 \times 10^{-3} \pm 1.5 \times 10^{-4}$ (Figure 3.13) and $\chi_{c,calculated} = 2.64 \times 10^{-3} \pm 1.7 \times 10^{-4}$ (Figure 3.14) (these results are determined from Table 3.1 or Figure 3.11). In both cases a negative

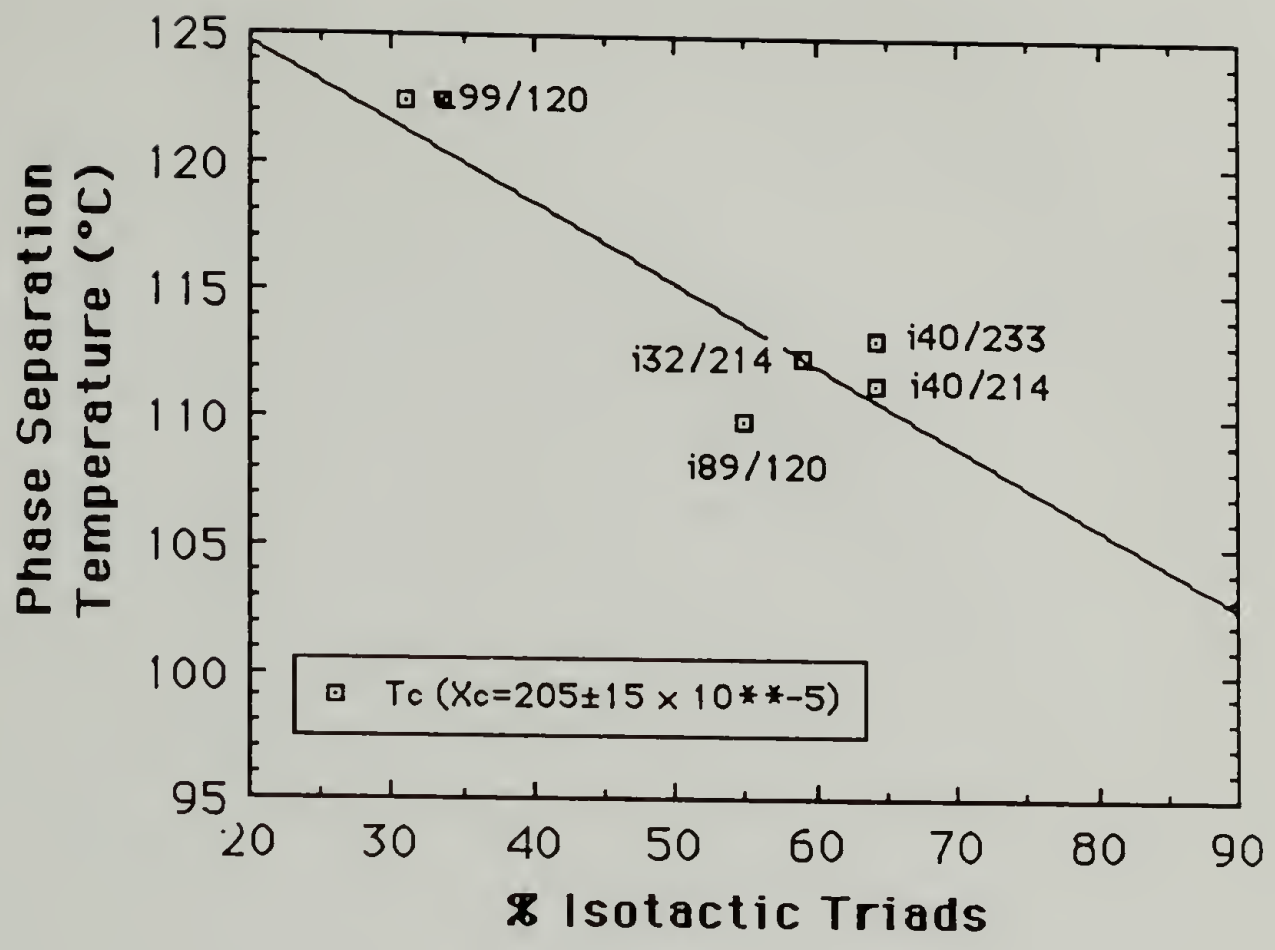

Figure 3.13 Cloud Point for 25% PS Blend Versus % Isotactic Triad Content of PVME for $\chi_{c\ calculated} = 205 \times 10^{-5} \pm 15 \times 10^{-5}$.

slope is indicated, implying the tacticity effect. The slope appears to be about -0.18 °C/Isotactic Triad %. Thus a 10% change in tacticity would be expected to produce a shift in T_{cp} at 25% PS of about 2°C.

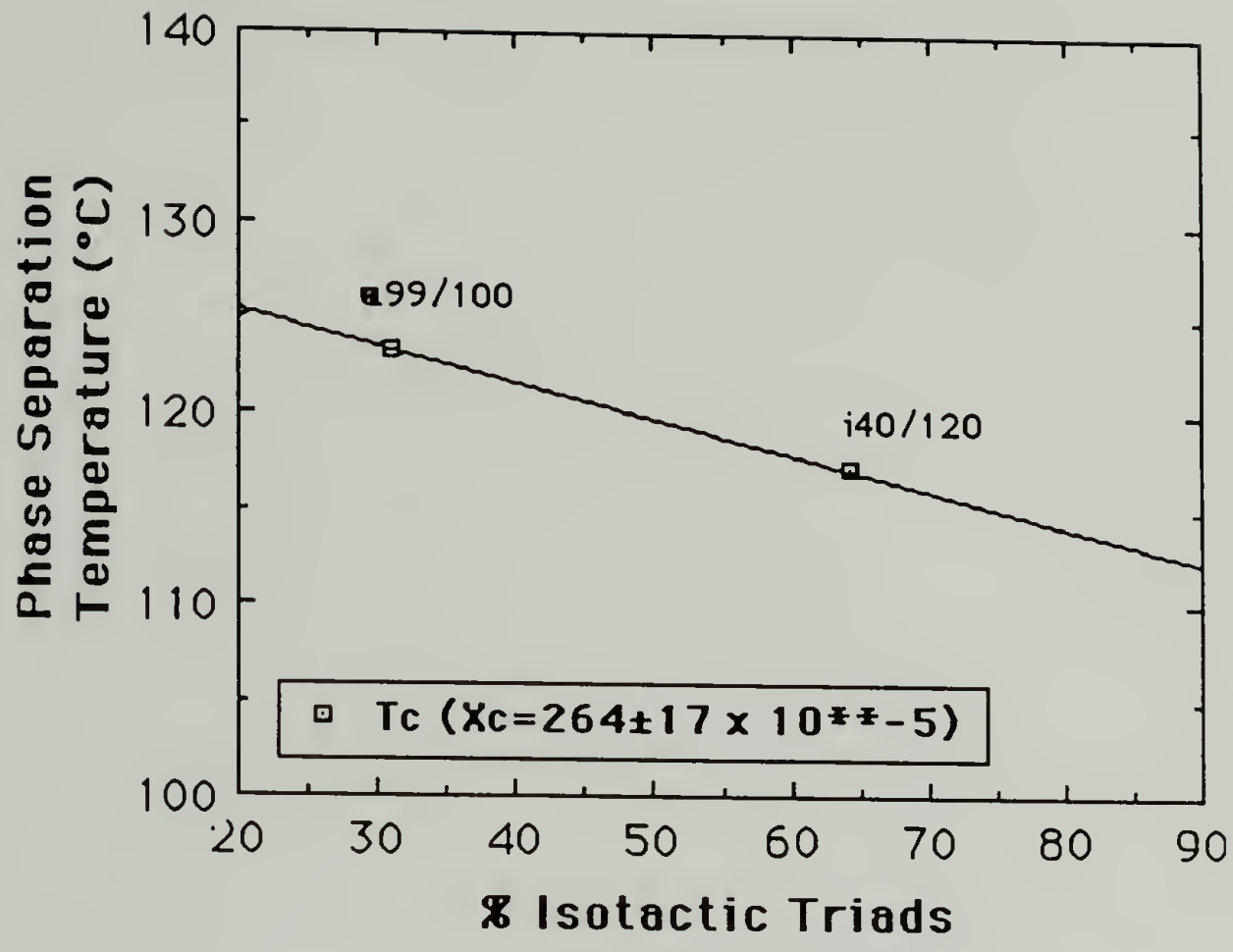

Figure 3.14 Cloud Point for 25% PS Blend Versus % Isotactic Triad Content of PVME for $\chi_{c\ calculated} = 264 \times 10^{-5} \pm 17 \times 10^{-5}$.

F. Conformational Effects in the PS/PVME Blend System

Short range ordering of the isotactic sequences may have an effect on the phase behavior of the i-PVME/PS blend. Such correlations of molecular orientation (CMO) above the crystalline melting point have been postulated as being an explanation for aberrant LCST behavior of polyolefins in concentrated solution[14,15]. Delmas explained the lower LCST for polyethylene (PE) when compared to polypropylene (PP) in concentrated solutions as due to

short range ordering which can occur in PE above the crystalline melting point but not in PP. Copolymers of PP and PE show intermediate behavior. A more elaborate analysis of the CMO effect will be undertaken in Chapter 7 with regard to small angle neutron scattering results.

Schurer, de Boer and Challa[16] have noted that conformational differences between polymers of differing tacticities can have an impact on blend phase behavior. For the system PMMA/PVF_2, the 5_1 helical conformation of the isotactic PMMA may cause a steric interference to ester-group interactions. Isotactic PVME occurs in a 3_1 helical conformation[17] with similar steric interferences to interactions for the methoxy group. Atactic PVME segments, probably exists in a conformation which minimizes methoxy-methoxy interactions. In such a conformation the methoxy groups would experience minimal steric interference to interaction with other polar groups.

G. Conclusions

A shift in the phase diagram for PS/PVME blends of similar molecular weights is observed due to changes in the tacticity of PVME resulting in lower miscibility for more isotactic PVME. Additionally, solution cast blends of lower molecular weight isotactic PVME show crystallization induced phase separation below the CPC. A clearing point is observed for these blends which corresponds to a crystalline melting point and/or a matrix phase glass transition. Molecular

weight and tacticity effects have been qualitatively separated. Changes in the tacticity chiefly effect the entropic component of χ as might be expected since stereospecificity chiefly effects the structure and may cause an increase in the ordering of one of the blend components.

In general, the phase behavior of the isotactic blends is compatible with the concepts proposed in Chapter 1 (Figure 1.1). It would appear that a phase separated blend having physically crosslinked rubbery domains could be produced from this system. Materials similar to that described in Chapter 1 were produced by solution casting of the isotactic PVME blends as described in this chapter. The clearing point behavior is indicative of the desired material properties (i. e. crystallinity in the PVME domains). In these materials, phase separation occurs due to crystallization of the PVME from solution. As will be discussed in the next chapter, these materials actually come closer to the idealized system proposed in Chapter 1 than melt blended and phase separated samples. The reasons for this will be discussed in Chapter 5 in terms of a more elaborate analysis of the cloud point curves based on Flory-Huggins-Staverman (F-H-S) theory. The ability of the F-H-S analysis to predict kinetic behavior (Chapter 6) affirms its usefulness in modeling the tacticity effect. An in depth, quantitative analysis of the tacticity effect using small angle neutron scattering data and the F-H-S approach is presented in Chapter 7. The CMO concept introduced above will be further developed with regard to neutron scattering data.

References

1. R. Koningsveld, L. A. Kleintjens, A. R. Schultz, *J. Poly. Sci. A2*, **8**, 1261 (1970).

2. E. Roerdink and G. Challa, *Colloid and Poly. Sci.*, **263**, 361 (1985).

3. W. Herman, Ph.D. Dissertation, University of Massachusetts, Amherst, 1987.

4. J. W. Schurer, A. de Boer and G. Challa, *Polymer*, **16**, 201 (1975).

5. E. Roerdink and G. Challa, *Polymer*, **21**, 1161 (1980).

6. F. E. Karasz, W. J. MacKnight, *Macromolecules*, **1**(6), 229 (1963).

7. S. Reich, Y. Cohen, *J., Polymer Sci., Poly. Phys. Ed.*, **19**, 1255 (1981).

8. M. T. Berard, Ph.D. Dissertation University of Massachusetts, Amherst, 1991.

9. W. Cheung, G. Beaucage, R. S. Stein, poster presented at the American Physical Society Meeting, Cincinnati OH March, 1991.

10. O. Aoki, Ph.D. Dissertation University of Massachusetts, Amherst, 1990.

11. G. Beaucage, R. S. Stein, T. Hashimoto, H. Hasegawa, *Macromolecules* (in press)

12. H. Yang, M. Shibayama, R. S. Stein, T. Hashimoto, S. Suehiro, *Macromolecules*, **19**, 1667 (1986).

13. H. Yang, Ph.D. Dissertation University of Massachusetts, Amherst, 1985.

14. G. Charlet, G. Delmas, *Polymer*, **22**, 1181 (1981).

15. A. Barbalata, T. Bohossian, K. Prochazka, G. Delmas, *Macromolecules*, **21**, 3286(1988).

16. J. W. Schurer, A. de Boer, G. Challa, *Polymer*, 16, 201 (1975).

17. G. Natta, P. Corradini, *Chim. Ind.* (Milan), 45, 229 (1963).

CHAPTER 4

MECHANICAL BEHAVIOR AND MORPHOLOGY OF ISOTACTIC PVME/PS BLENDS

A. Introduction

Two types of mechanical test specimens were investigated in this work. Solution cast rectangular films which were about 0.05 to 0.1 mm thick, 0.5 cm wide and 6 cm in length. These films were produced by solvent casting 15% PVME blends from toluene at room temperature (total polymer content of 20% by weight) on Teflon sheets, allowing the films to air dry for at least three days followed by drying in a vacuum oven at about 35°C for at least three weeks. Phase separation occurred due to crystallization of the i-PVME from the solution as the toluene was evaporated. X-ray diffraction from these blends indicated the presence of a slight degree of crystallinity however, due to the limited net amount of crystallinity (i.e. 15%(PVME) x 10%(crystallinity for example) = 1.5% total crystallinity in blend) an absolute determination of the degree of crystallinity could not be made. For similar blends having higher percentages of PVME estimates of about 10% crystallinity in the PVME phase (by X-ray diffraction) were common. An attempt was made to induce thermal phase separation in these blends, however, due to the thinness of the films, inhomogeneities resulted which made mechanical testing impossible. PVME phase sizes of 1-25 μ were observed in the

crystallized blends by light scattering, optical microscopy and TEM (courtesy Peterman U. Hamburg).

When larger quantities of i-PVME were synthesized (at Polysar LTD's Sarnia, Ontario pilot plant), melt blended materials were produced at Polysar's Leominster, MA facility in a Braybender® mixer (50 g capacity). These blends were ground into granules and pressed under vacuum into dog bone tensile bars according to ASTM standards (ASTM standard D 638 Type V). The melt blended dog bones were 3/32" thick and 1/8" wide at the center. The gauge length was 1/2".

It should be noted that different stress/strain conditions may exist in the two sample types. For example, in the limit of an extremely thin sample, plane stress conditions would exist in a tensile experiment since a very thin sheet of material can contract laterally. Under these conditions dilatational strain is minimized. Crazing is a dilatational deformation, that is localized volumetric strains occur (the craze is a localized region of lower density). Shear banding, on the other hand, occurs in the absence of volumetric changes. Thus, in very thin samples, one would expect to be more likely to observe shear banding rather than crazing. At the opposite extreme, i.e. a very thick specimen, plane strain conditions would exist at the center of the specimen causing large amounts of dilatational strain (favoring crazing). The samples discussed above are somewhere in between these two extremes. It would be expected that the thinner sample would experience less dilatational strain than the dog bone sample, thus one might be more likely to observe shear banding in the thinner sample.

B. Solution Cast Samples

Figure 4.1 shows 4 typical stress strain plots for solution cast PVME/PS blends (a HIPS plot is included for comparison). The curves have been shifted along the strain axis in order to facilitate comparison.

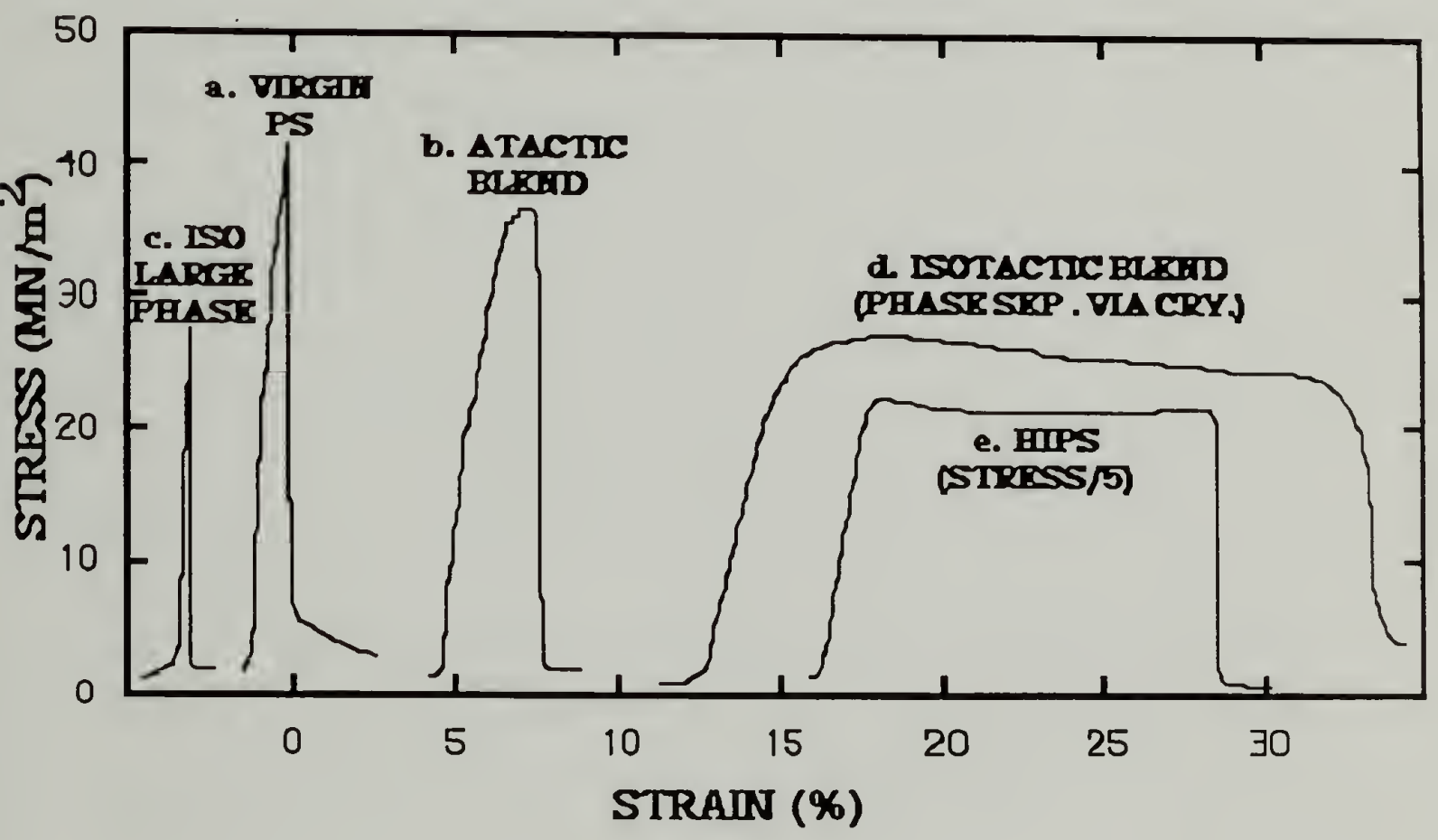

Figure 4.1 Stress-strain plots for solution cast samples. (a) A typical tensile test for a pure polystyrene cast film. (b) A typical tensile test for a miscible blend of 15% a-PVME/PS. (c) An isotactic PVME blend of the same composition with large crystalline domains (25μ). (d) A 15% blend of isotactic PVME with PS having crystalline domains of about 1 to 5 μ. (e) A film sample of Polysar HIPS. All materials were prepared under the same conditions. (Curves have been shifted to fit onto one plot, scales are identical in all cases except for (e).)

All of the experiments were under a constant strain of 10 mm/min. Figure 4.1 (a) is a typical tensile test for a pure polystyrene cast film (120K g/mole). Brittle failure occurs at about 1.6% strain. Figure 4.1 (b) is a typical tensile test for a miscible blend of 15% atactic (non-crystalline) PVME (99K g/mole) blended with PS (no phase separation present). Brittle failure occurs after about 3% strain. The modulus (the initial slope of the stress-strain plot) is reduced when compared with pure PS. Figure 4.1 (c) is an isotactic PVME blend of the same composition with large crystalline domains (25μ). Brittle failure occurs after a small degree of strain. The initial modulus is not significantly different from that of PS indicating that the matrix is predominantly PS (most of the PVME presumably being tied up in crystalline domains). Figure 4.1 (d) is a 15% blend of isotactic PVME with PS having crystalline domains of about 1 to 5 μ. A significant increase in the strain at failure occurs in this material. A broad yield point is observed and failure is by a ductile mechanism. The modulus is reduced in this case in comparison with Figure 4.1 (c) and 4.1 (a), but is not as low as the atactic blend (non-crystalline PVME) 4.1 (b). The initial modulus would indicate that the matrix phase in 4.1 (d) contains more PS than that of 4.1 (c) but less than that of Figure 4.1 (b) (non-crystalline PVME). Figure 4.1 (e) shows similar stress strain data for a film sample of Polysar HIPS. The behavior of Figure 4.1 (d) is similar to the behavior of the HIPS sample. The yield strain for the HIPS film is close to 125 MN/m^2. The isotactic PVME blend shows a lower yield stress of about 35 MN/m^2 (a careful comparison of absolute stresses and strains is not justified due to inhomogeneity of the solution cast samples). Pure PS showed a yield stress of about 40

MN/m^2. The absolute stress numbers in Figures 4.1 are, however, very crude due to inhomogeneity in the film thickness and the small sample dimensions (i.e. a stress of 40 N/m^2 is derived from 1 mg stress (± 0.2 mg) divided by .05 mm (±.03 mm). The sample width (about 0.5 cm ± 0.05cm) is fairly accurate). Thus, errors close to 100% are easily imaginable in the measured stress. For ASTM standard dog bones (discussed below), HIPS gives a yield stress of about 20 MN/m^2. Due to the inherent variability in thickness, the very small stresses measured and the inability to perform impact tests on the thin solution cast films, it was impossible to obtain quantitative estimates of the energy absorbed or the initial modulus of the solution cast films, although the larger strain at failure of the isotactic PVME blend (about 20%) in comparison with HIPS (12%) would indicate a similar or larger energy absorption.

Qualitatively one may compare the tensile stress-strain curves of HIPS and Figure 4.1 (d). HIPS shows a very linear region at the onset of stress with a modulus similar to that of pure PS. This indicates that the matrix phase is not significantly plasticized by the rubber inclusions. The linear elastic region is followed by a yield point. This has been explained[1] as resulting from a minimum stress value for the initiation of crazing (as well as a minimum time period). Once the required yield stress (and time) is reached the onset of crazing occurs leading to dilatational elongation of the sample. The energy which is applied to the sample is absorbed by the formation of localized regions of high orientation and low density. Optical micrographs (between

Figure 4.2 Optical micrographs under crossed polars of solution cast samples. Regions of high birefringence (orientation and or crystallinity) appear bright. The samples are similar to those used in Figure 4.1 (Bar is equal to 200 microns.)

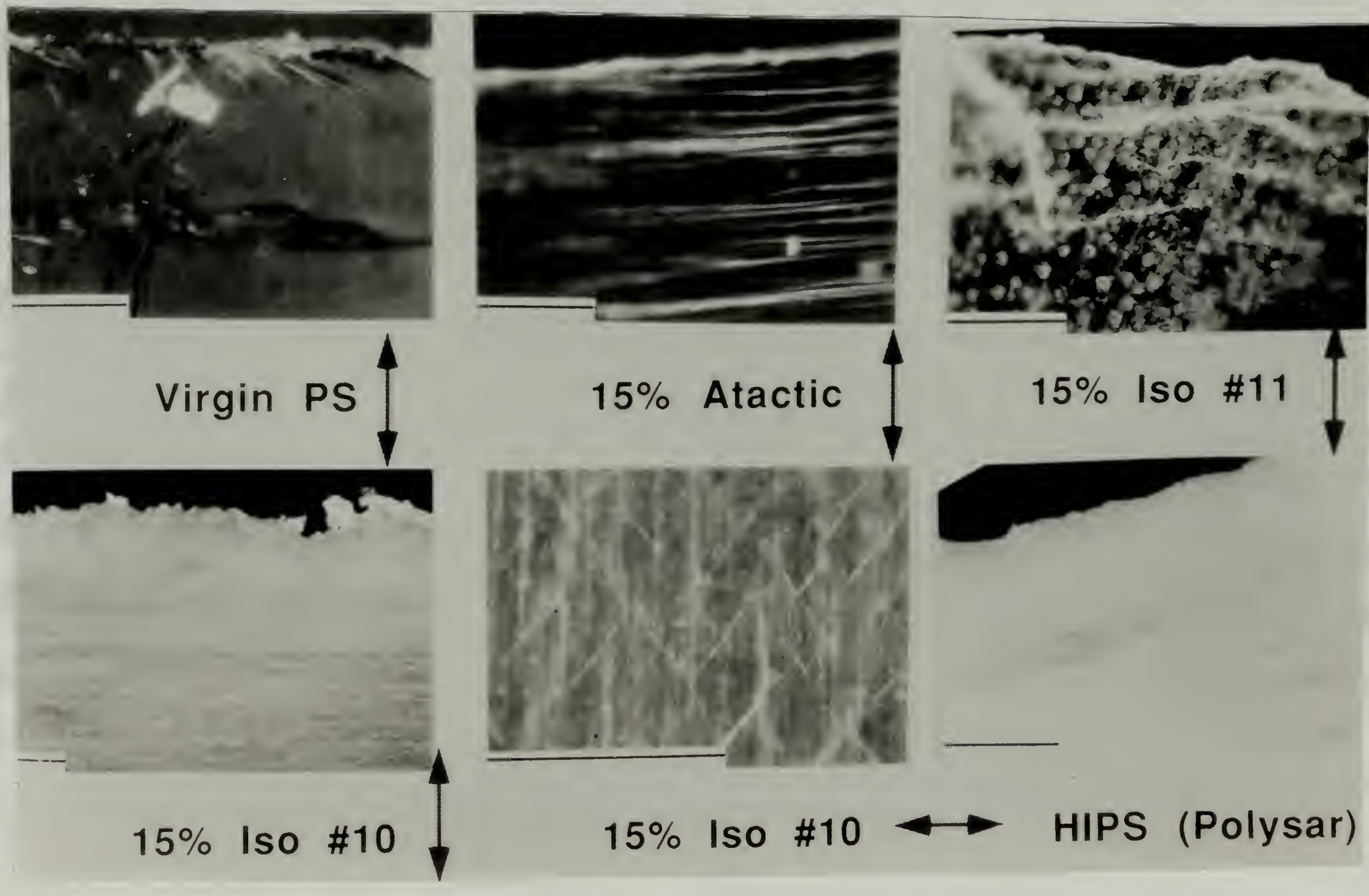
Virgin PS
15% Atactic
15% Iso #11
15% Iso #10
15% Iso #10
HIPS (Polysar)

crossed polars) of the same samples as were used in Figure 4.1 are shown in Figure 4.2. In Figure 4.2 virgin PS can be compared with the HIPS sample. In virgin PS a sharp concoidal fracture surface reflects brittle failure. Crazes are seen to diverge from the failed surface. The HIPS sample fails ductally with a highly deformed failure surface. Crazes are so numerous in the HIPS sample that the micrograph (between crossed polars) is very bright. Crazes form at 90° to the stress direction indicated by the large arrow. It has been proposed that there is a minimum size beyond which a craze will degenerate into a crack (Chapter 1). The effect of the added rubbery domains in HIPS is to increase the number of crazes, decreasing the average length thereby delaying the onset of failure.

The stress-strain curve of Figure 4.1 (d) shows subtle differences from that of HIPS. The initial linear modulus is reduced from that of PS and HIPS. This indicates a plasticization of the matrix phase. Further, the material shows a gradual reduction in modulus before a broad yield point occurs. It should be noted that a yield point followed by a drop in stress is not expected for materials which exhibit shear banding in the absence of crazes[1]. In Figure 4.2 the micrograph labeled "15% Iso #10" is of a recently failed sample with stress-strain behavior similar to Figure 4.1 (d). In addition to crazes which occur at 90° to the stress direction (indicated by the horizontal arrow), shear bands appear at 45° to the stress direction (along the principle planes of stress). Under crossed polars these highly oriented regions appear as bright lines. At many of the intersection points between crazes and shear bands crystalline domains of PVME (observed by x-ray) show up

as bright spheres. There is a dispersity in the sphere sizes with spheres of about 5 μm being most predominant at the intersection points. Returning to Figure 4.1 (d) it would appear that the initial lowering of the linear modulus before the broad yield point (lowering in slope) is due to the formation of shear bands since both features are absent in the HIPS sample. As noted above, this shear banding may be inhanced by the thinness of the films. The drawing behavior (large elongations) occur both in HIPS and in the material of Figure 4.1 (d). In both of these materials a large number of small crazes appear in the micrographs. Thus it is possible that the yielding and the crazes are related. If this is the case, then the initial stress level for the formation of crazes is reached at a slightly higher stress level and over a longer time span for the material of Figure 4.1 (d) when compared with HIPS. The broadened yield region may be due to inhomogeneities in the modulus of the partially yielded matrix phase. Following the onset of crazing the material is dilatationally strained. Crazes appear to be limited in size by termination (or initiation) at both rubber phases and at shear bands. The micrograph of the failed "Iso #10" surface shows that the material fails ductally with a highly deformed failure surface. This should be compared with the less deformed surface of HIPS and the brittle surface of virgin PS.

In Figure 4.2 the micrograph labeled "15% Atactic" is a similar optical micrograph of the one phase atactic PVME blend (non-crystalline). As was noted above (Figure 4.1 b.) this material shows a reduced linear modulus followed by brittle failure. Crazes very similar to those of pure PS clearly form in this material, however, no evidence

for shear banding was observed. From this data it would appear that the presence of a disperse phase is required for the formation of shear bands in these blends. A brittle failure surface is also shown.

The "15% Iso #11" micrograph is of a different isotactic PVME (#11) which produced larger crystalline phases (about 25μm). In this case shear bands did not form. Failure occurred at the interface between phases leading to large cracks. The initial tensile modulus (initial slope in Figure 4.1 (c)) was similar to that of pure PS indicating a greater degree of immiscibility due to crystallization in this blend when cast from solution. Due to differing solvent evaporation rates and other factors not under experimental control a comprehensive study of the relationship between phase size and mechanical properties could not be performed. Further, with the synthesis of larger quantities of isotactic PVME attention was shifted to the more industrially applicable melt blended samples.

Shear bands are known to exhibit relaxation[1]. This behavior was clearly observed in the shear banded blends studied. The micrographs of Figure 4.2 labeled "Iso #10" were taken a day after failure for the micrograph which shows the failed surface and immediately after failure for the micrograph which show the bulk material. In the aged sample the shear bands have relaxed. This effect has been explained as evidence that molecular cohesion is retained in shear bands. On the other hand crazes are said to destroy molecular cohesion and therefore do not show this relaxation behavior. The deformation behavior shown in the shear banded PVME blend is similar to the

deformation behavior displayed by ABS toughened PS (about 50% crazing and 50% shear band deformation).

C. Melt-Blended Samples

Isotactic PVME synthesized by the author at Polysar's Sarnia pilot plant was melt blended with Polysar polystyrene of molecular weight, M_w = 395 kg/mole ($M_w/M_n \approx 2$). None of the isotactic blends produced by melt blending followed by melt pressing showed the drastic improvement in mechanical properties observed for some of the solution cast samples. Shear bands were not observed in the failed samples, although it was difficult to examine the thick samples using optical microscopy. (Thin samples obtained from the mold flashing also failed to show shear banding.) Isotactic PVME domains in the phase separated blends did not show strong birefringence indicating that the domains were not significantly crystalline. Similarly, DSC failed to show the presence of PVME crystallinity. Failure, in all of the melt blended samples occurred by fairly localized crazing. In all of the samples brittle failure occurred with a concoidal failure surface. Figure 4.3 is a plot of strain at failure versus percent PVME for phase separated blends of atactic and isotactic PVME.

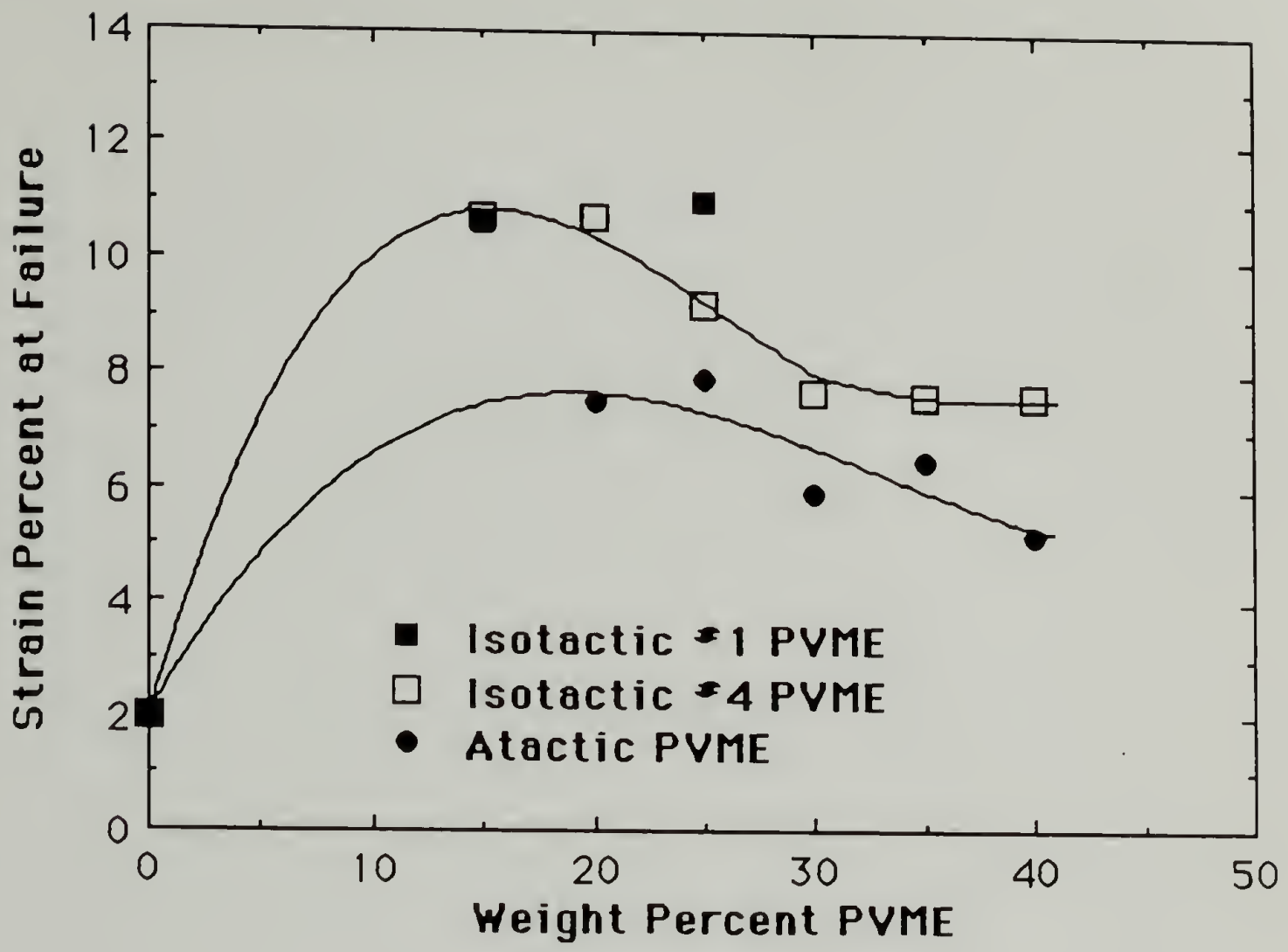

Figure 4.3 A plot of strain at failure versus percent PVME for phase separated blends of atactic and isotactic PVME.

A slight improvement over the atactic blends was observed, but when compared to a similarly prepared HIPS sample the improvement was deemed insignificant, Figure 4.4. It is interesting to note that the addition of isotactic PVME to HIPS appears to improve the strain at failure. This is probably due to plasticization of the matrix PS by PVME indicating miscibility for the PVME in this complex system.

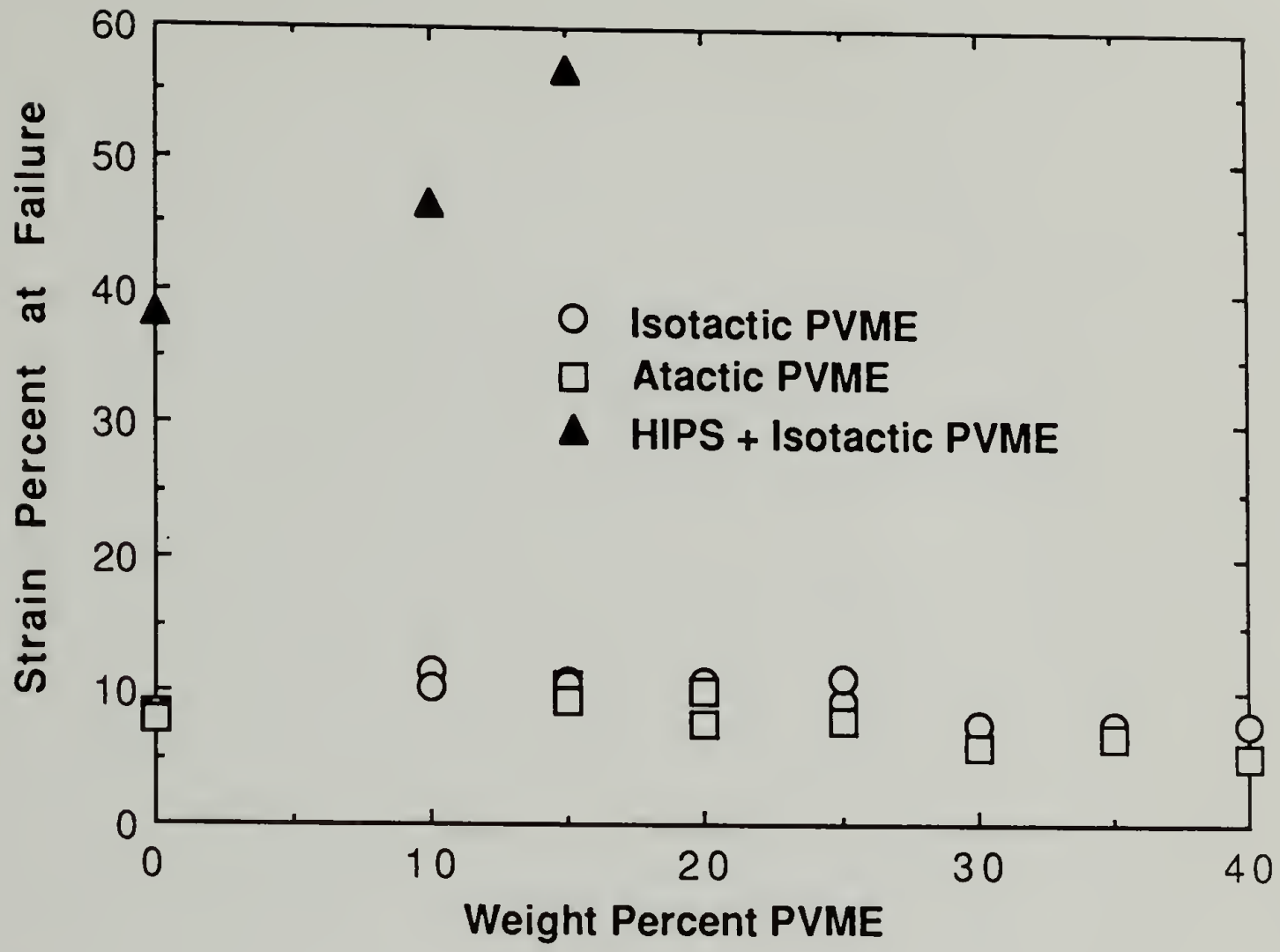

Figure 4.4 Same data as Figure 4.3 compared with HIPS prepared in the same manner.

An optimum in the strain at failure occurred at about 15% PVME for both the atactic and isotactic PVME blends. X-ray diffraction from the melt blended samples failed to show any trace of crystallinity in the PVME phase.

Since the blends of lower concentration PVME are more miscible, the initial increase in strain at failure may be due to increasing plasticization of the matrix phase. At about 15% this increased plasticization may be offset by the reduced miscibility of the PVME at higher concentrations. Data on the initial modulus of the

blends, Figure 4.5, shows a linear decrease in the tensile modulus with increased weight fraction PVME to about 15% PVME followed by a leveling off to about 30% PVME.

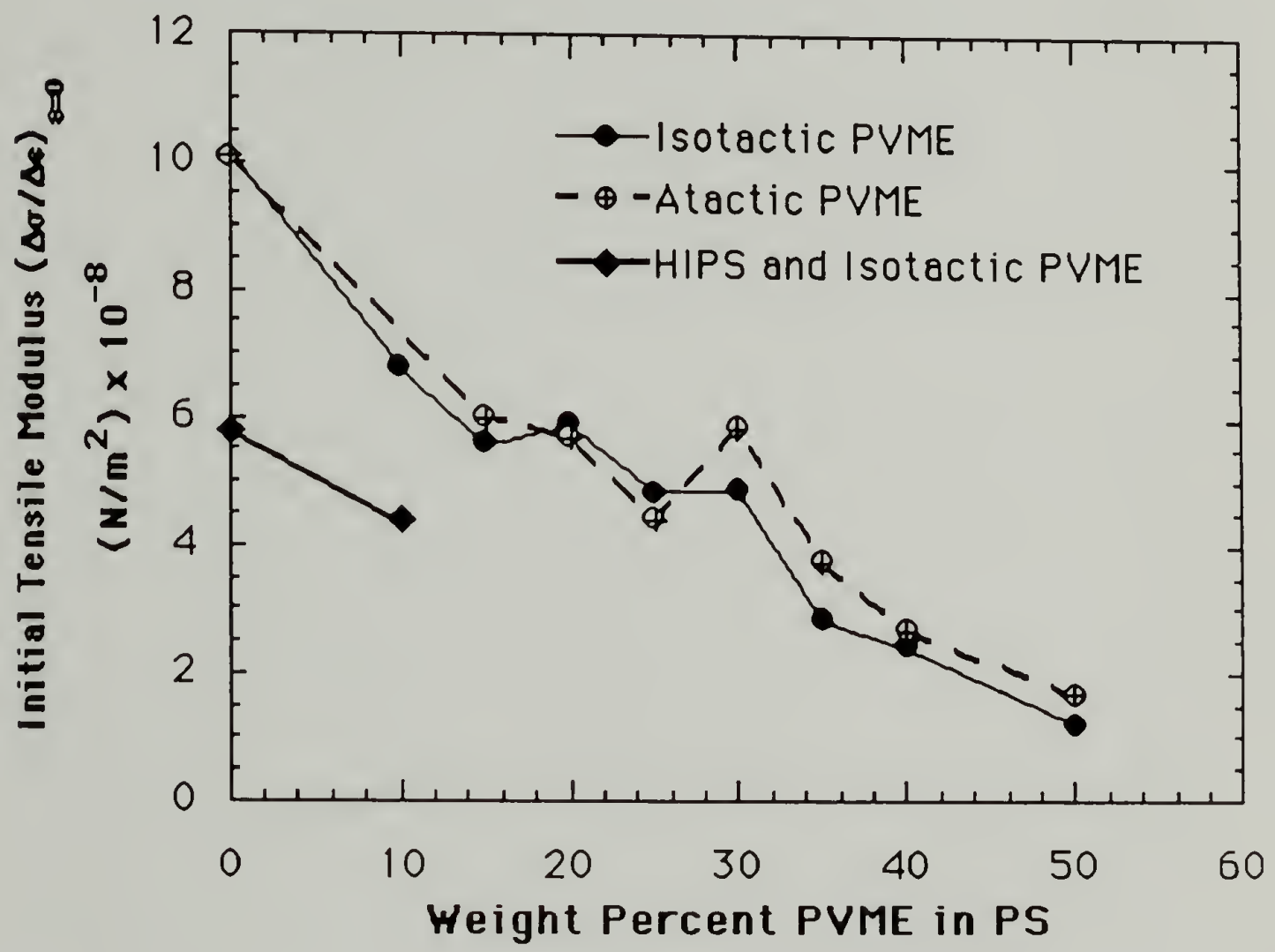

Figure 4.5 Initial modulus of the blends versus weight percent PVME. (Lines merely connect the data points for clarity.)

After the tendency towards a plateau in the 15 to 30% PVME range, the modulus drops less precipitously above 30% PVME. This behavior is consistent with the phase diagram (Figure 4.6) which drops rapidly in the low concentration PVME region (up to 15% PVME).

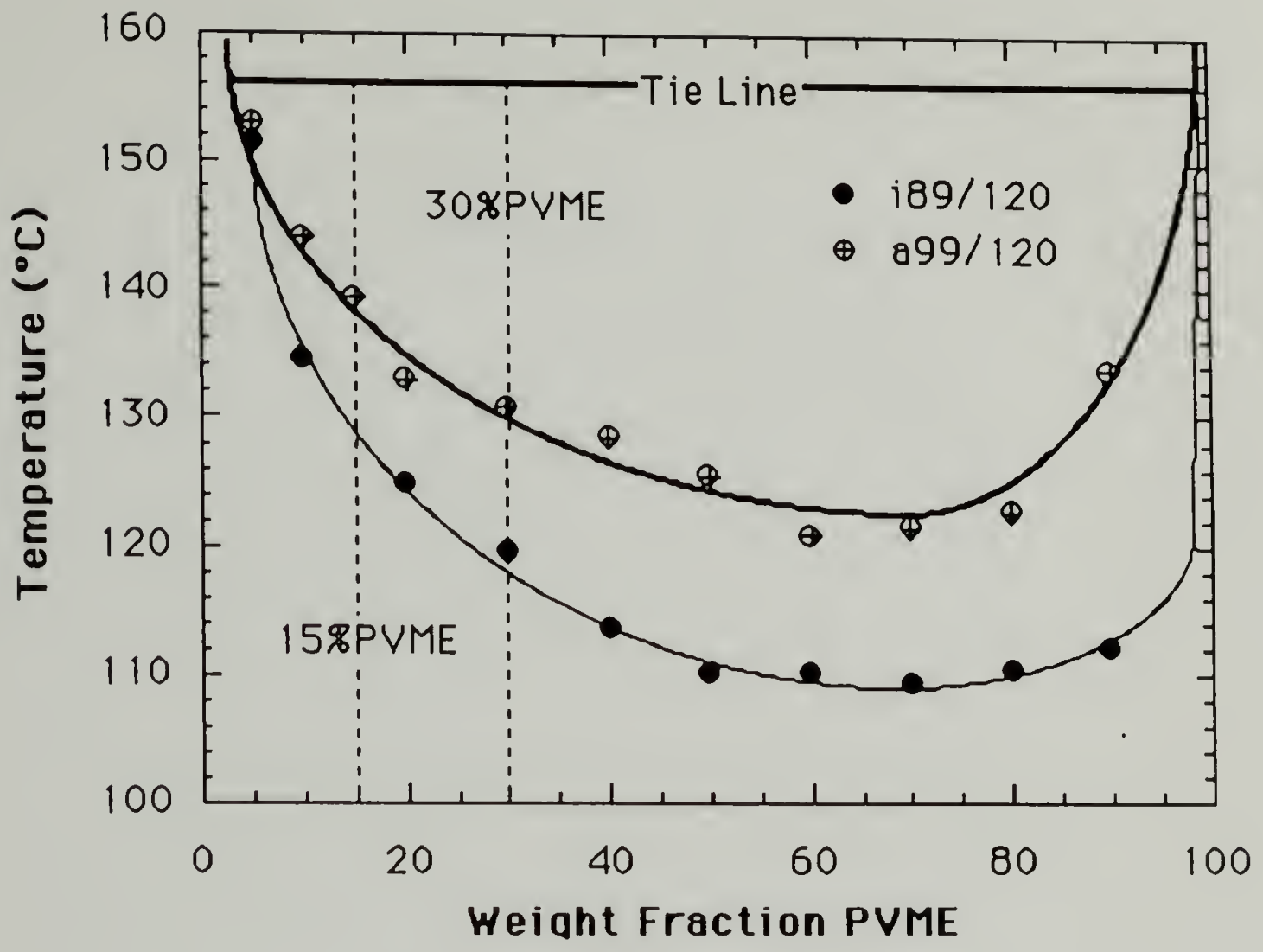

Figure 4.6 Phase diagram for isotactic and atactic PVME/PS. Lines are only for clarity and do not reflect a fit.

In the mid-composition range (15 to 75% PVME) the phase diagram is rather flat. Thus the low concentration fall of the modulus is in a high miscibility regime where most of the added PVME plasticizes the matrix leading to linear behavior. At about 15% the majority of the PVME goes into the formation of phase separated domains, and the matrix composition remains fairly constant. The second regime may reflect the result of larger PVME domains on the initial modulus. Finally, at higher compositions PVME, the PVME phases may begin to show continuity as the PS modified PVME becomes the majority phase

(this should occur at about 52% PVME following the tie line in Figure 4.6).

The large scatter in the mechanical data make generalizations difficult. Figures 4.3-5 are compilations of a number of different blends made under various annealing conditions and with additives, 1% heat stabilizer (Santonox White Crystals®) and 1% crystallizing agent (silica and sodium benzoate) either present or absent. These additives were found to have no effect on the mechanical tests. Annealing of the phase separated blends had slight effects (discussed below) although materials with behavior comparable to HIPS were not produced.

The stress at failure data is presented in Figure 4.7.The PVME blends showed a failure stress comparable with pure polystyrene (intercept at % PVME=0 in Figure 4.7). Data for HIPS and HIPS blends with isotactic PVME are shown for comparison. There is essentially no difference in the stress at failure for the isotactic and atactic melt blends. The stress at failure for the PVME blends shows a rise until about 10% PVME. This demonstrates the effect of added non-crystalline domains and the plasticization effect at moderate percentages of PVME. Shear banding may be a factor in this rise at low concentrations PVME. The drop in stress at failure and the plateau in the 10 to 30% range is reminiscent of the behavior of the initial modulus. The behavior of the stress at failure might be expected to follow the modulus in this way and similar reasoning could be applied to explain the behavior. At 35 to 40% PVME the stress at failure appears to show a change in slope although the data is less than

conclusive. Such a drop in slope might be related to changes in the stress field with differing blend structure, i.e. related to the PVME phase becoming continuous. The HIPS blends show a similar, though less pronounced increase in the stress at failure at low concentrations PVME indicating the possibility of plasticization induced shear banding, although these could not be observed in the blends due to turbidity.

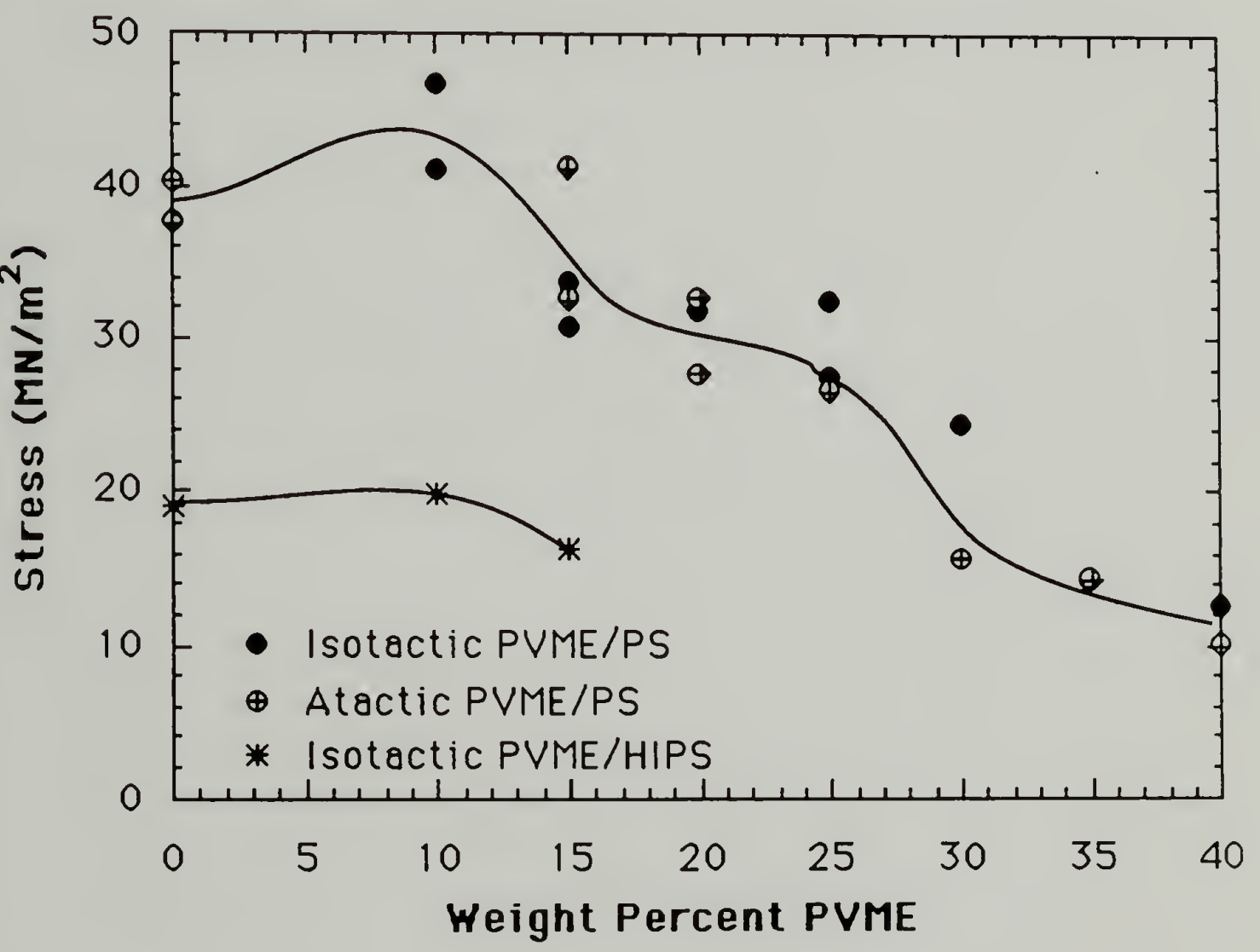

Figure 4.7 Stress at Failure versus weight fraction PVME in PVME/PS blends.

The energy absorbed in the tensile tests was calculated from the areas under the stress-strain curves. Figure 4.8 shows that none of the

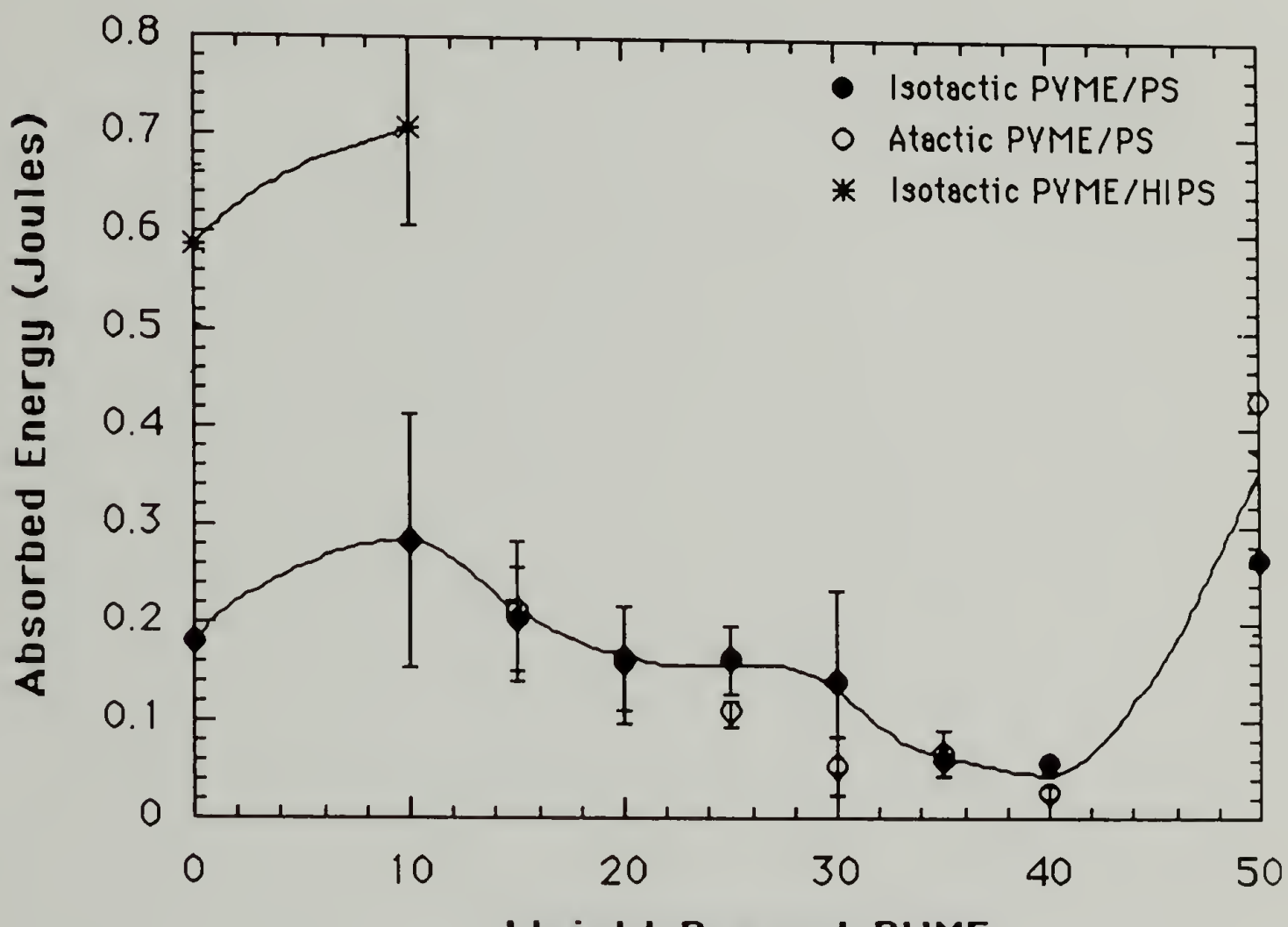

Figure 4.8 Absorbed energy vs weight percent PVME. Lines do not reflect a fit.

PVME melt blends showed energy absorption comparable to HIPS. The absorbed energy behaves in a very similar manner to that of the strain and stress. The initial increase in absorbed energy is due to plasticization. This increase reaches a maximum at the plateau region of the phase diagram at which point most of the PVME goes into phase separated domains (perhaps reducing the plasticization of the matrix). The behavior above 30% PVME is believed to be due to various stages

of PVME phase continuity. The 50% PVME blend showed an anomalous increase in energy absorption due to large extension in the low modulus material (Figure 4.3 and 4.5). This increase in the absorbed energy and decrease in the modulus may be related to the PVME phase reaching continuity. Due to the turbidity of the samples these postulates could not be proven by optical microscopy or light scattering.

In practice, it was impossible to drastically alter the final phase sizes in the phase separated blends by annealing or by pressing tensile bars at different temperatures. Generally, homogeneous phases of about 10 μm could be produced (estimated from crude optical microscopy of the mold flashing which was fairly thin). This behavior is probably due to the limitations of kinetic phenomena in the phase separation process. It was attempted to reduce the PVME phase size by annealing the blends below the phase separation temperature. Figures 4.9 and 4.10 are an example of such an attempt for the 30% PVME blends. The large scatter in the data and lack of drastic effects are characteristic of the results. The tensile bars were annealed at 50°C for 8 days and at 120°C for 5 days. Generally, the isotactic blends showed higher absorbed energies although this difference was within the scatter of the data. Annealing above the glass transition temperature of the blend (about 55°C for the 30% blend) yielded a slightly lower modulus and a higher energy absorption, however the small differences may be due to relaxation of internal stresses present in the melt pressed blends. Annealing below the experimental

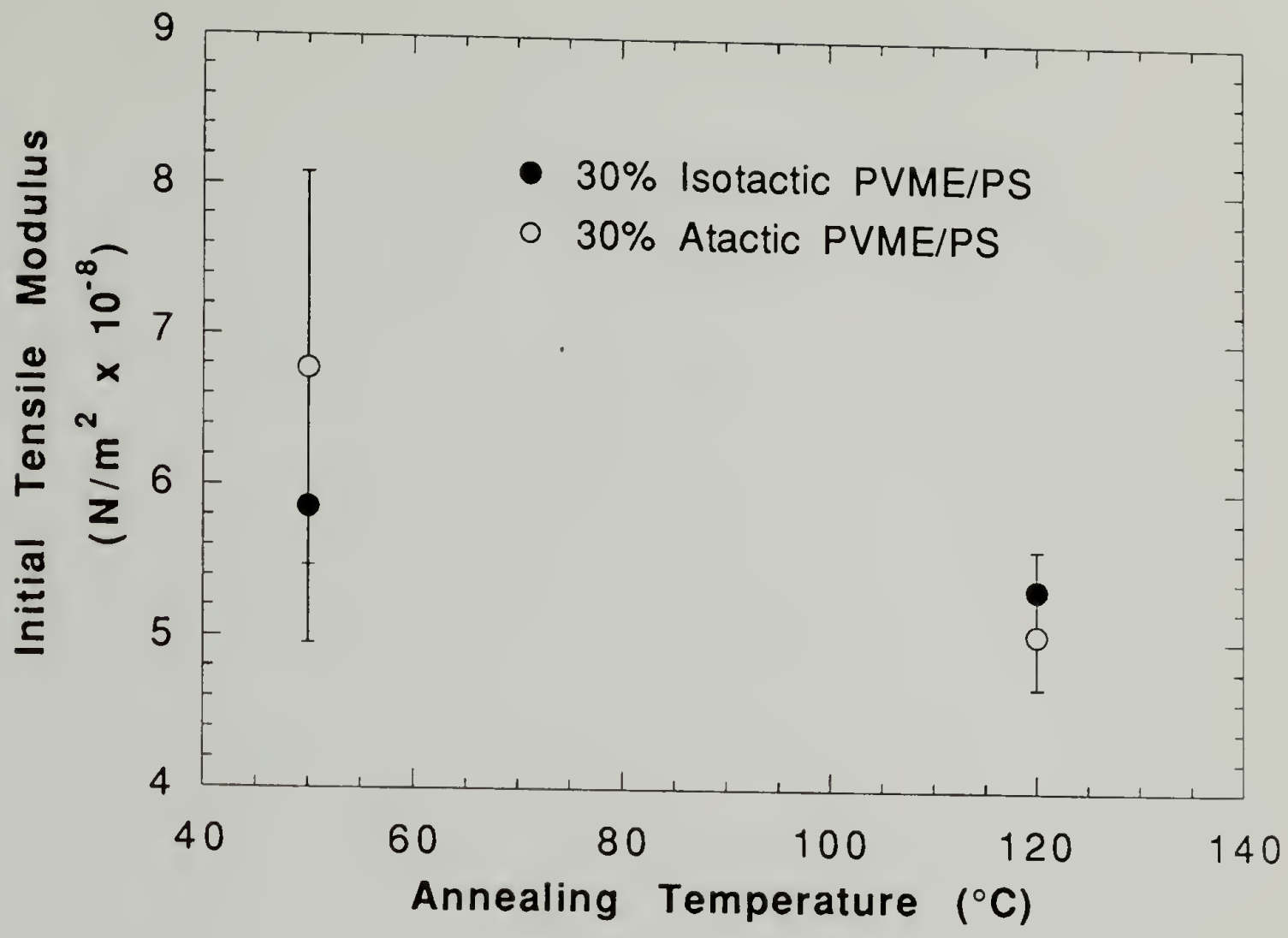

Figure 4.9 Initial modulus versus annealing temperature for 30% PVME blends.

melting temperature of about 50°C also failed to produce improved mechanical results. Annealing for longer periods was limited by the thermal stability of the PVME even in the presence of antioxidants (blends annealed at 120°C for more than a week became brown).

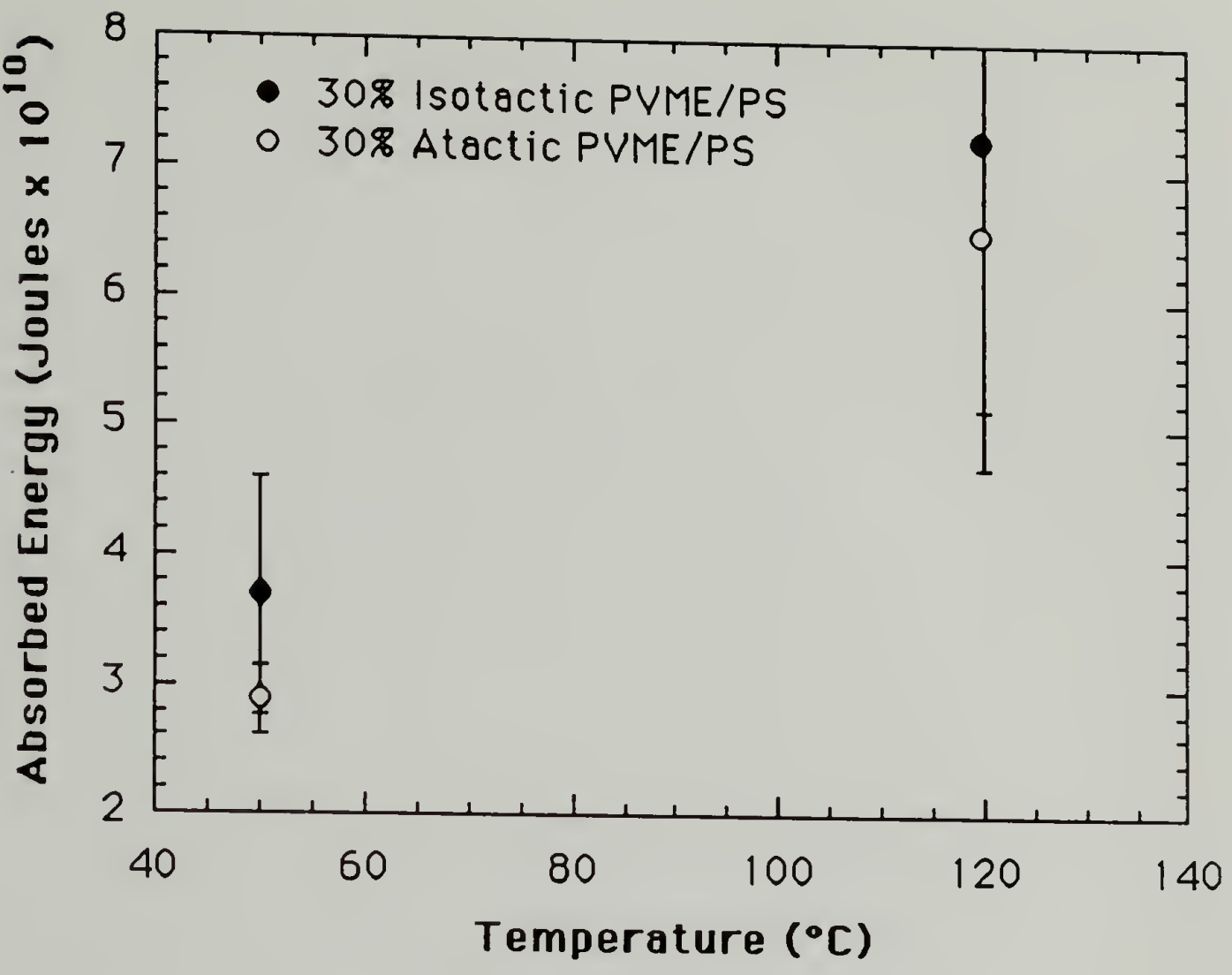

Figure 4.10 Absorbed energy versus annealing Temperature for 30% PVME blends. (Identical samples as in Figure 4.9.)

D. Crystallization of i-PVME

It is believed that the absence of crystallinity in the phase separated isotactic blends prevents the formation of a resilient rubbery phase which appears to be necessary for improved toughness (although the reasons for this remain vague). An attempt was made to improve the crystallization kinetics of the rubbery phase by the introduction of crystallizing agents (sodium benzoate and silica for example). These agents serve as seeds for crystallization acting to

increasing the rate of nucleation. (If the crystallization is limited by kinetics rather than nucleation these additives would be expected to have little effect.) X-ray diffraction is the most sensitive of standard techniques to observe small amounts of crystallinity. A study was conducted adding various amounts of crystallizing agents to pure PVME in order to increase the rate of nucleation. Figure 4.11 shows x-ray patterns from pure atactic PVME (a), isotactic PVME (b) and the subtracted crystalline pattern (c) after subtraction of the background. A comparison of the area under the amorphous and crystalline patterns yields the degree of crystallinity which shows a maximum value of about 10% after several weeks. The addition of crystallizing agents had no effect on the rate or on the final degree of crystallinity (x-ray). The different crystalline peaks in Figure 4.12 are for various times after melting (about 2 days separates the neighboring crystalline patterns). Generally traces of crystallinity (by x-ray) appeared after about one day, and full crystallinity occurred after about two weeks at room temperature. This corresponded well with the mechanical resiliency of the i-PVME. Additionally, annealing the PVME at temperatures above and below room temperature served only to reduce the rate and amount of crystallinity. It should be noted that a marked small angle pattern occurs in the highly crystalline PVME samples. This indicates the presence of larger scale structures (but smaller than a spherulite since these could not be observed under the optical microscope) such as axialites in this material.

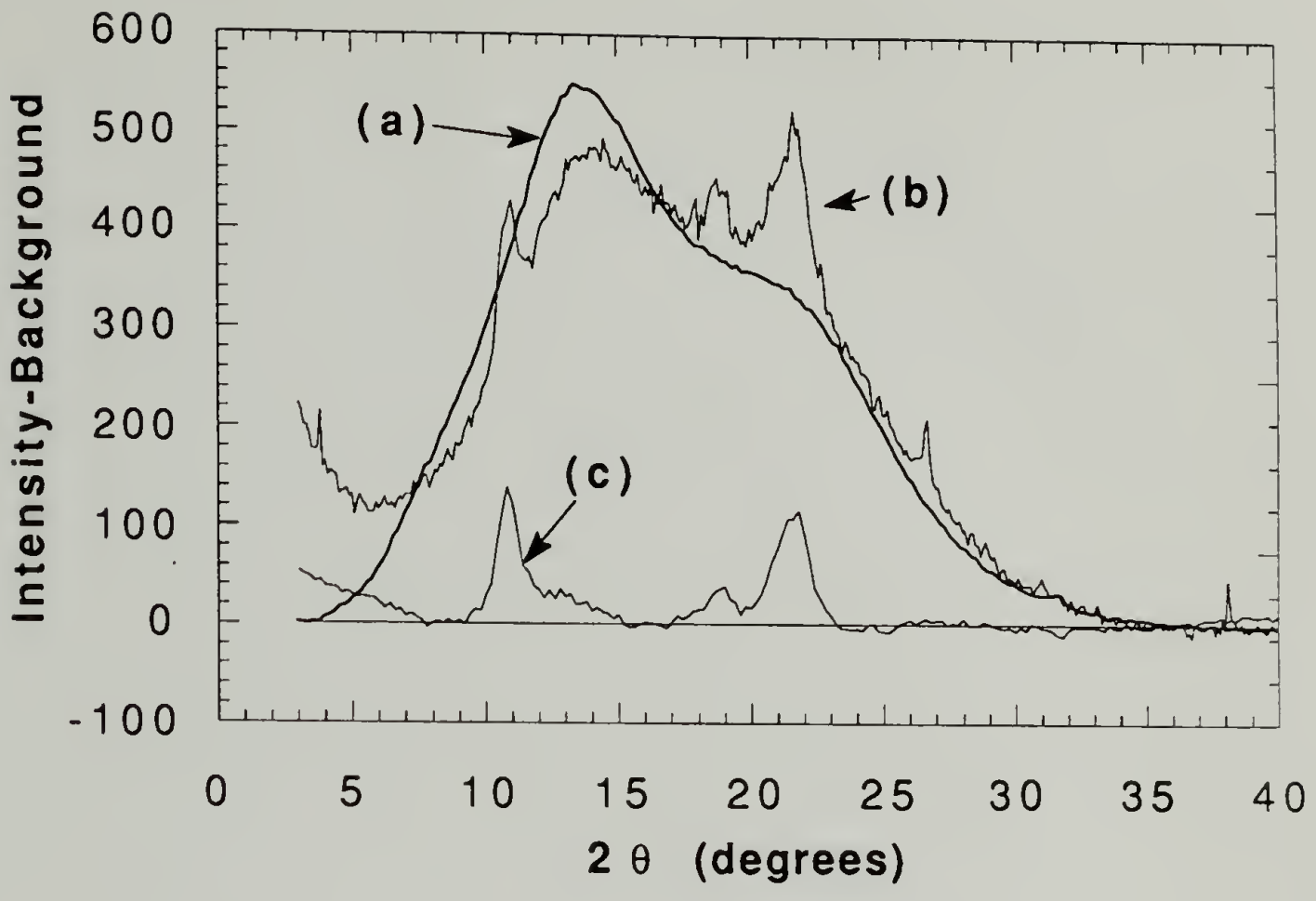

Figure 4.11 X-ray patterns for isotactic PVME (a = amorphous PVME, b = amorphous and crystalline, c = the subtracted crystalline pattern).

Further fractionation of the PVME was attempted in order to increase the degree of isotacticity. Repeated fractionation by heating an aqueous solution of the PVME (PVME has an LCST in water) followed by a solvent/non-solvent fractionation using benzene (solvent) and heptane (non-solvent) yielded PVME with a higher degree of isotacticity and a lower polydispersity. Figure 4.13 shows the X-ray

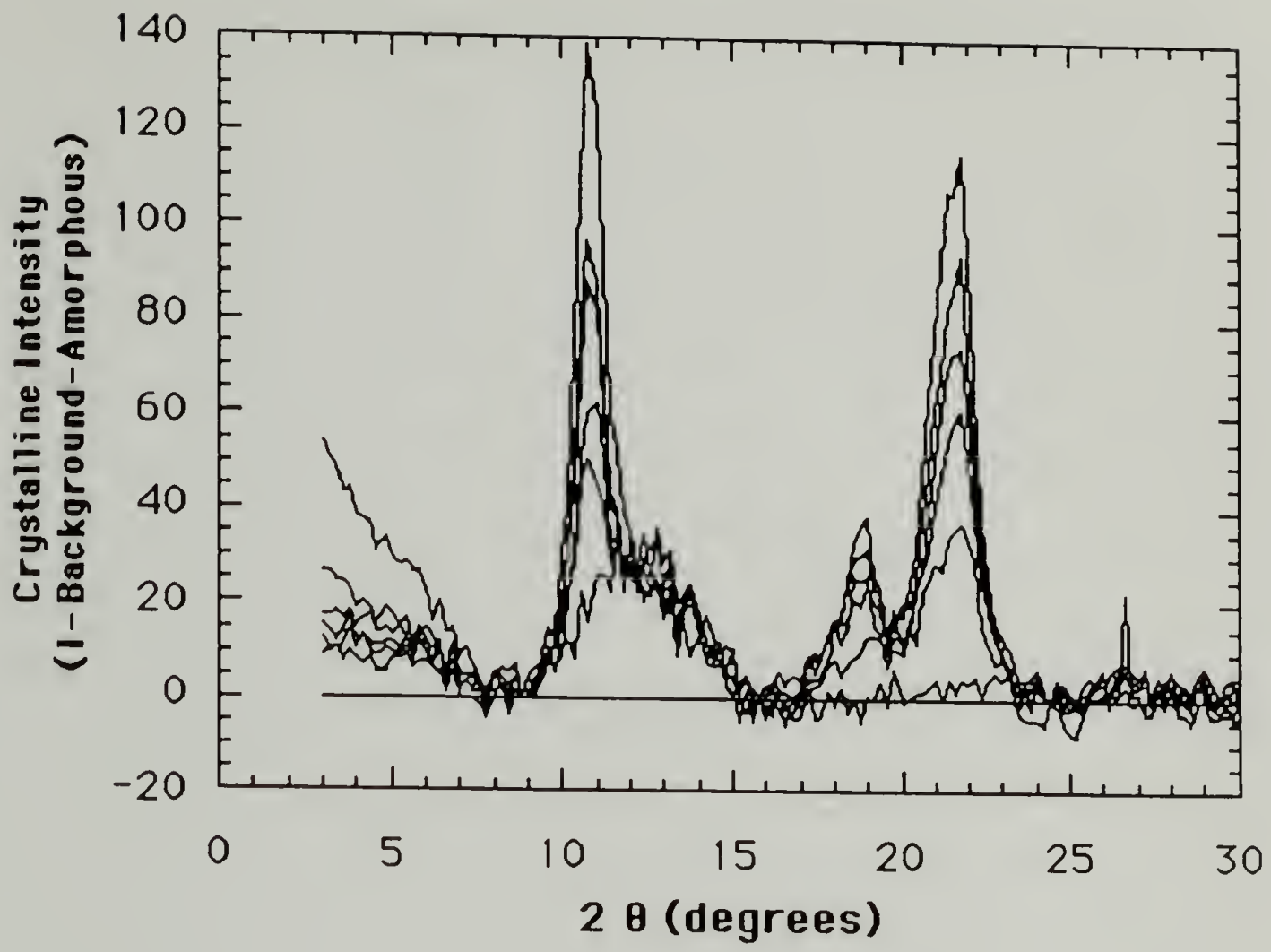

Figure 4.12 Crystalline pattern after subtraction of amorphous and background (amorphous pattern is also shown for area comparison). Crystalline curves are separated in time by about one day. (Maximum crystallinity is identical with crystalline pattern in Figure 4.11.)

patterns for the Sarnia PVME purified by the toluene/heptane procedure (labeled old purified) and the same PVME after two further fractionations as described above (labeled fractionated). (A 10% crystallinity PVME is included for comparison). Although this material showed a slightly faster rate of crystallization, melt blends of this PVME failed to show improved mechanical properties.

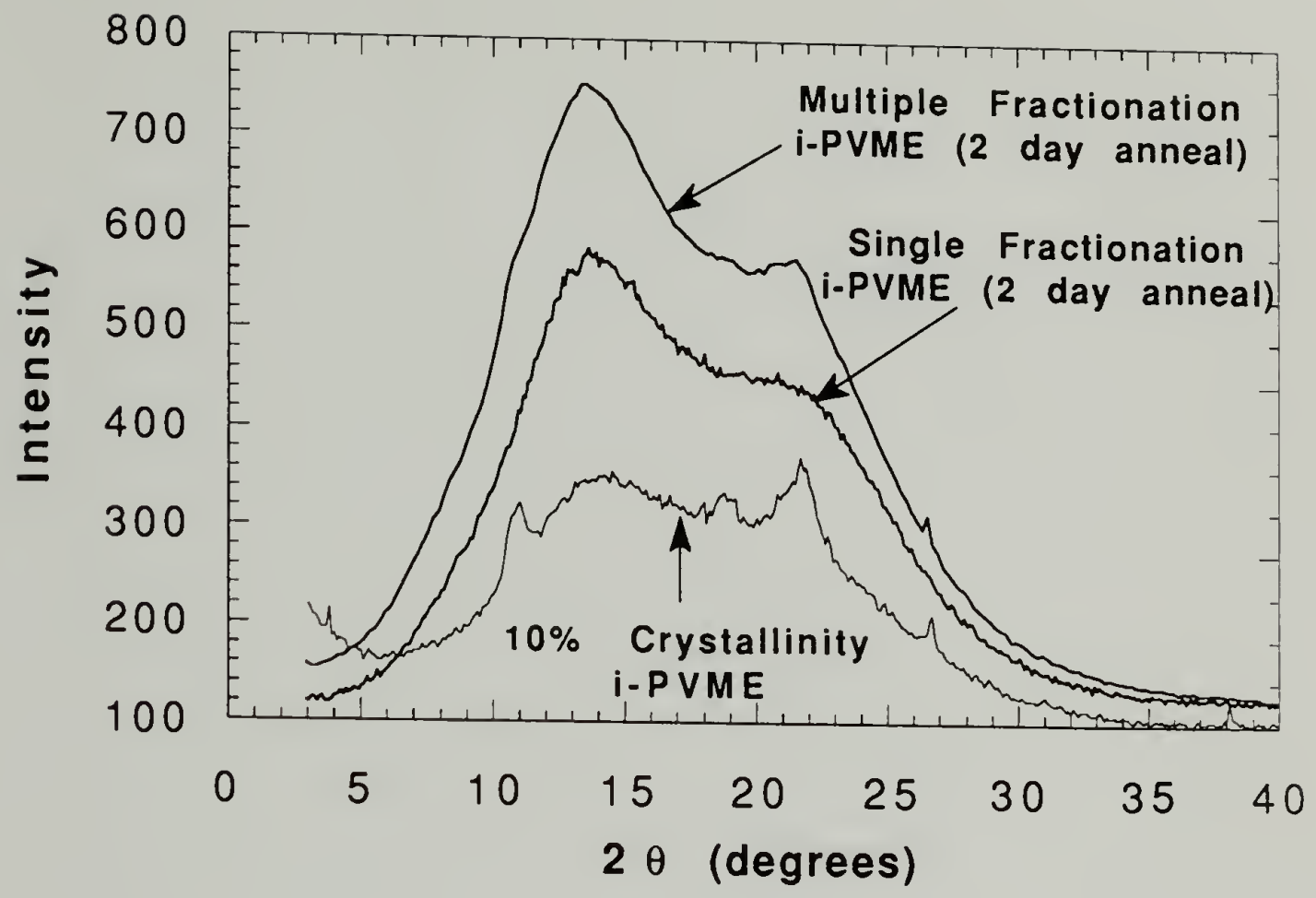

Figure 4.13 Improvement in degree of crystallinity in multiply fractionated i-PVME over i-PVME from a single fractionation. Note larger peak at 22° for the multiple fractionation sample.

E. Conclusions

Isotactic PVME/PS blends produced by solution casting relatively thin films showed (in some cases) the presence of shear bands and extensive crazing. In these materials a dramatic increase in tensile strain and energy absorption occurred comparable to commercial high impact polystyrene (HIPS). It is believed that a combination of plasticization of the matrix phase by the miscible PVME and the presence of resilient crystalline PVME domains of

about 5μm are necessary conditions for this toughening mechanism. Phase separation for the solution cast samples was driven by crystallization of the isotactic PVME from the solution during evaporation. These materials have a final morphology which mimics the morphology produced in Figure 1.1.

It was attempted to produce similar materials following the scheme outlined in Chapter 1 and Figure 1.1, that is by melt blending in the miscible regime and pressing ASTM tensile bars above the phase separation temperature followed by quenching. However, mechanical properties similar to those obtained by solution crystallization were not obtained. Isotactic PVME domains from the melt phase separated material did not show crystallinity either by DSC, observation of birefringence under crossed polars or by X-ray diffraction. Some degree of control over the mechanical properties was obtained by extensive annealing of the phase separated blends above their glass transition temperature and below their phase separation temperature, however, although this succeeded in reducing the phase size, crystallinity could not be produced in the isotactic PVME domains.

In the next chapter Flory-Huggins-Staverman theory is used to explain the failure of the melt blended samples to produce crystalline PVME domains and mechanical properties similar to the solution cast samples. Additionally, the shift in phase miscibility observed in Chapter 3 will be explained in more useful terms.

References

1. C. B. Bucknall, *Toughened Plastics*, Applied Science Publishers LTD, London, 1977.

CHAPTER 5

FLORY-HUGGINS-STAVERMAN ANALYSIS OF THE TACTICITY EFFECT

A. Introduction

The solution cast samples phase separated by solvent crystallization produce dramatic improvements in energy absorption and changes in the mechanisms of energy absorption in the samples containing 1 to 5 micron crystalline PVME phases. The failure of LCST phase separated samples of similar phase size to reproduce this behavior lead to further theoretical analysis of the nature of the LCST phase separation in this system. Chiefly, it is desired to determine the difference between these two mechanisms for producing a phase separated blend in terms of predictable thermodynamic properties.

The mechanical tests indicate that in the LCST phase separated blends the matrix material is of similar composition as that in the successful crystallization phase separated samples. However, x-ray analysis indicates that crystallinity can not, in practice, be induced in the phase separated PVME even after annealing and/or addition of crystallizing agents. Parallel to this, in the solution cast blends which do not show dramatic decreases in the initial modulus (plasticization of the matrix phase), shear bands also do not form even in the presence of physically crosslinked domains (phase sizes are also

larger). It appears that the presence of a resilient rubbery phase in which crystallinity acts as physical crosslinks serves as a necessary but not complete requirement for the formation of shear bands which can interact with crazes to increase energy absorption.

It is desirable to ascertain at least in a qualitative manner the reason for the lack of crystallinity in the melt blended samples. Additionally, a better understanding of the tacticity effect is desired including a physical picture of the reasons for the shift in miscibility. To some extent this has been accomplished using Flory-Huggins-Staverman theory in analyzing the cloud point curves. A more elaborate analysis of the tacticity effect will be given in Chapter 7 where χ values were directly determined using small angle neutron scattering (SANS). The SANS results, however, pertain to deuterated blends which show modified miscibility as will be discussed.

B. Theoretical Background

Phase separation in the polystyrene/poly(vinylmethylether) (PS/PVME) blend system exhibits LCST behavior and can be conveniently studied using light scattering due to the large difference in index of refraction between PVME and PS (1.467 and 1.592 respectively). By slowly raising the temperature of a polymer blend of composition ϕ (where ϕ is the PVME volume fraction) the optical cloud point (T_{CP}) can be determined. The cloud point curve (CPC) determined by extrapolating T_{CP} versus ϕ_2 data to zero heating rate can be related to the binodal phase diagram (the locus of coexisting

phase compositions in T::ϕ_2 space) for monodisperse polymer blends. It is not permitted to identify the cloud point curve (CPC) with the binodal for polydisperse blends. The polystyrene samples studied here have a narrow molecular weight distribution which is represented by a single component in this analysis. The distribution of the PVME samples, however, is rather broad and cannot be ignored. The significance of a two-dimensional phase diagram (temperature versus composition) for a non-binary system has been amply discussed[2,3], here the situation is summarize in Figure 5.1 which shows that cloud points coexist with incipient phases (shadow phase) whose overall concentration differs from those lying on the CPC (the tie line phase) except at the critical point. The polymer fractions in the incipient phases, connected by the shadow curve (SHC) also differ from the original polymer in molecular weight distribution (i.e. a fractionation of molecular weight occurs on phase separation for polydisperse blends). Thus, a blend at the cloud point (a) on the left side of Figure 5.1 is in equilibrium with the shadow phase (b) on the right side and the molecular weight of the shadow phase differs from that of the parent, cloud point phase.

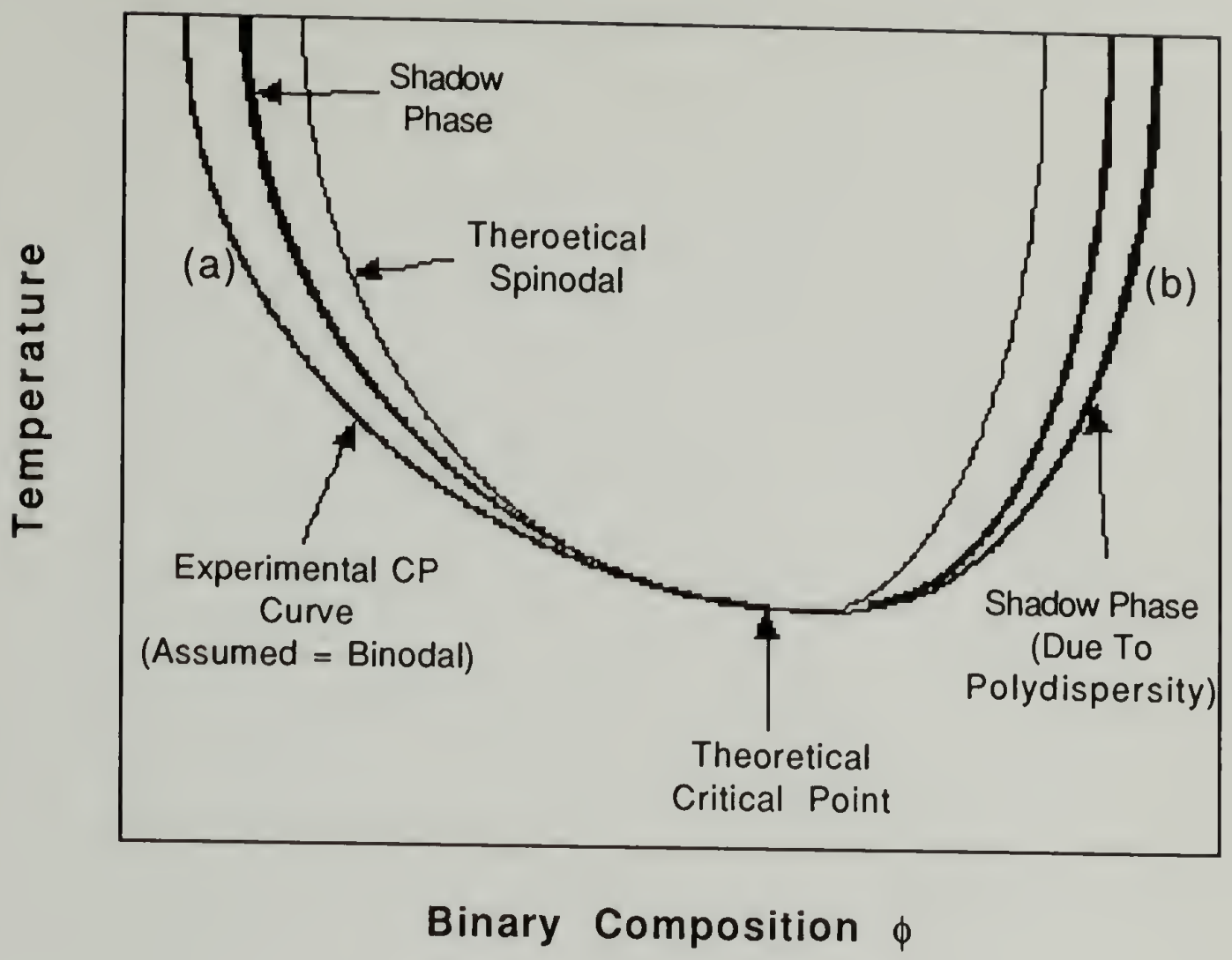

Figure 5.1 Theoretical and experimental CP curves (one of the components is polydisperse).

C. Flory-Huggins-Staverman Approach

Modeling the systems as quasi-binary mixtures in which constituent 1, polystyrene, is monodisperse and constituent 2, PVME, contains a distribution of chain lengths, we have, at two-phase equilibrium,

$$\Delta\mu_1^a = \Delta\mu_1^b \qquad (5.1)$$

$$\Delta\mu_{2i}^{a} = \Delta\mu_{2i}^{b} \qquad (5.2).$$

In these equations $\Delta\mu_k^l$ is the chemical potential of component k in phase l minus the value for the pure component k in the liquid state at the same pressure and temperature. There are as many equations as there are components in constituents 1 and 2.

To find expressions for the $\Delta\mu$'s we assume the system to obey the Flory-Huggins rigid lattice equation for the free enthalpy of mixing ΔG amended for the difference in size between styrene and vinylmethylether units (F-H-Staverman approach[1,2,3,4,5]),

$$\frac{\Delta G}{NRT} = \frac{\phi_1}{m_1} \ln \phi_1 + \Sigma\left(\frac{\phi_{2i}}{m_{2i}} \ln \phi_{2i}\right) + g\,\phi_1\,\phi_2 \qquad (5.3)$$

where ϕ_1 and ϕ_2 are the volume fractions of PS and PVME respectively, m_j is the number of lattice sites occupied by macromolecules "j", N is the total amount of lattice sites in moles and RT has its usual meaning. We have,

$$\phi_2 = \Sigma\,\phi_{2i} \qquad (5.4)$$

and define the interaction function g (we use g for a composition dependent χ parameter) by,

$$g = a + \frac{(b_0 + b_1/T)}{(1 - c\,\phi_2)} \qquad (5.5)$$

where a and b_0 are parameters correcting for possible shortcomings in the first two combinatorial entropy terms on the right hand side of equation 5.3. The parameter b_1 is of an enthalpic nature,

$$\frac{b_1}{T} = \frac{z_2\,\Delta w_{12}}{RT} \qquad (5.6)$$

and

$$c = 1 - \frac{z_2}{z_1} \approx 1 - \frac{s_2}{s_1} \qquad (5.7)$$

c will here be referred to as the Staverman Parameter. The coordination numbers z_2 and z_1 refer to the two repeat units in the system and are supposed to reflect their difference in size and shape. We follow Staverman in further assuming the ratio $\frac{z_2}{z_1}$ as equaling the ratio of molecular surface areas $\frac{s_2}{s_1}$ which can be estimated with Bondi's method of group contributions[6]. Alternatively , c, can be used as an adaptable parameter.

It should be noted that the Flory-Huggins (F-H) lattice model assumes equally sized and symmetrically shaped lattice sites such as

would exist in a polymer/symmetric solvent system where the size of the solvent molecule defines the lattice cell size. For real polymer/polymer systems a symmetric lattice cell with one mer unit per cell is probably not the case. Regardless of the real situation, the statistics involved in deriving the F-H theory as originally formulated do not allow for deviation from a strictly symmetric and generally small sized lattice site. Thus, the present discussion (and the discussion in Chapters 6 and 7) must be taken as indications of where newer theories for polymer blends (such as the Curro-Schweitzer RISM theory[7]) should be directed and as a qualitative indication of the results to be expected from such modern theories. (The RISM theory is not at this date capable of describing the phenomena involved in this thesis but does account for surface area differences similar to those described by the Staverman parameter.)

If $z_2 = z_1$, the interaction function, g, is independent of concentration and is usually denoted by χ. We note that the entropic and enthalpic contributions to χ, χ_s and χ_h, respectively, are then given by,

$$\chi_s = a + b_0 \qquad (5.8),$$

and,

$$\chi_h = \frac{b_1}{T} \qquad (5.9).$$

It has been demonstrated that the parameters a and b_0 are not merely empirical in nature. They can be shown to arise from combinatorial entropy corrections due to a disparity between z_1 and z_2. In the present work we use a and b_0 as adaptable parameters.

Within this framework the chemical potentials are given by,

$$\frac{\Delta\mu_1}{m_1 RT} = \frac{\ln \phi_1}{m_1} + \left(\frac{1}{m_1} - \frac{1}{m_{n2}}\right)\phi_2 + g_1 \phi_2^2 \qquad (5.10)$$

$$\frac{\Delta\mu_{2i}}{m_{2i} RT} = \frac{\ln \phi_{2i}}{m_{2i}} + \frac{1}{m_{2i}} - \frac{1}{m_1} + \left(\frac{1}{m_1} - \frac{1}{m_{n2}}\right)\phi_2 + g_2 \phi_1^2 \qquad (5.11)$$

where,

$$g_1 = a + \frac{b\,(1-c)}{(1 - c\,\phi_2)^2} \qquad (5.12)$$

$$g_2 = a + \frac{b}{(1 - c\,\phi_2)^2} \qquad (5.13)$$

$$b = (b_0 + \frac{b_1}{T}) \qquad (5.14)$$

and,

$$m_{n2} = \Sigma \frac{\phi_2}{\phi_{2i}/m_{2i}} \qquad (5.15).$$

D. Polydispersity

Dealing with equations (5.1), (5.2), (5.10) and (5.11) we are faced with the problem of the molecular weight distribution in constituent 2. Three average molecular weight values are available, viz. number-, weight-, and z-average, M_N, M_W and M_Z. The following definitions may be formulated,

$$\sum w_i = 1 \qquad (5.16)$$

$$\sum \frac{w_i}{M_i} = \frac{1}{M_N} \qquad (5.17)$$

$$\sum w_i M_i = M_W \qquad (5.18)$$

$$\sum w_i M_i^2 = M_W M_Z \qquad (5.19)$$

where the w_i represent the mass fraction of component "i" with molecular weight M_i, the total mass being normalized to one gram.

Since there are only four equations, the molecular weight distribution (w_i,M_i) can be established in a unique fashion only for a binary polymer mixture, where we have four unknowns (w_1, w_2, M_1 and M_2) representing the distributions of the PVME samples.

E. Determination of the Parameters a, b_o and b_1 and c

The principle effect of the introduction of a molecular weight distribution is a shift of the critical solution point away from the minimum in the CPC. The CPC and its coexistence curve (SHC) are determined by equations (5.10) and (5.11), the use of which calls for knowledge of the parameters a, b and c. If the molecular weight distribution in constituent 2 were completely known one might represent it either by an arbitrary number of components or by a continuous function and fit the data to equations (5.10) and (5.11). Alternatively, one might use the spinodal and critical conditions given respectively by,

$$\frac{1}{m_{W1}\,\phi_1} + \frac{1}{m_{W2}\,\phi_2} = 2a + \frac{2b\,(1-c)}{(1 - c\,\phi_2)^3} \qquad (5.20)$$

$$\frac{\alpha_1}{m_{W1}\,\phi_1^{\,2}} + \frac{\alpha_2}{m_{W2}\,\phi_2^{\,2}} = \frac{6\,b\,c\,(1-c)}{(1 - c\,\phi_2)^4} \qquad (5.21)$$

where m_{Wj} is the weight-average site-number of constituent "j" and $\alpha_j = \left(\frac{M_Z}{M_W}\right)_j$.

F. F-H-S Cloud Point Analysis

Data discussed in Chapter 3 for the i89/120 and a99/120 blends will be used in the F-H-S analysis of the cloud point curves. Figure 5.2

(same as Figure 3.9) is the cloud point curve (CPC) for the i89/120 and a99/120 blends.

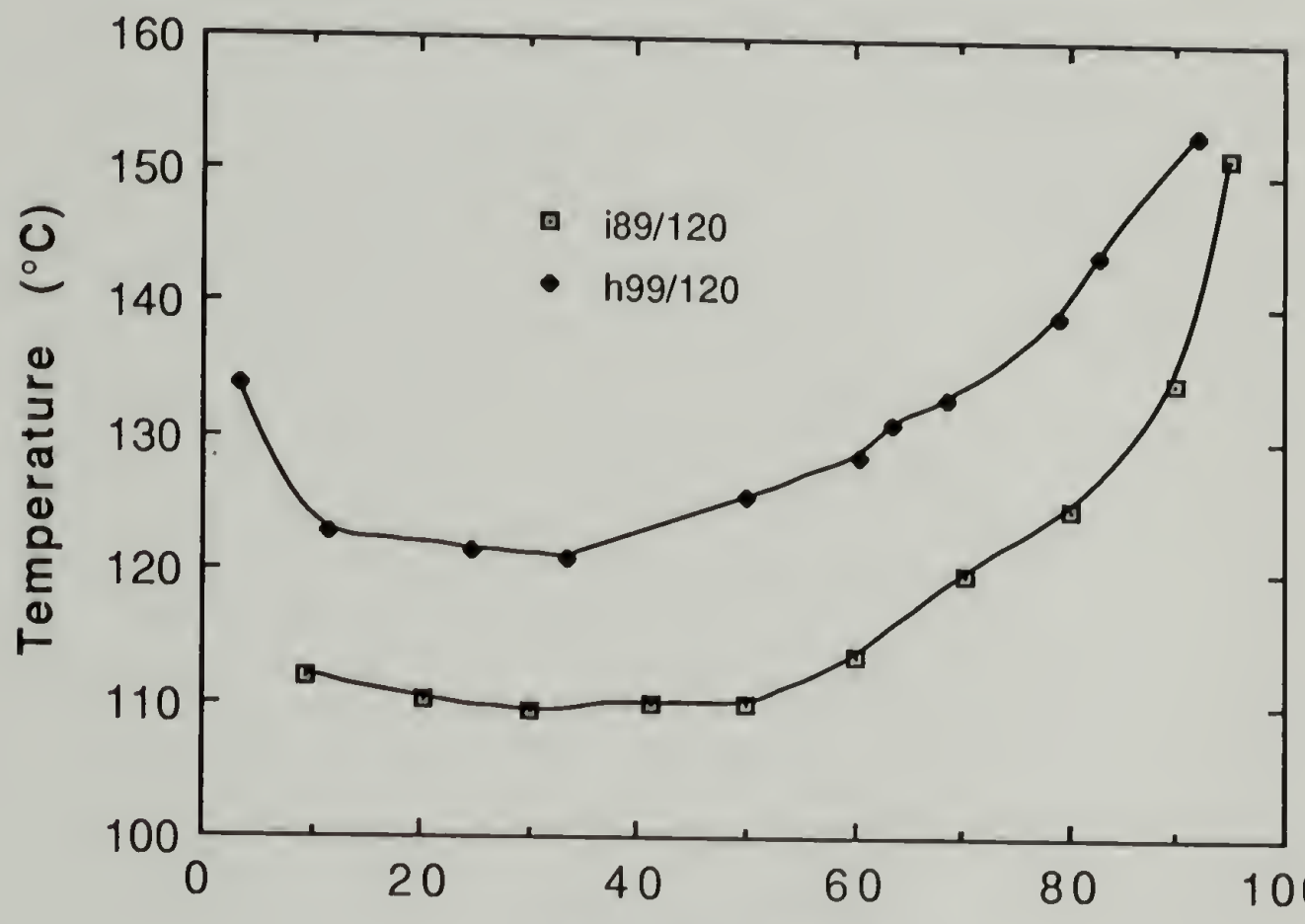

Figure 5.2 Cloud point curves for i89/120 and h99/120 blends. (same as Figure 3.9)

Both blends contain the same molecular weight PS, but different M_W for the two PVME's. In spite of the fact that the molecular weight of the PVME in a99/120 is higher than that for i89/120, the cloud point curve for a99/120 is higher than that for i89/120, implying a tacticity effect. Thus the isotactic PVME is less miscible with PS than the atactic PVME. Figure 5.3 shows the Flory-Huggins-Staverman fit to the CPC of the 99 kg/mole atactic PVME/120 kg/mole PS blend

(a99/120). Polydispersity significantly shifts the composition of the coexisting incipient phase (SHP) from the binodal line.

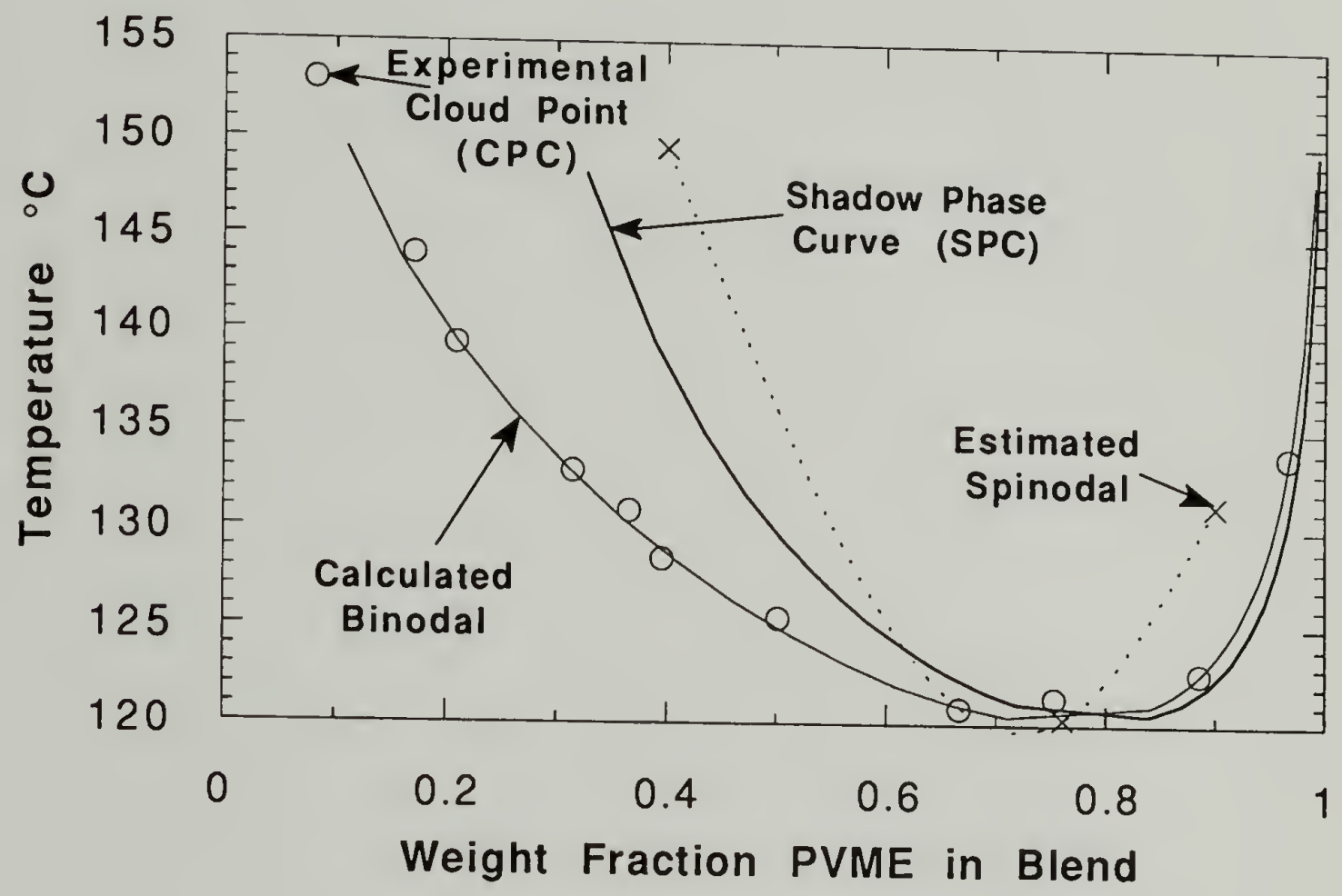

Figure 5.3 Flory-Huggins-Staverman fit to the CPC of the 99 kg/mole atactic PVME/120 kg/mole PS blend (a99/120).

The procedure involved calculating two monodisperse PVME fractions , M_1 = 26.9 kg/mole w_1 = 0.499 and M_2 = 170.8 kg/mole w_2 = 0.501, from the molecular weight distributions and equations 5.16 to 5.19 . Next, three spinodal points were estimated such that the central spinodal point would approximate T_{CP} for a 0.75 weight fraction PVME blend. Equations 5.20 and 5.21 were then used to calculate a, b_0 and b_1 using c = 0.36 as calculated from Bondi[4]. These values for a, b_0 and b_1 were then used in equations 5.1, 5.2, and 5.10

through 5.15 to generate the binodal and shadow curves. This procedure was iterated, varying the off critical spinodal points (x in Figures 5.3 and 5.4), until a suitable fit to the CPC was obtained. The final values for a, b_0 and b_1 are reported in Table 5.1. (It should be noted that the monodisperse molecular weight fractions do not necessarily have values close to 0.5 . For the isotactic PVME M_1 = 34.1 kg/mole w_1 = 0.623 and M_2 = 179.6 kg/mole w_2 = 0.377.)

Figure 5.4 is a similar fit to the i89/120 blend. In this case use was made of the inherent relationship between b_1 and c derived from equations 5.6 and 5.7 (the definition of c). If it is assumed that the coordination number z_1 or the surface area s_1 for the PS component is the same for both the isotactic and atactic blends, then

$$\frac{b_{1i}}{b_{1a}} = \frac{(1 - c_i)}{(1 - c_a)} \qquad (5.22).$$

Thus, using the Bondi value for c_a (the atactic Staverman parameter), one may obtain a value for c_i, a_i, b_{0i}, and b_{1i} (the isotactic values), using the same iterative scheme. In this way a value for c_i of 0.425 was obtained, indicating a smaller PVME surface area for the isotactic blend in relation to the atactic blend. It should be noted that the fit to the CPC at high and low concentrations is strongly effected by c, such that if one were to use the Bondi value of 0.36 for the isotactic blend a noticeable mismatch with the CPC would occur.

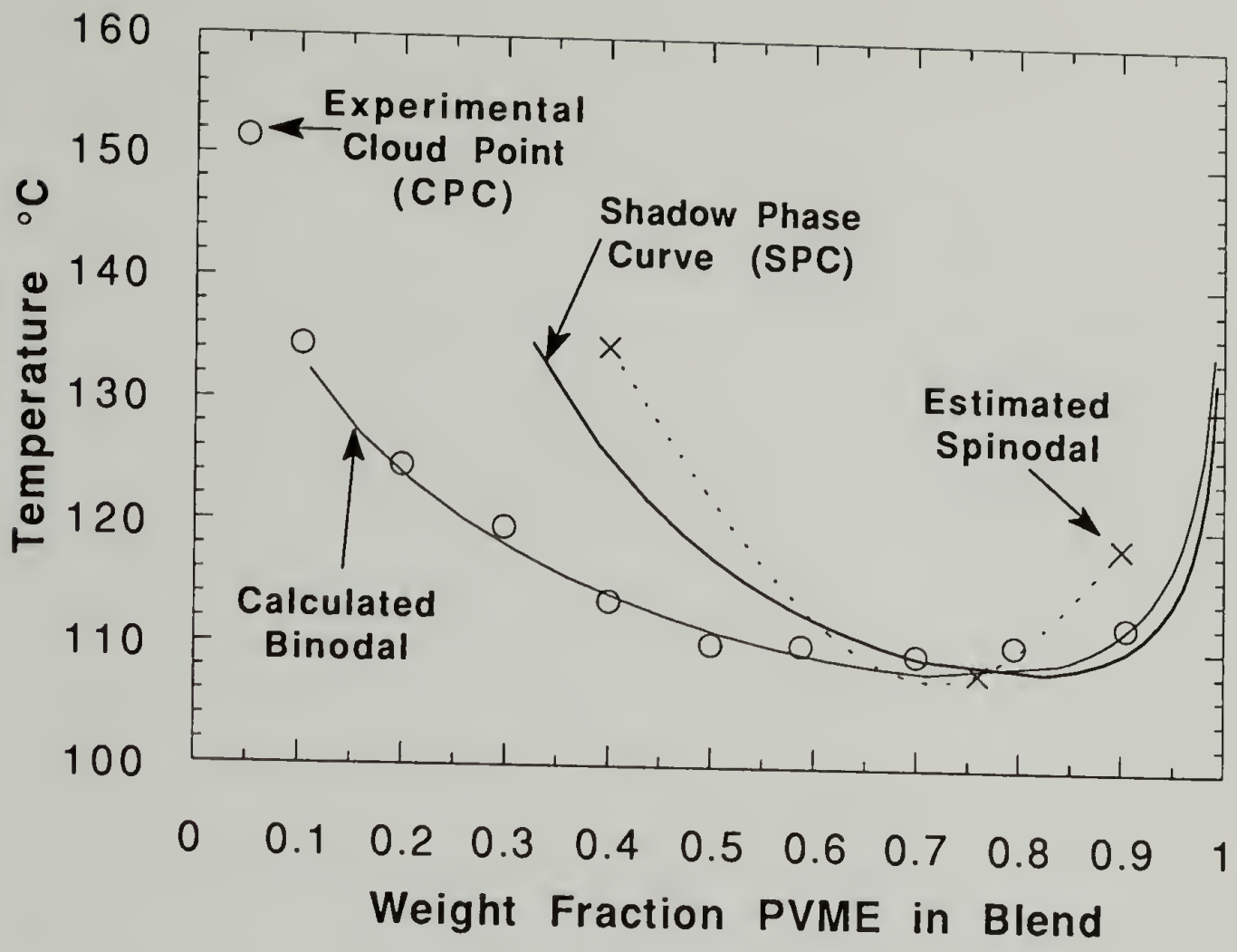

Figure 5.4 Flory-Huggins-Staverman fit to the CPC of the i89/120 blend.

Values for a, b_0, b_1, and c for the isotactic and atactic blends are presented in Table 5.1. The fractional change relative to an average value are also reported.

The tacticity difference most strongly effects the entropic terms, a and b_0 as well as the Staverman parameter, c. Since g is related to $\Delta G/T$ and $\Delta G/T = \Delta H/T - \Delta S$, the change in the entropic terms is related to a negative change in the entropy. That is to say, in comparing the ground state for the blend components with their state in the blend there is a smaller change in the non-composition dependent entropy, "a", on mixing for the isotactic PVME than for the atactic PVME and this change is towards a more random state for

both. The composition dependent entropy term, b_0, shows a larger change on mixing for the isotactic PVME and this is a change towards

Table 5.1 Flory-Huggins-Staverman analysis parameters from fits to the cloud point curves. (* = from Bondi)

	a ($\times 10^3$)	b_0 ($\times 10^2$)	b_1	c
HETERO	-1.43	1.36	-4.69	0.36*
ISO	-0.57	1.77	-4.08	0.425
$\frac{\Delta VALUE}{AVG\ VALUE}$	0.86	0.20	0.14	0.17

a more ordered state. The change in the Staverman parameter, c, reflects a smaller surface area for the isotactic PVME in comparison to the atactic PVME which will be discussed with respect to simple molecular models in the next section. In considering the net effect of the parameters listed in Table 5.1 a plot of the composition dependence of the entropic [a+b0/(1-c ϕ)] and the enthalpic [b_1/{T (1-c f)}] components of g (composition dependent χ) will be considered (Figure 5.5).

Figure 5.5 shows a more positive value for g in the isotactic blend which leads to the tacticity effect (a more positive value for g indicates lower miscibility). The difference in the enthalpic component of g, for the isotactic and atactic PVME blends, is small compared with the entropic component. The differences in the

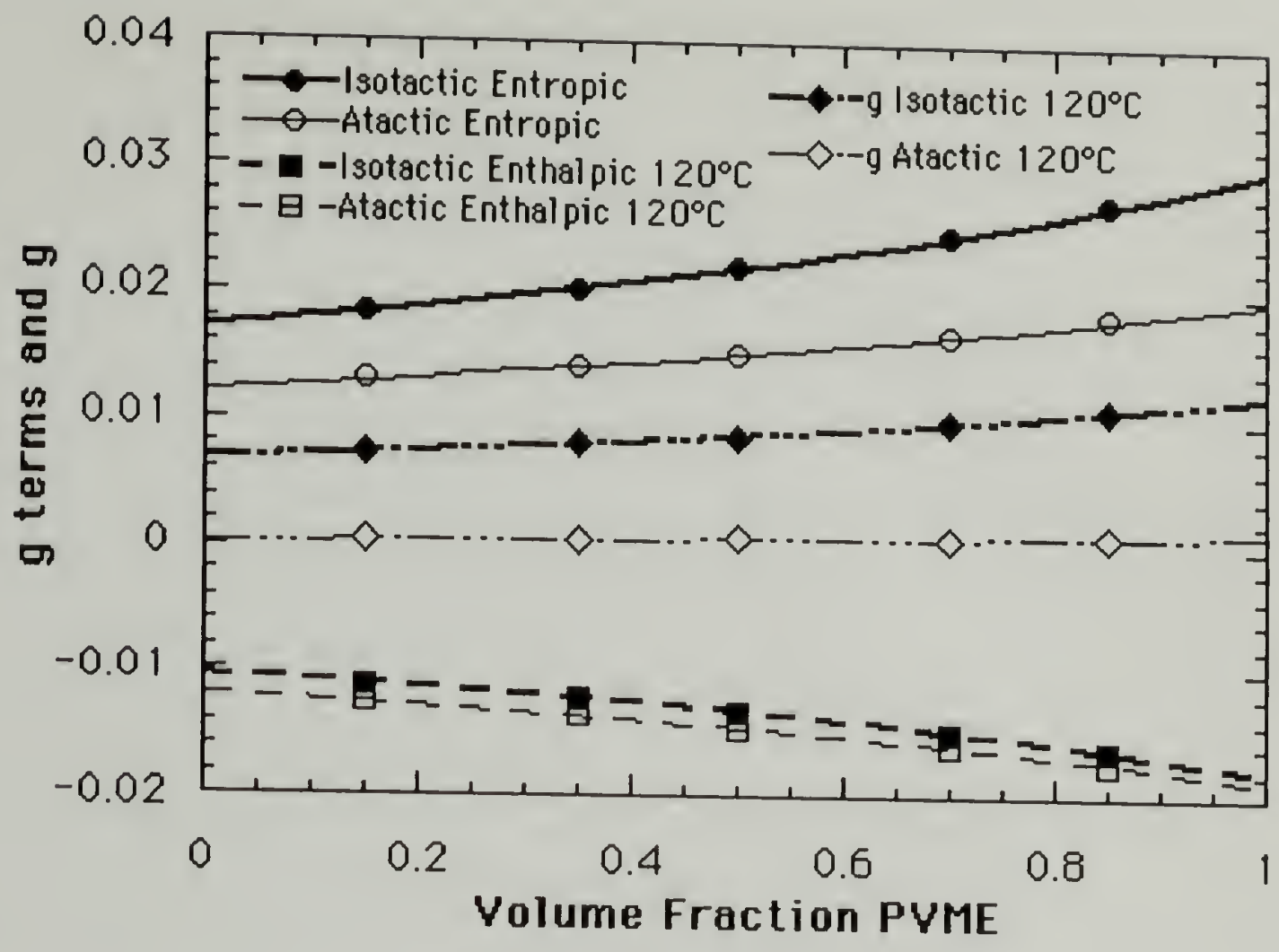

Figure 5.5 The entropic $[a+b_0/(1-c\,\phi)]$ and the enthalpic $[b_1/(1-c\,\phi)]$ components of g (composition dependent χ) at 120°C for the isotactic and atactic PVME/PS blends.

entropic component become larger at higher fractions PVME, while the enthalpic differences become smaller. The dominance of the entropic terms as well as the changes in the Staverman parameter, c, indicate that the isotactic PVME in the blend shows a higher degree of ordering (and tighter packing) than the atactic PVME in comparison to the melts for the two materials. This leads to a relatively large decrease in entropy (the negative of the entropic terms as discussed above). Thus one is lead to the conclusion that the isotactic PVME in some way becomes more ordered in the blend, that is, interactions with PS in the blend increase the ordering of the isotactic PVME

more than atactic PVME. The ability of isotactic PVME to order in minimum energy conformations will be discussed in regard to simple molecular models in the next section. It is noted that this purported ordering increases with the fraction PVME in the blend. Thus it is probably a property which relates to the structural nature of the PVME component, specifically the tacticity.

The dominance of the entropic term in the shift in miscibility for the isotactic PVME/PS blends agrees with the critical point analysis given in Chapter 3.

G. Fractionation in Phase Separated Blends

Crystallization of polymers is known to proceed with a fractionation of molecular weight and exclusion of chains less likely to crystallize (such as less tactic chains)[8,9,10]. Such exclusion may play a role in the solvent cast blends described in Chapter 4. The fractionation of polymers in phase separation from polydisperse blends has not been extensively described in the literature. This may play a large role in the behavior of the LCST blends described in Chapter 4. A dramatic fractionation of the polydisperse PVME is predicted by the F-H-S theory. Figures 5.6 and 5.7 show M_W, M_N and M_W/M_N for the shadow phase versus the initial blend composition (cloud point phase composition) for the isotactic and atactic PVME blends respectively.

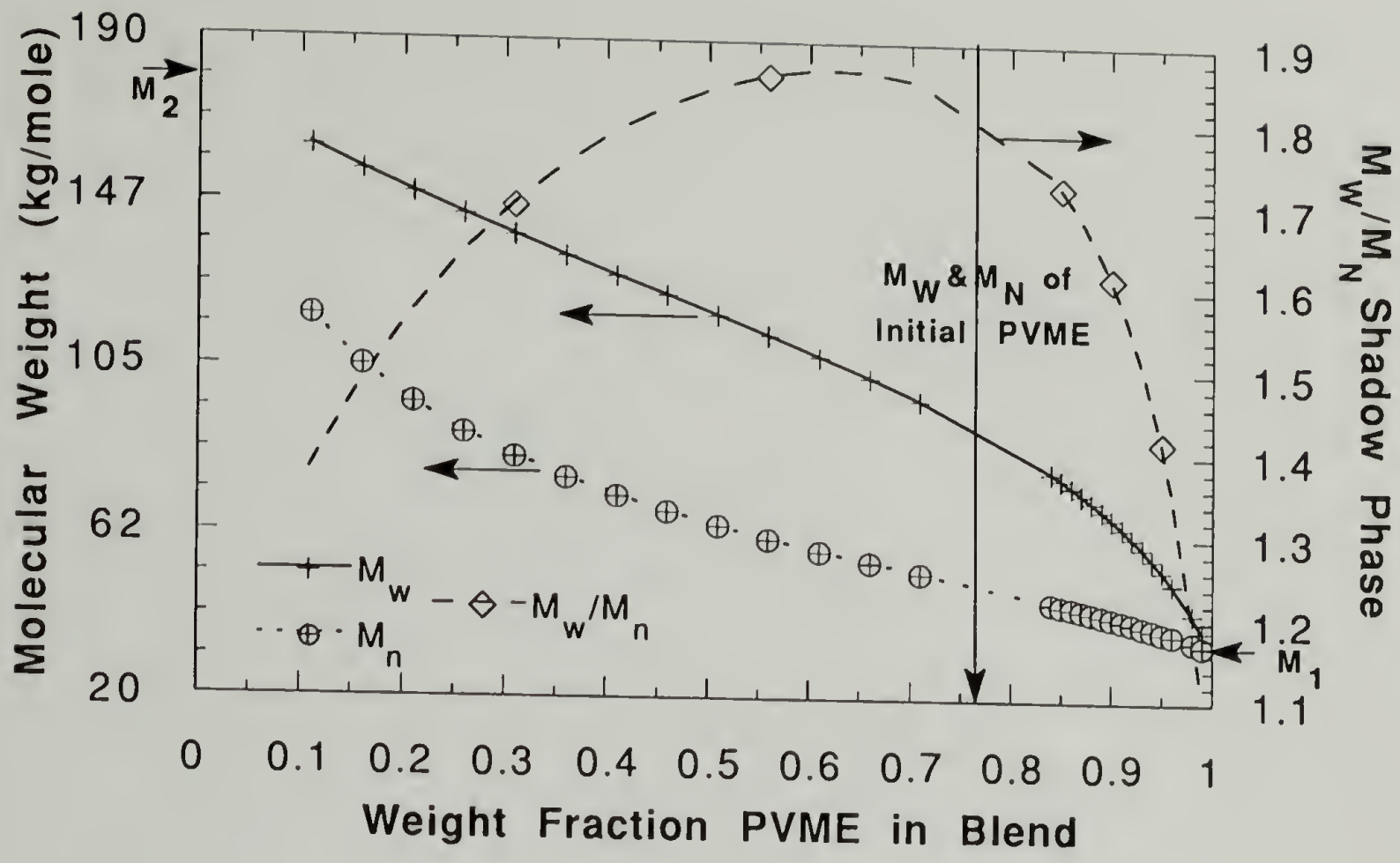

Figure 5.6 Fractionation of PVME in the incipient phase for the isotactic blend. M_W, M_N and $\frac{M_W}{M_N}$ of the incipient phase versus initial blend composition in weight fraction PVME (initial phase polydispersity is indicated by the arrow).

In both blends a fractionation effect is felt at the extremes of concentration. The polydispersity goes to 1 at the extremes of composition. For a blend close to pure PVME, only the high molecular weight monodisperse fraction, M_2 is phase separated at the CPC. Similarly, for a blend close to pure PS only the low molecular weight PVME, M_1, is phase separated at the cloud point. Further, by comparing Figures 5.3 and 5.4, with 5.6 and 5.7 it can be seen that only at the critical point are the original M_W and M_N of the PVME maintained (indicated by the large arrow in Figures 5.6 and 5.7). It should be noted that this fractionation effect probably has important

consequences with regard to the T_g, viscosity, degree of crystallinity and modulus of the incipient phase which is formed. In the above

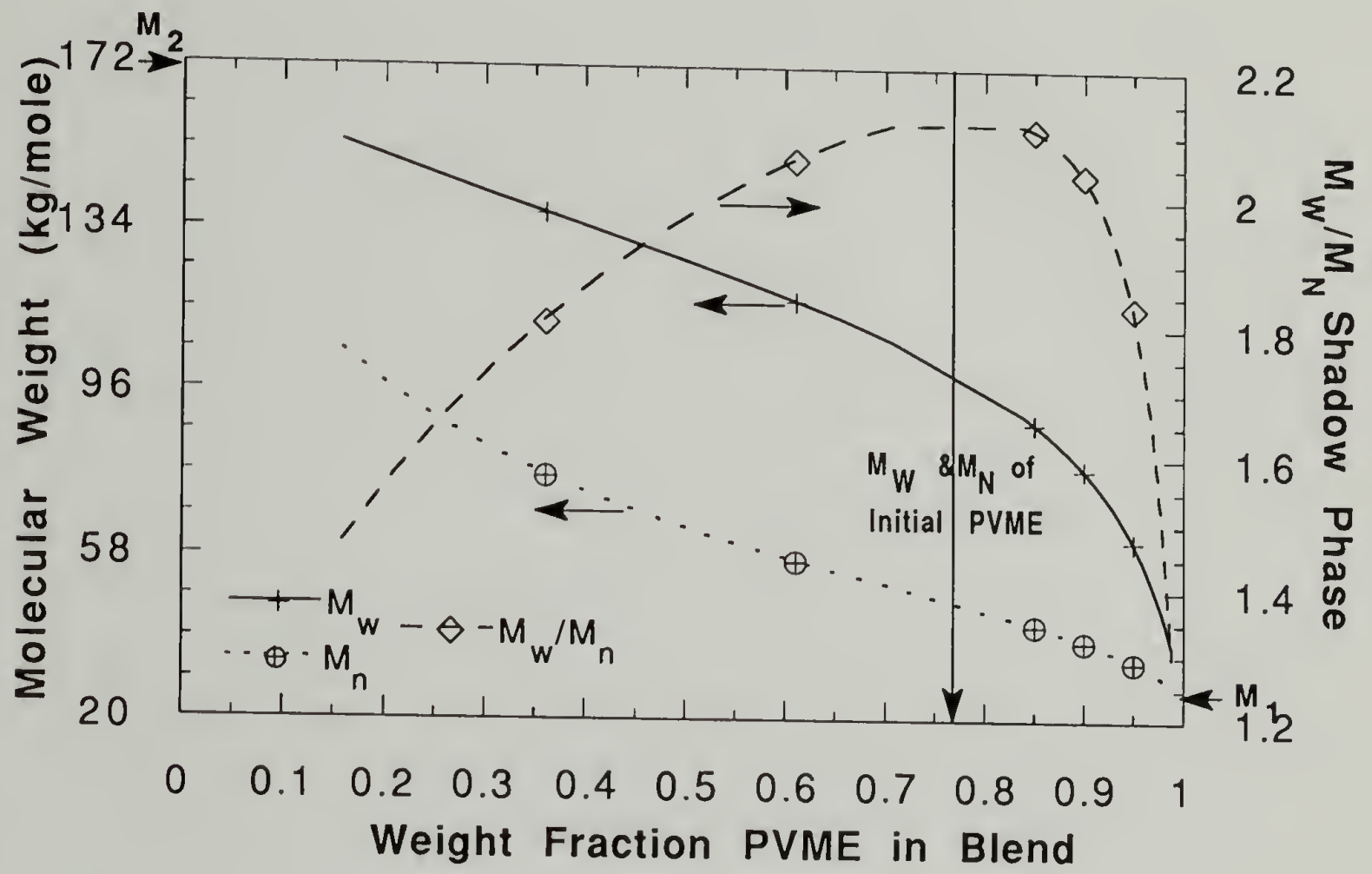

Figure 5.7 Fractionation of PVME in the incipient phase for the atactic blend. M_W, M_N and $\frac{M_W}{M_N}$ of the incipient phase versus initial blend composition in weight fraction PVME (initial phase polydispersity is indicated by the arrow).

analysis we have only considered thermodynamic behavior which dominates at the earliest stages of phase separation. In practice the later stages of phase separation would be governed by transport properties, interfacial properties of the phases being formed and thermodynamic driving forces which would change with the composition of the phases and depth of quench. The fractionation and

shifting of the incipient phase composition shown for the initial conditions should, however, serve as an indication of the general behavior for phase separation in a polydisperse blend of this type.

With respect to a 15% PVME blend such as was used in the LCST mechanical tests of Chapter 4, a fractionated PVME rich phase of high molecular weight PVME with lower polydispersity will be produced. It is believed that the higher molecular weight material may not crystallize in the presence of the small amount of PS which also exists in this phase.

H. Estimation of $c_{pvme/ps}$ Using Simple Molecular Models.

In addition to the cloud point determination of $c_{PVME/PS}$ for the isotactic material an estimation was made using a simple molecular modelling program[11] based on Allinger's MM2 conformational analysis technique[12,13]. Projections of the molecules were produced (shown in Figures 5.8, 5.9 and 5.10) after performing an energy minimization for isolated isotactic and heterotactic PVME chains and heterotactic PS chains all of 20 mer units. As discussed in section 5.F, the ordering achievable in the isotactic blends and not in the atactic blends becomes apparent after referring to Figures 5.8 and 5.9. The isotactic material is capable of forming a sheet like structure in these simple models formed of helical chains (more apparent in non-space filling models).

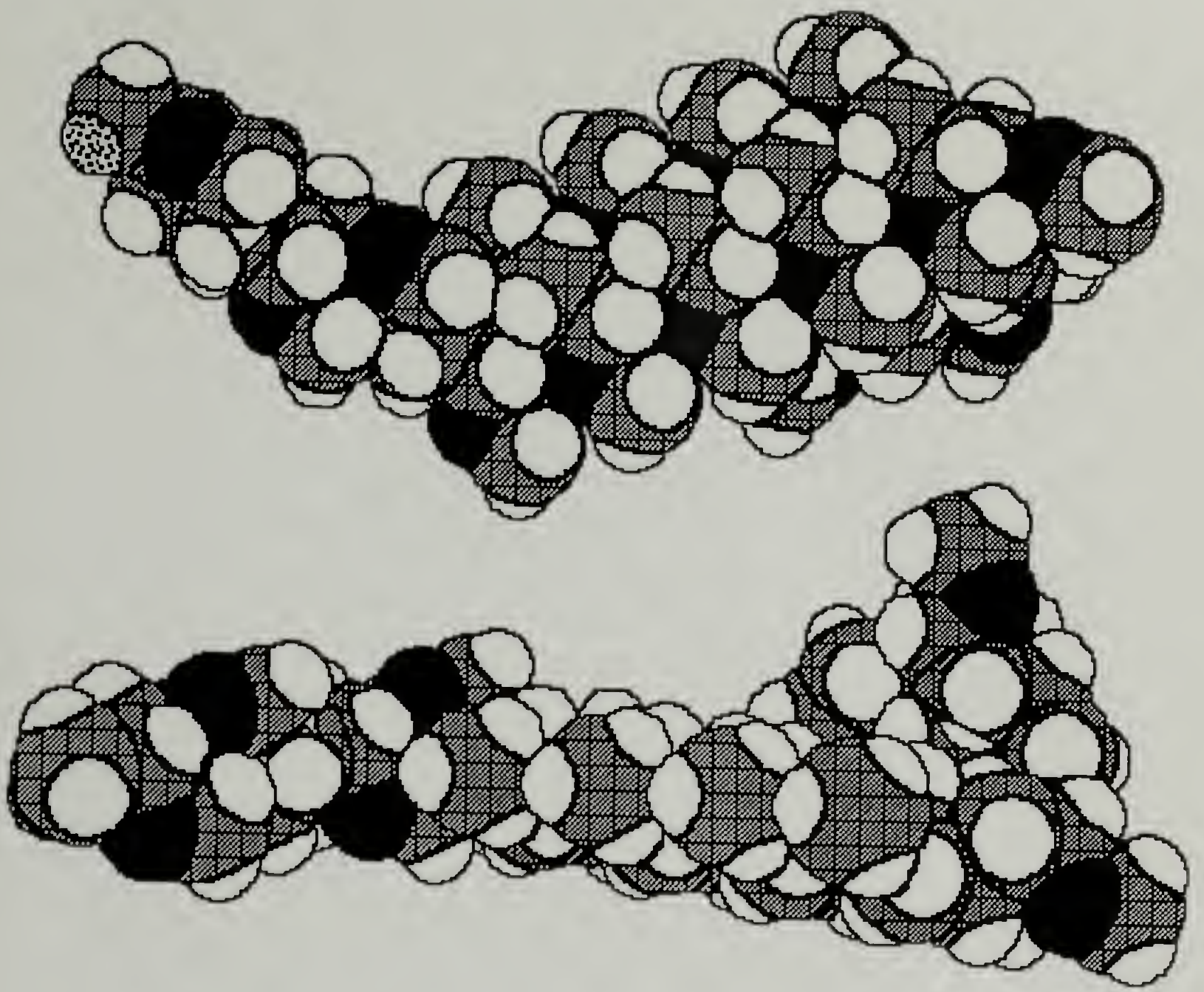

Figure 5.8 Isotactic PVME (two space filling projections at 90°) with a degree of polymerization of 20. Estimated $c_{PVME/PS} = 0.411$ (a value of 0.425 was obtained from the cloud point fits). White regions are hydrogen, black are oxygen and grey are carbon. The speckled hydrogen in the top view is a deuterium tag at the end of the chain.

A heterotactic oligomer produced in the same way is shown in Figure 7.11. This isomer forms a completely different structure in these rudimentary models. The sheet like form is absent. Instead, a more worm like chain with kinks is seen. The regular structure caused by the tacticity acts to reduce the surface area of the oligomer on a scale of 6 to 15 mer units. Thus, it is apparent that simple models of chain

interactions, such as the Hildebrand theory, which do not account for larger scale, conformational differences may be deficient.

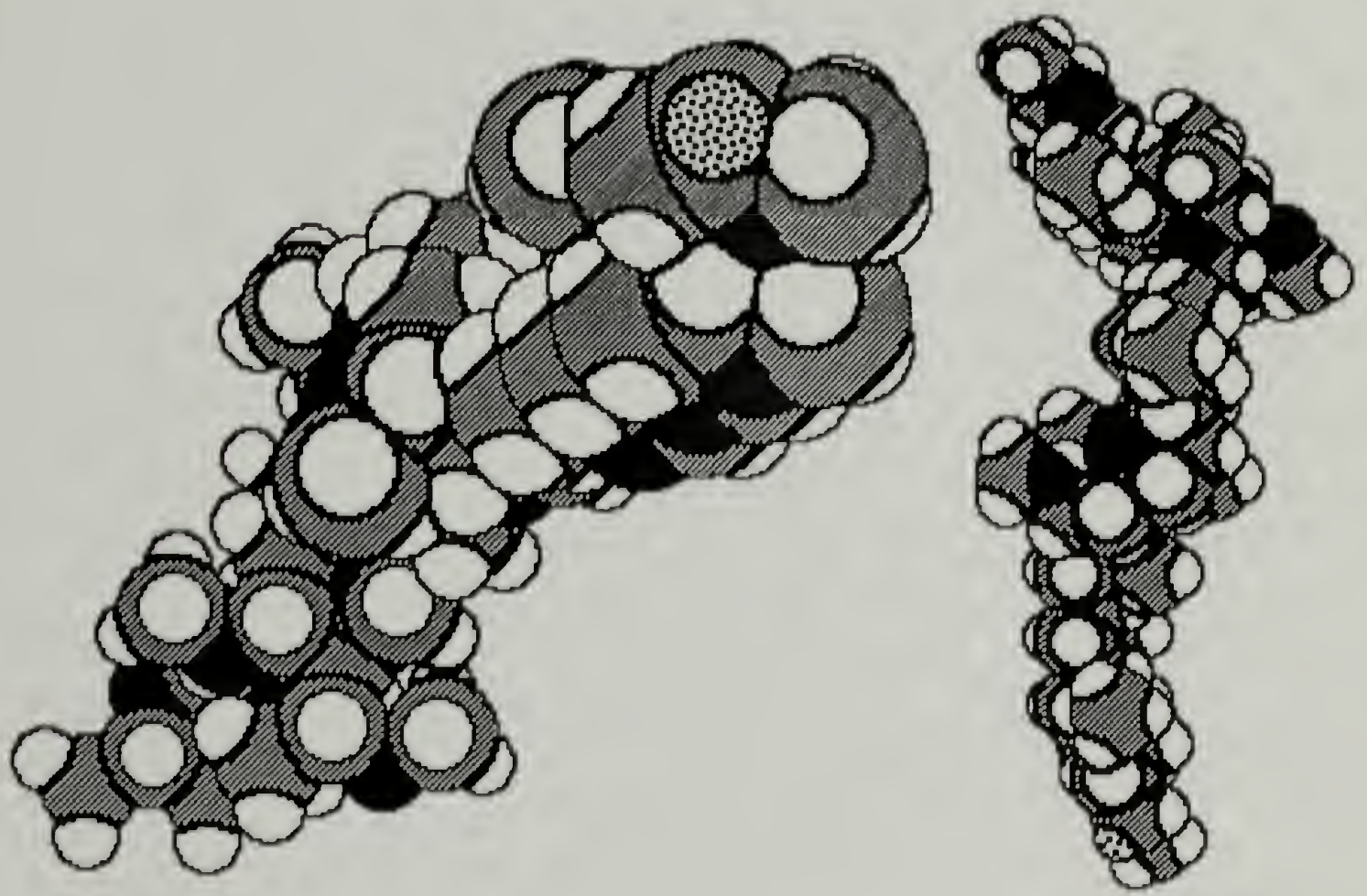

Figure 5.9 Heterotactic PVME with a degree of polymerization of 20. Two space filling projections at 90° are shown, one being an end view and the other a side view. Estimated $c_{PVME/PS} = 0.393$. A value of 0.36 was used in the cloud point fits as determined from low molecular weight materials using the method of Bondi.

A model for oligomeric PS of 20 mer units was also made, Figure 5.10. This model showed a worm like chain with kinks as in the heterotactic PVME. A marked orientation of the aromatic side groups is observed.

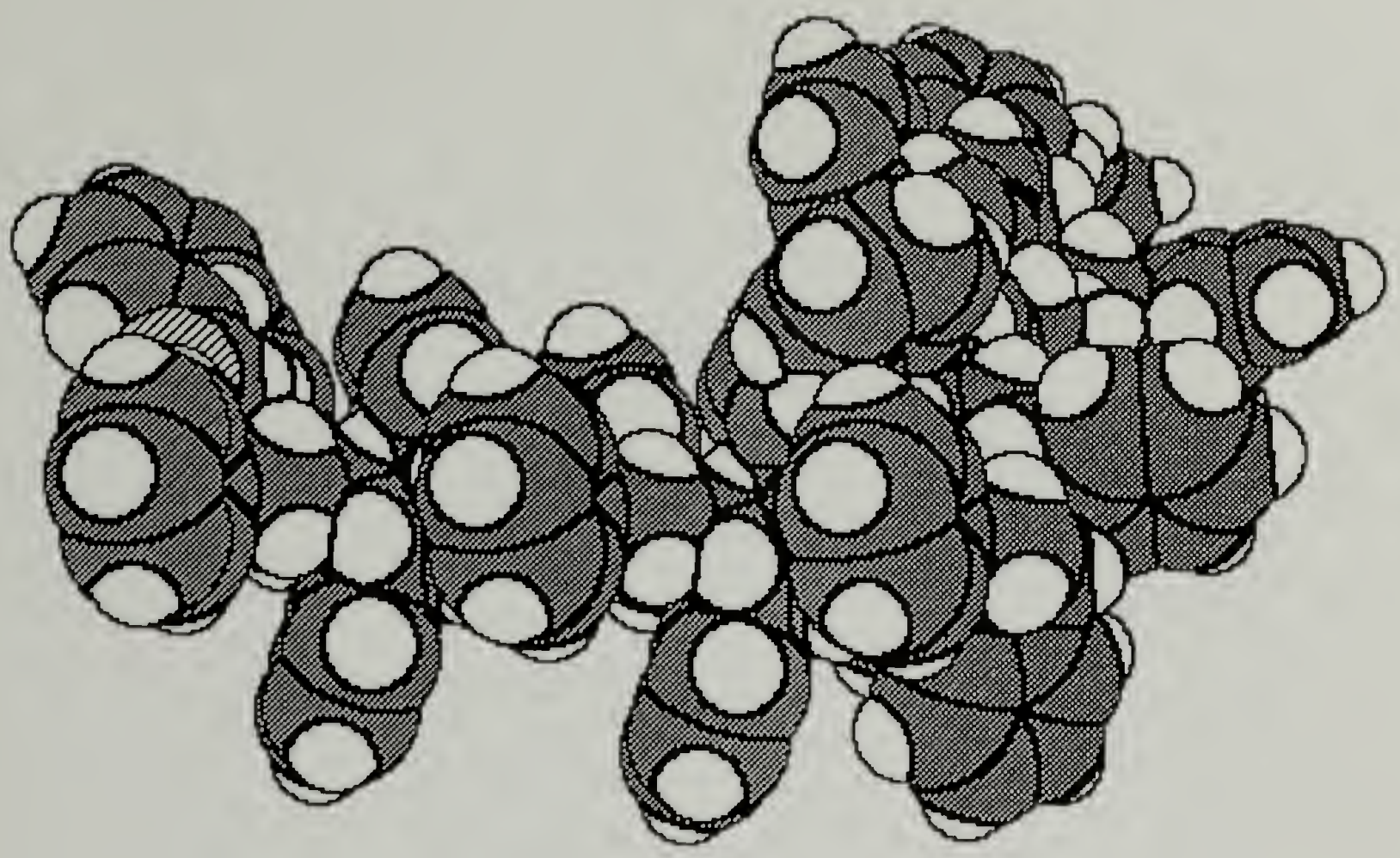

Figure 5.10 Heterotactic PS with a degree of polymerization of 20. Model was used to estimate the surface area of a PS chain for use in the calculation of $c_{PVME/PS}$. Grey areas are carbon, white areas hydrogen and hatched areas deuterium tagged end groups.

From various projections of the models an estimate for the surface areas was made. These surface areas were used to calculate $c_{PVME/PS}$. Values of 0.393 for the heterotactic and 0.411 for the isotactic were obtained in this way. An increase in $c_{PVME/PS}$ for the isotactic material agrees with the cloud point measurements and the results in Table 5.1 (an increase in c was caused by a smaller surface area per mer in the isotactic oligomer). For oligomers with such low degree of polymerization it was impossible to mix different tacticities in the percentages observed experimentally. If this were possible the surface area differences between isotactic and atactic PVME could be estimated more accurately. The tacticity of the PS used in the

experiments is not know but most likely contains at least 25% isotactic triads. Thus the heterotactic PS surface area is probably over estimated in these models. Since $c_{PVME/PS} = 1 - \frac{S_{PVME}}{S_{PS}}$ this would have the effect of increasing $c_{PVME/PS}$. It should be noted that localized regions of isotactic material, Figure 5.8, several mer units long in a heterotactic chain, Figure 5.9, might serve as strong bending points in the structure leading to a reduced available surface area such as observed experimentally and calculated using the Bondi method.

I. Predictions Concerning the Kinetics of Phase Separation from F-H-S Analysis of Cloud Point Curves

Using the calculated values for a, b_0, b_1, and c, it is possible to predict g (composition dependent χ-parameter) over a range of temperatures. One use for such predicted g values is in the estimation of the growth rate for phases in the immiscible regime. Since the behavior of g is predicted from data at the miscibility limit (for the case of cloud point data) a successful prediction into the immiscible regime could be considered a test of the formalisms used in deriving the g function.

The thermodynamic driving force for phase separation in the immiscible regime is given by the ratio,

$$\frac{D_{app}}{D_c(T)} = \frac{(g - g_s)}{g_s} \qquad (5.23),$$

where g_s is the composition dependent χ-parameter at the spinodal temperature (see Chapter 6 for a discussion of the Cahn-Hillard analysis of phase separation). Considering only a composition of 75% PVME by weight (close to the critical composition so as to avoid the binodal region) it is possible to predict the thermodynamic driving force for phase separation for the isotactic and atactic blends, Figure 5.11.

In this analysis g_s was calculated using the FHS parameters of Table 5.1 in equation 5.5 and the cloud point temperature for a 75% PVME blend under the assumption that this is the critical composition and the critical temperature ($T_{cp\ iso} \approx 109°C$, $T_{cp\ atactic} \approx 121°C$). $\frac{g - g_s}{g_s}$ values calculated in this way are much smaller for the isotactic blend for similar quenches above the critical temperature. Drastically slower kinetics are therefore predicted ($D_c(T)$ is expected to have very similar values for the different tacticities since they have essentially identical glass transition temperatures).

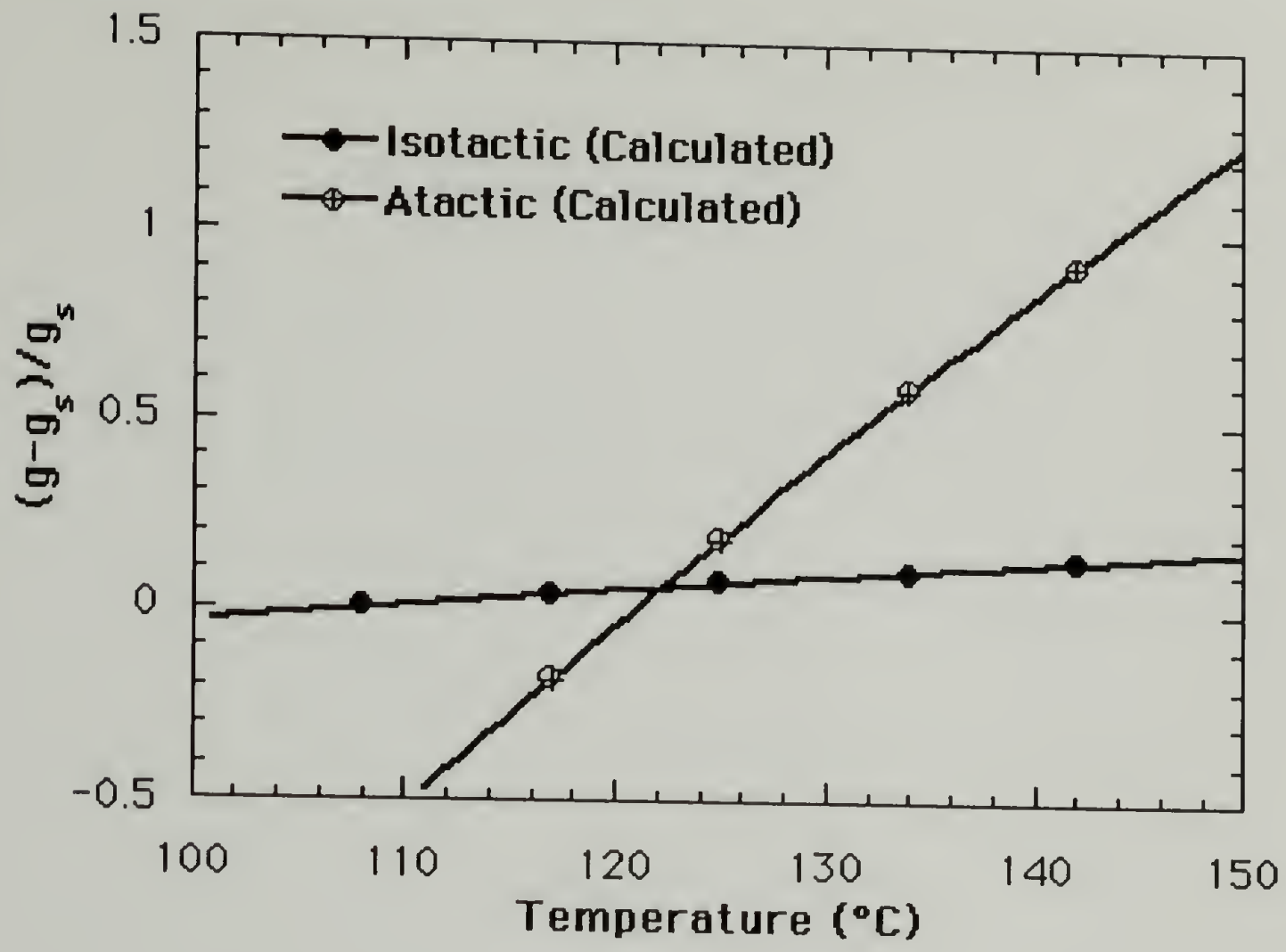

Figure 5.11 Predicted behavior for $\frac{g - g_s}{g_s}$ from the F-H-S analysis. This is the thermodynamic driving force for phase separation above the coexistence curve. Isotactic PVME shows lower miscibility and much slower kinetics above the miscibility limit $\frac{g - g_s}{g_s} = 0$.

Combining equations 5.5 and 5.23 it is possible to estimate the sensitivity of $\frac{g - g_s}{g_s}$ to changes in the various F-H-S parameters,

$$\frac{D_{app}}{D_c(T)} = \frac{b_1 (T_s - T)}{T(T_s a + T_s b_0 + b_1 - T_s a c \phi_2)} \qquad (5.24),$$

$$\left(\frac{\delta(Dapp/Dc(T))}{\delta b_0}\right)_{a,b1,c,Ts,T,\phi 2} =$$

$$\frac{b_1 T_s (T_s - T)}{T(T_s a + T_s b_0 + b_1 - T_s a c \phi_2)^2} \qquad (5.25)$$

$$\left(\frac{\delta(Dapp/Dc(T))}{\delta a}\right)_{b0,b1,c,Ts,T,\phi 2} =$$

$$(1 - c \phi_2)\left(\frac{\delta(Dapp/Dc(T))}{\delta b_0}\right)_{a,b1,c,Ts,T,\phi 2} \qquad (5.26)$$

$$\left(\frac{\delta(Dapp/Dc(T))}{\delta b_1}\right)_{a,b0,c,Ts,T,\phi 2} =$$

$$\frac{(ac\phi_2 - a - b_0)}{b_1}\left(\frac{\delta(Dapp/Dc(T))}{\delta b_0}\right)_{a,b1,c,Ts,T,\phi 2} \qquad (5.27)$$

$$\left(\frac{\delta(Dapp/Dc(T))}{\delta c}\right)_{a,b0,b1,Ts,T,\phi 2} =$$

$$-a \phi_2 \left(\frac{\delta(Dapp/Dc(T))}{\delta b_0}\right)_{a,b1,c,Ts,T,\phi 2} \qquad (5.28)$$

In equation 5.26 (for δa) , $(1 - c \phi_2)$ is always less than one (close to 0.7), in equation 5.27 (for δb_1) , $\frac{(ac\phi_2 - a - b_0)}{b_1}$ is generally less than one

(close to 0.003) and in equation 5.28(for δc) , -a ϕ_2 is generally very small (close to 0.0007). The magnitude of the change in the parameters must also be taken into account ($\Delta a \cong 0.001$, $\Delta b_0 \cong 0.004$, $\Delta b_1 \cong 0.6$, and $\Delta c \cong 0.06$). When this is done it is clear that $\frac{g - g_s}{g_s}$ is most sensitive to the change in the entropic parameter 'b_0' for the conditions under consideration. The change in the enthalpic parameter, 'b_1',has about 1/4 the effect of 'b_0', change in 'a' has about 1/6 the effect of 'b_0', and change in the Staverman parameter, 'c', has about 1/100 of the effect of 'b_0'. Since b_0 is related to the composition dependence of g (equation 5.5), it would be expected that differences in the kinetics of phase separation would be greater at higher concentrations of PVME in the initial blend and for larger Staverman parameters. Equations 5.24 and 5.25 show, however, that this effect is of additive (5.24) or second order (5.25) importance.

J. Mechanical Properties and the F-H-S Analysis

The failure of the LCST phase separated blends (discussed in Chapter 4) to display shear bands and significantly improved energy absorption over a-PVME phase separated blends can now be discussed in terms of the F-H-S analysis. As was discussed above, the selective fractionation of higher molecular weight PVME into the incipient phase (rubbery domains) reduces the opportunity for crystallization to occur, thereby rendering the isotactic and atactic materials mechanically very similar.

The isotactic material is less miscible with PS than the atactic material, however, the much slower kinetics of phase separation for the isotactic material would probably produce smaller phases than the atactic phases (as will be discussed in Chapter 6). This may account for the slight difference in mechanical behavior between the isotactic and atactic melt blends which was observed.

The solution cast blends, on the other hand, have PVME phases which are inherently crystalline. In fact, crystallization may serve to fractionate the more isotactic and lower molar mass materials from the melt.

Thus, the F-H-S analysis has given a picture of the reasons for the poor results in the LCST phase separated blends and has made predictions towards the kinetics of phase separation which will be investigated in the next chapter. In Chapter 7, the ideas which have been presented here will be further pursued in regard to SANS measurements on blends of the isotactic and atactic PVME with deuterated PS.

References

1. H. Tompa, *Trans. Farad. Soc.*, **45**, 1142 (1949)

2. R. Koningsveld, A. J. Staverman, *J. Polym. Sci., Part A2*, **6**, 305, 325, 349 (1968).

3. R. Koningsveld, A. J. Staverman, *Koll. Polym. Z.*, **218**, 114 (1968).

4. R. Koningsveld, *Adv. Coll. Interface Sci.*, **2**, 151 (1968).

5. R. Koningsveld, *Disc. Farad. Soc.*, **49**, 144 (1970).

6. A. Bondi, *J. Phys. Chem.*, **68**, 441 (1964).

7. K. S. Schweitzer, J. G. Curro, *J. Chem. Phys.*, **91**(8), 5059 (1989).

8. M. Satkowski, PhD Dissertation, University of Massachusetts, Amherst, 1990.

9. B. Morra, Ph.D. Dissertation, University of Masssachusetts, Amherst, 1981.

10. T. Russell, Ph.D. Dissertation, University of Massachusetts, Amherst, 1979.

11. M Rubenstein and S. Rubenstein, *Chem 3D, The Molecular Modeling System Version 2*, Cambridge Scientific Computing Inc., Cambridge, MA 1989

12. N. L. Allinger, *J. Amer. Chem. Soc.*, **99**(25), 8127 (1977).

13. U. Burkert and N. L. Allinger, *Molecular Mechanics, ACS Monograph 177*, Amer. Chem. Soc., Washington D.C. 1982.

CHAPTER 6

TACTICITY EFFECTS ON THE KINETICS OF PHASE SEPARATION

A. Introduction

The equilibrium thermodynamics of the phase behavior governs the direction in which phase separation will tend. In a practical blend, such as those discussed in Chapter 4, the domain sizes and final morphology will be governed by the kinetics of phase separation. The early stages of phase separation are, to some degree of accuracy, described by Cahn-Hilliard theory. The mid-stage of phase separation has been a matter of recent investigation and will be discussed at the end of this chapter. Late stage phase separation is generally described by Ostwald ripening[1,2]. Late stages depend on surface tensions between components, the viscosity of components and and a variety of other parameters such as stresses in the material. In this chapter the early stages of phase separation will be discussed with a brief indication of possible extension of this analysis to mid-stage phase separation.

This analysis is of importance not only in predicting the kinetic factors at work in the final morphologies of the LCST blends of Chapter 4, but as a test of the F-H-S analysis given in the last chapter. The F-H-S analysis has predicted drastically slowed kinetics of phase separation for the isotactic blends.

B. Cahn-Hillard Theory

The linear Cahn-Hillard theory of the early stages of phase separation was used to analyze light scattering data[3,4], During the initial stages of phase separation the intensity of light scattered at all angles is expected to increase exponentially,

$$I(q,t) = I(q,t=0) \exp(2R(q)t) \qquad (6.1),$$

where $q = \frac{4\pi}{\lambda} \sin\left(\frac{\theta}{2}\right)$, t is the time of phase separation and R(q) is the amplification factor for phase separation or the growth rate. Cahn-Hillard theory defines R(q) for an incompressible blend as,

$$R(q) = D_c\, q^2 \left(-\left(\frac{\delta^2 f}{d\phi_2^2}\right) - 2\kappa q^2 \right) \qquad (6.2),$$

where D_c is the translational diffusion constant, f is the free energy density of the system at composition ϕ_2, and κ is the coefficient of the composition gradient in the development of the Cahn-Hillard theory.

For binary blends of linear polymers under the mean field approximation equation (6.2) can be given as,

$$R(q) = D_c\, q^2 \left(\frac{(\chi - \chi_s)}{\chi s} - \frac{R_0^2\, q^2}{36} \right) \qquad (6.3),$$

where χ is the Flory-Huggins interaction parameter, χ_s is the interaction parameter at the spinodal and R_0 is the unperturbed chain

dimension. Equation 6.3 suggests plots of $\frac{R(q)}{q^2}$ versus q^2 in order to determine the apparent diffusion constant, D_{app},

$$D_{app} = D_c \left(\frac{\chi - \chi_s}{\chi_s} \right) \qquad (6.4),$$

and $\left(\frac{D_c R_0^2}{36} \right)$. As is indicated by equation 6.4, D_{app} is equal to zero at the spinodal temperature. The value of q for which R(q) = 0 is "q"-critical (q_c). Composition fluctuations with wave numbers larger than this q value will not decompose into a phase separated structure. Equation (6.3) also predicts a balance between transport and thermodynamic effects which leads to a maximum in R(q) at "q_m". "q_m" is related to "q_c" by,

$$q_m^2 = \frac{q_c^2}{2} \qquad (6.5).$$

"q_m" is the q value at the initial stages for the scattering "halo" from spinodal decomposition of the blend discussed in Chapter 3 (Figure 3.2).

C. Experimental

Isotactic PVME, i89 (M_W = 89kg/mole, M_N = 49.1 kg/mol, M_Z = 144.9 kg/mol), was prepared using cationic polymerization followed by solvent fractionation as reported in Chapter II. Atactic PVME, a99 (M_W = 99 kg/mole, M_N = 46.5 kg/mol,

M_Z = 151.3 kg/mol), was purchased from Scientific Polymer Products Inc. and fractionated (as discussed in Chapter 2). The triad tacticities of the two polymers were determined using proton NMR (a99 : 31% isotactic, and 69% heterotactic; i89 : 55% isotactic, 40% heterotactic, and 5% syndiotactic). The glass transition temperature for the two polymers was essentially identical, -29°C, in accord with the findings of Karasz and MacKnight[5] for other monosubstituted vinyl polymers. Relatively monodisperse PS , M_w/M_n = 1.03, of molecular weight M_w =120 kg/mole (Polymer Laboratories, Amherst, MA) was blended with each of the two PVME samples. Molecular weights of all polymers are reported as measured by GPC in terms of polystyrene standards. A Mark-Houwink analysis of the isotactic and atactic PVME indicated that this lead to errors in the molecular weight of less than 5% which is within the accuracy of the measured values.

Blends of PVME/PS were cast from toluene solutions at 30°C and allowed to air dry. The films were further dried in a vacuum oven at 70°C for a week and finally in a vacuum oven at 100°C for at least 6 hours before scattering measurements were made.

Cloud point measurements were performed on relatively thick films, 50-100 μ cast on one microscope cover slip. Kinetic measurements were made on much thinner films generally close to 10 μ thick held between two cover slips. These thinner samples are necessary in order to reduce multiple scattering and obtain a wide angle pattern. The cloud point samples can be very thick using the apparatus described in Chapter 3. Integrated scattering intensity from an angular range of about 50° to 140° was measured using the

apparatus shown in Figure 3.1 which has been previously described[1]. A one dimensional multichannel analysizer, OMA (Princeton Instruments) coupled with a PC was used to perform the kinetics studies, also shown in Figure 3.1. A screen was used to produce a real image of the scattering pattern and a macro-zoom lens was attached to the OMA. The OMA, lens and screen were set at an angle of 30° from the main beam. The hot stage and sample were set at an angle of about 25° in order to circumvent internal reflection from the cover slip/air interface. In this way angles from 0° to 75° could easily be observed. Adjustments for a smaller angular range could be made in minutes with this setup. All kinetics measurements reported were performed on 75% by weight PVME blends prepared as described above. This composition has been determined to be close to the critical composition for these blends, thus, only spinodal decomposition is expected in the early stages. (Off critical compositions will only produce spinodal decomposition in deep quenches.)

Samples for the cloud point measurements were equilibrated on the hot stage at temperatures close to the phase separation temperature prior to measurements. Measurements at several heating rates were taken and the phase separation temperature was extrapolated to zero heating rate as described in Chapter 3. Samples for the kinetics measurements were equilibrated at about 100°C on a hot stage near the apparatus and quickly transferred to the apparatus which was at the experimental temperature. Due to the small mass of the cover slips and samples thermal equilibrium was reached in much

less than a minute as measured with a thermocouple attached to the cover slip.

D. Kinetics of Phase Separation

Figures 6.1 and 6.2 show a series of light scattering patterns (reduced intensity versus q) for isotactic and atactic PVME blended

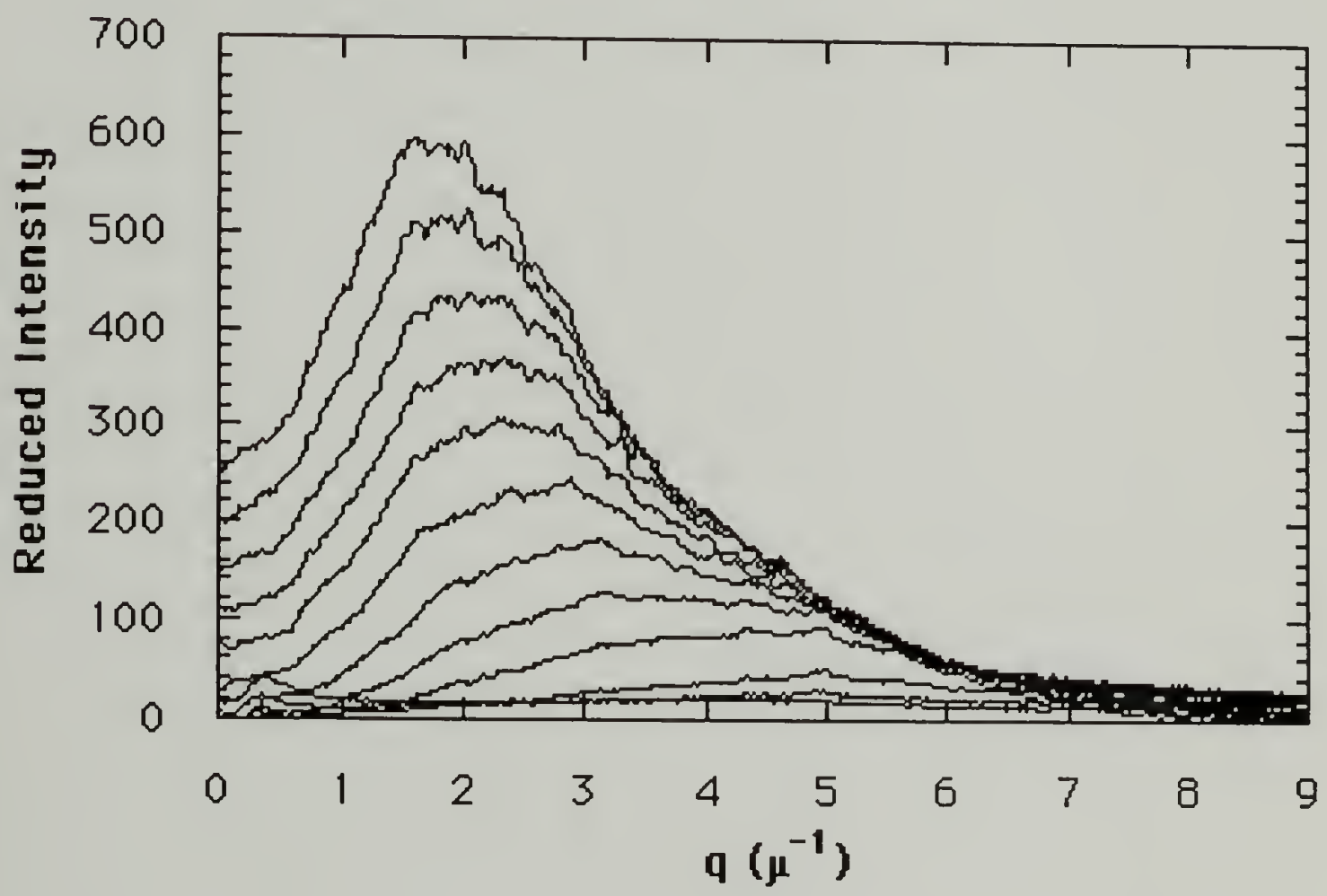

Figure 6.1 A series of light scattering measurements for isotactic PVME blended with PS (75% PVME) at 130°C. (Critical temperature is 109°C.) The patterns are separated by about one minute.

with polystyrene (75% by weight PVME). In both cases the intensity monotonically increases as a function of time, the curves being separated by about 1 min in both cases. As will be noted from Figure

5.2, the cloud point occurs at about 109°C for the isotactic blend and at about 121°C for the atactic blend. The patterns for Figure 6.1 (isotactic) were measured at 130°C (a quench depth of 21°C). Figure 6.2 was measured at 123°C (a quench depth of 2°C). Curves in both Figures are separated by about one minute. Since the kinetic data

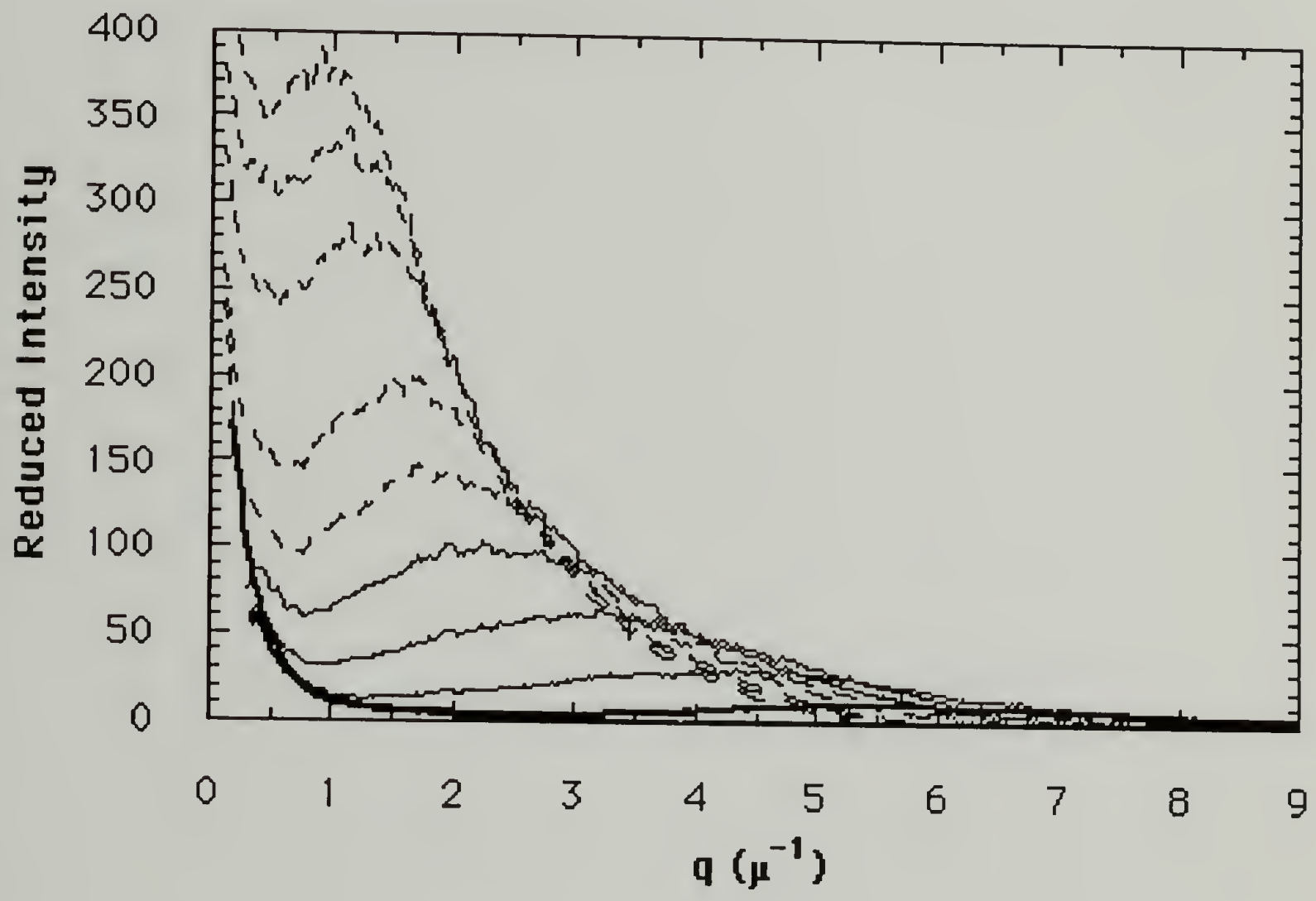

Figure 6.2 A series of light scattering measurements for atactic PVME blended with PS (75% PVME) at 123°C. (Critical temperature is 121°C.) The patterns are separated by about one minute.

in Figures 6.1 and 6.2 are comparable for drastically different quenches, they dramatically show a tacticity effect on the phase separation kinetics. Since the 21°C quench of the i-PVME/PS blend does not show large differences in rate of phase separation when

compared with smaller quenches for the same blend, the weak slope of Figure 5.11 for the isotactic blend is affirmed qualitatively.

Plots of the q value for the maximum in scattering intensity, q_{max}, versus time and the corresponding reduced intensity I_{max} versus time are given in Figures 6.3 and 6.4 for the isotactic and

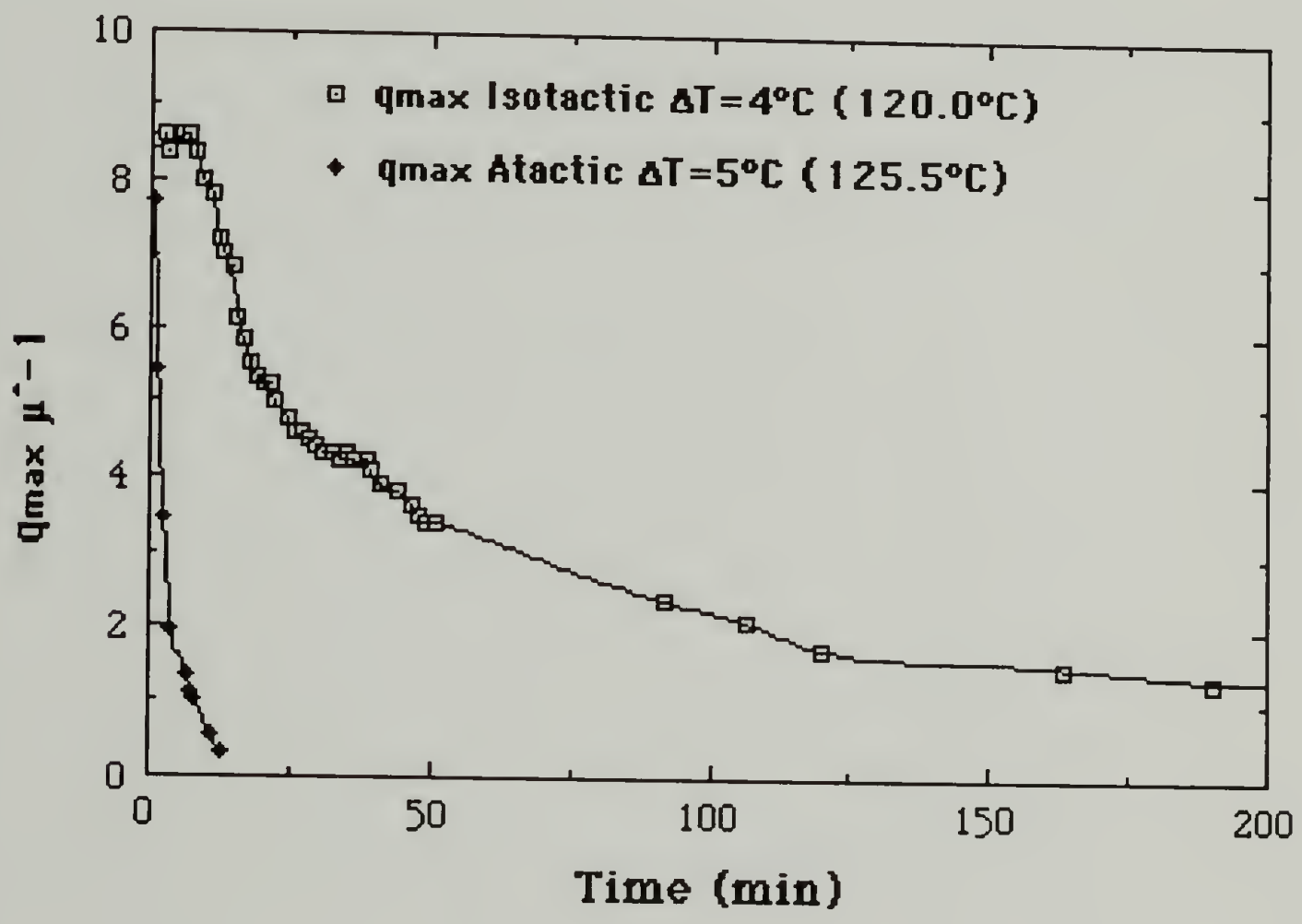

Figure 6.3 q_{max} versus time for isotactic and atactic PVME/PS blends.of about 4°C quench.

atactic blends at a quench depth of about 4°C (120°C and 126°C respectively). At this quench depth the isotactic material shows a region of constant q_{max} for about 10 minutes followed by movement of q_{max} to smaller angles. The atactic material shows little if any region of constant q_{max} and q_{max} rapidly decays to very low values.

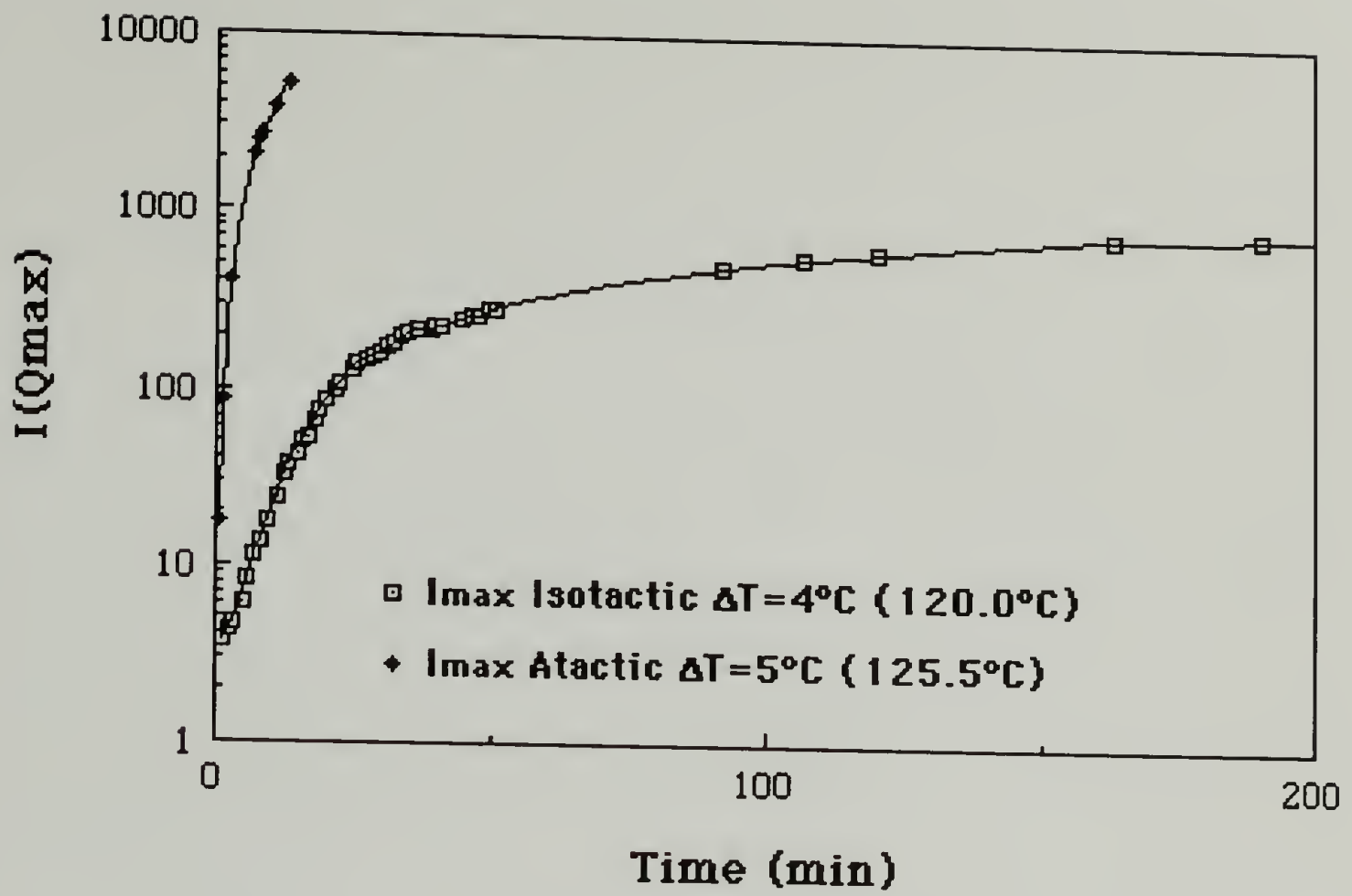

Figure 6.4 Dependence of the maximum in scattering intensity on time for isotactic and atactic PVME/PS blends.

In Figure 6.4 the isotactic blend shows a large region of linear growth followed by a nonlinear region (mid-stages of phase separation) and a broad late stage region. The atactic material on the same time scale rapidly decays. Clearly, the growth in size of the phases is much slower in the isotactic blend. In measurements at equal quench depths the kinetics are effected by the temperature dependence of D_c. This effect would increase the rate of phase separation (through $D_c(T)$) for the isotactic blend since it is measured at a higher temperature. The observed rate is, however, slower than that of the atactic PVME making this argument moot.

In Figure 6.5, ln(I) is plotted against time for a 16°C quench of the isotactic blend as suggested by equation 6.1. A series of q values are plotted.

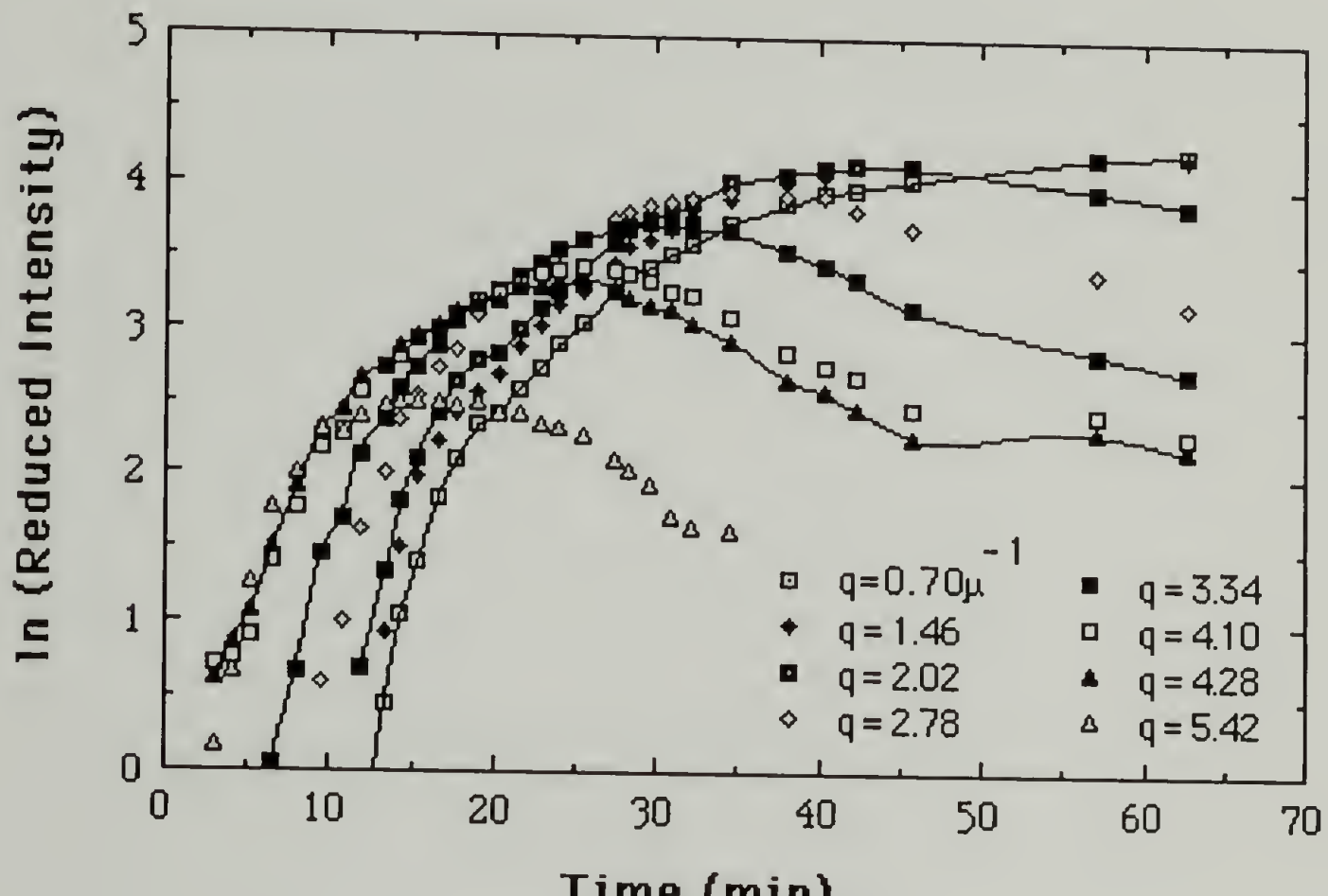

Figure 6.5 ln(I) versus time for a 16°C quench of the isotactic blend as suggested by equation 6.1.

At early stages (t < 10 min) a linear regime is observed for most of the q range. This corresponds to the early stages of phase separation for the isotactic blend. Deviation from linear Cahn-Hillard behavior occurs at later times. The slopes of the linear region of Figure 6.5 are plotted versus q in Figure 6.6. A maximum in R(q) occurs as indicated by Cahn-Hillard theory.

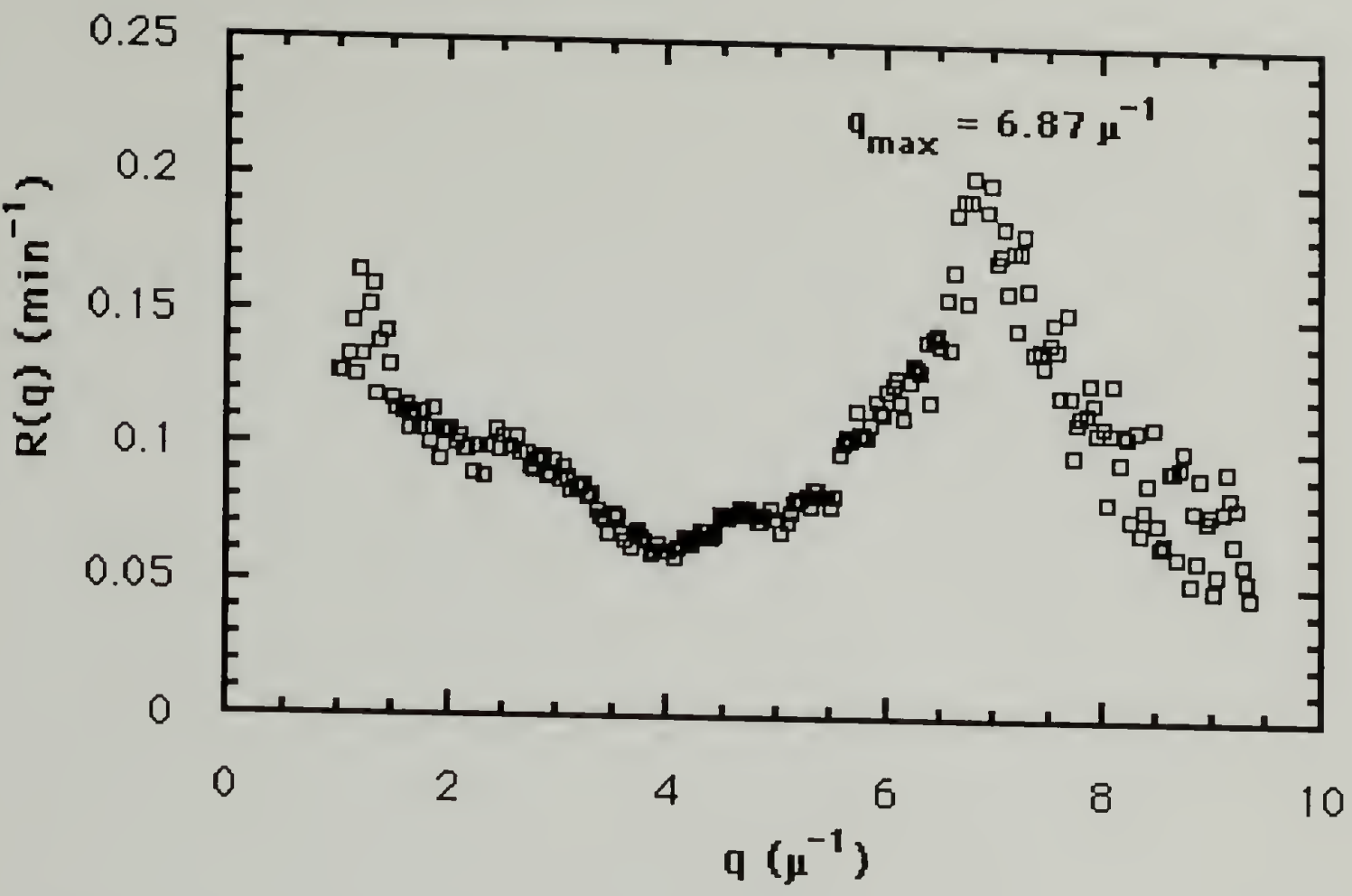

Figure 6.6 R(q) vs q for the isotactic blend of Figure 6.5 .

As noted above, equation 6.2 suggests plots of $\frac{R(q)}{q^2}$ versus q^2. Figure 6.7 shows such a plot for the data of Figures 6.5 and 6.6. A linear region is observed and a value for the apparent diffusion constant of 7.6×10^{-3} is obtained. For this case $q_c = 15\ \mu^{-1}$ and $q_m = 10\ \mu^{-1}$. This value is higher than the value indicated in Figure 6.7 (about 8.5 μ^{-1}), however the extrapolated q_c is an order of magnitude from the measured values in Figure 6.7 .

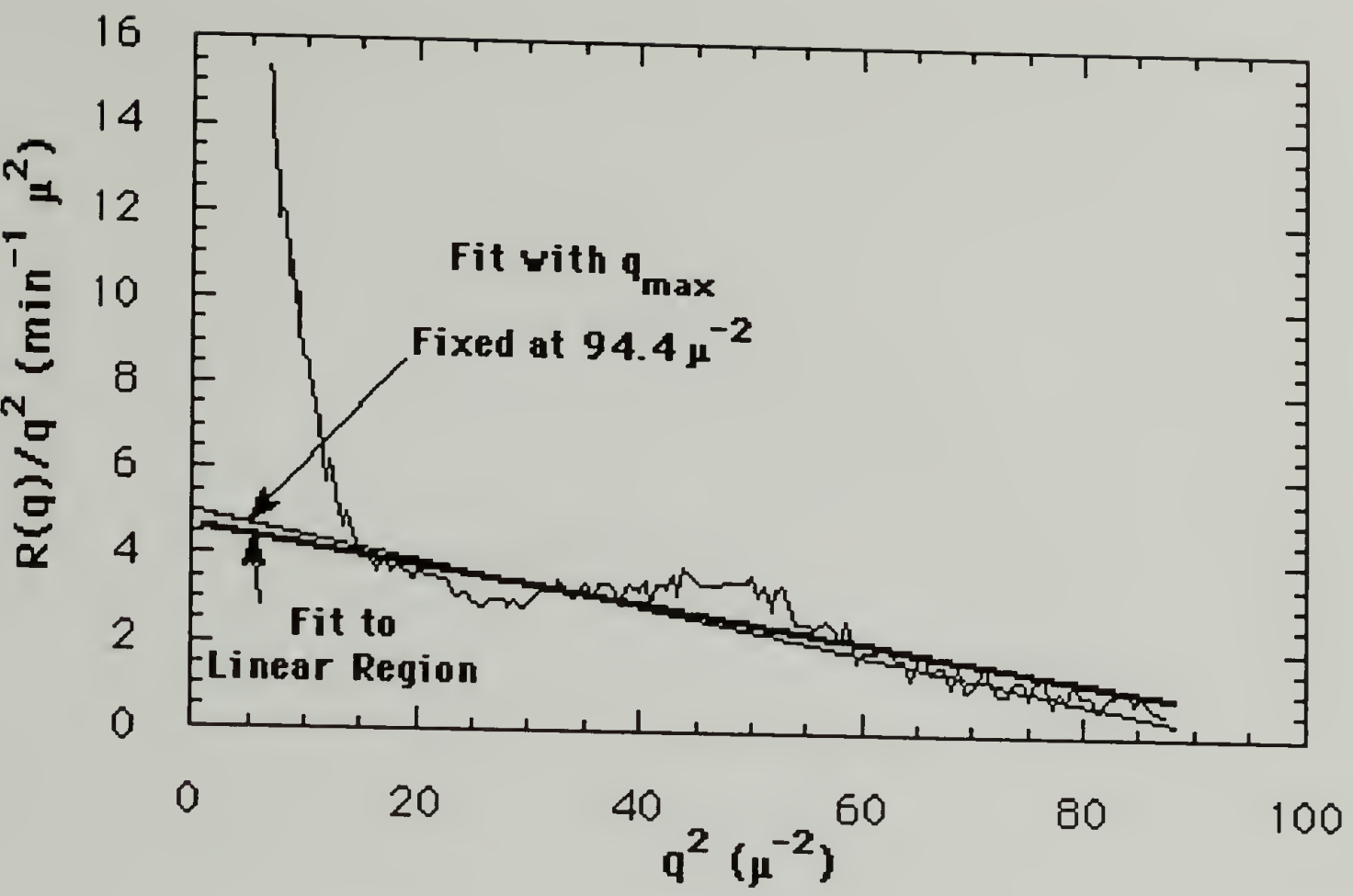

Figure 6.7 $\frac{R(q)}{q^2}$ versus q^2 for the isotactic blends of Figures 6.5 and 6.6 .

Values for D_{app} versus temperature are plotted in Figure 6.8. An extrapolation to $D_{app} = 0$ is made in order to determine the spinodal temperature (equation 6.4) whose values are given in Table 6.1 (T_s). Three spinodal temperatures are indicated in Table 6.2 for the 75% PVME blends. Values obtained by the above extrapolation differed by about 2°C from those measured using the cloud point technique. T_{min} (Thin Films) is the minimum temperature at which phase separation

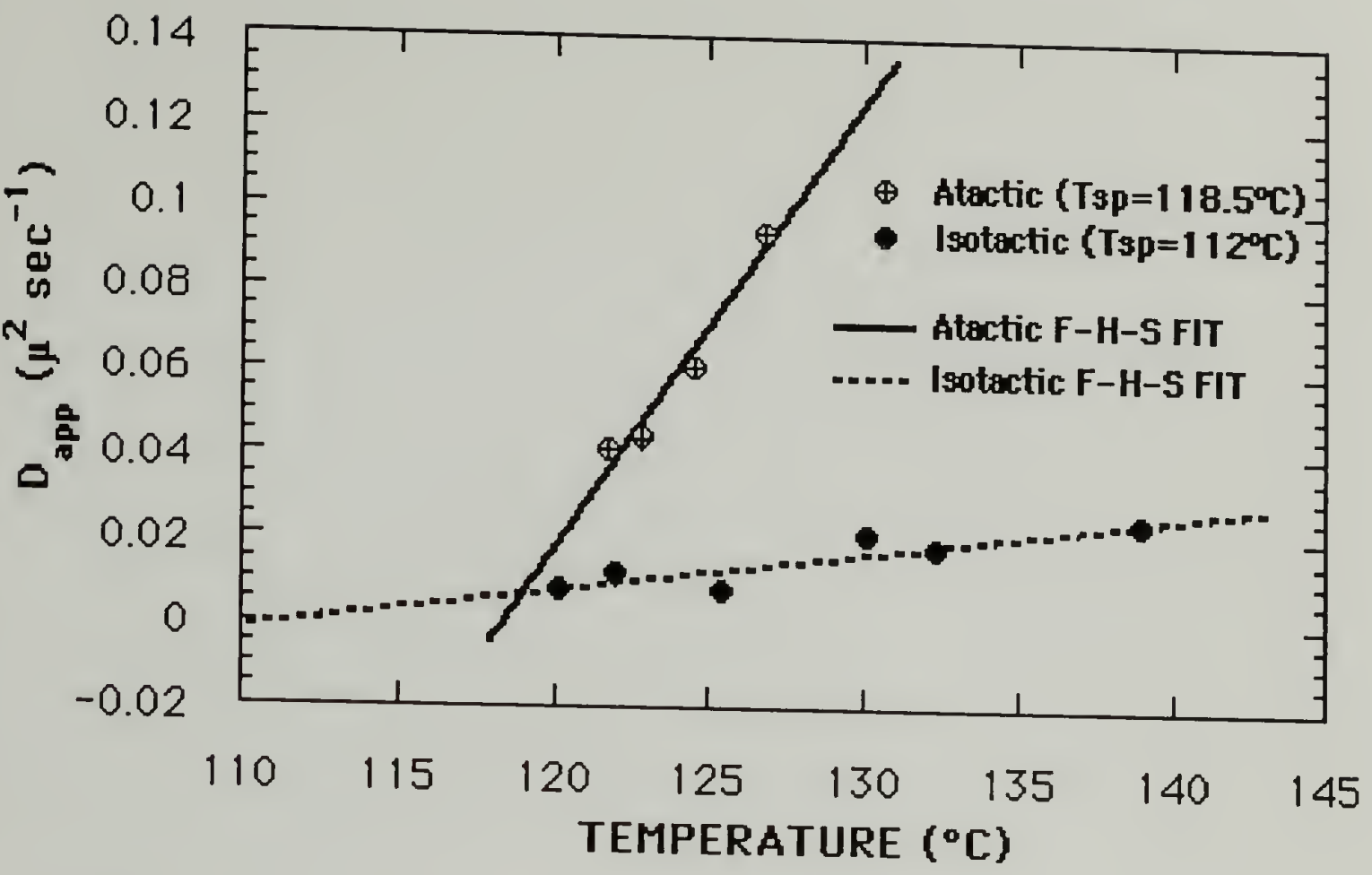

Figure 6.8 D_{app} versus quench temperature for 75 weight percent isotactic and heterotactic PVME/PS blends for extrapolation to the spinodal point at D_{app}=0. Lines are F-H-S predictions for $(-K_c T)\left(\frac{(g - g_s)}{g_s}\right)$ with K_c = -0.22 and -0.24 for the isotactic and atactic blends respectively (g is used for a composition dependent χ).

could be induced by the quenching technique used in the kinetics measurements. The difference between the latter and the cloud point measurement may be due to the difference in film thickness, indicated in the experimental section, as has been noted by Cohen and Reich[6]. The small driving force for phase separation in the isotactic blends discussed above may be over powered by surface tension effects in the isotactic blends leading to a larger discrepancy in the T_{min} and T_{cp} values in Table 6.1 .

Table 6.1 Spinodal temperatures for isotactic and heterotactic PVME/PS blends of 75 weight percent PVME as measured by D_{app} extrapolation, quench measurements for thin films and cloud point measurements for thick films.

	Isotactic Blend	Atactic Blend
T_s (D_{app})	113°C	119°C
T_{min} (Thin Films)	115°C	121°C
T_{cp} (Thick Films)	109°C	121°C

E. Correlation Between F-H-S Analysis and Kinetics Measurements

Clearly there is qualitative agreement between the predictions of the F-H-S analysis and the measured kinetics data (Figures 5.11 and 6.8). In Figure 6.8 a fit of the F-H-S analysis has been applied to the measured D_{app} data. It is assumed that the translational diffusion constant has a linear temperature dependence such that,

$$D_{app} = D_c(T) \frac{(\chi - \chi_s)}{\chi_s} = K_c\, T \frac{(g - g_s)}{g_s} \qquad (6.6).$$

(g is used for a composition dependent χ.) It would be expected that tacticity would have little effect on the translational diffusion constant $D_c(T)$. The values for $D_c(125°C)$ obtained from the fit of Figure 6.8 are,

$$D_{c,iso}(125°C) = -0.22 \frac{\mu^2}{sec}$$

$$D_{c,atactic}(125°C) = -0.24 \frac{\mu^2}{sec}.$$

These values are close to other experimentally determined values such as those of Nishi, Wang and Kwei[7] (determined using NMR $D_c \approx -0.28$). The agreement between the two D_c values, and the agreement with literature values, supports the F-H-S analysis of the CPC and gives credence to the predictions of that analysis concerning shifts in the composition and molecular weight distribution for the rubbery domains (shadow phase) discussed in Chapters 1 and 3.

F. Conclusions

The Flory-Huggins-Staverman theory predicts drastically slowed phase separation kinetics for the isotactic blend. Analysis of the thermodynamic driving force for phase separation, $\frac{(g - g_s)}{g_s}$, indicates that the entropic term, b_0, dominates the predicted shift in the phase separation kinetics.

Qualitatively, measurements of the phase separation kinetics surprisingly supported the prediction of the F-H-S analysis. The translational diffusion constants, D_c, of the two tacticities of PVME were very similar and agree with literature values obtained using an unrelated technique. (It is expected that these two values should agree for different tacticity mono-substituted vinyl polymers which do

not show a shift in T_g.) Thus, a quantitative assessment of the agreement between the theoretical prediction and the measured kinetics was upheld.

G. Intermediate Stages of Phase Separation

The above analysis was based on the initial stages of phase separation in which linear regions of ln(I) versus time plots are observed. This regime is described to some degree of satisfaction by linear Cahn-Hillard theory. As can be seen from from Figure 6.5 this regime (about 15 minutes in Figure 6.5) accounts for a very small portion of the data and for larger quenches in blends with sizable values of D_{app} this region may not be observed at all. (Many polymer blend systems have been reported in the literature for which a linear regime can not be measured[8].) Therefore, it is desirable to understand, at least in an empirical manner, the rich data which follows the initial linear region. It should be noted that the behavior which is observed in Figure 6.5 is fairly universal occurring over the quench depth spectrum for both isotactic and atactic PVME of critical composition as well as for other blend systems reported in the literature[8].

As shown schematically in Figure 6.9 the linear theory assumes that $(\chi-\chi_s)/\chi_s$ is constant in the equation,

$$R(q) = D_c\, q^2 \left(\frac{(\chi - \chi_s)}{\chi_s} - \frac{R_0^2\, q^2}{36} \right) \qquad (6.3).$$

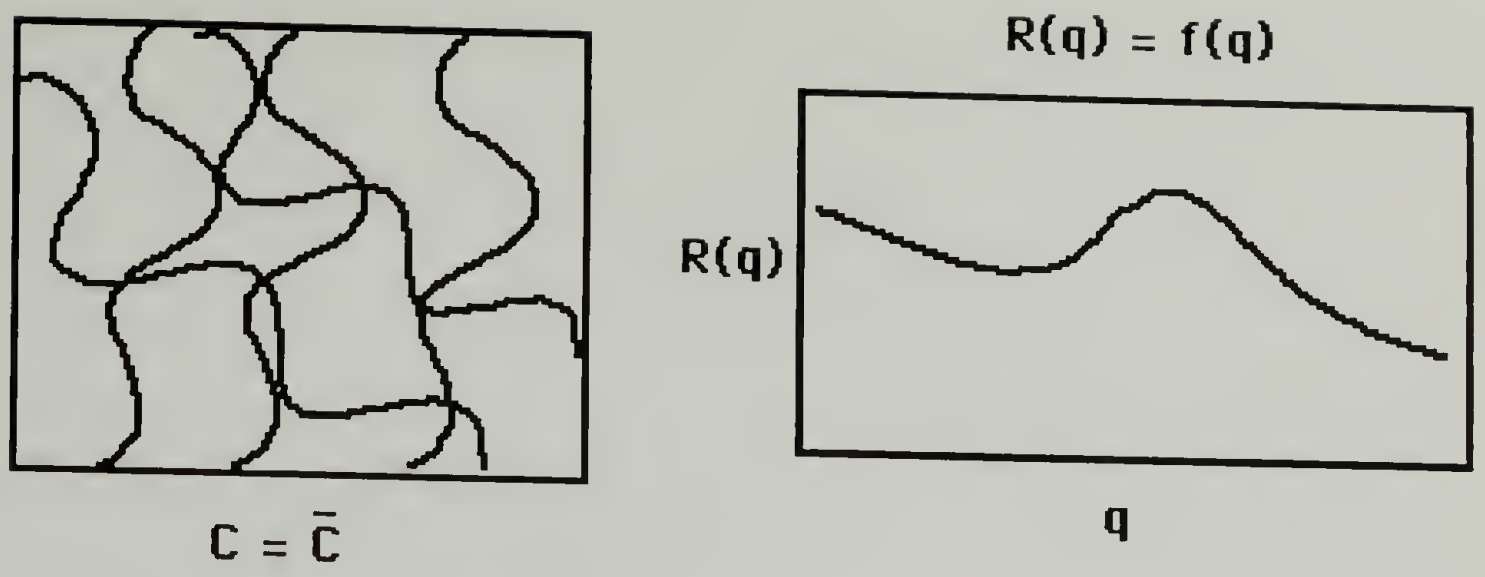

$$I = Io \exp(2\, R(q)\, t)$$

$$R(q) = Dc\, q^2 \{(\chi-\chi s)/\chi s - Ro^2\, q^2/36\}$$

Figure 6.9 A schematic of linear Cahn-Hilliard theory. Left structure of spinodal decomposition, right dependence of R(q) on q.

Since $(g-g_s)/g_s$ (g is used for a composition dependent χ) depends on composition and spinodal temperature, T_s, for real blends and as modeled with the F-H-S equation (T_s also depends on composition) the linear theory assumes that composition is constant through out the phase separation. This is valid over a limited range due to the flatness of the spinodal curve near the critical point (Figure 6.10, A) and due to the small change in composition at the initial stages of phase separation ($\phi = \bar{\phi} = \phi_{\text{initial blend}}$).

Recently[9], Hashimoto and coworkers have ascertained that the early stages of spinodal phase separation in polymer blends gives way to an intermediate stage of pseudo-spinodal phase separation characterized by a self-similar growth of composition fluctuations. That is, the size scale of the fluctuations grow while the structure

remains similar to that of the early stages of spinodal decomposition (Figure 6.10). In this scheme it can be postulated that the composition which could be considered an average concentration at the earliest stages of spinodal decomposition due to the small size of the fluctuations gives way to a changing composition, specifically at the growing fronts of the pseudo-spinodal structure. In this way, the thermodynamic driving force for the phase separation, $(g-g_s)/g_s$, decreases with time.

In reference to equation 6.3 given above, initially this decreasing $(g-g_s)/g_s$ yields a smaller value for R(q) and consequently a decreasing slope of $\ln(I) = \ln(I_0) + 2\ R(q)\ t$ (equation 6.1). At some point $(\chi-\chi_s)/\chi_s$ becomes equal to $(R_0^{\ 2}\ q^2)/36$ and the slope of ln(I) goes to zero (B in Figure 6.10). Beyond this time in the phase separation, the slope (2 R(q)) becomes negative (since $(R_0^{\ 2}\ q^2)/36$ is larger than $(g-g_s)/g_s$ as is observed in the data. As time progresses further (C in Figure 6.10), composition becomes approximately linear in time in a region of composition for which the spinodal temperature is linear in composition, thus $(g-g_s)/g_s$, which depends roughly on the inverse of the spinodal temperature for a constant quench, becomes linear in 1/time and ln(I) becomes independent of time. At later stages one

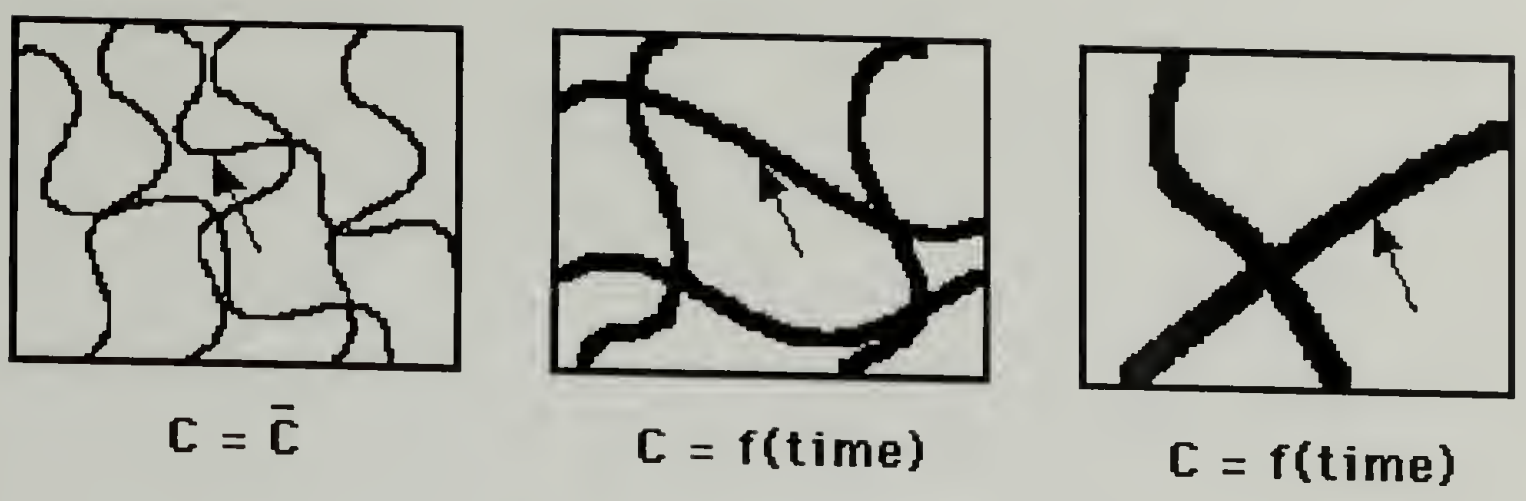

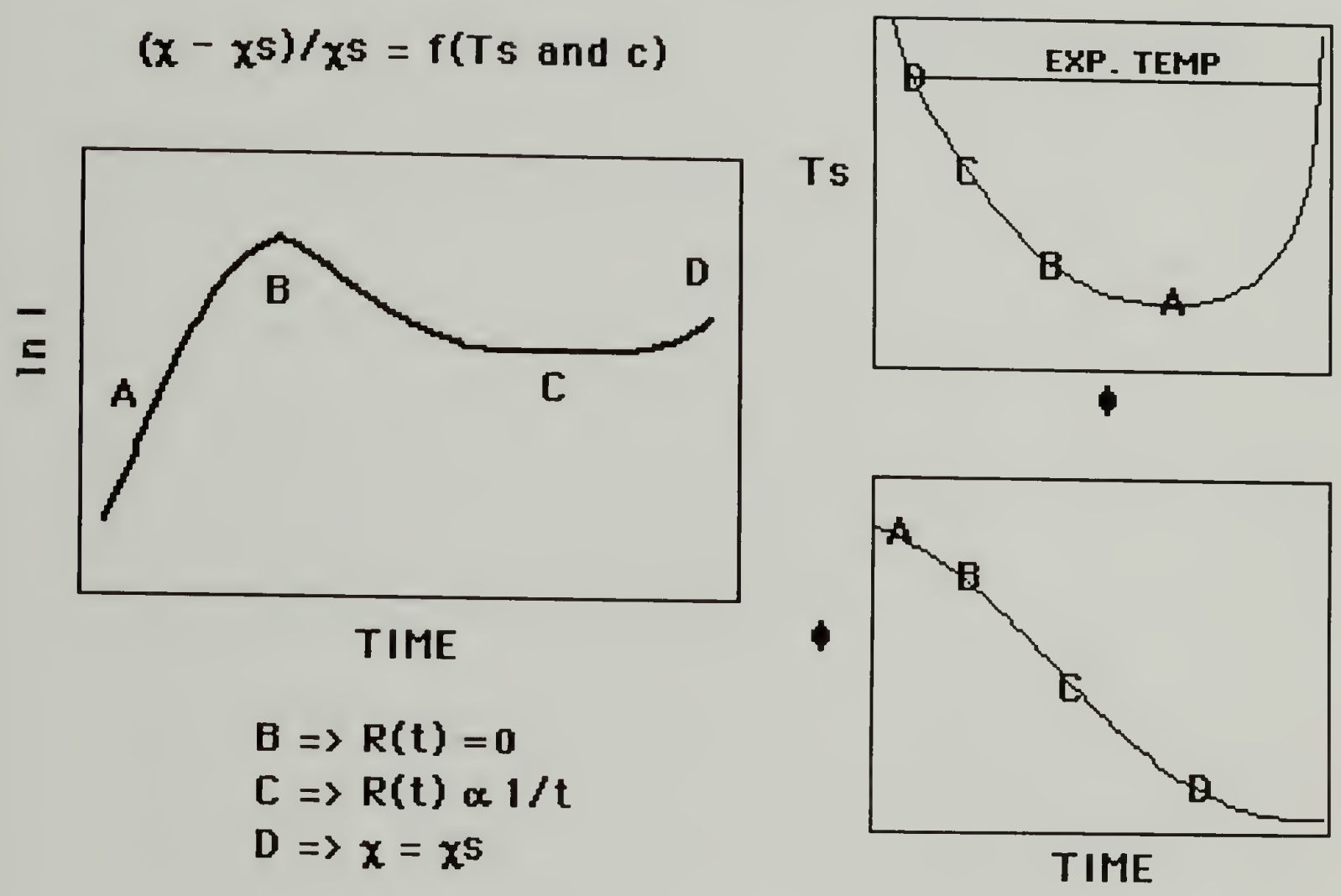

Figure 6.10 Self-similarity in intermediate stages of polymer phase separation.

would predict a linear decrease of intensity with time as $(g-g_s)/g_s$ goes to zero. Actually, a slight increase in intensity is observed at very long time scales in the blends studied here (D in Figure 6.10) indicating that the pseudo–spinodal model is no longer appropriate.

Figure 6.11 is a typical fit of the data using this approach and the F-H-S equation for $(g-g_s)/g_s$ (equation 5.24). An exponential

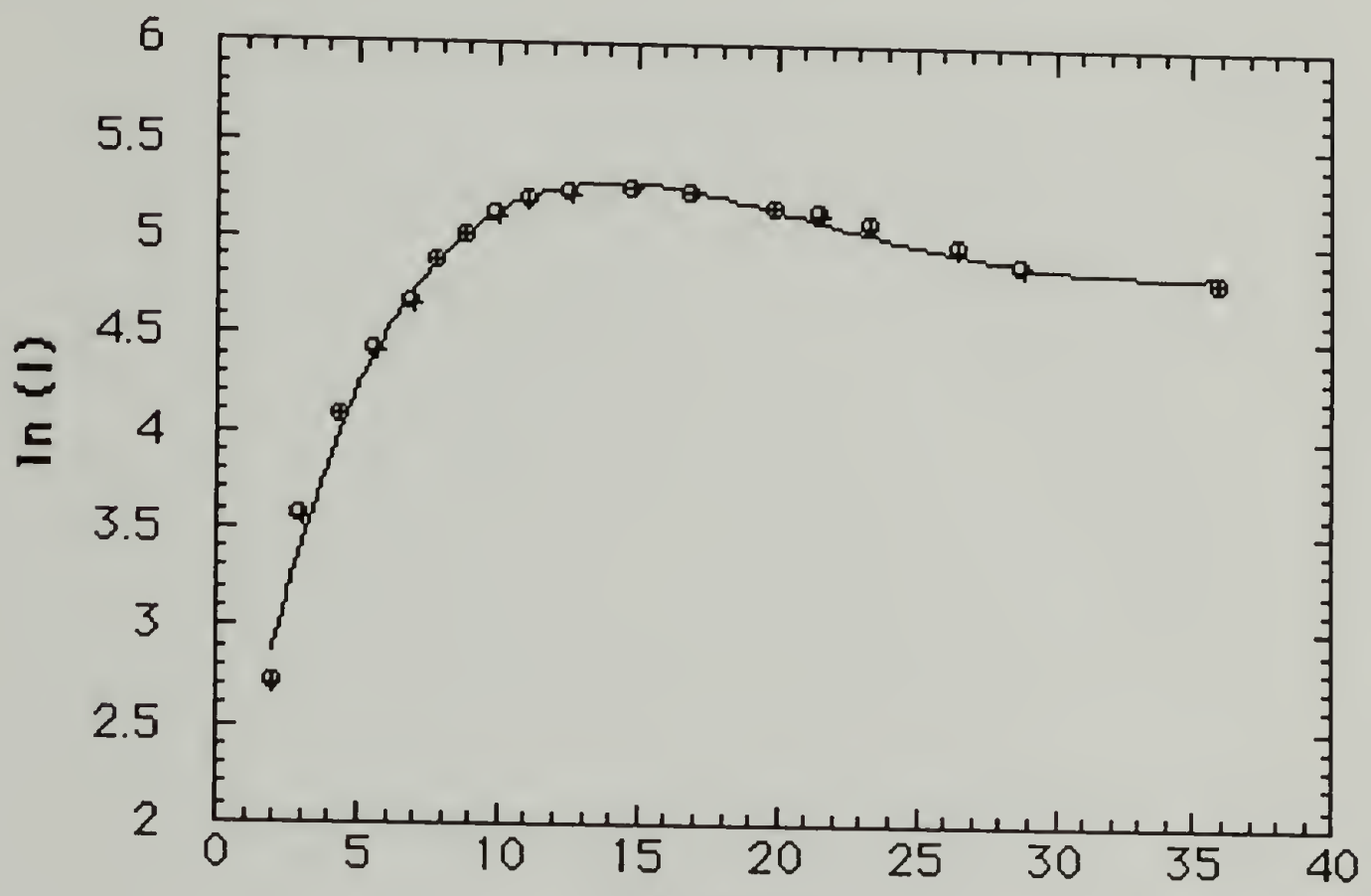

Figure 6.11 A typical fit of the scattering data using the pseudo-spinodal approach and the F-H-S equation for $(g-g_s)/g_s$ (equation 5.24). (123.5°C Heterotactic PVME/PS q=1.84 μ^{-1})

decrement in composition was used to model the behavior shown schematically in Figure 6.10, yielding two unknown fitting parameters. These parameters, however, can be determined from the data if it is assumed that the composition change with time is not dependent on the size scale of measurement (i.e. the q value) within the range of q values measured. (In this case the previous assumption yields 500 plots for each quench similar to Figure 6.11 for which these two constants must remain the same). The spinodal temperatures and the

a, b_0, b_1 and c values ascertained in the F-H-S analysis were used to generate $(g-g_s)/g_s$ and R(q) data. Values of R_0 (the unperturbed radius of gyration for an average polymer chain in the blend) may be obtained in this way (one of the two fitting parameters). Generally the radius of gyration was in the 100Å range which would agree with a theta chain of similar degrees of polymerization.

This approach to analyzing the scattering data yields fits to the data over a wide range of q and time. Although not used in the present chapter due to time constraints (each quench generated 500 I versus q data files each with time dependencies similar to Figure 6.11), it is believed to be a very promising approach which can result in a Cahn-Hillard type analysis of scattering data on systems which show a very small (or no) linear regime in the ln(I) versus time data. For the quenches examined, values for D_{app} did not significantly vary for quenches in which the linear regime was well defined. The use of a much broader range of q values and the loss of the linear assumption are hoped to yield more accurate fits and values for D_{app}.

An independent experimental measurement of the average concentration (at the interface between phases) versus time behavior would be helpful in extending this approach. Ellipsometric or neutron reflection experiments may serve to yield such data in the near future.

References

1. O. Olabisi, L. M. Robeson, M. T. Shaw, *Polymer-Polymer Miscibility*, Academic Press, New York, 1979.

2. S. Wu, *Polymer Interface and Adhesion*, Marcel Dekker Inc., New York, 1982.

3. T. Hashimoto, J. Kumaki, and H. Kawai, *Macromolecules*, **16**(4), 641 (1983).

4. M. Shibayama, H. Yang, R. S. Stein, and C.C. Han, *Macromolecules*, **18**, 2179 (1985).

5. F. E. Karasz and W. J. MacKnight, *Macromolecules*, **1**(6), 537 (1968).

6. S. Reich, Y. Cohen, *J. Polymer Sci., Poly. Phys. Ed.*, **19**(8), 1255 (1981).

7. T. Nishi, T. T. Wang and T. K. Kwei, *Macromolecules*, **8**, 227 (1975).

8. For example Polycarbonate/PMMA blends. T. Kyu, J. M. Saldanha, *Macromolecules* , **21**, 1021, 1988.

9. T. Hashimoto, personnel communication.

CHAPTER 7

NEUTRON SCATTERING ANALYSIS OF ISOTACTIC PVME/PS BLENDS

A. Introduction

Small angle neutron scattering (SANS) from blends in the miscible region was used to determine the effects of tacticity on the temperature and composition dependence of the interaction parameter using the random phase approximation (RPA) analysis[1] and the Flory-Huggins-Staverman (F-H-S) analysis discussed in Chapters 5 and 6. Additionally, the correlation length approach was used to determine the spinodal temperatures for two compositions. Experiments were performed at Los Alamos National Lab's LANSCE Facility. In neutron scattering selective deuteration of one of the the blend components enhances the contrast between regions of differing neutron scattering cross-section (similar to index of refraction contrast in light scattering or electron density contrast in x-ray scattering). In general the substitution of deuterium for hydrogen in a low molecular weight compound has only a small effect on the structure and thermodynamic interactions (for instance the melting point of heavy water is 3.8°C). However, in many polymer blend systems (including PVME/PS) the cumulative effect of deuteration dramatically alters the miscibility. This effect has been studied in our lab by H. Yang[2].

B. Background

Data obtained from a modern small angle neutron scattering facility is converted by the user facility (LANSCE in this case) to a reduced intensity, R(q) which is analogous to the Raleigh factor obtained in light scattering. R(q) is defined as,

$$R(q) = \frac{I(q)}{I_0 V_{IR}} p^2 \qquad (7.1),$$

where q is related to the angle of scattering, θ, and the wavelength of neutrons, λ, by,

$$q = \frac{4\pi}{\lambda} \sin\left(\frac{\theta}{2}\right) \qquad (7.2),$$

I(q) is the scattered intensity, I_0 is the main beam intensity, V_{IR} is the irradiated volume and p is the sample to detector distance. The data is circularly averaged for an isotropic scatterer such as a polymer blend. The intensity of scattering is calibrated by the user facility to an absolute value, thus data taken on different instruments should be completely comparable. Scattering experiments are done on the pure components of a polymer blend in order to estimate the incoherent scattering and a weighted average of these runs based on the blend composition is subtracted from the sample's R(q) yielding $R_c(q)$, the reduced intensity produced by composition fluctuations in the absence of incoherent scattering. All runs were done at temperature using a heating cell which was accurate to within about 0.1 °C. The q range of

the data was from about 0.008 to about 0.18 $Å^{-1}$, which is characteristic of the wide q range available at a spallation source such as LANSCE. (Differences between spallation sources and reactor sources are well documented in the literature and the interested reader is referred to reference 3.)

Einstein fluctuation theory relates $R_c(q)$ from a scattering experiment to the inverse of the change in osmotic pressure with composition. The latter can be directly related to the change in chemical potential with composition. Thus the scattering data is directly related to the second derivative of the free energy with respect to composition. Generally this leads to a direct interpretation of the scattering data in terms of thermodynamic parameters such as the interaction parameter, χ. However, in all of the polymer blends which have been studied using SANS a composition dependence of χ occurs. Thus, χ_{sc} measured in a scattering experiment can not be directly equated with the χ given by standard Flory-Huggins theory. This will be discussed below in terms of the F-H-S analysis. Generally, a composition dependent χ is denoted by g

de Gennes[4] has developed an equation for the determination of χ_{sc} based on the RPA theory. Generally,

$$\frac{k_n}{R_c(q)} = \sum_{i=1,2} \left(\frac{1}{v_i \, z_i \, \phi_i \, g_D(U_i)} \right) - \frac{2 \, \chi_{sc}}{v_0} \qquad (7.3),$$

where $g_D(U_i)$ is the Debye scattering function for a single randomly coiled chain given by,

$$g_D(U_i) = \frac{2}{U_i^2}\left[e^{-Ui} - 1 + U_i\right] \qquad (7.4).$$

U_i is given by,

$$U_i = q^2 R_{gi}^{\ 2} \qquad (7.5),$$

where R_{gi} is the radius of gyration for random coil 'i'. The radius of gyration for a Gaussian chain is given by,

$$R_{gi}^{\ 2} = \frac{z_i b_i^2}{6} \qquad (7.6),$$

where z_i is the degree of polymerization (generally the weight average is used $z_{i\,z}$ is the "z" average used below) and b_i is the statistical segment length for polymer "i" (similar to a Kuhn step length). In the scattering experiment an average statistical segment length is measured, $\bar{b}$. After accounting for molecular weight distributions it has been given by[5],

$$\frac{\bar{b}^2}{v_0} = \phi_1 \phi_2 \left(\left(\frac{z_{1\,z}}{z_{1\,w}}\right)\frac{b_1^2}{v_1 \phi_1} + \left(\frac{z_{2\,z}}{z_{2\,w}}\right)\frac{b_2^2}{v_2 \phi_2}\right) \qquad (7.7).$$

In analyzing the SANS results the approximation[2],

$$R_{gi}^{\ 2} = \frac{z_i v_i}{6}\left(\frac{\bar{b}^2}{v_0}\right) \qquad (7.8),$$

is used, where v_0 is the average segmental volume which has been estimated as [6],

$$v_0 = \sqrt{v_1 v_2} = \sqrt{\left(\frac{M_{w\ mer\ 1}}{\rho_{mer\ 1}}\right)\left(\frac{M_{w\ mer\ 2}}{\rho_{mer\ 2}}\right)} \qquad (7.9).$$

$g_D(U_i)$ behaves in q-space as the concentration fluctuation correlation function behaves in real space (they are related by a Fourier transform). That is, at low q, $g_D(U_i)$ scales like 1/q and at high q, $g_D(U_i)$ scales like e^{-q^2}. Clearly, at some size scale (in r or q) there is a transition between these two scaling forms of $g_D(U_i)$. This size scale is termed the correlation length, ζ, and will be important in determining the spinodal temperature for a polymer blend. ζ can also be thought of as an average size scale between concentration fluctuations in the miscible region.

Since $g_D(U_i)$ scales like $1/(q\ z_i\ b_i^2)$ at low q and since $g_D(U_i)$ is multiplied by z_i in equation 7.3, z_i essentially drops out of equation 7.3. This is important to note since data fits are made in the low q regime. Thus, the free fitting variable for the scattering data is clearly the statistical segment length b rather than R_g. This will be used in sections I, J and O.

k_n in equation 7.3 is given by,

$$k_n = N_A \left(\frac{a_1}{v_1} - \frac{a_2}{v_2}\right)^2 \qquad (7.10)$$

where a_i is the neutron scattering length (defined in reference 6) and v_i is the segmental molar volume of component i. v_0 in equation 7.3 is the average segmental molar volume The calculation of v_0 is a matter of some dispute so generally χ_{sc} is reported as $\frac{\chi_{sc}}{v_0}$, the experimentally measured quantity. z_i and ϕ_i in the above equations are the degree of polymerization and the volume fraction of component i in the blend.

The constants in equation 7.3 are generally known and fits of the scattering data can be made over a large q range in order to determine $\frac{\chi_{sc}}{v_0}$ and $\frac{\bar{b}^2}{v_0}$. Equation 7.3 can also be simplified for the case of small q and rearranged in an Ornstein-Zerniker form yielding,

$$\frac{k_n}{R_c(q,T)} = \frac{(1 + q^2\,\zeta^2(T,\phi))}{R_c(q=0,T)} \qquad (7.11).$$

This form suggests the so called modified Zimm[7,8] (or correlation length) approach in which plots of $\frac{1}{R_c(q,T)}$ versus q^2 are made over the low q range where linear behavior applies, in order to obtain values for $\zeta^2(T,\phi)$ and $R_c(q=0,T)$. In Flory-Huggins (F-H) theory,

$$\frac{1}{R_c(q=0,T)} = \frac{2}{v_0}(\chi_s - \chi) \qquad (7.12),$$

and,

$$\zeta^2(T,\phi) = \frac{\bar{b}^2}{36\,\phi_1\,\phi_2\,(\chi_s - \chi)} \qquad (7.13),$$

where,

$$\frac{2\,\chi_s}{v_0} = \sum_{i=1,2}\left(\frac{1}{v_i\,z_i\,\phi_i}\right) \qquad (7.14).$$

χ_s is the interaction parameter at the spinodal point for a particular composition. Since $(\chi_s - \chi)$ goes to zero as the spinodal point is approached (in temperature or composition), $\frac{1}{\zeta^2(T,\phi)}$ also goes to zero at the spinodal and linear plots of $\frac{1}{\zeta^2(T,\phi)}$ versus temperature will yield the spinodal temperature. Since $R_c(q,T,\phi)$ is proportional to $\frac{1}{\zeta^2(T,\phi)}$, the scattering intensity will increase in magnitude (especially at low q) as the spinodal temperature is approached in composition or temperature.

It should be noted that the F-H theory as originally proposed uses a Hildebrand type equation for χ whose functional form is B/T where B is a constant (in composition) enthalpic interaction. χ's with the form A+B/T (where A is a non-combinatorial entropy term) can also be accommodated in the F-H theory, however, χ's which display a composition dependence (referred to using the symbol g) will not strictly follow the equations given above. For instance, the derivation

of equation 7.14 assumes no composition dependence to χ. Terms reflecting the second derivative of g with respect to composition would be required in order to estimate g_s for a composition dependent χ (g_s is determined by setting the second derivative of the the free energy with respect to composition to zero). Since the second derivatives would themselves, generally, depend on temperature one is faced with an actual $g_{s\ lm}$ where $T=T_s$ for a given composition, and an apparent $g_{s\ ap}$ using the temperature of observation. It is believed that $g_{s\ lm}$ is only of importance at the limit of miscibility (i.e. in determining the spinodal point), where as $g_{s\ ap}$ is the value of g_s which the blend uses to determine its relative miscibility (i.e. $g-g_s$) at a particular temperature.

As was noted in Chapter 5, the F-H theory will not, in general, accommodate non-symmetric lattice sites or different sized lattice sites for different blend components. This is because the F-H theory was a direct development from polymer solution theory in which the lattice site referred to one symmetric solvent molecule, and the polymer mer unit was assumed to occupy exactly the same sized symmetric lattice site. Since the tacticty effect depends on at least three mer units (the definition of triad tacticity), and since this group of three mer units can not generally be regarded as symmetric in shape, one is faced with the need to either develop a new approach to polymer blends (such as the Curro-Schweitzer theory mentioned in Chapter 5) or to ignore the limitations of the F-H theory and to proceed as if the F-H theory could accommodate non-symmetric lattice sites which may have different surface areas and volumes for

the two blend components. The latter approach was used in this thesis since modern theories of polymer blends have not yet been shown capable of analyzing complicated phenomena such as the tacticity effect. The results presented here must be taken as an indication of the aspects of polymer blend theory which remain to be fully addressed, and as empirical models for predictive use. Such predictive use has already been shown to be very useful and at least qualitatively correct in Chapters 4, 5, and 6. A functional form for χ (even an empirical form) is a prerequisite for predictions of blend behavior.

C. Approximation for the Thermal Expansion Differences Between Isotactic and Atactic PVME

The volumes, volume fractions (at a fixed weight fraction) and densities used in section B are subject to thermal expansion and it is important to account for this dependence on temperature in analyzing the thermal behavior of the scattering data. Data concerning the thermal expansion of atactic PVME and PS were collected by Shibayama, Yang and Stein[9]. The data analysis presented in this Chapter assumes similar thermal behavior for isotactic and atactic PVME in the melt. This assumption was tested by observation of the index of refraction as a function of temperature using an Abbe refractometer. This is a very simple technique which yields highly accurate values for index of refraction. Under the assumption of a spherical molecule, the density, ρ, can be related to the index of refraction, n, using the Lorentz-Lorenz equation,

$$\left(\frac{(n^2 - 1)}{(n^2 + 2)}\right) = \rho\, C \qquad (7.15),$$

where C is the specific refraction which depends on the polarizability of the molecules (temperature independent)[10]. Equation 7.15 results in a monotonically decreasing index of refraction with decreasing density.

Taking the derivative of the Lorentz-Lorenz Equation with respect to temperature, T, one obtains,

$$\frac{dn}{dT} = \left(\frac{(n^2+2)(n^2-1)}{6n}\right)\frac{1}{\rho}\frac{d\rho}{\delta T} = - q(n)\,\alpha \qquad (7.16).$$

Figure 7.1 shows the thermal behavior of n for isotactic and atactic PVME. Linear fits to the high temperature data (T > 70°C) indicate very little difference between the non-crystalline isotactic and atactic PVME. It is interesting to note that the crystalline melting of the i-PVME can be clearly observed. Since the crystalline PVME has a higher density its index of refraction is slightly higher. i-PVME's treated with three different annealing conditions show different melting points. This is consistent with DSC data which indicates a wide range for i-PVME melting points (T_m's of 35 to 70°C have been observed). The melting temperature increases from about 40°C for the material annealed at room temperature (RT) to 60°C for a material annealed at 48°C. Annealing at temperatures higher than 48°C failed to induce crystallinity from the melt in the time available (about one day). As has been noted previously in the discussion of x-ray

diffraction, the rate of crystallization from the melt is very slow for isotactic PVME of about 70% isotactic triad content (trace crystallinity

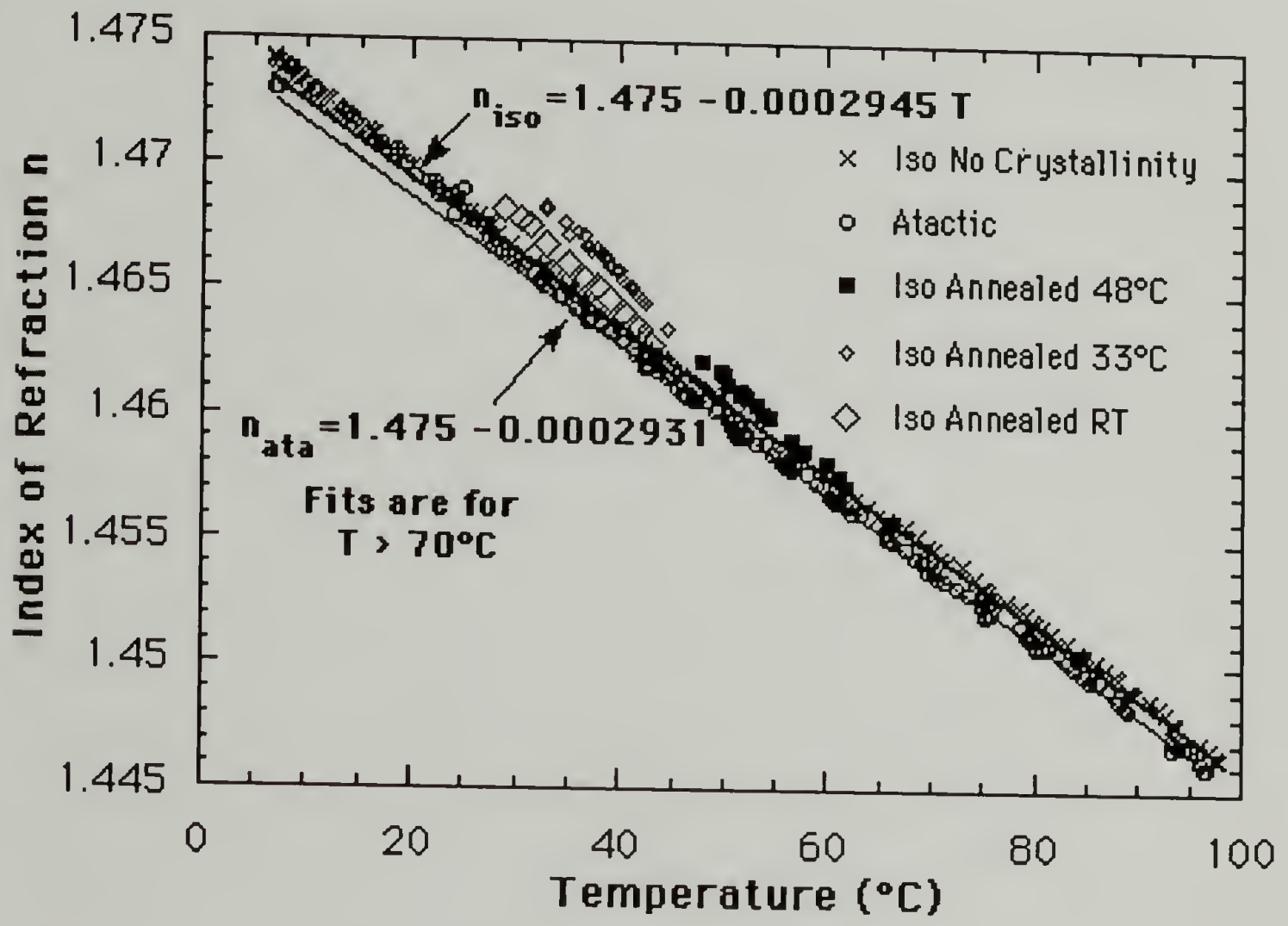

Figure 7.1 Index of refraction as a function of temperature for isotactic and atactic PVME. (Measurement error is similar to the scatter in the data.)

after 1 day, full crystallinity of about 10% after several weeks). This has been advantageous in the index of refraction measurements and SANS experiments.

Equation 7.15 was used to estimate the thermal behavior of the density. Figure 7.2 shows a decrease in density with temperature for the non-crystalline PVME which is very similar to the atactic PVME.

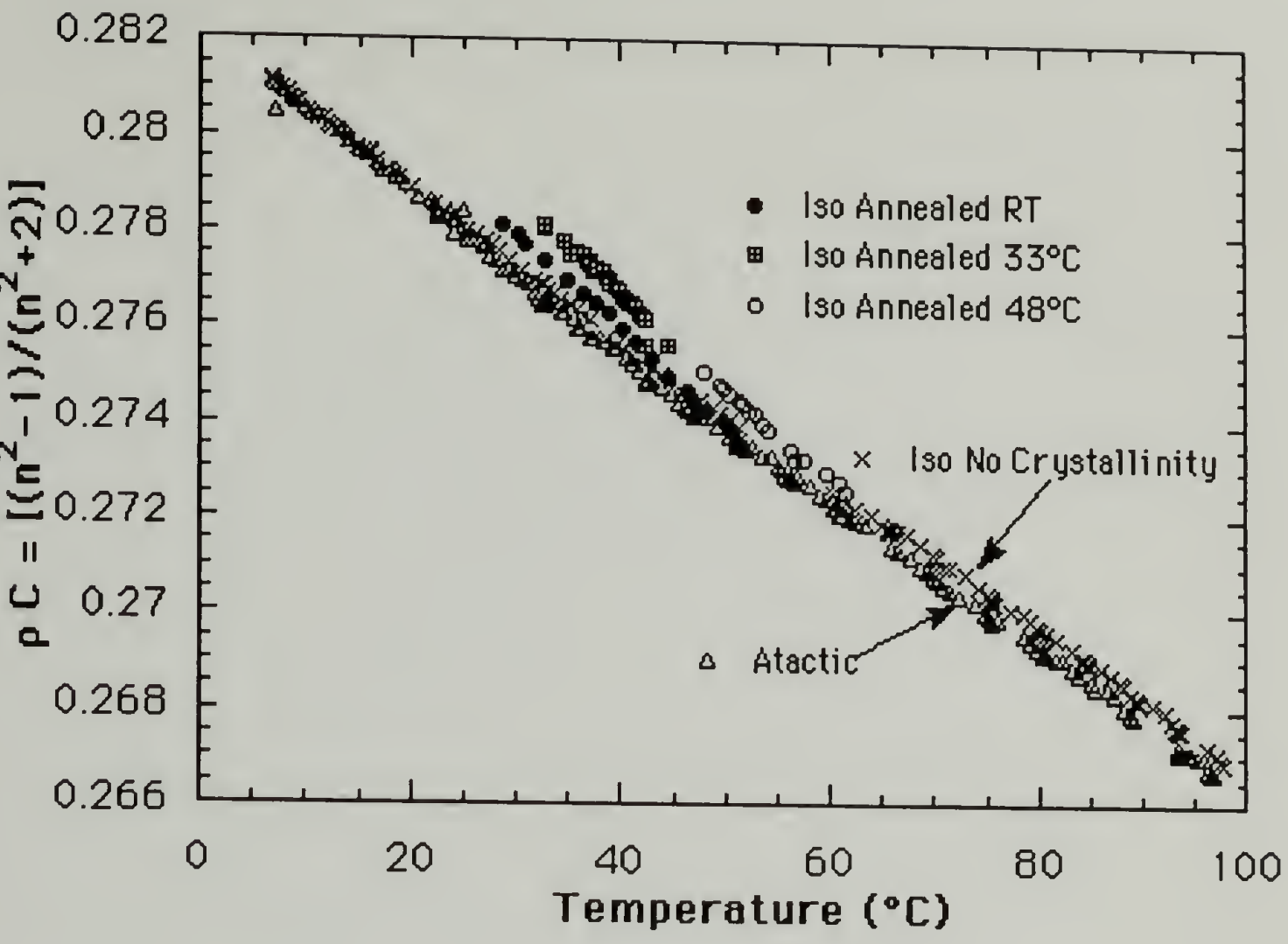

Figure 7.2 Density times the specific refraction (C) versus temperature for isotactic and atactic PVME. (Measurement error is similar to the scatter in the data.)

The crystalline PVME again shows a higher density when compared with the non-crystalline PVME as would be expected if the isotactic material were thought to be a more ordered material in the melt. The difference in densities decrease at lower temperatures due to differing thermal expansion coefficients as described below.

The thermal expansion coefficients were also calculated for the two tacticities using the slopes of the high temperature index of refraction from Figure 7.1 as $\frac{dn}{dT}$, Figure 7.3.

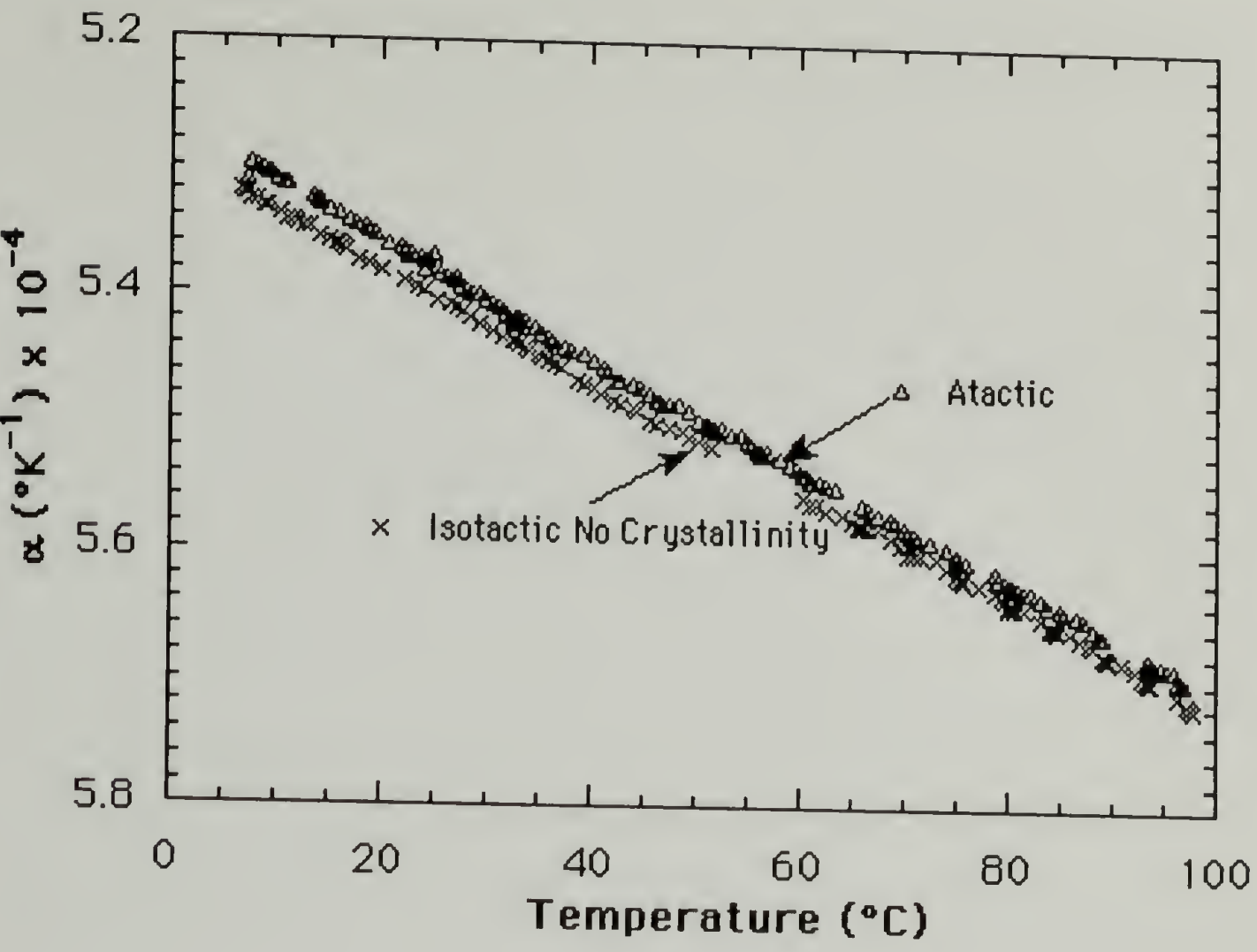

Figure 7.3 Calculated thermal expansion coefficient for isotactic (no crystallinity) and atactic PVME versus temperature. (Measurement error is similar to the scatter in the data.)

These values show a drift of about 10% over the 100°C temperature range observed. A value of $5.8 \times 10^{-3}\ K^{-1}$ is reported in the Polymer Handbook[11]. A thermal expansion coefficient of $6.2 \times 10^{-3}\ K^{-1}$ is obtained from density measurements reported by Murray[12]. The isotactic PVME has a slightly lower thermal expansion coefficient which appears to merge with the atactic values at higher temperatures. The isotactic material in the melt can therefore be describes as a slightly more dense material with a slightly lower thermal expansion coefficient whose thermal expansion coefficient merges with that of the atactic material at higher temperatures. This

data could be indicative of an isotactic material which is more 'ordered' than the atactic material. Since α is given by,

$$\alpha = \sqrt{\left(\frac{(C_P - C_V)\,\kappa}{V\,T}\right)} \qquad (7.17)$$

and C_P, C_V are given by,

$$\frac{C_P}{T} = \left(\frac{dS}{dT}\right)_P \quad \frac{C_V}{T} = \left(\frac{dS}{dT}\right)_V \qquad (7.18)$$

merging of the two thermal expansion coefficients would indicate that differences in the thermal behavior of the entropy vanish at high temperatures. This observation will be of more importance in discussing the thermal behavior of the interaction parameter as determined by SANS. (reference should be made to the simple molecular models shown in Chapter 5 Figures 5.8 and 5.9 for an indication of the type of "ordering" which can occur in the isotactic PVME when compared with the atactic PVME.)

D. Neutron Scattering Results for Isotactic PVME/PS Blends Using the Correlation Length Approach

i-PVME was blended with perdeuterated polystyrene of the molecular weight and polydispersity listed in Table 7.1. The blends were made by freeze drying a benzene solution followed by vacuum drying at various temperatures depending on the T_g of the blend. The resulting fluffy powder was pressed under vacuum at a temperature

above T_g but below the cloud point for the blend. Samples prepared in this way were dried under vacuum below their T_g for at least three days and stored for transportation in a sealed desiccator. The cloud points for these blends are elevated by about 10°C from that of the hydrogenous PS due to the deuteration effect[13].

TABLE 7.1 Molecular weights and polydispersity of polymers used in SANS experiments (as measured by GPC with the deuteration mass differences and the universal constant for PVME accounted for).

	M_w kg/mole	$\frac{M_w}{M_n}$	$\frac{M_z}{M_w}$
Isotactic PVME	121	1.73	1.51
dPS	85	1.04	1.51

Figure 7.4 shows the temperature dependence of scattering for three runs of isotactic PVME/PS blends in which the composition is 50% by weight d-PS. In agreement with the discussion in section B, the scattering is seen to increase with temperature at low q.

In analogy to Figure 7.4's temperature dependence, Figure 7.5 shows three runs in which the composition is varied for a constant temperature of 100°C. Since the critical composition corresponds to about 75% i-PVME this composition is closer to the spinodal and shows the highest intensity at low q. The 90% i-PVME blend is closer

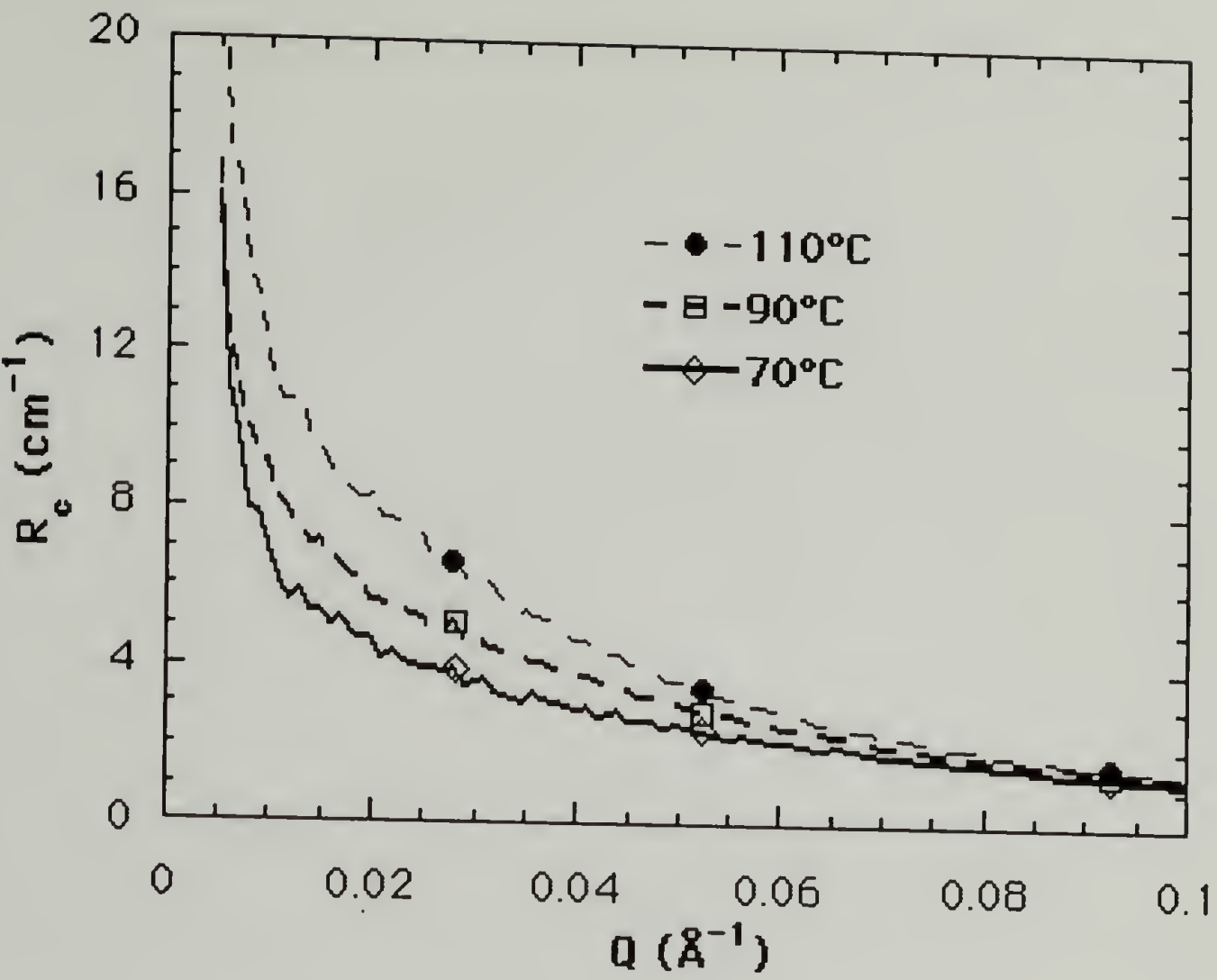

Figure 7.4 Absolute intensity, R_c, versus q for a 50% dPS/i-PVME blend. Three temperature runs are shown indicating the increase in low q intensity as the critical point is approached. (Statistical error is smaller than the data points.)

to the spinodal than the 10% blend due to the non-symmetric phase diagram, thus the 10% has a higher intensity than the 90% blend.

Plots of $\frac{1}{R_c(q,T)}$ versus q^2 corresponding to Figures 7.4 and 7.5 are shown in Figures 7.6 and 7.7. Equation 7.11 indicates that plots of this kind will yield $\frac{2}{v_0}(g_s - g)$ (equation 7.12) at the

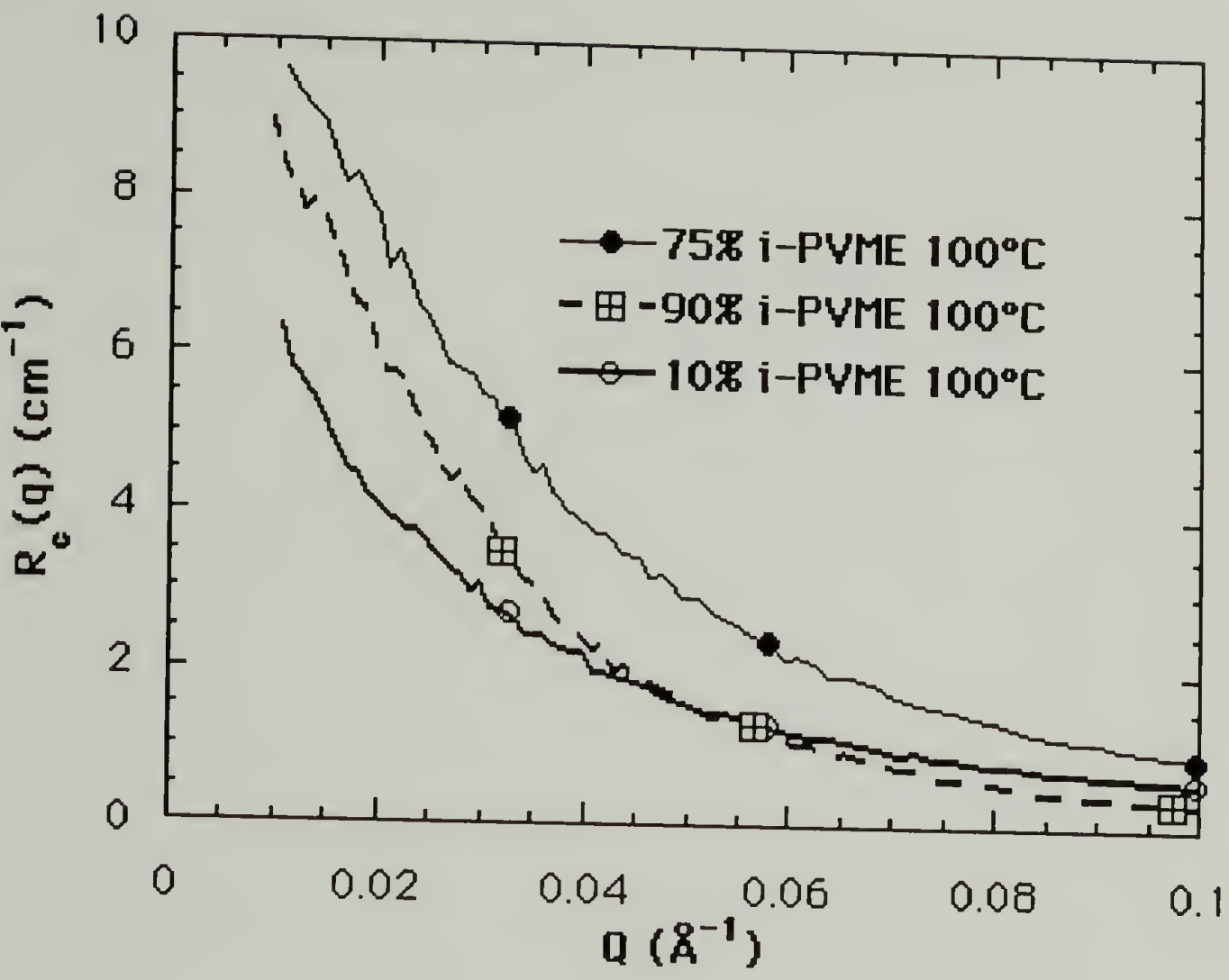

Figure 7.5 Absolute intensity, R_c, versus q for dPS/i-PVME blends at 100°C. Three composition runs are shown indicating the increase in low q intensity as the minimum in the phase diagram is approached (75% i-PVME). (Statistical error is smaller than the data points.)

q^2=0 intercept and will have a slope which is related to the correlation length and, by assuming Gaussian chains, with the average statistical segment length (equation 7.13) for the two blend components.

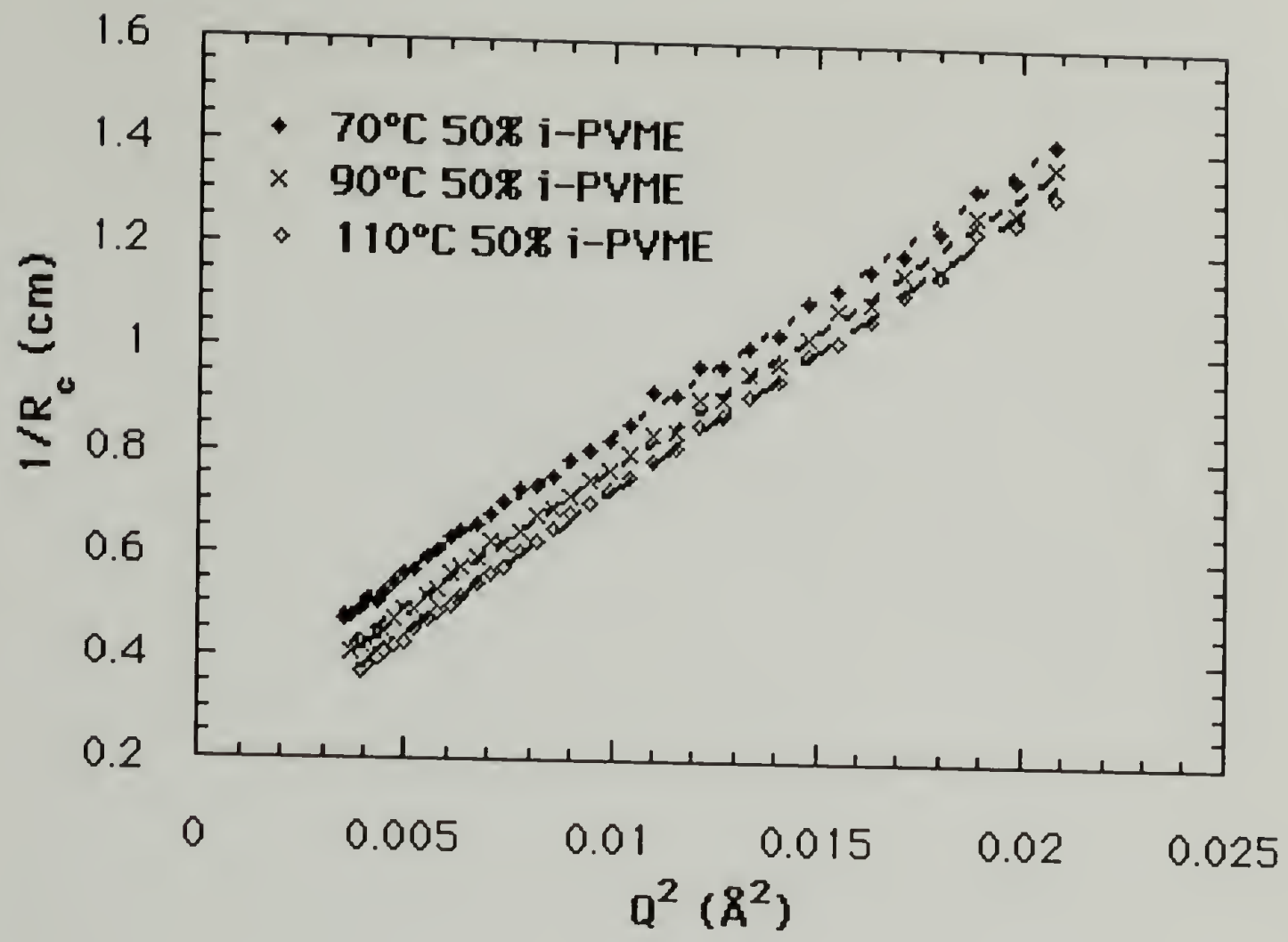

Figure 7.6 Plots of $1/R_c$, versus q^2 for a 50% dPS/i-PVME blend. Three temperature runs are shown. (Statistical error is smaller than the data points.)

In accordance with the discussion of the correlation length approach given in section B, the data show linear regimes from about 0.003 to 0.025 $Å^{-2}$ (corresponding to q values of .05 to .16 $Å^{-1}$). In Figure 7.6 the intercept at $1/R_c(0)$ decreases with increasing temperature indicating that the spinodal is approached (equation 7.12).

Figure 7.7 illustrates the composition dependence of the scattering data. The top two curves are from the extremes of composition. The slope for the 90% i-PVME is the largest observed

indicating the largest correlation length (since the intercept is relatively small). The 10% i-PVME blend has the largest intercept

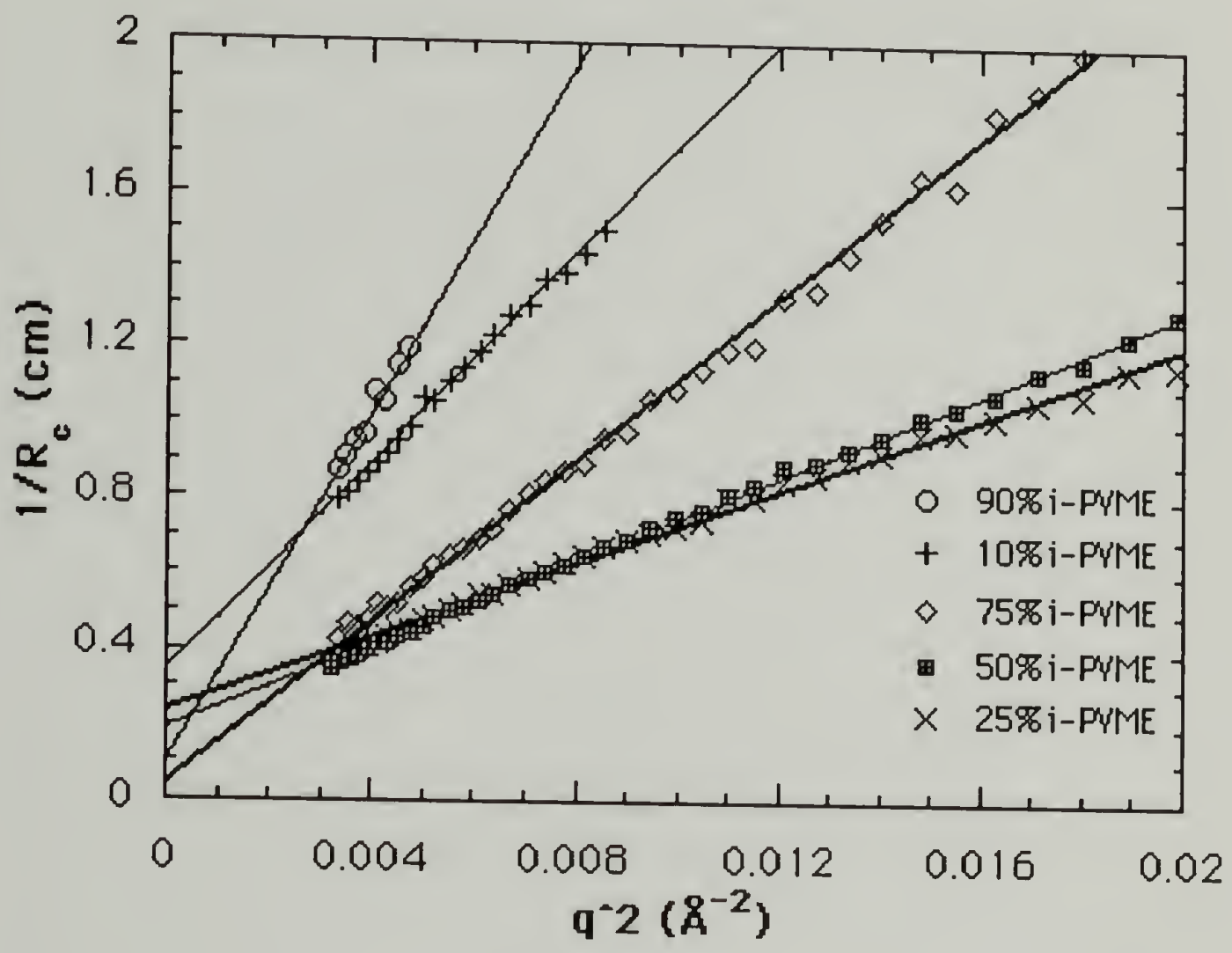

Figure 7.7 Plots of $1/R_c$, versus q^2 for various i-PVME/dPS Blends at 100°C. The q=0 intercept reflects the distance from the spinodal and the slope reflects the (correlation length)^2/intercept. (Statistical error is smaller than the data points.)

($1/R_c(0)$) indicating the greatest miscibility. The lowest miscibility (smallest intercept) occurs for the 75% i-PVME blend which is close to the critical composition. Atactic PVME shows a smaller dependence of both the correlation length (as reflected in the slopes) and $1/R_c(0)$ on composition. In order to compare the atactic PVME correlation lengths determined by Yang with the isotactic correlation

lengths observed in this work, ζ must be normalized to account for differences in distance from the phase separation temperature. This was done by dividing the measured correlation lengths by the value at 50% composition. In Figure 7.8 the composition dependence of this reduced correlation length is illustrated for the isotactic and atactic PVME/PS blends. Isotactic PVME shows a stronger temperature dependence at high percentages PVME leading to much larger values for $(\zeta)/(\zeta_{50\%,T})$. For compositions in the 20-50% PVME region there is little temperature dependence, The low composition PVME $(\zeta)/(\zeta_{50\%,T})$ shows a slight up turn. This behavior might be explained by differences in the statistical segment length, b, between dPS and i-PVME. The relationships between the statistical segment length and the correlation length for randomly coiled polymers are given by equations 7.3-7.7 and 7.11. A larger statistical segment length for the dPS in comparison to i-PVME could explain both the rise at low concentrations and at higher PVME concentrations observed in Figure 7.8. From equation 7.13 we see that $\zeta^2(T,\phi)$ is equal to $\bar{b}^2/(36\phi_1\phi_2(g_s-g))$. $\bar{b}^2$ is given in equation 7.7 as having the form $A_2' \phi_1 + B_1' \phi_2$,where A_2' is proportional to b_2^2 (component 2) and B_1' to b_1^2. The χ dependence of $\zeta^2(T,\phi)$ can be removed by multiplying by $1/R(0)$ yielding the slope of the $1/R(q)$ versus q^2 plots. Thus,

$$\frac{\zeta^2}{R(0)} = A_1/\phi_1 + B_2/(1-\phi_1) \qquad (7.19),$$

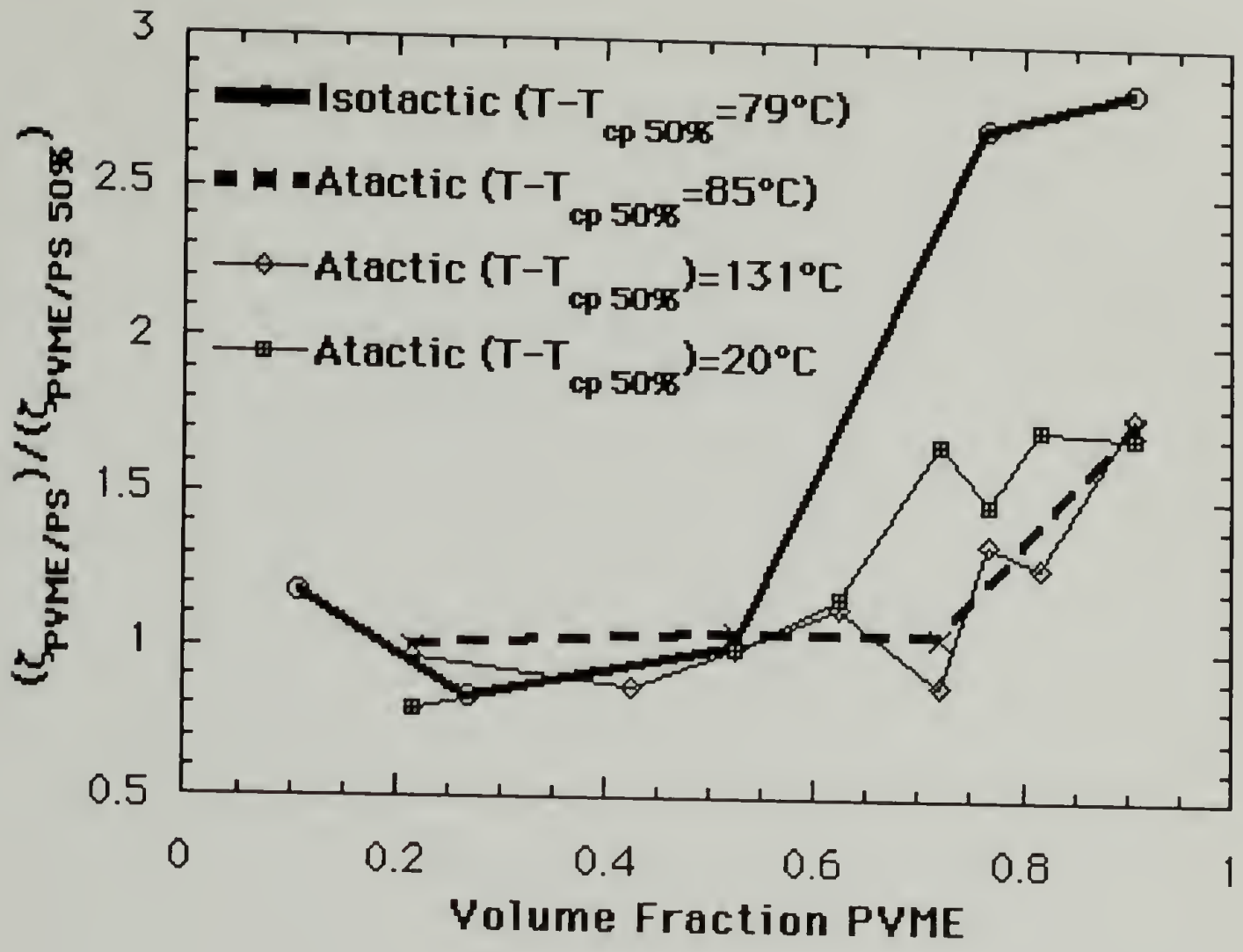

Figure 7.8 Reduced correlation length $(\zeta)/(\zeta_{50\%,T})$ versus composition. Isotactic PVME (at 100°C) shows a much stronger composition dependence at high percentages PVME. Atactic data for room temperature, 71°C and 136°C ($T_{cloud\ point}$ = 156°C) are presented for comparison from Yang. [The statistical error in the data (obtained from the scattering counts) is smaller than the data points, the actual error depends on the choice of the linear region in the $1/R_c$ plots. This is very small for the isotactic data which had a much larger linear region and is related to the scatter in the data for the atactic points.]

$$B_2 = \left(\frac{z_{2z}}{z_{2w}}\right)\frac{b_2^2}{18\, v_2\, k_n} \qquad (7.20\ a),$$

$$A_1 = \left(\frac{z_{1z}}{z_{1w}}\right)\frac{b_1^2}{18\, v_1\, k_n}. \qquad (7.20\ b).$$

This analysis is applied to the data of Figure 7.8 in Figure 7.9 yielding

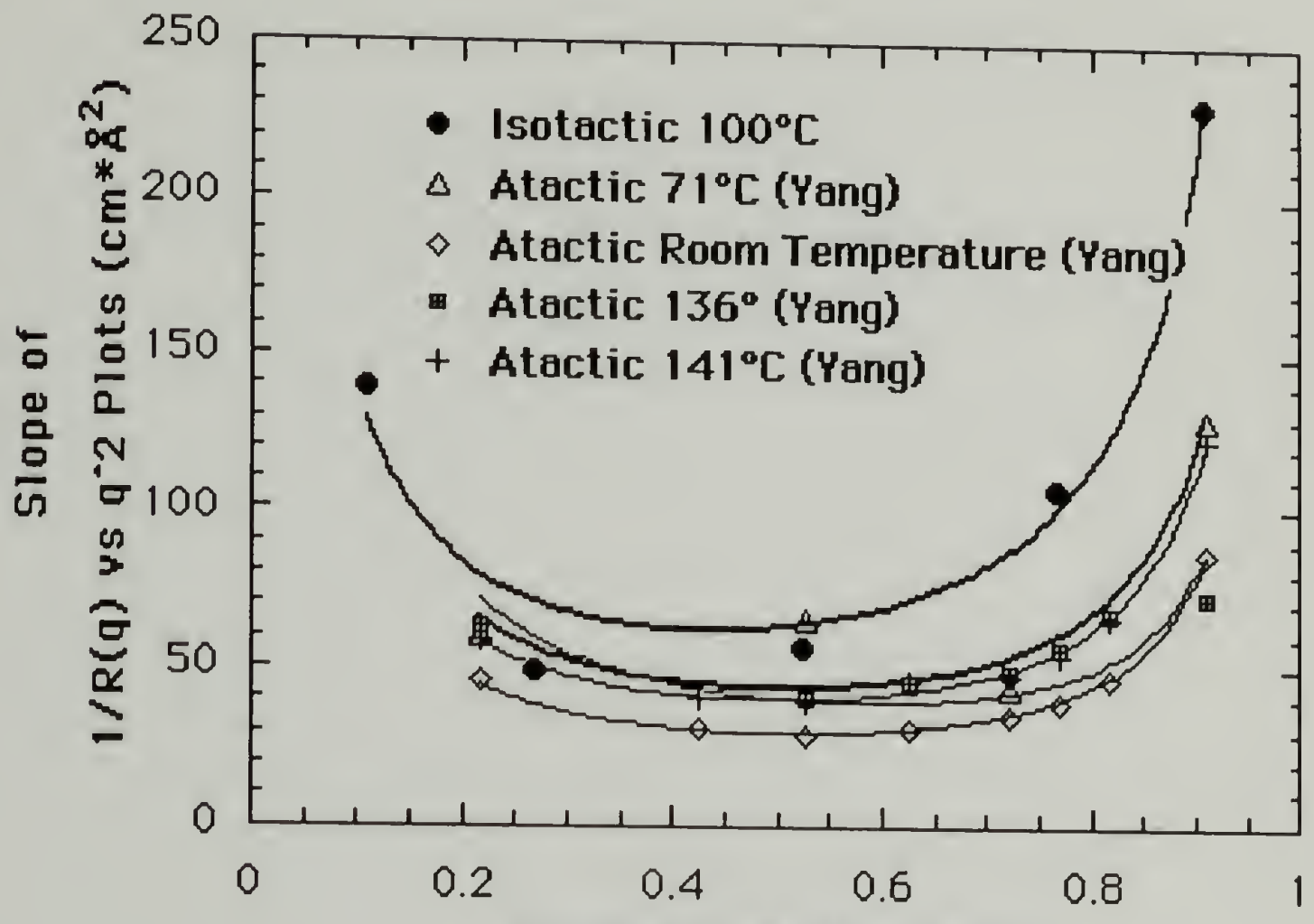

Figure 7.9 $\zeta^2/R(0)$ (slope of Figure 7.7) versus volume fraction PVME fit using equation 7.19. Values for A_{PVME} and B_{dPS} are presented in Table 7.2. [Error is discused in the legend of Figure 7.8.]

values for A_{PVME} and B_{dPS} which are tabulated in Table 7.2. The values in Table 7.2 for b_{PVME} give crudely similar values for the atactic PVME blends. Generally, it would appear that b for PVME is slightly smaller than b for PS. It would be expected, however, that b_{PS} would be the same for the isotactic and atactic blends which is clearly not the case.

It could be assumed that the use of a constant value for b_{iPVME} across the composition range is not an accurate assumption.

Table 7.2 A_{PVME} and B_{dPS} are used to calculate $b_{PVME/dPS}$ and b_{dPS} for the isotactic and atactic blends.

	A_{PVME}	B_{dPS}	Calculated b_{PVME} (Å)	Calculated b_{dPS} (Å)
Isotactic 100°C	11.75	19.70	7.0	14.4
Atactic 25°C	7.73	7.00	5.5	6.9
Atactic 71°C	11.19	10.65	6.6	10.7
Atactic 136°C	13.58	6.57	7.1	8.2
Atactic 141°C	9.86	10.09	6.1	10.2

A more in depth discussion of the behavior of b_{iPVME} and b_{aPVME} will be given with the discussion of the RPA analysis since $\bar{b}$ is fit directly in this approach (sections I, J, and O).

E. Extent of Linearity in $1/R_c(q)$ vs q^2 Plots.

It should be noted that the linear regime is significantly smaller for blends at the extremes of the phase diagram, i.e. 10% and 90% i-PVME. From equation 7.3 $1/R_c(q,T)$ is proportional to the sum of the inverse of the two volume fractions times their respective Debye factors. The linear regime is defined where at low q the Debye factors

behave as $1/U_i$ for a single random coil. This occurs where U_i is smaller than 1. Since the cumulative scattering intensity for the blend contains a modifying volume fraction term which serves to reduce the effect of the minor component in the blend for a particular composition the reduction in the linear regime for the 90% blend might be explained by a larger radius of gyration for the isotactic material ($U_i = q^2 R_g^2$). This is in fact the case for the blends studied ($z_{PVME} = 2080$, $z_{PS} = 757$ where z is the degree of polymerization).

The reduction in the linear regime for the low composition PVME can not be explained using classic F-H reasoning. The reduction appears to follow a reduction in the correlation length for the low composition. Plots of log $R_c(q,T)$ versus log q illustrate this behavior. In these plots the break in the intensity curve is a crude measure of the correlation length, Figure 7.10. If a comparison of the break in the scattering pattern from Figure 7.10 with the linearity of the $1/R_c(q)$ versus q^2 plot is made, Figure 7.11, a direct relationship is observed for the 10% i-PVME blend. This relationship does not exist for the higher concentration i-PVME blends.

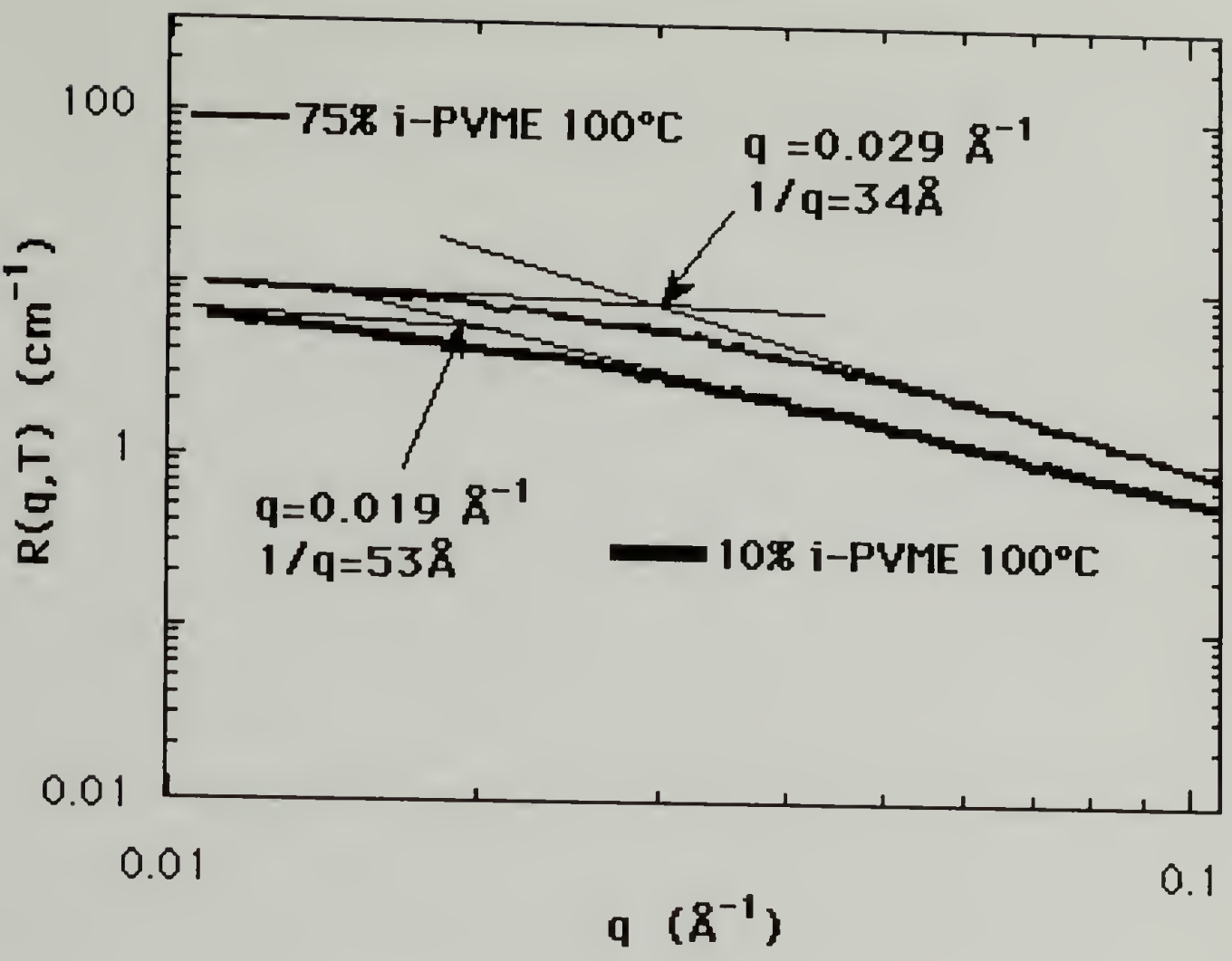

Figure 7.10 log Rc versus log q for 10% and 75% i-PVME/dPS blends at 100°C. The break in the curve at low q (indicated by the arrow) is a measure of the transition from large scale phenomena (small q) and large scale phenomena (large q). [Statistical error is smaller than the lines.]

Since F-H theory, with no composition dependence to χ, predicts that the correlation length should dramatically decrease in the low composition region ($q_{crossover}$ should increase) following equation 7.13, as large scale (small q) thermodynamic effects dominate small scale (large q) effects, the observed decrease in the linear region

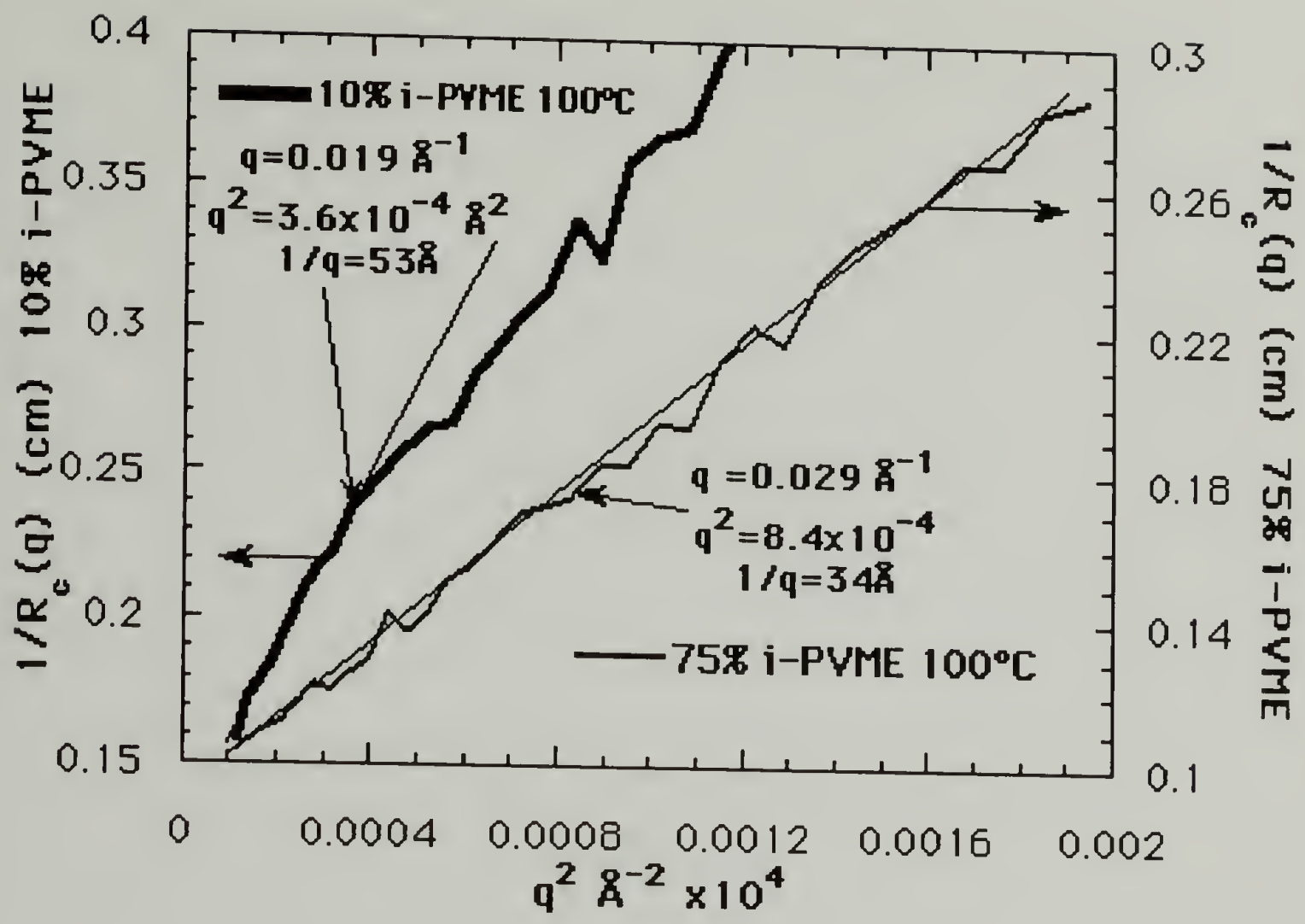

Figure 7.11 $1/R_c(q)$ versus q^2 for high and low fraction i-PVME blends. The linear region for the high composition blend is not limited by the correlation length. The low composition shows non-linearity directly above the correlation length shown in Figure 7.10. [Statistical error is smaller than the lines. Data scatter is related to actual error.]

(increase in ζ) can not be explained. It should be noted, and will be discussed in more detail later, that a composition dependent χ which showed reduced composition dependence in the low i-PVME concentration regime might explain the observed behavior.

F. $(g-g_s)$ as Determined by the Correlation Length Approach

$1/R_c(0,T)$ data was obtained from plots of $1/R_c$ versus q^2 as qualitatively discussed above and in section B. The composition dependence of $-(1/R_c(0,T))$, which should be related to $(g-g_s)$ according to equation 7.12, is plotted in Figure 7.12. Data from Yang's work on atactic PVME is compared with data on isotactic PVME obtained in this study.

Figure 7.12 demonstrates a dramatically larger composition dependence for $(g-g_s)$ for the isotactic PVME/dPS blends. The composition dependence is much greater in the low concentration regime. A non-linear drop in $(g-g_s)$ is observed for the high concentration data point. The advantage of the correlation length approach lies in its simplicity and ability to predict qualitative results. Numerical analysis of the g values obtained through direct application of the RPA theory (equation 7.3) will be more useful and are presented later.

Figure 7.13 shows the temperature dependence of $(g-g_s)$ for isotactic and atactic PVME/dPS blends.

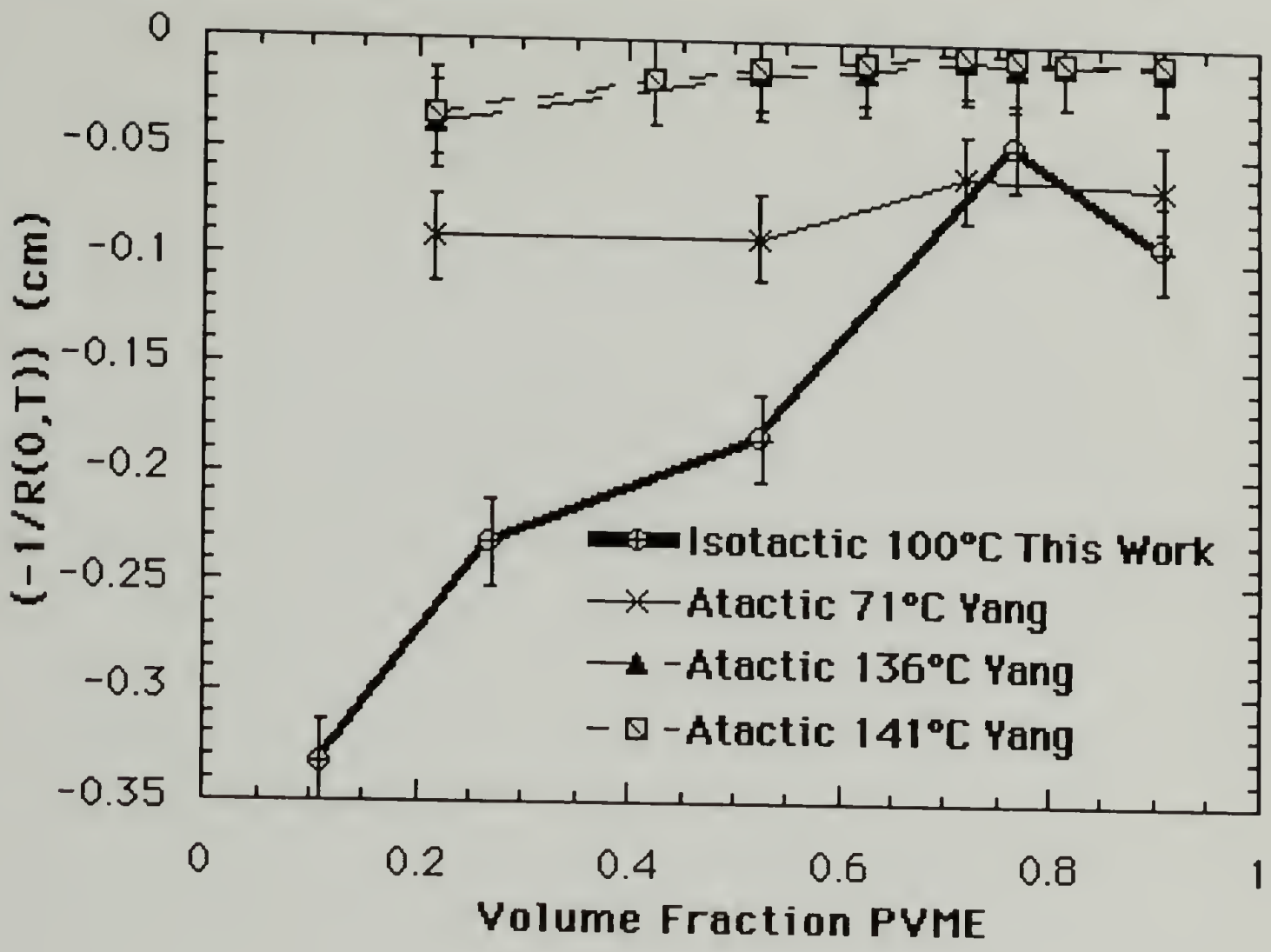

Figure 7.12 $(-1/R_c(0,100°C))$ versus volume fraction PVME for isotactic and atactic PVME blended with dPS. (Lines merely connect the data points. Actual error, estimated from the data scatter, is shown.)

Qualitatively, the isotactic data appears to merge with the atactic data as 1/T goes to zero. Additionally, the data does not appear to have a linear behavior in 1/T as would be predicted by a classically modified Hildebrand theory (χ=A+B/T). This is true for both the atactic and isotactic data, although it is much less pronounced in the

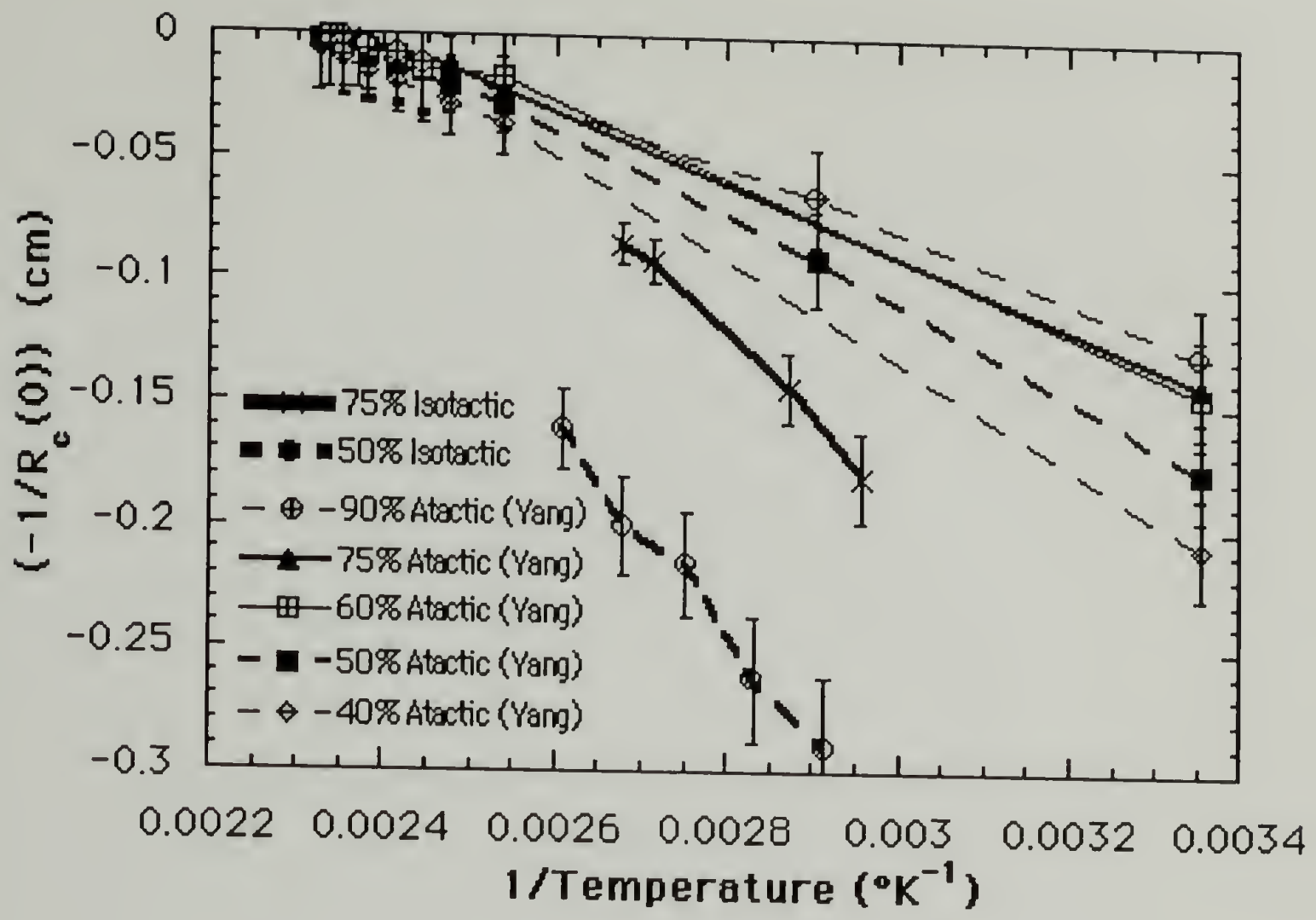

Figure 7.13 $-1/R_c(0,T)$ versus $1/T$ for two compositions of isotactic PVME and several compositions of atactic PVME (data of Yang). Istotactic PVME shows a much stronger temperature dependence to $(g-g_s)$. (Lines are not fits but merely connect the data points. Actual error, estimated from the data scatter, is shown.)

atactic data. The temperature dependence of $(g-g_s)$ appears to be modified by the the composition dependence as might be predicted by the F-H-S equation, $g=a+(b_0+b_1/T)/(1-c\phi)$. The thermal behavior of g will be discussed extensively in the RPA fit section below.

G. Temperature Dependance of the Correlation Length

Equation 7.13 predicts that as the spinodal temperature is approached the inverse of $\zeta^2(T,\phi)$ will go to zero. This behavior has been used to directly measure the spinodal temperature. Generally, this type of analysis is applicable only for data points in the vicinity of the cloud point temperature due to composition dependence and non-linear temperature dependence of χ not predicted by the Hildebrand theory. Since the data measured in this study is far from the cloud point temperature a comparison of the cloud point temperature and the estimated spinodal temperature becomes a measure of the non-linearity of χ. Additionally, a model (fit to the data) which accounts for the non-linear thermal behavior is expected to estimate the spinodal temperature as a value close to the cloud point temperature especially for critical compositions. Plots of $\zeta^{-2}(T,\phi)$ versus T are given in Figures 7.14 and 7.15 for a 50% i-PVME/dPS blend and a 75% iPVME/dPS blend respectively (M_w dPS for the 75% blend is 110 kg/mole blend).

From equation 7.13 the extrapolated temperature where $(1/\zeta^2) = 0$ should correspond to the spinodal temperature. The cloud point for the 50% blend occurs at about 179°C. This discrepancy may be explainable in view of the absence of a concentration dependence to χ in the classically modified F-H theory (i.e. χ=A+B/T). The modified F-H theory also fails to account for possible temperature dependences to the entropic component of χ, A.

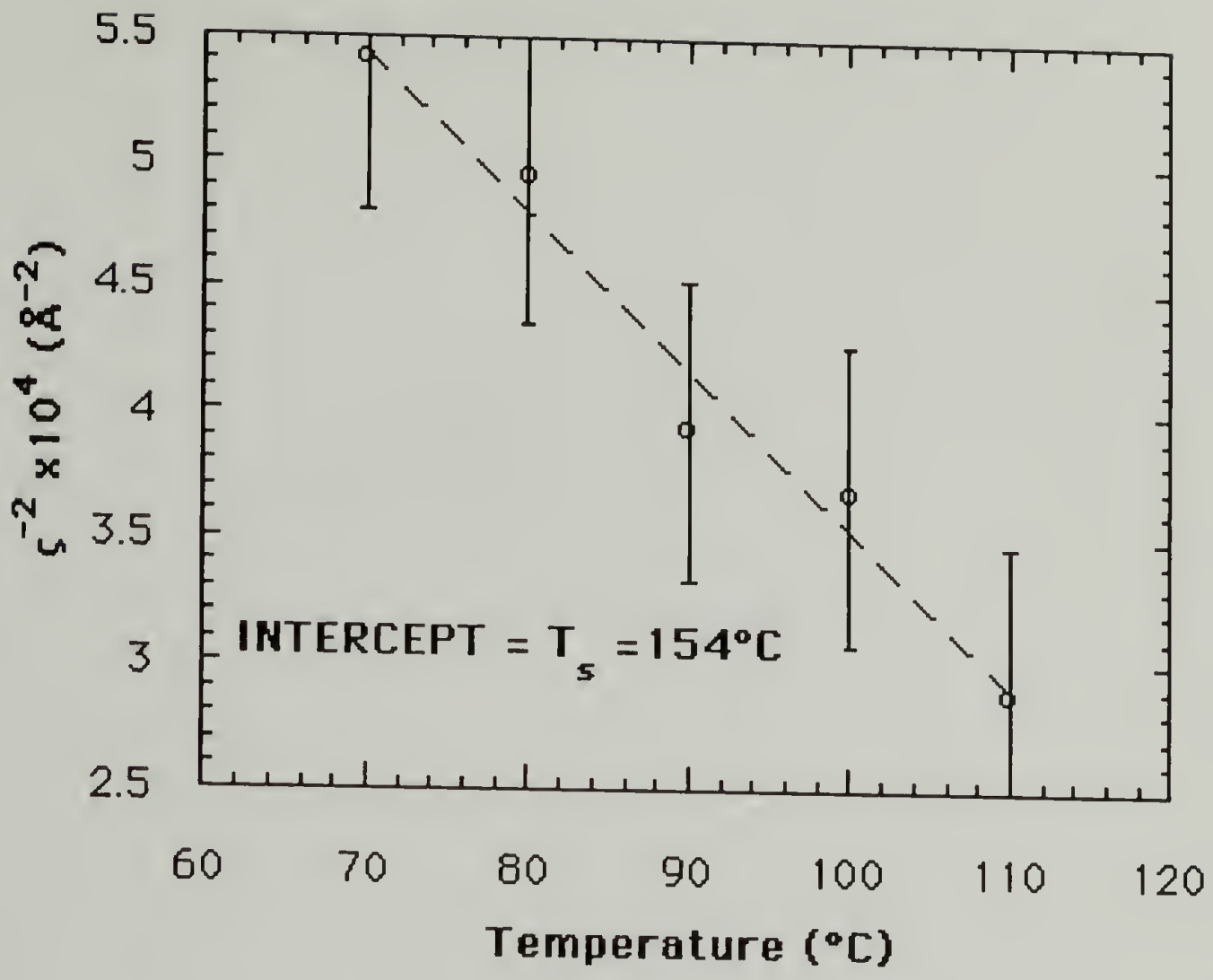

Figure 7.14 The inverse of the correlation length squared, ζ^{-2}, versus temperature for a 50% i-PVME blend (M_w dPS=85kg/mole). The extrapolated value should give the spinodal temperature using the correlation length approach and F-H theory. Error is estimated from data scatter.

Figure 7.15 is a similar plot for a 75% i-PVME blend (near the critical point) with a higher molecular weight dPS (110 kg/mole). The extrapolated spinodal temperature is 126°C where as the measured cloud point is about 176°C. Two explanations for this rather large difference may be made. First, the difference may be real, due to polydispersity and a large composition dependence to g. Secondly, very slow phase separation kinetics in the isotactic blend

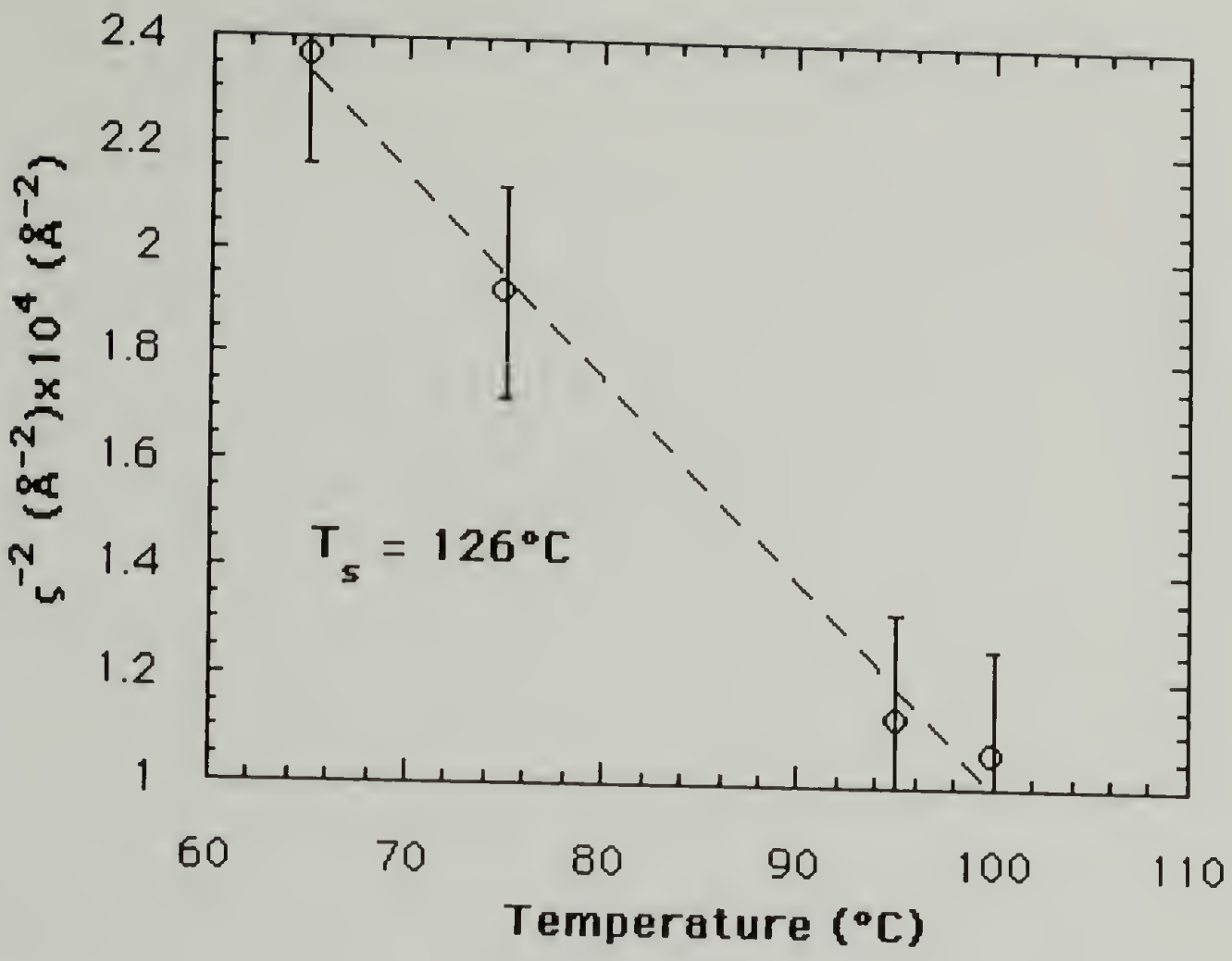

Figure 7.15 The inverse of the correlation length squared, ζ^{-2}, versus temperature for a 75% i-PVME blend (M_w dPS=110kg/mole).

may inhibit the measurement of the initial phase separation point in the isotactic blends (T_{CP}) until the blends are heated well into the spinodal regime. A combination of these two effects may lead to the observed difference.

H. Random Phase Approximation

In addition to the correlation length approach given above, the data was fit to deGennes' RPA equation (equation 7.3) in order to obtain χ_{sc}/v_0 and $\bar{b}^2/v_0$ directly as fitting parameters. Figure 7.16 shows a typical fit to the isotactic data using a non-linear regression software[14].

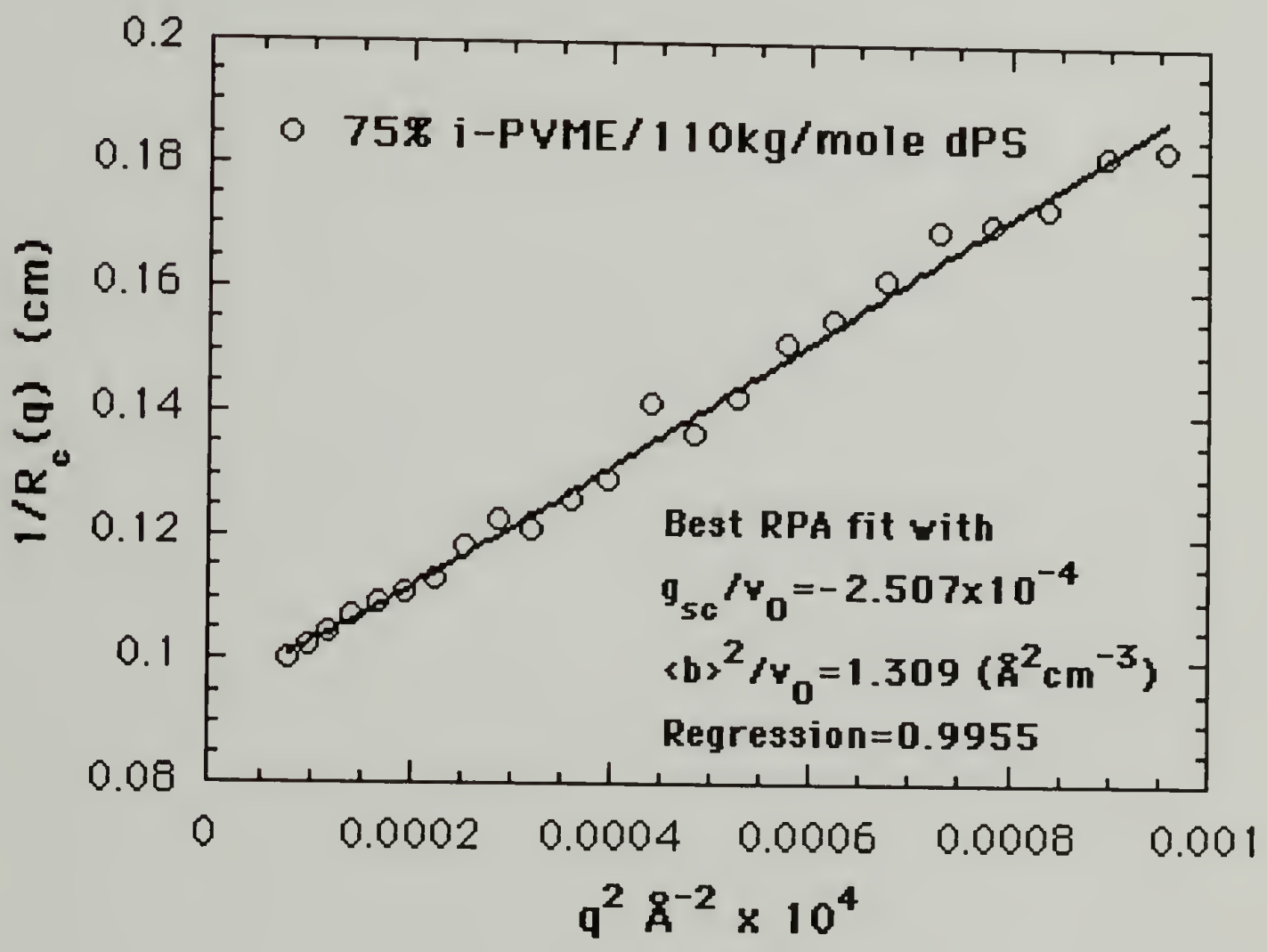

Figure 7.16 Typical RPA fit (equation 7.3) to SANS data using χ_{sc}/v_0 and $\bar{b}^2/v_0$ as fitting parameters. Note slight up turn of fit at low q^2 which alters χ_{sc}/v_0 by as much as 20% from a linear fit.

The most significant difference between the linear correlation length approach and the direct RPA approach is the slight up turn of the fit in the critical region of very low q. This slight up turn may alter the value obtained for χ_{sc}/v_0 by as much as 20% from a linear fit. Additionally, the fit is optimized in terms of the two independent experimental parameters of interest, χ_{sc}/v_0 and $\bar{b}^2/v_0$ rather than in terms of the slope, $\zeta^2/R_c(0)$, and the intercept, $1/R_c(0)$, which are themselves interdependent functions of the parameters of interest. Finally, it has been shown that the RPA fit is applicable to higher q^2 values since it is able to accommodate some degree of non-linearity, there by relieving some of the need to obtain extremely low q data. The main drawback of the RPA analysis is the complexity of the fit which makes qualitative understanding of the fit difficult.

I. Composition Dependence of the Statistical Segment Length

As was noted above, the RPA theory yields χ_{sc}/v_0 and the average statistical segment length, $\bar{b}^2/v_0$, directly as fitting parameters to the scattering data. The average statistical segment length is related to the statistical segment lengths of the components of a polydisperse blend by equation 7.7 as derived by Joanny[5]. The statistical segment length is a physical parameter for a polymer chain akin to the Kuhn step length[15]. The Kuhn step length is, however, a derived quantity which expands the usefulness of the freely jointed random coil theories to non-freely jointed chains. "b", in contrast, is a physical measure of the average base unit of a polymer chain. Along this line of reasoning it is possible to think of the statistical segment length of

one component of a polymer blend as being related in some way to the average length of an interacting unit (since they are both dimensional parameters on similar size scales for the same material).

(As was noted in section B, it is $\bar{b}^2/v_0$ rather than R_g which is measured in the RPA approach used here. z_i for the two components is fixed in this analysis. z_i is essentially removed from equation 7.6 in the low q regime by cancelation in equation 7.3 .

Following the reasoning of Staverman[16] and later Koningsveld[17], differences in the size (specifically the surface area) between interacting units of a polymer blend can account for shifts in the critical point from the composition predicted by theory,

$$\phi_{c\ PVME/PS} = \frac{z_{PVME}^{1/2}}{z_{PVME}^{1/2} + z_{PS}^{1/2}} \text{ (= 0.62 for the i-PVME/dPS blend)} \qquad (7.21)$$

The experimental value for $\phi_{c\ PVME/PS}$ is 0.72 to 0.76. Differences in the surface areas of blend components are thought to be the origin of a composition dependent χ. Further, since "b" is a physical quantity, it can be thought of as being effected by structural changes in the polymer chain such as tacticity. It is believed that isotactic PVME, having a more ordered structure, will have a smaller sized interacting unit in comparison with atactic PVME. Support for this comes from the index of refraction data given above, the molecular models previously discussed, and shifts in the Staverman parameter, $c_{PVME/PS}$, necessary to fit optical cloud point data. This belief has

been useful in predicting a dramatic shift in the phase separation kinetics for the isotactic PVME blends of close to critical composition discussed in Chapter 6. The $\bar{b}^2/v_0$ data has been analyzed in view of this postulate.

Figure 7.17 is a plot of $\bar{b}_{PVME/PS}$ versus composition for isotactic and atactic PVME blends. v_0 was calculated as $v_0 = \sqrt{v_{PVME}\, v_{PS}}$ where

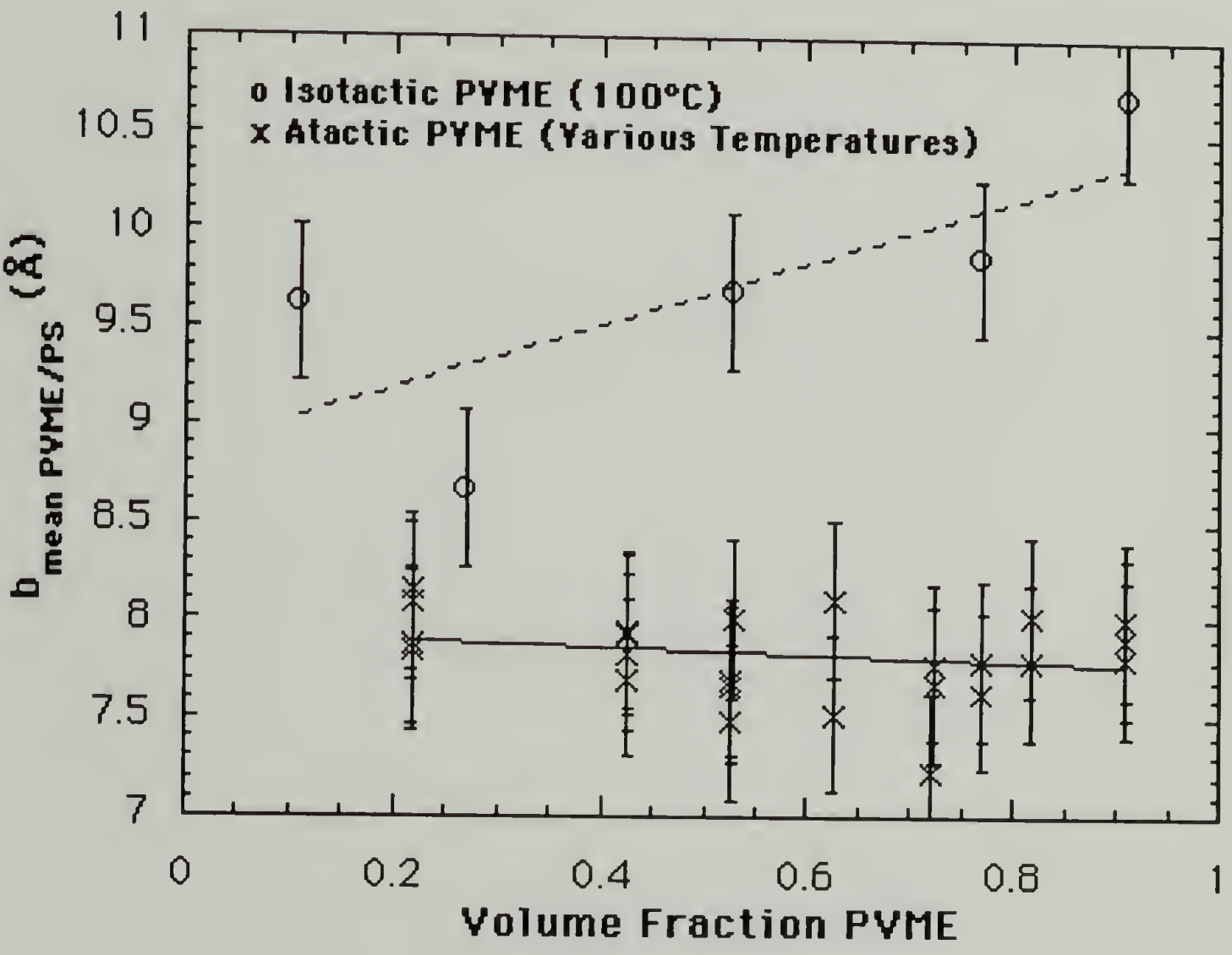

Figure 7.17 $\bar{b}_{PVME/PS}$ versus volume fraction PVME for isotactic PVME (this work) and atactic PVME (Yang reference 2). Linear fits are applied to show the general trend of the data. Isotactic PVME shows a strong composition dependence absent in the atactic data.

the thermal expansion of v_{PVME} and v_{PS} is accounted for. Linear fits are provided in order to show the general trend of the data. $\bar{b}_{i\text{-}PVME/PS}$ shows a strong composition dependence. The behavior is reminiscent of the behavior shown in Figure 7.9 for the correlation length, however fits of the form, $\bar{b}_{i\text{-}PVME/PS} = (A\,\phi_{PVME} + B\,(1\text{-}\phi_{PVME}))^{1/2}$, following equation 7.7, give poor results, similar to the linear fit shown in Figure 7.17. Since the atactic PVME data shows comparatively no composition dependence it is assumed that b_{dPS} and $b_{a\text{-}PVME}$ are not significantly composition dependent (see section D for implications of a variable $\bar{b}_{i\text{-}PVME/PS}$). Thus, one can use equation 7.7 to isolate the dependence of $b_{i\text{-}PVME}$ from that of $\bar{b}_{i\text{-}PVME/PS}$. The values of b_{dPS} and $b_{a\text{-}PVME}$ are known from the work of Yang to be close to 6.8 and 6.9Å respectively. These values were calculated from the characteristic ratio, $C=\langle R_0^2\rangle^{1/2}/M^{1/2}$ as given in the Polymer Handbook and the mer molecular weight, m_i, (these are, strictly speaking values for the Kuhn step length which, as has been noted above, is conceptually different, although not necessarily numerically different, from the statistical segment length),

$$\text{"}b_i\text{"} = m_i^{1/2}\, C_i \qquad (7.22).$$

Yang used these values together with equation 7.7 and the polydispersities, to calculate $\bar{b}_{a\text{-}PVME/PS}$ for his blends to be about 8.5Å which agreed with his data fairly well. Thus, polydispersity serves to significantly increase the mean value as can be seen directly in equation 7.7 since $\left(\frac{z\ z}{z_w}\right)$ is always equal to or greater than one. If one

cancels the volume fractions in equation 7.7, equation 7.23 is obtained,

$$\frac{\bar{b}^2}{v_0} = \left(\left(\frac{z_{PVMEz}}{z_{PVMEw}}\right)\frac{b^2_{PVME}\,\phi_{PS}}{v_{PVME}} + \left(\frac{z_{PSz}}{z_{PSw}}\right)\frac{b^2_{PS}\,\phi_{PVME}}{v_{PS}}\right) \qquad (7.23).$$

Therefore, a relatively larger $\left(\frac{z_{PVMEz}}{z_{PVMEw}}\frac{1}{v_{PVME}}\right)$ will be felt in the low PVME concentration regime (this ratio is about 0.026 for i-PVME and 0.010 for dPS at 100°C). Using b_{dPS} = 6.8Å, as discussed above, in equation 7.7 the data in Figure 7.18 is derived. If different values for b_{dPS} are used, specifically in the range b_{dPS} = 10 to 5Å, the general features of Figure 7.18 do not change (the fit, discussed below becomes worse using these values since the data no longer behaves monotonically).

The calculated $b_{i\text{-}PVME}$ displays a very strong composition dependence. At low concentrations i-PVME it approaches a limiting value of 6.55Å which is somewhat smaller but comparable to the value of 6.9Å given by Yang for atactic PVME. At high concentrations i-PVME the value becomes very large. The behavior is reminiscent of a binary chemical reaction which depends on the concentration squared. Using this analogy one could qualitatively say that an initial value for the statistical segment length at zero concentration, $b_{\phi=0\ i\text{-}PVME}$ is augmented by an orientational correlation which involves two statistical segment lengths (of size $b_{\phi\ i\text{-}PVME}$) associating. Thus

one could say $b_{\phi\ \text{i-PVME}} = b_{\phi=0\ \text{i-PVME}} + \kappa\,\phi^2$, where κ represents the amount added to $b_{\text{i-PVME}}$ per successful interaction times the

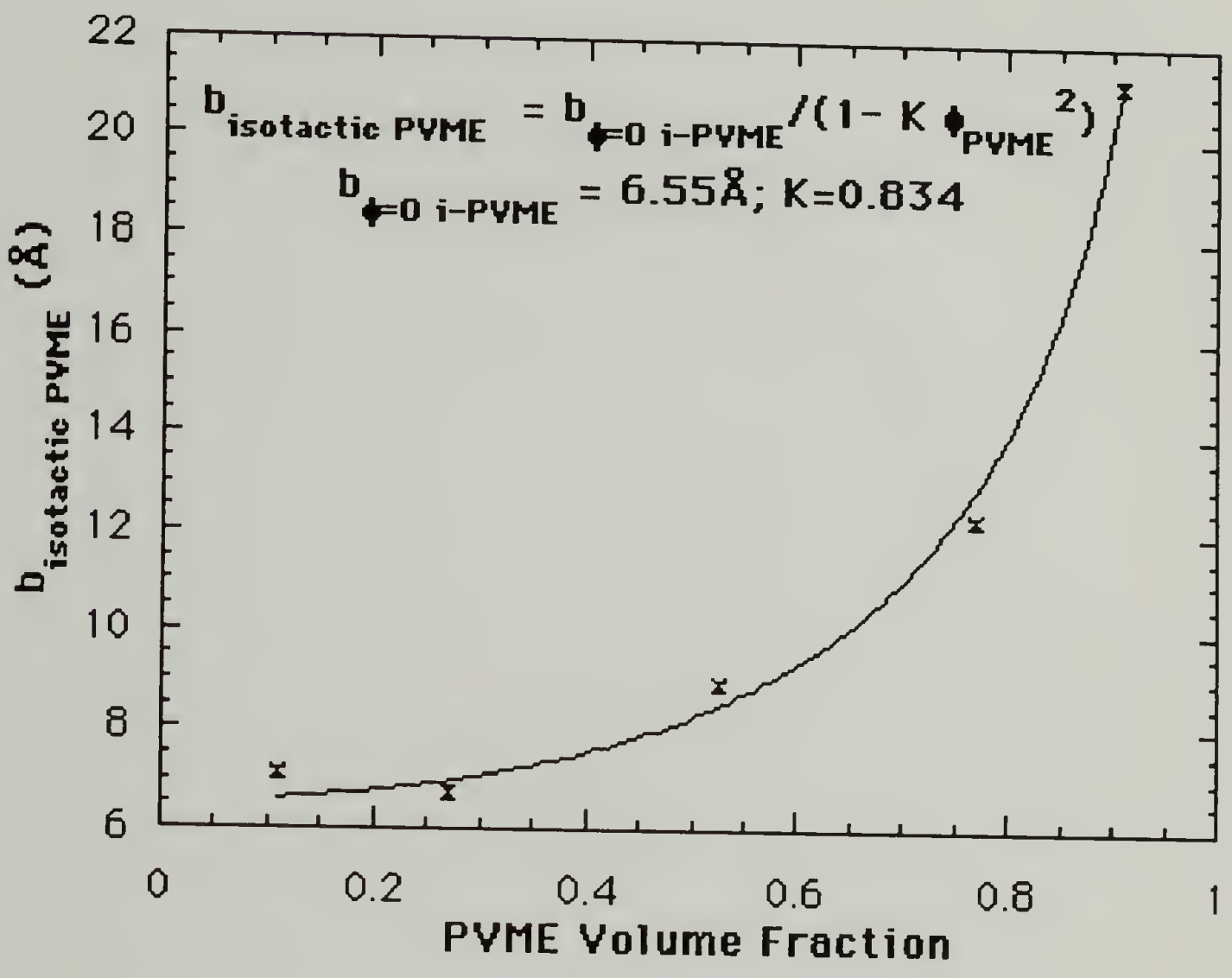

Figure 7.18 $b_{\text{i-PVME}}$ versus volume fraction isotactic PVME at 100°C as calculated using $\bar{b}_{\text{PVME/PS}}$ from Figure 7.17 and $b_{\text{dPS}} = 6.8$Å from the work of Yang (reference 2).

probability for success. κ, in this scenario, will be proportional to the value of $b_{\text{i-PVME}}$ itself since the larger the size of a correlated region the larger the influence on a correlating partner. Thus,

$$b_{\phi\ \text{i-PVME}} = \frac{b_{\phi=0\ \text{iPVME}}}{(1-K\,\phi^2)} \qquad (7.24),$$

where K is a non-dimensional factor which measures the probability of an interaction adding one $b_{\phi\ \text{i-PVME}}$ to $b_{\phi=0\ \text{i-PVME}}$ at a concentration ϕ. Equation 7.24 was used to fit the data for $b_{\phi\ \text{i-PVME}}$ in Figure 7.18 yielding $b_{\phi=0\ \text{i-PVME}}$ =6.55 and k=0.834 (regression of 0.997). $b_{\phi=0\ \text{i-PVME}}$ is smaller than the reported value of 6.9Å which might be expected if the isotactic material were more ordered than the atactic material 'ab initio' (better ordered materials such as crystals tend to be more compact, i.e. denser, than less ordered materials such as liquids for example). The extrapolated $b_{\phi=1}$ in this scenario has a finite value of 39.5Å at 100°C (at other temperatures this value is not finite as will be discussed below).

A parallel derivation of equation 7.24 can be obtained if one considers the probability of two statistical segments of i-PVME interacting as being proportional to the correlation function for the two chains which is given by[18],

$$g(r) = \frac{3}{\pi}\frac{b}{r}\phi^2 \qquad (7.25),$$

where $b=b_{\phi\ \text{i-PVME}}$. r, in this case would be considered the distance over which the correlation occurs. Thus,

$$b_{\phi\ \text{i-PVME}} = b_{\phi=0\ \text{i-PVME}} + \frac{3\,b_{\phi\ \text{i-PVME}}}{\pi}\left(\frac{\delta}{r}\right)\phi^2 \qquad (7.26),$$

which gives $K=\frac{3\lambda}{\pi r}$ where λ is a length factor which accounts for the probability of adding to the statistical segment length a value of $b_{\phi\ i\text{-}PVME}$ for an approach distance r at $\phi_{PVME}=1.0$. If k=0.83, then $\delta/r = 0.87$. δ will be discussed in more detail below.

As was discussed above, the type of ordering which may occur in the isotactic PVME can be visualized by reference to the simple molecular models of Chapter 5.

J. Temperature Dependence of the Statistical Segment Length

Figure 7.19 shows the temperature dependence of $\bar{b}_{a\text{-}PVME/PS}$ from Yang's data. The data indicates a slight increase in $\bar{b}_{a\text{-}PVME/PS}$ with temperature, although this may be within actual experimental error. Figure 7.20 is a plot of b_{iPVME} for the isotactic data where b_{dPS} was considered constant as discussed above (the temperature ranges do not coincide so that plots on the same scale were not possible for the isotactic and atactic blends).

The isotactic data shows a decrease in $\bar{b}_{i\text{-}PVME/PS}$ with temperature outside of experimental error. Following the discussion given in the previous section specifically the analogy with chemical equilibrium, K, in equation 7.24 could be thought of as behaving like a

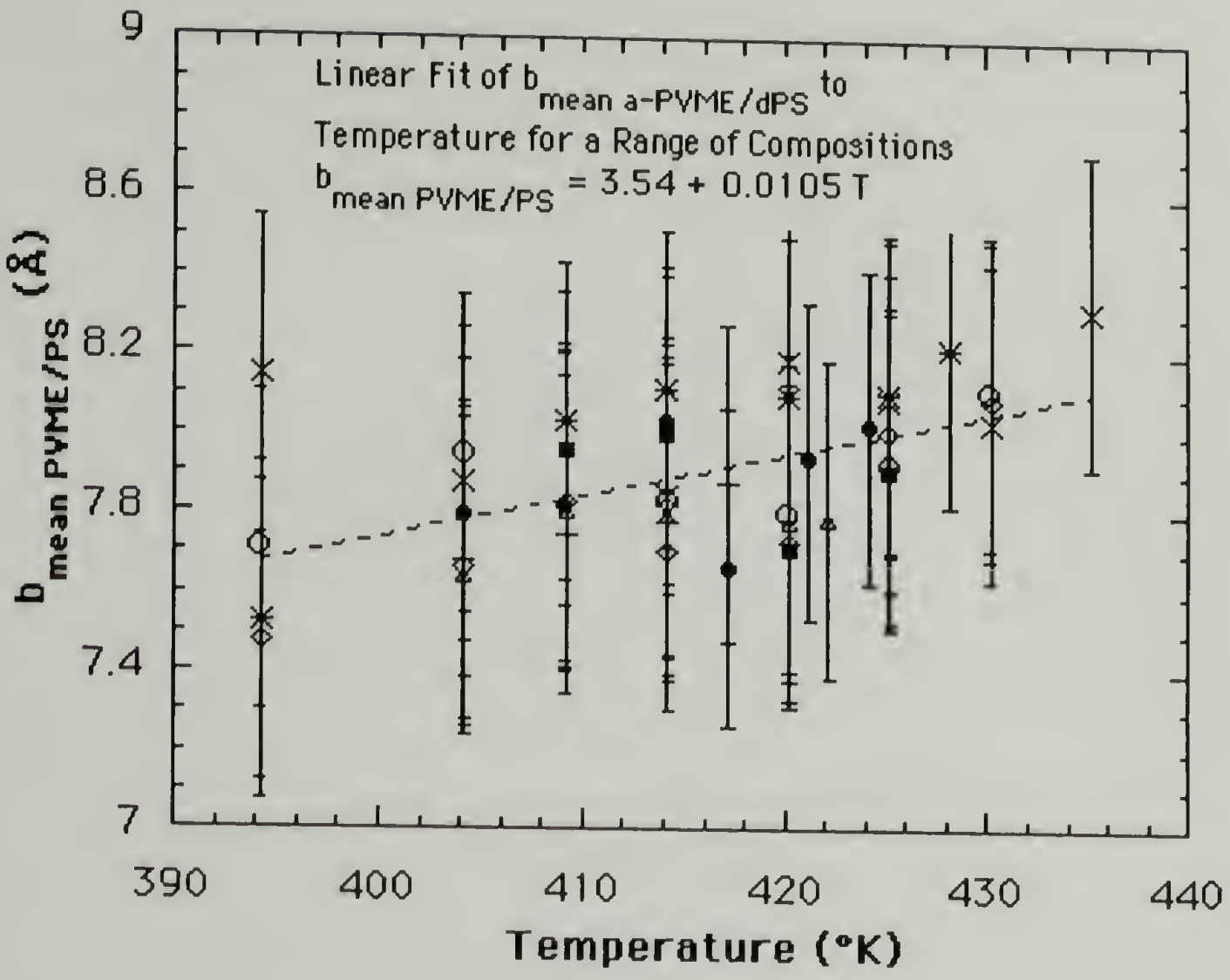

Figure 7.19 Temperature dependence of $\bar{b}_{a\text{-PVME/PS}}$ from Yang's data (reference 2). Data shows a high degree of scatter and the temperature dependence is comparatively small (about a 5% or 0.2 Å change over 50°C). Error bars indicate actual error obtained from scatter in the data.

chemical equilibrium constant. One could therefore surmise that K would have a temperature dependence given by,

$$K = 1 \exp\left(\frac{-\Delta G}{RT}\right) \qquad (7.27),$$

where "l" is a scaling factor which relates the distance of interaction r with the distance added to the statistical segment length at T=∞ and

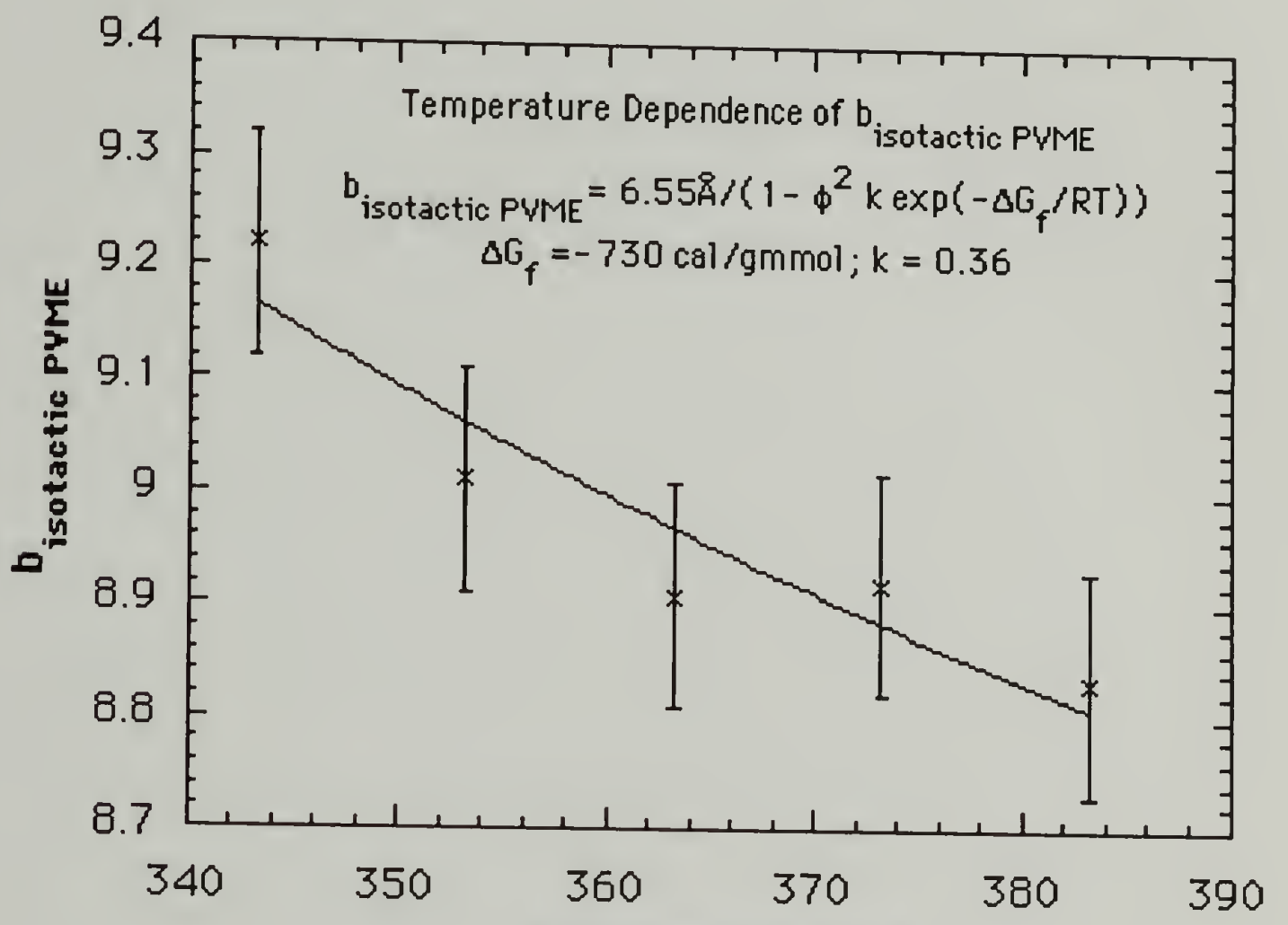

Figure 7.20 Temperature dependence of $\bar{b}_{i\text{-}PVME/PS}$. The change with temperature is about 5% as in the atactic data however the slope is in the opposite direction (absolute value of change is larger 0.35Å). Error bars indicate actual error as obtained from scatter in the data. Statistical error is smaller than the data points.

ϕ=1, thus, combining the temperature dependence with the composition dependence we have,

$$b_{\phi\ \text{i-PVME}} = \frac{b_{\phi=0\ \text{iPVME}}}{\left(1 - \frac{3\,\lambda\,\exp(-\Delta G/RT)}{\pi\,r}\,\phi^2\right)} \qquad (7.28).$$

Figure 7.20 shows a fit of the temperature dependence with this equation using $b_{\phi=0\ \text{iPVME}}$=6.55Å from the composition data which yields a value for $\frac{3\,\lambda}{\pi\,r}$ of 0.36 and a value for ΔG of -730 cal/gmmol. If λ, the amount added to b_{iPVME} per correlation, is given a value of 1 to 10Å then r, the distance for such a correlation, will be 2.7 to 27Å which seems to be a reasonable distance range. The ΔG value of -730 cal/gmmole is in the range of a crystallization free energies for polymers[19].

K. χ_{sc} as Applied to the Flory-Huggins-Staverman Empiricism

The χ_{sc}'s obtained using the RPA theory were fit to the F-H-S equation presented in Chapter 5. As discussed above, χ_{sc} is related to the second derivative of free energy with respect to composition. For a composition dependent χ, Sanchez[20] (among others) has derived,

$$g_{sc} = g - (\phi_1 - \phi_2)\frac{dg}{d\phi_1} - \left(\frac{\phi_1\,\phi_2}{2}\right)\frac{d^2g}{d\phi_1^{\,2}} \qquad (7.29).$$

Using this equation with the F-H-S description of χ we have,

$$g_{sc} = a + \frac{(b_0 + b_1/T)}{(1 - c\,\phi_2)} - \frac{c\,(1 - 2\,\phi_2)\,(b_0 + b_1/T)}{(1 - c\,\phi_2)^2} - \frac{c^2\,(\phi_2 - \phi_2^{\,2})\,(b_0 + b_1/T)}{(1 - c\,\phi_2)^3}$$

(7.30),

in which the first two terms represent χ in the F-H-S nomenclature and the second two terms are due to the composition dependence of χ.

L. g_{sc} as a Function of Temperature

Figure 7.21 shows the temperature dependence of g_{sc} for the isotactic blends and for Yang's atactic PVME/PS blends at 50% and 75% a-PVME which corresponds to the compositions of the isotactic blends ($v_0 = \sqrt{v_{PVME}(T)\, v_{PS}(T)}$).

Isotactic PVME blends show a much stronger temperature dependence which appears to asymptotically approach that of the atactic blends at high temperatures. The temperature dependence does not appear to be strongly affected by composition, although the absolute value of χ is strongly affected. The 75% isotactic PVME data point (box with a line in it) corresponds to a dPS molecular weight of 85kg/gmmole, the temperature scan data (filled diamond) corresponds to 110kg/gmmole dPS. There is a shift of χ with molecular weight of the dPS component, however, as was noted above the data remains strongly temperature dependent relative to the atactic data.

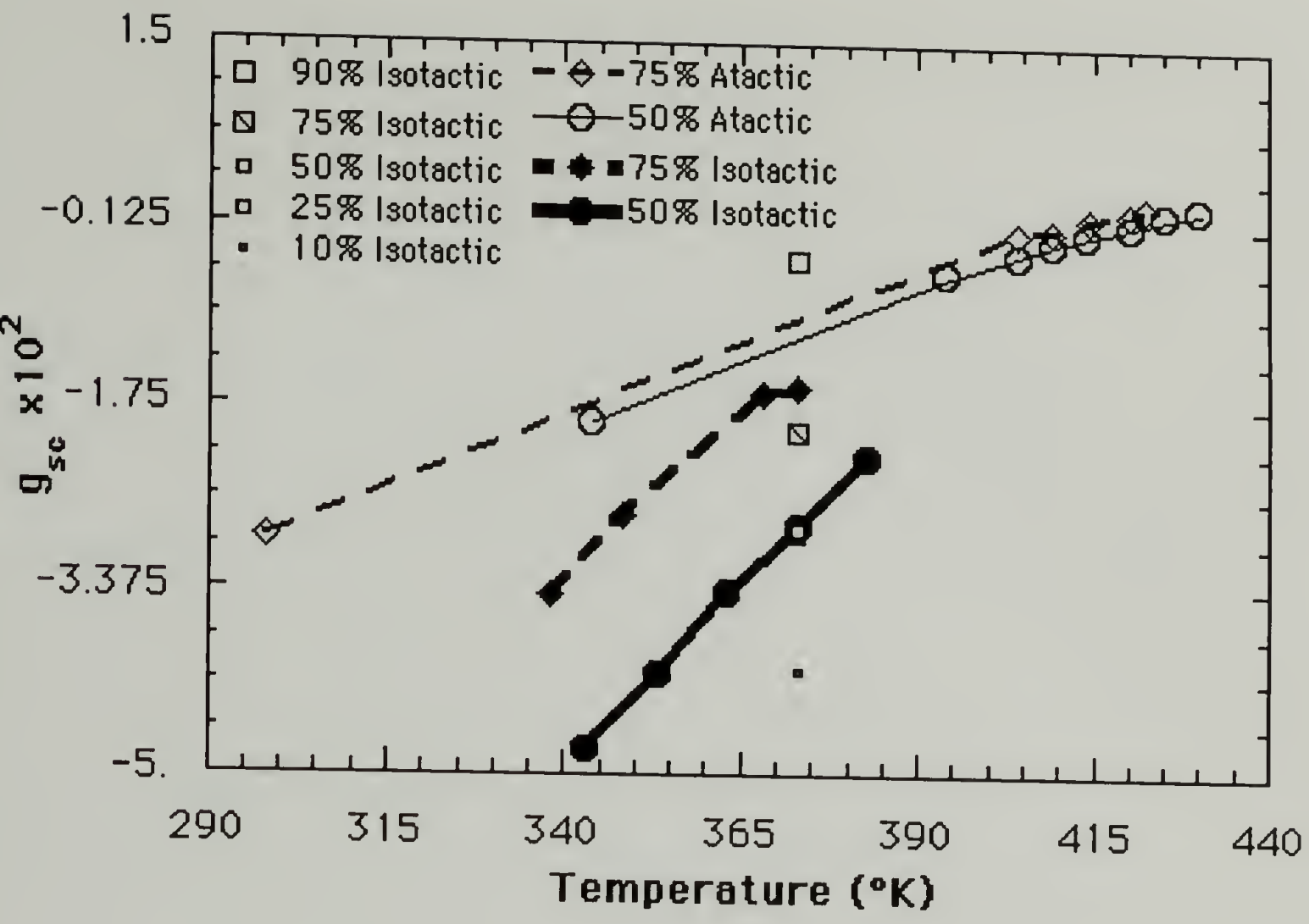

Figure 7.21 Temperature dependence of g_{sc} for 75% and 50% i-PVME blends, 75% and 50% a-PVME blends and 10 to 90% g_{sc} values at 100°C. Isotactic PVME blends display a much stronger temperature dependence. (Lines merely connect the data points for clarity. 75% i-PVME blend used 110kg/gmmole dPS. Statistical error is smaller than the data points.)

The temperature data for the atactic PVME could not be fit using equation 7.30 and a $c_{PVME/PS}$ of 0.36 (which fit the cloud point data for a-PVME/hydrogenous PS) over all of the temperature ranges and compositions reported by Yang (6 compositions and at least four temperature per composition were measured). It is believed that this is due to the deuteration effect. This failure to match the hydrogenous PS data might be expected since cloud points for a-PVME/hPS and a-PVME/dPS differ by 10 to 20°C over the composition range. It was

possible to fit all of Yang's rather extensive data using the F-H-S theory if a different (but constant) $c_{PVME/PS}$ was used. It was found that the best fit to all of Yang's composition and temperature scan data occurred when $c_{PVME/PS}$ = -0.189, or when the surface area ratio was $\frac{S_{a\text{-}PVME}}{S_{dPS}}$ = 1.189. This should be compared to $\frac{S_{a\text{-}PVME}}{S_{PS}}$ = 0.64 using the Bondi method. If $S_{a\text{-}PVME}$ is constant in the two isotopic blends, then $S_{dPS} = 0.54\ S_{PS}$. Since the mass of deuterium is twice the mass of hydrogen, it conceivable that thermal motions in the dPS aromatic side groups are hindered causing a reduction in the volume and surface area.

Figure 7.22 shows the fit to the thermal data using equation 7.30 and $c_{PVME/PS}$ of -0.189, a=0.0136, b_0=0.0713, b_1=-36.9.

Perfect data fits are possible on individual temperature scans if one allows "b_1" to be a free fitting parameter and fixes a and b_0 to the values obtained from the composition fits. An iterative fitting between the composition and temperature data was the source of the values given.

The g values for the isotactic PVME/PS blends were also fit using equation 7.30. It was impossible to obtain a good fit to both the temperature dependence and the composition dependence using a fixed $c_{PVME/PS}$, even when $c_{PVME/PS}$ was used as a fitting parameter. Fits to the temperature data alone, or the composition data alone were

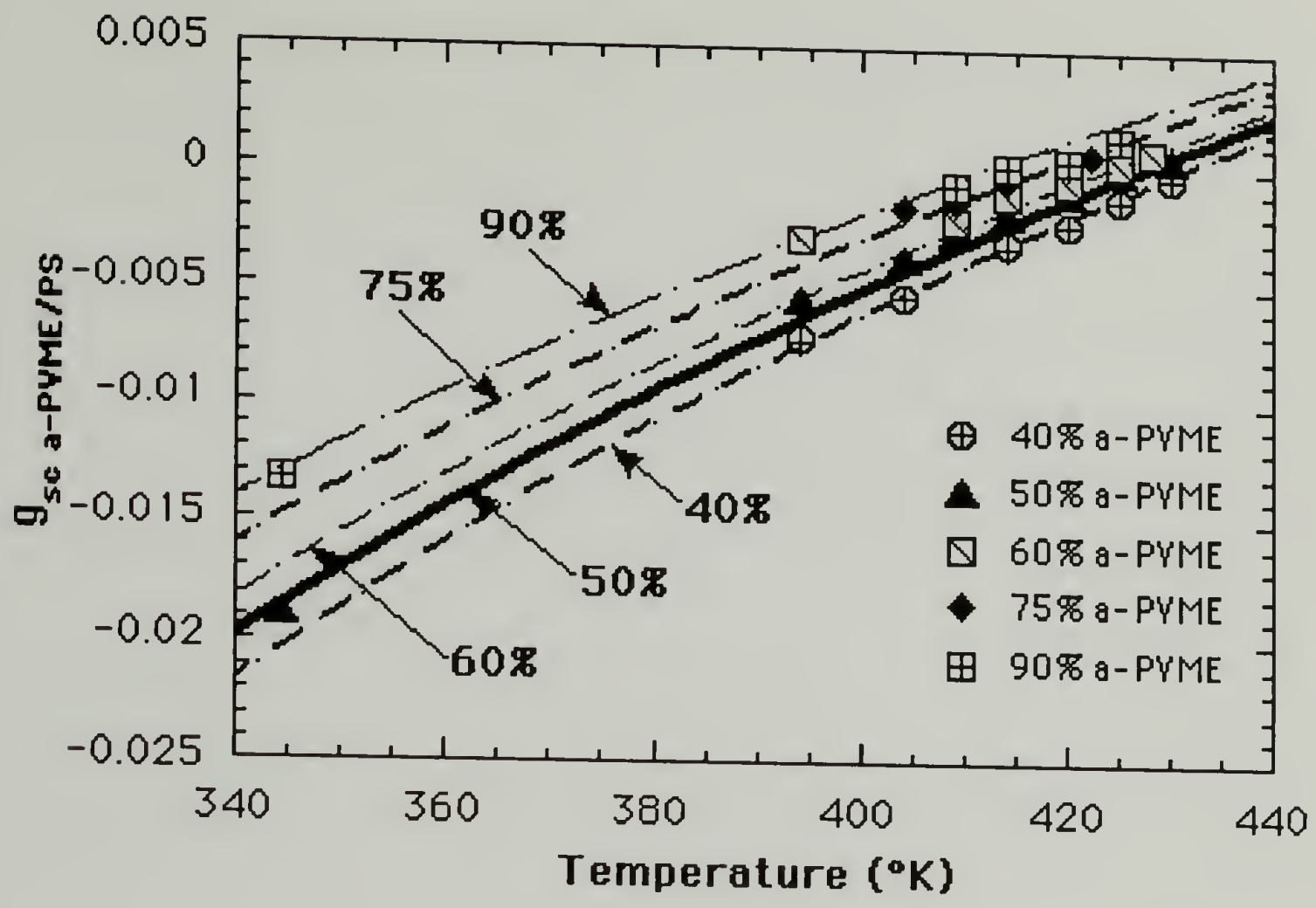

Figure 7.22 Fit of equation 7.30 to the temperature dependence of g_{sc} using $c_{PVME/PS}$ = -0.189, a=0.0136, b_0=0.0713, b_1=-36.9. Data points are from Yang.

possible and lead to good fits. The aim in this work, however, is to gain an understanding of the nature of the tacticity effect and such single parameter fits, although useful as a predictive tool for that single variable (T or ϕ), are useless in terms of gaining an understanding of the effect. The fits to the data for the correlation length given above were capable of simulating both the concentration and temperature dependence. It was thought that changes in the statistical segment length might correlate in some way with changes in $c_{PVME/PS}$ since they are both geometric parameters for the same material and since atactic PVME showed relatively little change in both $c_{PVME/PS}$ and $\bar{b}^2$, where as isotactic PVME showed strong

temperature and composition dependencies. Many relationships were attempted, such as a simple proportionality between the ratio of the statistical segment lengths of PVME and dPS and the surface areas.

The first point to note in deriving a relationship between b_{iPVME} and S_{iPVME} is that S_{iPVME} has a limiting value at $\phi_{PVME}=1.0$. That is, correlated PVME has a finite surface area per interacting unit on the size scale of the surface area per interacting unit of dPS. This is a minimum value which expands as less of the isotactic PVME units are correlated (i.e. as the PVME becomes less ordered with increasing dPS concentration). The second point is that the concentration dependence of the change in S_{PVME} behaves inversely to the behavior of b_{PVME}, that is, as b_{PVME} gets larger and exceeds the size scale of measurement (for our purposes it goes to infinity) ΔS_{PVME} goes to zero, and as b_{PVME} goes to a finite value at $\phi_{PVME}=>0$, ΔS_{PVME} goes to a finite value $S_{PVME\ \phi=0}$ which is close to but not identical to $S_{atactic\ PVME}$. The limiting condition at $\phi=0$ defines a relationship between $b_{isotactic}$ and S_{iPVME}/S_{dPS} given by,

$$\frac{S_{iPVME}(\phi)}{S_{dPS}} = \frac{S_{iPVME\ \phi=1}}{S_{dPS}} + \frac{b_{iPVME\ \phi=0}}{b_{iPVME}(\phi)}\left(\frac{S_{iPVME\ \phi=0}}{S_{dPS}} - \frac{S_{iPVME\ \phi=1}}{S_{dPS}}\right)$$

(7.31).

Since $c_{iPVME/PS} = 1 - (S_{iPVME}/S_{dPS})$, we have,

$$c_{iPVME/PS}(\phi) = c_i(\phi=1) - \frac{b_{iPVME}(\phi=0)}{b_{iPVME}(\phi)}[c_i(\phi=0)-c_i(\phi=1)] \qquad (7.32),$$

or, substituting in equation 7.28 for $b_{iPVME}(\phi)$,

$$c_i(\phi) = c_i(\phi=0) + \frac{3\,\lambda\,\exp(-\Delta G/RT)}{\pi\, r}\,[c_i(\phi=1)-c_i(\phi=0)]\,\phi^2 \qquad (7.33).$$

Equation 7.33 was used in equation 7.30 to fit the g_{sc} data. The parameters $c_i(\phi=0)$ and $c_i(\phi=1)$ were adjusted to fit the composition and temperature dependence using values for a, b_0 and b_1 from the atactic PVME blend. These values were then used to estimate a, b_0 and b_1 using the isotactic data. A second iteration adjusting $c_i(\phi=0)$ and $c_i(\phi=1)$ was performed and from these values the best fit to the isotactic data was ascertained. Figure 7.23 shows the temperature dependence of g_{sc} fit to equation 7.33 using values of $3\,\lambda\,[c_i(\phi=1) - c_i(\phi=0)]/\pi\, r = 0.02$ and $c_i(\phi=0)=0.4$. A value of 352.6 was used for $(-\Delta G/R)$ which was obtained from the fit to $b_{isotactic}$. A value of $c_i(\phi=0)=0.4$ indicates that the deuterated blend of the isotactic PVME has a surface area ratio similar to that of a hydrogenous blend of the atactic PVME. This is a logical result of the fits since the deuteration effect increases miscibility by about 10°C, while the tacticity effect reduces miscibility by about 10°C. An attempt will not be made to relate the 75% i-PVME data taken with a different molecular weight dPS (M_w=110kg/mole). It should be noted that values for b_0 and b_1 from this blend using the "a" determined for the

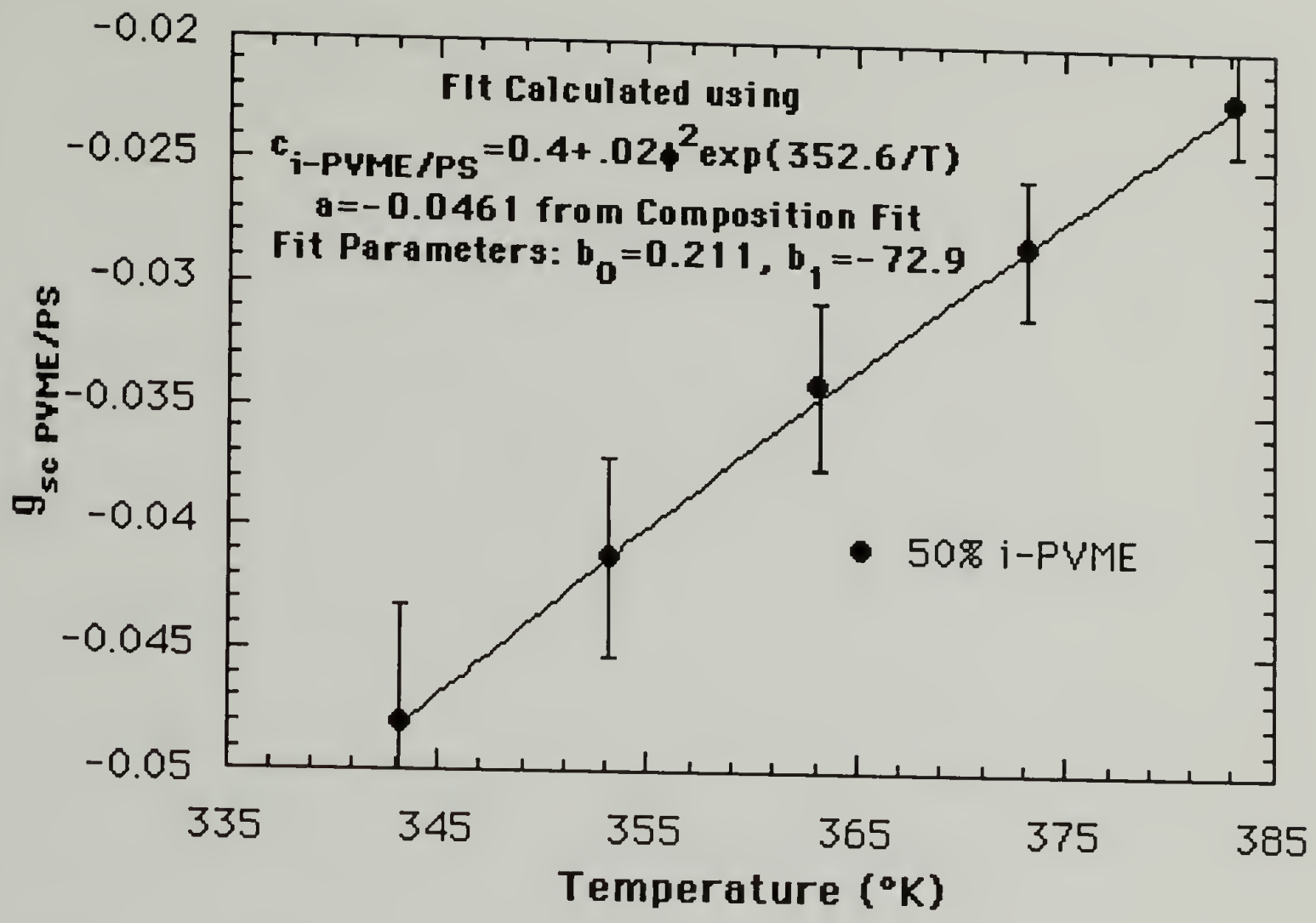

Figure 7.23 F-H-S fit of $g_{sc\ isotactic}$ using equation 7.30 and 7.33. The fit values are given above. Data is for a 50% isotactic PVME/dPS blend. (Error bars are an estimation of actual error from scatter in the data.)

lower molecular weight dPS agree in direction of shift from the atactic blends but disagree in magnitude of shift. Obviously, in order to obtain a complete picture of the behavior of the isotactic blends more data is needed.

M. g_{sc} as a Function of Composition

Figures 7.24 is a plot of g_{sc} versus composition for atactic PVME/PS blends at several temperatures measured by Yang and Shibiyama[9] at NIST (PS=244 kg/mole polydispersity of 1.06 and

$M_{W\ PVME}$ = 99 kg/mole polydispersity about 2.2). The larger extent of scatter in the composition data reflects the use of several different samples which may have differed slightly (as to thickness for instance). The data was fit to equation 7.30. As was noted above, the composition data could be fit using the value for c found with the hydrogeneous materials (cloud point c) but the same fit couldn't be used with the temperature data. The best overall fit occurred with a c of -0.189 reflecting differences between the hydrogeneous and deuterated PS component. The F-H-S equation gives a satisfactory prediction of the behavior of g for the atactic PVME/dPS blends.

Figure 7.25 is a fit to the isotactic composition data taken at 100°C. As is indicated in the figure the shape of the composition fit was strongly dependent on the c function given in equation 7.33. The curvature in the high PVME range was highly dependent on the k constant which reflects the difference between the surface area ratios for the pure PVME or pure PS limits. The slope in the low PVME

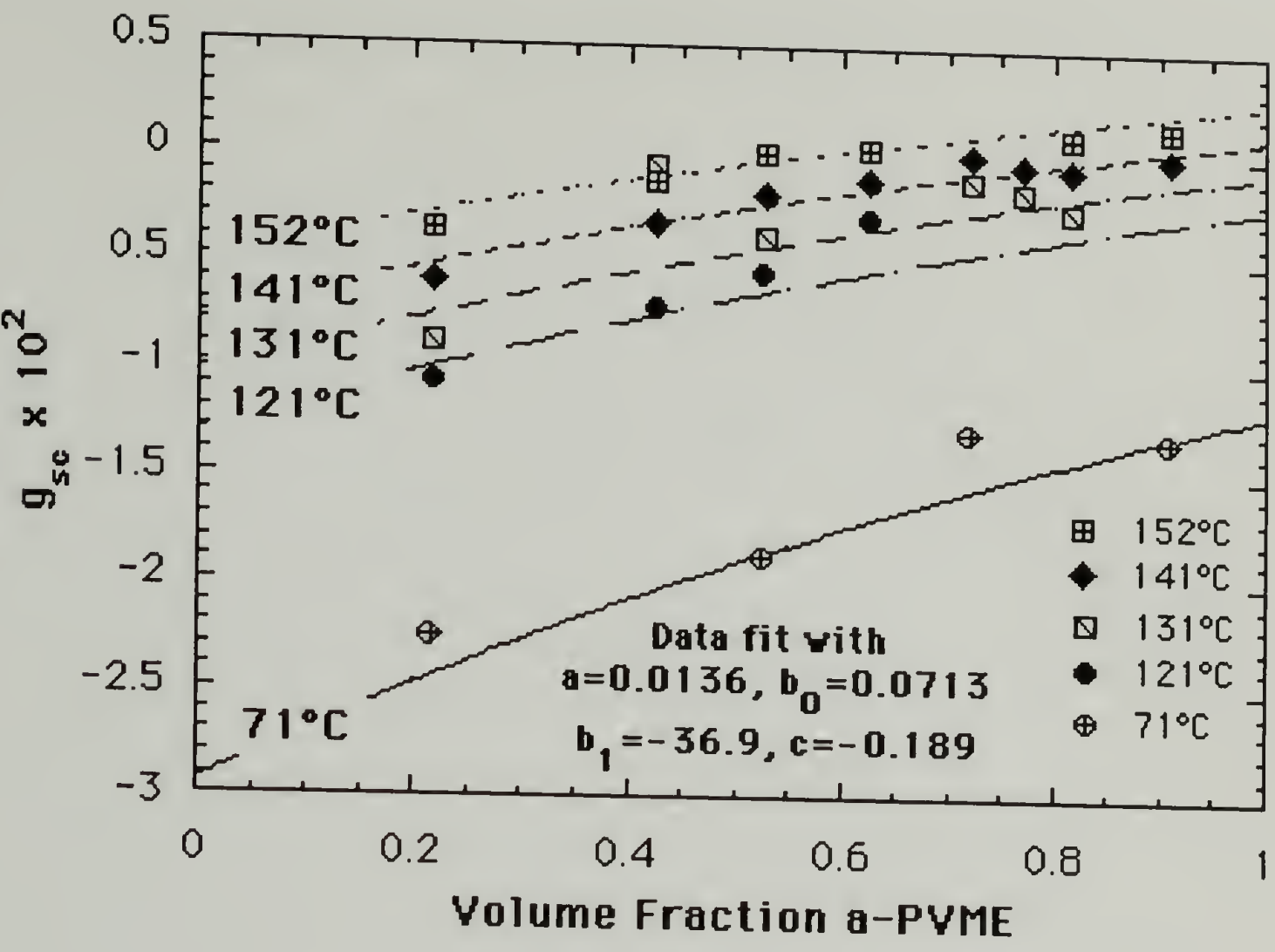

Figure 7.24 g_{sc} versus composition for atactic PVME/dPS. Fit parameters noted above were used in equation 7.30 (error bars are not included for clarity).

range was strongly dependent on the value of c in the pure PS limit. Generally the behavior is adequately predicted by the F-H-S equation. The fit parameters for Figure 7.25 are given in the caption. The numbers differ markedly from those of the atactic blends as will be discussed below.

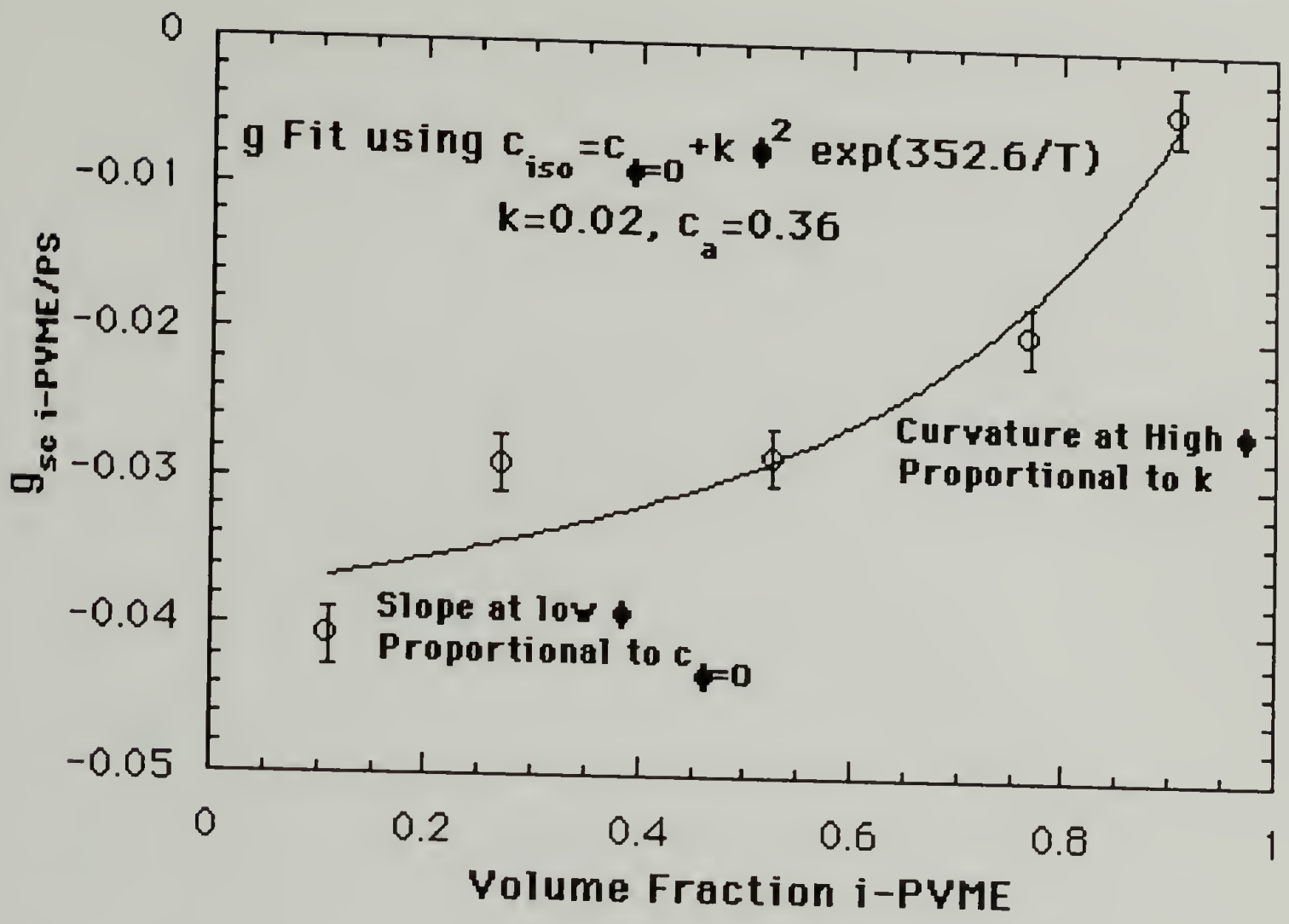

Figure 7.25 g_{sc} versus composition for isotactic PVME/dPS. Data is fit using equation 7.30 and 7.29 taking the derivatives with c as a function of ϕ. F-H-S fit parameters: a=-0.0461, b_0=0.211, b_1=-72.9 . (Error bars indicate the scatter in the temperature dependence data.)

N. The F-H-S Parameters

Table 7.3 gives the values obtained for a, b_0, b_1 and c for the isotactic and atactic materials blended with hydrogeneous and deuterated PS.

Table 7.3 F-H-S Parameters obtained from SANS (deuterated PS) and cloud point measurements (hydrogenous PS).

	a	b_0	b_1	c
a-PVME/dPS	0.0136	0.0713	-36.9	-0.189
i-PVME/dPS	-0.0461	0.211	-72.9	0.36 + f(ϕ)
a-PVME/PS ϕ=0.75	-0.00143	0.0136	-4.69	0.36
i-PVME/PS ϕ=0.75	-0.00057	0.0177	-4.08	0.425

A comparison between the hydrogenous and deuterated data will be presented later. It will be noted here that the hydrogenous data is for one composition only, and that is the critical composition wher e many of the composition dependences go to zero or become small (the critical composition is defined by any classical theory as the point at which the second and third derivatives of the free energy with respect to composition go to zero).

If one considers g as a free energy of mixing divided by temperature such that,

$$\frac{\Delta G_{mixing}}{T} = \frac{\Delta H_{mixing}}{T} - \Delta S_{mixing} \qquad (7.34),$$

"a" (Table 7.3) behaves as the negative of a change in entropy on mixing. Thus, in comparing the "a" terms for the deuterated blends one sees that the isotactic material shows an increase in this entropy where as the atactic material shows a decrease . This is understandable in terms of the difference between a crystalline and an amorphous lowest entropy state (the interacting blend of the amorphous material is more ordered than the pure amorphous material where as the interacting blend of the crystalline blend is less ordered than the crystalline material). One might expect that the change in entropy in this case might be related to the entropy of melting. The parameters b_0 and b_1 appear in the F-H-S equation multiplied by $1/(1-c\,\phi)$. In comparing two blends with different "c" values a bare comparison of these terms accounts for the blends' behavior at the $\phi=0$ limit. Thus, the bare numbers reflect a change on mixing in the absence of PVME self-interactions (the change for an isolated chain). b_0 reflects the negative of the entropic part of this change on mixing. In both cases the change in b_0 is towards a more ordered material (S is reduced), indicating that interactions in the blend tend to order the material to some extent. This change is larger in the isotactic material indicating that the isotactic PVME may be capable of more ordering than the atactic PVME in the blend. Similarly, b_1 is a larger negative enthalpic change in the isotactic material. The change in b_1 will be discussed below.

b_1 can be thought of as the enthalpic interaction per interacting grouping of PVME and PS (the lattice site) in the limit of infinite dilution of the PVME component. An interacting grouping is thought

to consist of more than one mer unit. This must be the case if there is to be a tacticity effect since tacticity is measured in terms of triads. It is believed that due to a more highly ordered and compact structure in the isotactic PVME, the interacting grouping has a smaller surface area . The ordering of the i-PVME may have an added effect in that for the same interacting grouping of dPS, more i-PVME methoxy units are available (due to i-PVME packing tighter than a-PVME for instance). An increase in the number of methoxy units which interact per grouping might increase the enthalpy per interacting group (defined in length for example by the length of a dPS interacting unit, Figure 7.26). If the ratio of atactic and isotactic PVME surface areas, $(1\text{-}c_{aPVME/PS})/(1\text{-}c_{iPVME/PS})$, is compared with the ratio of b_1's one finds a simple proportionality,

$$b_{1\,i} = b_{1a}\left(\frac{(1\text{-}c_{aPVME/PS})}{(1\text{-}c_{iPVME/PS})}\right) \qquad (7.35).$$

Thus, we have the intuitive result that enthalpy scales directly with surface area (in other words energetic interactions occur at the surfaces of the interacting units).

The change in b_0, however is larger than what would be expected from a proportionality with the surface areas. In fact the change in b_0, which dominates the tacticity effect (Chapter 5), is very close to twice what would be expected from a proportionality with the surface areas. If one were to consider the interacting units on the dPS and PVME chains to be rods, Figure 7.26, the length of which was

fixed by the length of the dPS rod (which remains constant with variation of PVME tacticity) and considered the higher ordering of the i-PVME chain to effectively decrease the radius of the rod thereby decreasing the surface area, effecting c and b_1, then one could consider the volume of such a conceptual rod as also decreasing. The relative change in volume of a rod of fixed length ($V_{rod} = \pi\, d\, r^2$ and $[\Delta V_{rod}/V_{rod}] = 2\, \Delta r/r$) is twice the relative change in surface area for a fixed length rod ($S_{rod} = 2\, p\, d\, r$ and $[\Delta S_{rod}/S_{rod}] = \Delta r/r$). Additionally, one would expect an entropic parameter which reflected changes in internal structure to follow volume rather than surface area. A decrease in the volume would be related to a decrease in ΔS and an increase in $-\Delta S$ as it relates to the fit. Thus, since the surface area ratios are given by $(1\text{-}c_{aPVME/PS})/(1\text{-}c_{iPVME/PS})$ we have,

$$b_{0\,i} = 2\, b_{0a} \left(\frac{(1\text{-}c_{aPVME/PS})}{(1\text{-}c_{iPVME/PS})} \right) \qquad (7.36),$$

which is roughly what is observed. This is a very important factor since the relatively large difference in the entropic parameter b_0 (possibly due to its dependence on volume rather than surface area) in comparison with the enthalpic parameter b_1 is the source of a more positive g above 72°C (as will be discussed below), with the "a" parameter playing a small role except at low temperatures (how low will be discussed below) and high compositions PVME. This more positive g defines the tacticity effect which leads to a reduced miscibility (under certain conditions as will be discussed).

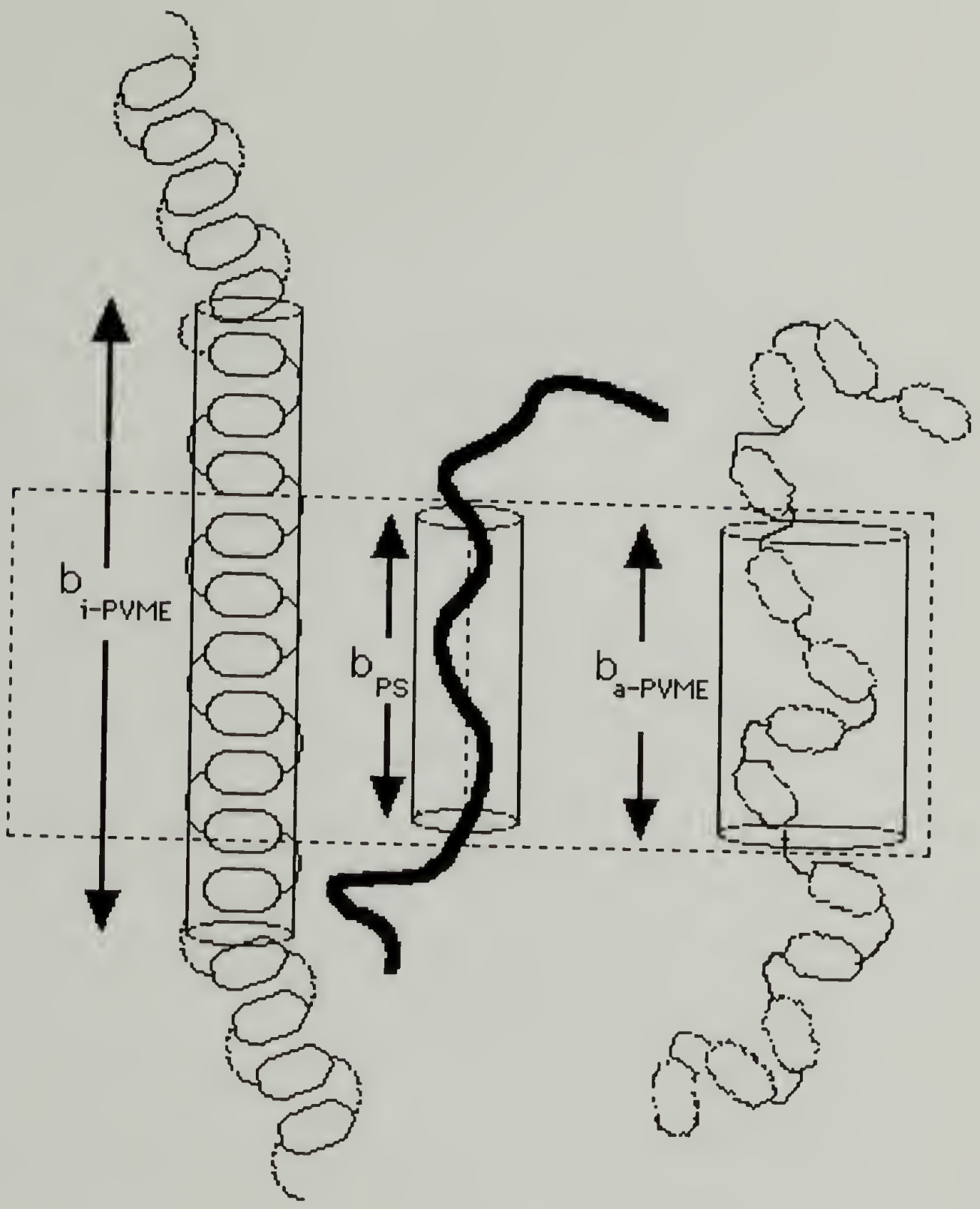

Figure 7.26 Geometric analysis (schematic) of changes in the F-H-S parameters with surface area and volume changes for interacting units (conceptualized as rods) organized into interacting groups. Interacting group (dotted box) is governed in length by the dPS unit. The reduction in surface area and volume of the isotactic PVME unit is related to an increase in the number of PVME mer units per interacting group and a decrease in entropy (randomness) for the group. $b_{i\text{-PVME}}$ increases relative to $b_{a\text{-PVME}}$.

O. Calculated Behavior of $g_{pvme/ps}$ from F-H-S fits to g_{sc}

Using the values for a, b_0 and b_1 discussed above, one can calculate the behavior of $g_{PVME/PS}$. Figure 7.27 is a plot of $g_{PVME/PS}$ versus T for atactic and isotactic PVME at various compositions.

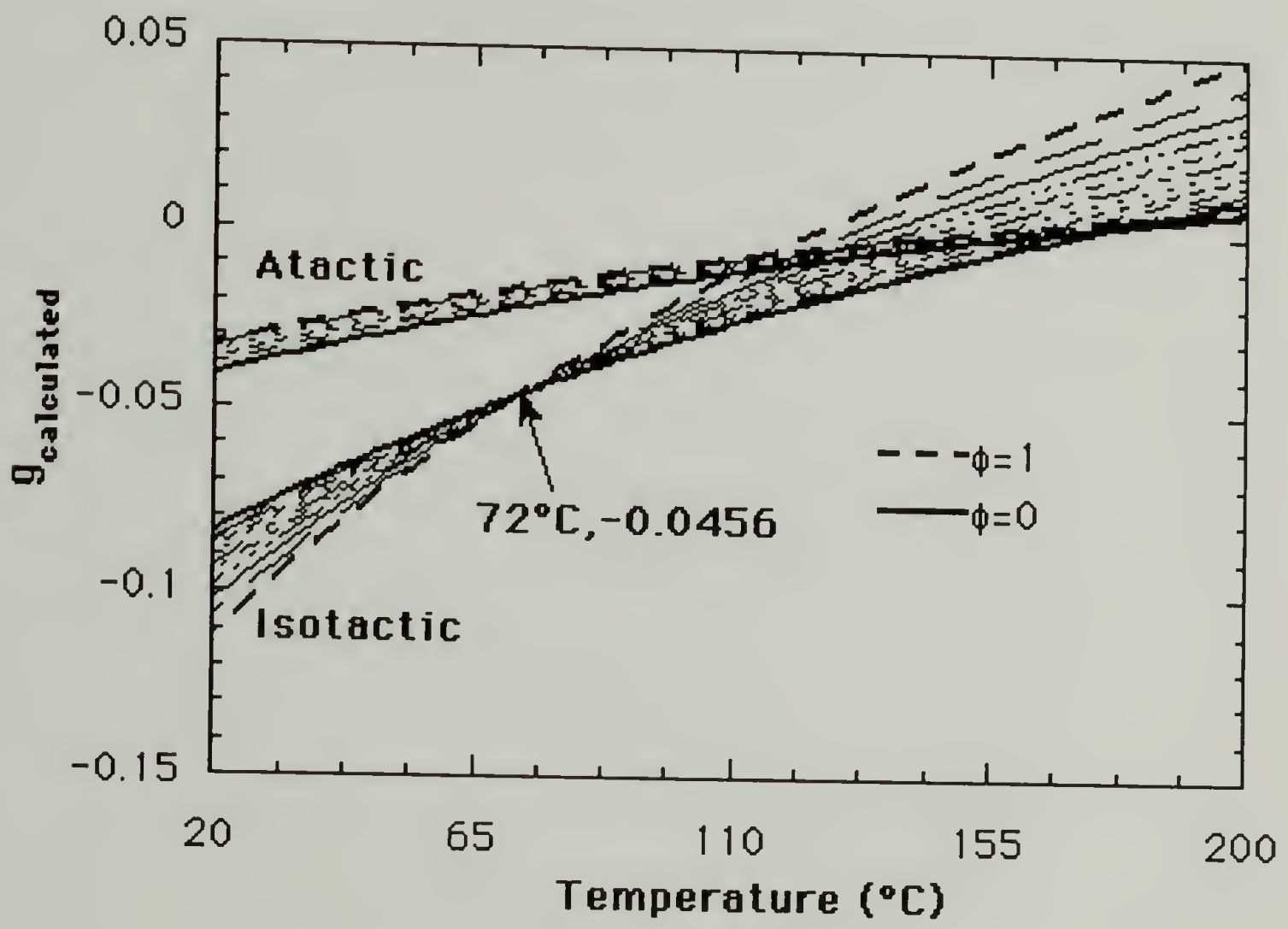

Figure 7.27 $g_{PVME/PS}$ versus T for atactic and isotactic PVME at various compositions. Bold dotted line is for composition of pure PVME, bold solid line is for composition of pure PS. Curves are calculated using F-H-S equation and parameters from Table 7.3. Light lines are for constant composition increments within the range of the bold lines.

The most striking difference between the behavior of the isotactic equation and the atactic equation is the reversal of the composition

dependence at about 72°C for the isotaetie material. This is believed to be a real phenomena sinee it is relatively close to the data (lowest data point was taken at 65°C). Above 72°C increasing PVME eoneentration serves to inerease g and make the blend less miseible. Below, inereasing eoneentration serves to decrease g making the blend more miseible. Sinee g is dominated by b_0 and b_1, it is ehiefly a balaneing between the entropie and enthalpie parameters whieh governs the g behavior. As was noted in the diseussion of the index of refraetion measurements, the highest observed melting point for the isotaetie PVME oeeurs at about 70°C. It would appear that there is a eorrespondenee between the ordering which is believed to oeeur in the melt and crystallization of the i-PVME.

The melting point is deseribed thermodynamieally as the balancing of the entropie and enthalpie eomponents of the free energy for the two phases.

$$T_f = \frac{\Delta H_f}{\Delta S_f} \qquad (7.37).$$

The value of g at 72°C is the F-H-S parameter "a" from Table 7.3 (for all compositions). Thus, b_0 and b_1 balanee each other at 72°C (or the equilibrium melting point). It is important to consider the ground state from which the blend is compared. The ground state for the isotactic PVME below 72°C is the crystalline state, even though it can not crystallize in the blends (in general). This leads to a large ehange in entropy for the miscible blend below 72°C. The greater the amount

of PVME present the greater will be this change in entropy. This leads to an increasing miscibility for increasing fractions of i-PVME. Above the melting point the ground state is amorphous, and the change in entropy is much smaller on mixing. (It should be noted that in all of the blends studied crystals can not form due to dilution by the PS component.) Above the melting point the change in entropy on mixing becomes small since the ground state is amorphous PVME. At this point the enthalpic interactions attracting PVME units can begin to be felt favoring demixing. The higher the concentration of PVME the larger the effect. This argument accounts for the reduced miscibility of higher concentrations PVME above 72°C.

At this point it is helpful to show the dependence of the statistical segment length function (equation 7.28) with temperature, Figure 7.28, since there appears to be a strong relationship between the statistical segment length and the proposed equilibrium melting point of 72°C. There is a discontinuity in b_{iPVME} with temperature which occurs at 72.2°C for the pure iPVME limit. The temperature for the discontinuity is a function of composition and decreases as more PS is added to the blend.

If the temperature at which the b_{iPVME} function goes to infinity is analogous to a melting point one would expect a melting point depression under conditions of a negative $g-g_s$ (this condition always exists for these blends at 72°C as will be discussed below. Nishi and

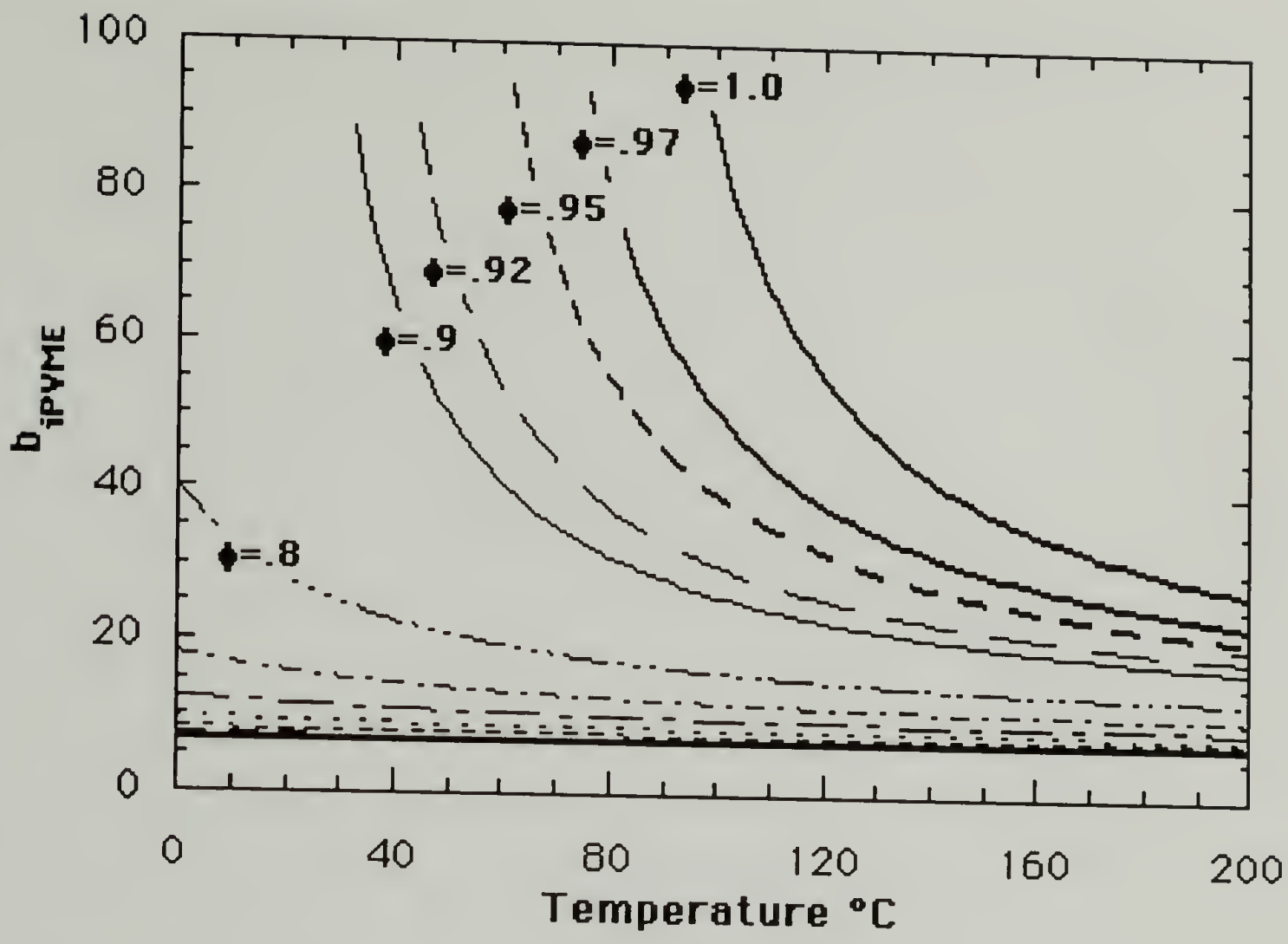

Figure 7.28 Thermal dependence of b_{iPVME}. Discontinuities occur at (composition : discontinuity temperature) ϕ=1:72.2°C, ϕ=0.97:=53.7°C, ϕ=0.95:41.5°C, ϕ=0.92:23.9°C, ϕ=0.90:14.3°C.

Wang[21,22] among others[23] have demonstrated that the relationship,

$$\frac{1}{T_m(\phi_1)} - \frac{1}{T_m^0} = -\frac{R v_1}{\Delta H_1 v_2} \chi_{21} (\phi_2)^2 \qquad (7.38),$$

is useful in determining the interaction parameter for polymer blends which show some degree of crystallization. T_m is the observed melting point, T_m^0 is the melting point of an infinite crystal at perfect equilibrium in the pure material, ΔH_2 is the heat of fusion of the purely crystalline material per mole of repeat unit, and v_i are the molar

volumes of diluent (PS), 2 ,and crystalline polymer (i-PVME), 1. Figure 7.29 is a plot of $(1/T_{b=\infty}(\phi_{PVME}) - 1/T^{\phi pvme=1}_{b=\infty})$ versus $(1 - \phi_{PVME})^2$ as suggested by equation 7.38. In Figure 7.29, $\phi_{i\text{-}PVME}$ is varied from 1.0 to 0.8. Blends with more than 92% i-PVME show a discontinuity in $b_{i\text{-}PVME}$ which decreases in temperature with decreasing percentage i-PVME in direct analogy to melting point depression behavior.

The plot suggested by equation 7.38 does not result in a linear fit. This suggests a composition dependent χ. The composition dependence used in the g_{sc} analysis improves the linearity but does not fully account for the behavior. The use of a larger k in the functionality of c, can account for the non-linearity, i.e. 0.02 was used for g_{sc} and 0.23 is used in the linear fit above. This results in a very small intercept (see fit equation in Figure 7.27). An intercept of zero with a linear fit is predicted by equation 7.38. The failure of the g_{sc} Staverman parameter, "c", to fit the data is understandable when it is considered that the extremely non-linear portion of the curves occurs at almost pure PVME where no g_{sc} data was taken (the highest experimental data point is ϕ_{PVME}=0.9 while the melting point depression analysis is based on extrapolation to above ϕ_{PVME}=0.92).

A linear fit to the lower concentration PVME data points (the last five data points shown above) using c from the χ_{sc} analysis results in a slope of 0.021 and an intercept of 0.00026. The slope can be calculated from equation 7.38 using values obtained in the g_{sc} and $b_{i\text{-}PVME}$ fits. At 72°C the values for $[-Rv_{PVME}/\Delta Hv_{PS}][(b_1/T)/(1-c\,\phi)]$ from the χ_{sc} analysis is 0.00052 using 352.6 as the value for $-\Delta H/R$

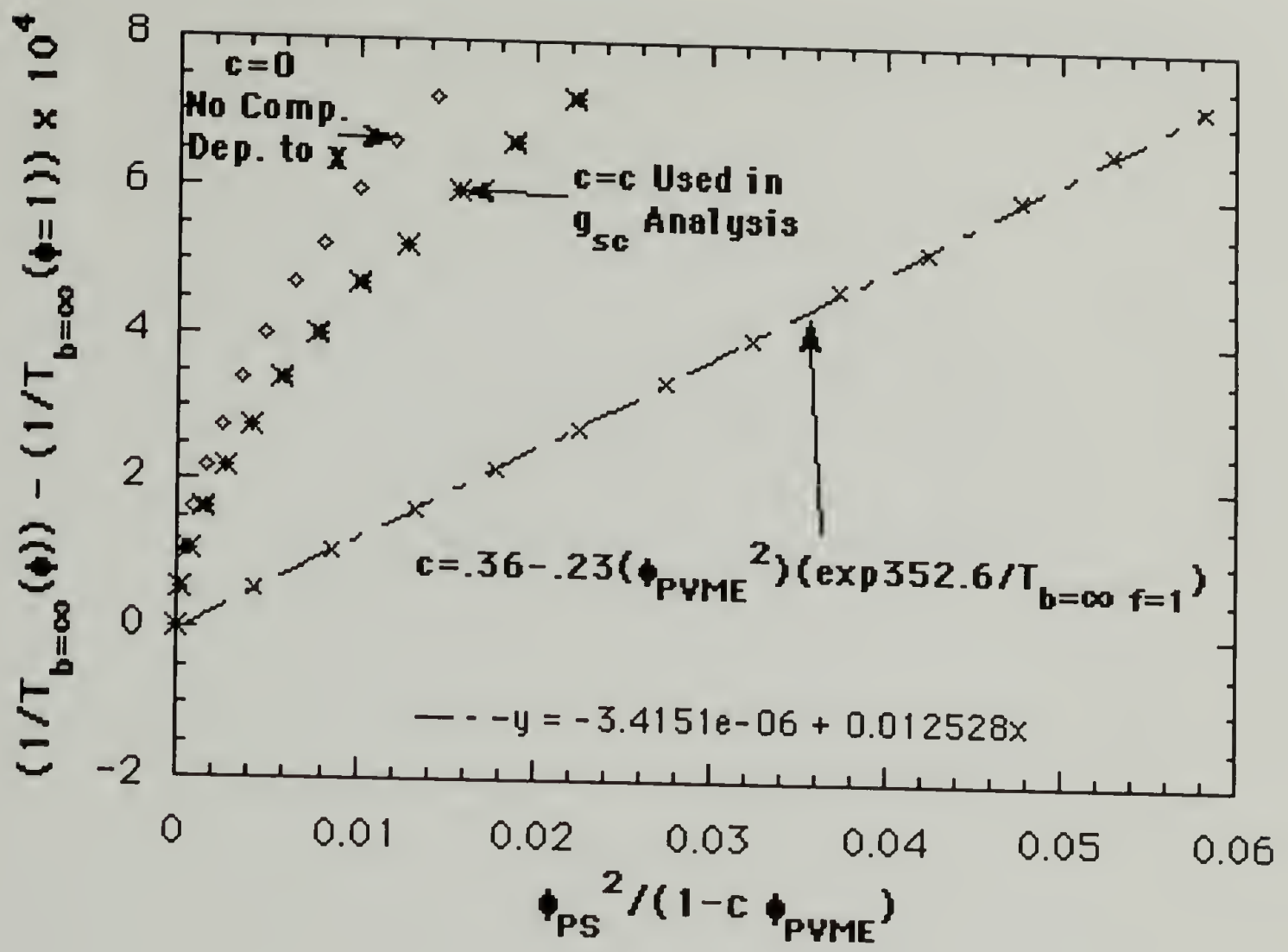

Figure 7.29 Flory-Mandelkern-type plot[24] of $(1/T_{b=\infty}(\phi_{PVME}) - 1/T^{\phi pvme=1}_{b=\infty})$ versus $(1 - \phi_{PVME})^2$ for isotactic PVME blended with dPS. Equation 7.38 suggests a linear fit for a non-composition dependent χ. Two curves with a F-H-S composition dependence to χ are included. The nonlinearity can be accounted for using a composition dependent χ and a composition dependent c from the F-H-S analysis.

(from the temperature dependence of b_1), $\bar{\phi}_{PVME}$=.9, and v_{PVME}=57.0, v_{PS}=99.4 cm^3/gmmole. This value disagrees with the slope given above. The intercept should equal $[-Rv_{PVME}/\Delta Hv_{PS}][(a+b_1/(1-c\,\phi)]$ which gives a value of 0.00046. The non-linearity of the behavior may be an important factor in the disagreement of the values.

The discontinuity point for $b_{i\text{-}PVME}$ displays a temperature and composition dependence which is directly analogous to what would be expected from an equilibrium melting point depression. The extrapolated equilibrium melting point for pure i-PVME agrees with the value obtained from index of refraction measurements, x-ray determinations of crystallinity and DSC measurements. The value of 72°C supports the ground state analysis of g given above. From this analysis it would appear that the composition and temperature dependences of g as reflected in the F-H-S parameters are intimately related to the crystallization phenomenon for i-PVME. The orientation of tactic PVME which has been postulated to occur in the blends above the crystalline melting point may be directly related to orientation which occurs in pure, crystalline PVME.

P. Calculated Values for g–g_s Using the F–H-S Parameters

The distance a polymer blend is in terms of free energy (or χ) from the spinodal point is a measure of the miscibility of the blend at a particular temperature and composition. Since the F–H–S equation gives a composition dependence to χ, the classic definition of χ_s (the spinodal χ) must be modified. Generally, χ_s is defined as the value of χ at which the second derivative of the free energy with respect to composition goes to zero, giving,

$$\chi_{s\ F\text{-}H} = \frac{v_0}{2}\left(\frac{1}{v_1 z_1 \phi_1} + \frac{1}{v_2 z_2 \phi_2}\right) \qquad (7.39).$$

In the presence of composition and temperature dependencies one obtains a spinodal g which depends on composition and temperature,

$$g_s^* = \chi_{s\ F\text{-}H} + (1 - 2\phi)\frac{\delta g}{\delta \phi} + \frac{(\phi - \phi^2)}{2}\frac{\delta^2 g}{\delta \phi^2} \qquad (7.40).$$

This is very similar to the definition of the scattering chi, g_{sc}, since they both are derived from the second derivative of the free energy,

$$g_s^* = g_{s\ F\text{-}H} - g_{sc}(\phi,T) + g(\phi,T) \qquad (7.41),$$

Thus, $(g(\phi,T) - g_s^*)$ is given by,

$$(g(\phi,T) - g_s^*) = g_{sc}(\phi,T) - g_{s\ F\text{-}H} \qquad (7.42).$$

When the F-H–S equation is inserted in equation 7.40 for g, one obtains,

$$g^*_{sF\text{-}H\text{-}S} = \chi_{s\ F\text{-}H} + \frac{c\,(1 - 2\phi)\,(b_0 + b_1/T)}{(1 - c\,\phi)^2} + \frac{c^2\,(\phi - \phi^2)\,(b_0 + b_1/T)}{(1 - c\,\phi)^3}$$

$$(7.43),$$

ignoring the partial derivatives in terms of $c(\phi,T)$. Equation 7.43 contains both composition and temperature dependences. Thus, one is faced with the awkward position of having a $g^*_{sF\text{-}H\text{-}S}(T=T_s)$ which fits the classic definition of χ at the spinodal point and $g^*_{sF\text{-}H\text{-}S}(T)$ which is the spinodal χ that the blend actually "feels" at a particular

temperature. Both values of $g^*_{sF\text{-}H\text{-}S}$ were used to calculate $(g\text{-}g^*_{sF\text{-}H\text{-}S})$ and were found to give similar general properties although $(g\text{-}g^*_{sF\text{-}H\text{-}S}(T=T_s))$ tended to show more linear behavior in temperature, as would be expected. Figure 7.30 is a plot of $(g\text{-}g^*_{sF\text{-}H\text{-}S}(T))$ versus temperature for the isotactic and atactic PVME/dPS blends.

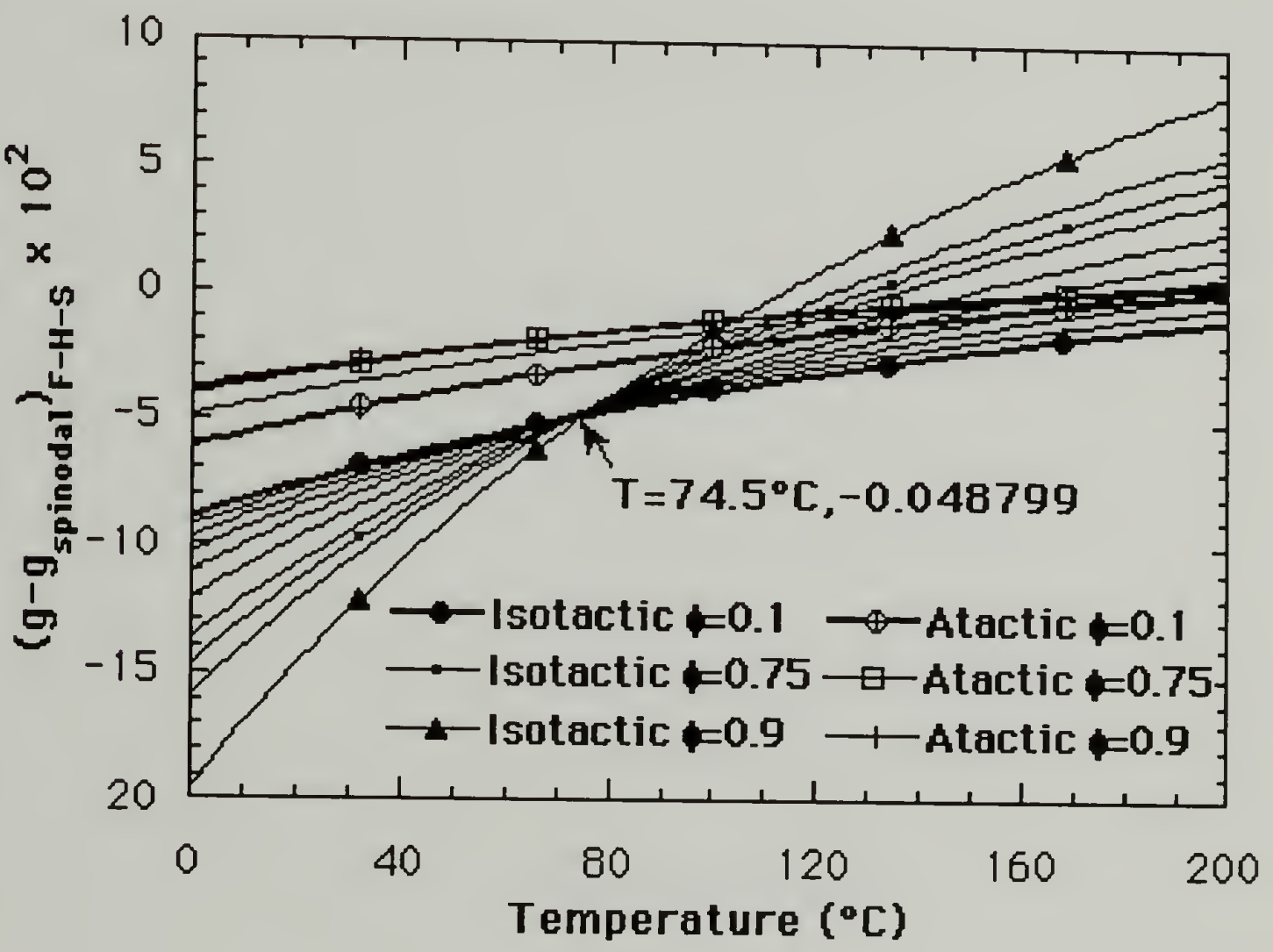

Figure 7.30 $(g\text{-}g^*_{sF\text{-}H\text{-}S}(T))$ versus temperature for the isotactic and atactic PVME/dPS blends.

The behavior of $(g\text{-}g^*_{sF\text{-}H\text{-}S}(T))$ to some extent shows the main features of g discussed above. There is a slight shift of the inversion point for the isotactic PVME blends due to the influence of g_s (72°C to 74.5°C).

The slope at low concentrations PVME (solid bold line is for ϕ=0.1) approaches the same value at low temperatures. This is expected since the blends become less different at low concentrations PVME. At high temperatures the low concentration data merge. This is the region where the orientation behavior of the isotactic material becomes less pronounced.

Since $(g - g^*_{sF\text{-}H\text{-}S}(T))$ goes to zero at the spinodal temperature and since equations can be written in terms of the F-H-S analysis for g and for $g^*_{sF\text{-}H\text{-}S}(T)$, one can solve for the spinodal temperature using the F-H-S parameters determined from the composition and temperature behavior of χ . This was done using the commercial software Mathamatica™[25]. Figure 7.31 is a plot of T_s versus composition for the isotactic and atactic blends calculated in this way.

Data for optical cloud points (SALS cloud points), SANS cloud points (determined by Yang for atactic PVME), and the spinodal temperatures as determined using the correlation length approach are included for comparison. The calculated spinodal points agree with the correlation length spinodal points, demonstrating the self-consistency of the data and F-H-S parameters (only one correlation length spinodal point was obtained for the isotactic data, the 75% PVME blend with a different molecular weight dPS showed a correlation length spinodal point of 126°C and a cloud point of 176°C following the behavior of the data shown above). The atactic spinodal curve behaves in a manner which might be expected for a polydisperse blend. This curve is shifted some what from the cloud point data

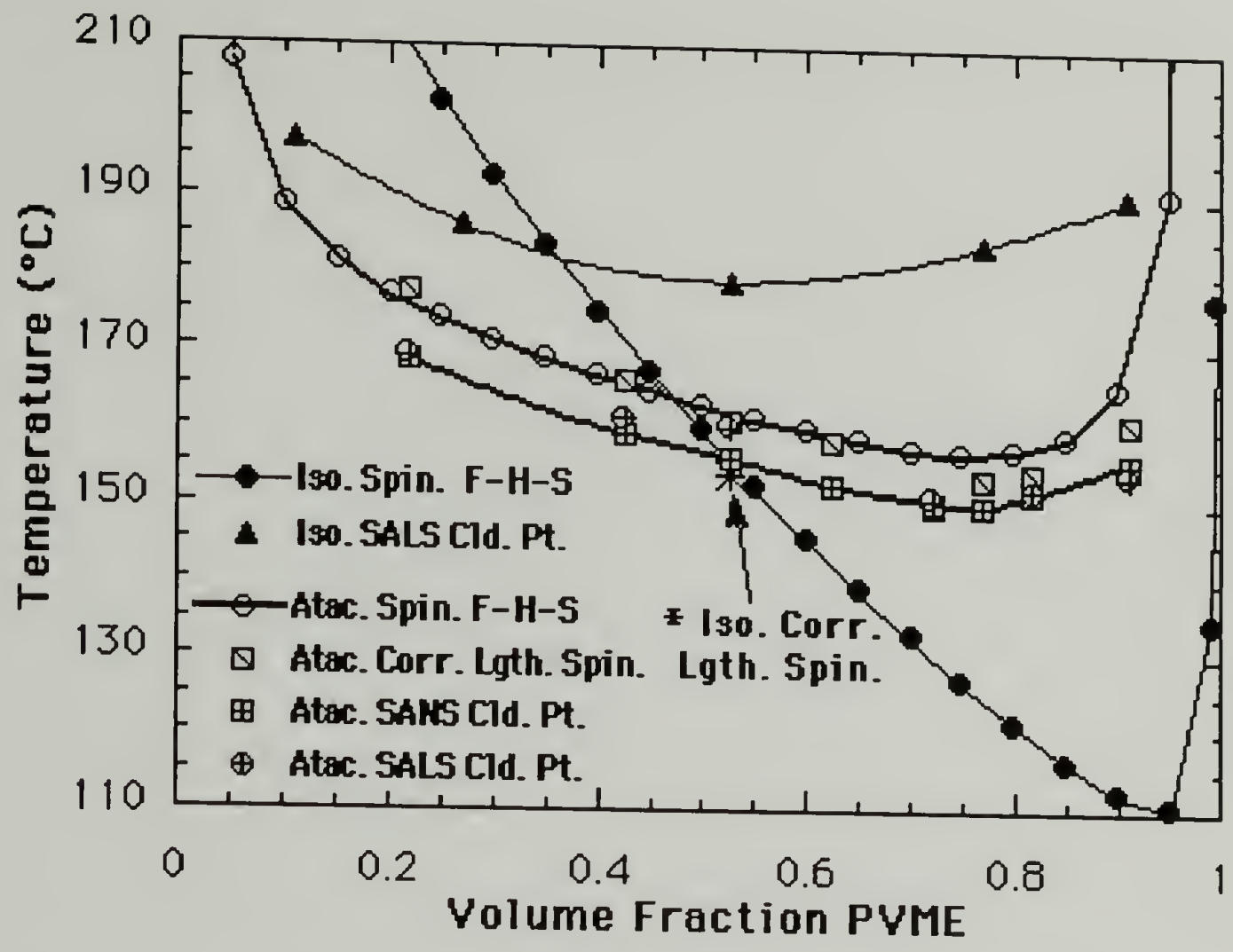

Figure 7.31 T_s versus composition as calculated using the F-H-S composition and temperature dependence of g. Lines merely connect calculated and data points.[Data for optical cloud points (SALS cloud points), SANS cloud points (determined by Yang[2] for atactic PVME), and the spinodal temperatures as determined using the correlation length approach are included for comparison.]

indicative of the presence of shadow phases as discussed in Chapter 5. The calculations indicate a highly skewed behavior for the isotactic PVME with monotonically decreasing spinodal temperatures with increasing PVME concentration until very close to pure PVME. The minimum in the spinodal curve no longer corresponds to the minimum in the phase diagram (as determined by cloud point measurements) due to the composition dependence of χ. The disagreement between the isotactic spinodal points and the cloud

point data indicates that the extrapolation from about 110°C (highest SANS data point) to 180°C (cloud point range) may not be justifiable in view of the strongly non-linear composition and temperature dependeneies of χ. Additionally, very slow kinetics of phase separation for the isotaetie blends may result in errors in the determination of an equilibrium cloud point. (In general, data obtained in the miscible regime, i.e. SANS data, is more reliable than data obtained at the miseibility limit or in the immiscible regime, i.e. cloud points.)

Figure 7.32 shows the composition dependence of $g_{spinodal}$ for the isotaetic and atactic blends (caleulated as in Figure 7.31). As diseussed above, the atactie ealeulation results in the expeeted behavior, while the isotaetic $g_{spinodal}$ becomes negative at eompositions above about 60% PVME. This is the result of the second and third derivative terms in equation 7.40. It should be noted that the temperature dependence of g for the atactic blends was known over eompositions ranging from 20 to 90% PVME while that of the isotaetic data was measured only at a 50% eomposition due to limitations in beam time. Further, the isotactic data was measured elose to (but above) the equilibrium erystallization temperature about 72°C). Thus, the F-H-S parameters for the isotaetie blend may be unduly effeeted by the taeticity effect as it relates to a erystalline ground state. The agreement of the atactie parameters should be taken as an indieation of the correctness of the approach, while the

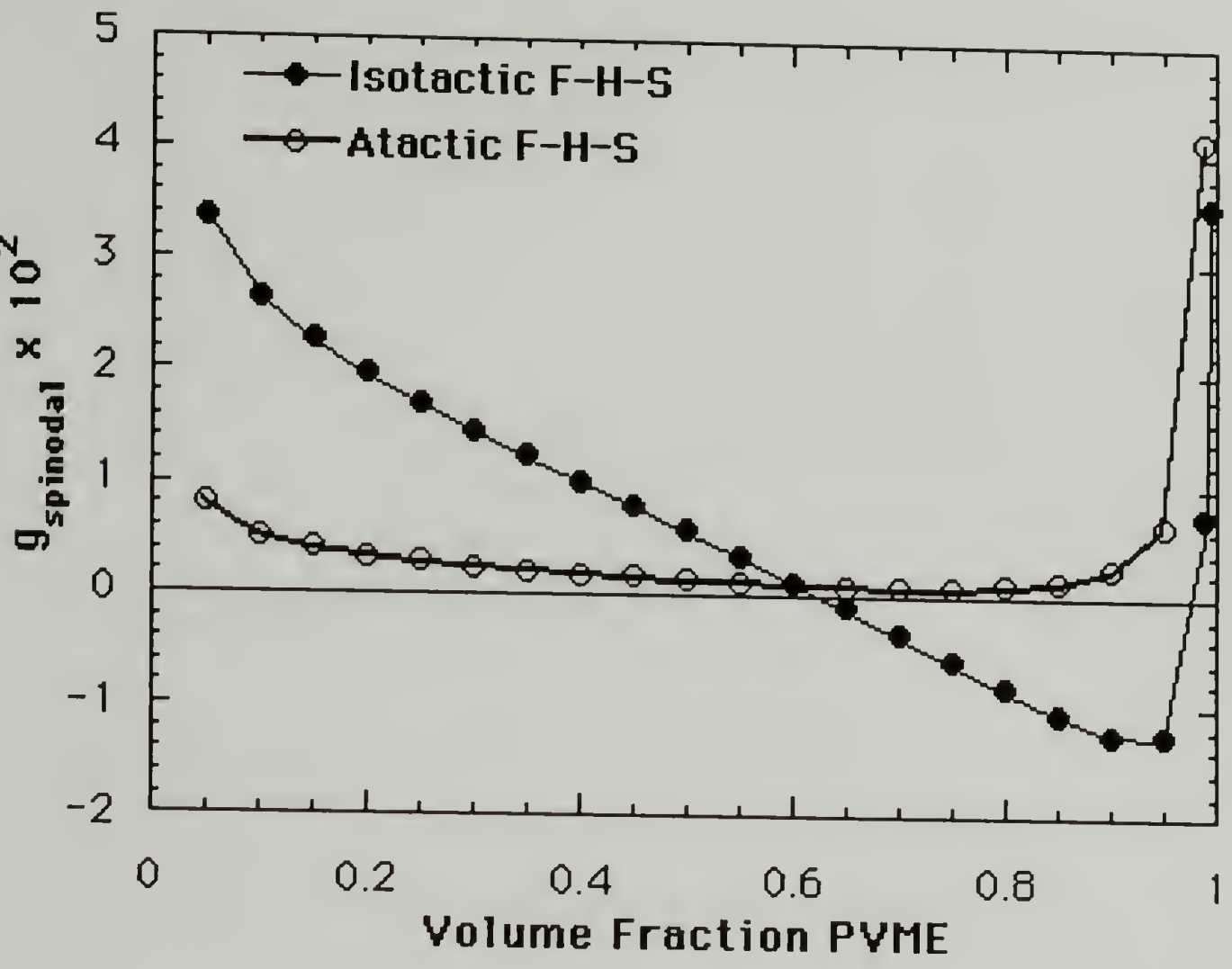

Figure 7.32 Composition dependence of $g_{spinodal}$ for isotactic and atactic blends (calculated as in Figure 7.29).

unexpected behavior of the isotactic parameters may be real or may be a manifestation of the limited data. It is believed that the general trends of the isotactic data reflect real behavior, but more data is needed to confirm the unexpected behavior observed in terms of the spinodal temperatures and $\chi_{spinodal}$.

In the discussion concerning light scattering kinetics of Chapter 6 it was noted that differences in the thermal behavior of $(g - g_s)/g_s$ governed the kinetics of phase separation. In the light scattering studies it was determined that although isotactic PVME was less miscible with PS than atactic PVME, it displayed a dramatically slower

phase separation above the cloud point. This slowed kinetics was successfully described using the F-H-S equation to model the cloud point curves. When plots of the calculated $(g - g_s)/g_s$ versus temperature were compared with plots of the apparent diffusion constant (experimentally determined) identical behavior was observed. Further, the constant which related $(g - g_s)/g_s$ with the apparent diffusion constant, D_c, was essentially identical for the two blends. Additionally, the translational diffusion constant, D_c, so determined, agreed with literature values obtained using NMR. It must be noted that the light scattering kinetics studies were conducted at compositions close to the critical composition (ϕ=0.75 was used). Although PVME/dPS blends can not be directly compared with PVME/hPS blends similar behavior near the critical composition is observed. Since g_s for the isotactic blend is negative in the critical composition range, and since it is essentially a normalization factor in obtaining $(g - g_s)/g_s$, the absolute value of g_s was used to normalize the $(g - g_s)$ data from the F-H-S parameters. Figure 7.33 is a plot of $(g - g_s)/abs(g_s)$ versus temperature for the deuterated blends as calculated using the F-H-S parameters described above. Clearly, fits limited to the immiscible region for isotactic blends (above $(g - g_s)/g_s = 0$) would give different parameters (a, b_0, b_1) than fits limited to the miscible regime. This, in combination with the deuteration effect, explains the discrepancy between the results of light scattering cloud point measurements and SANS results.

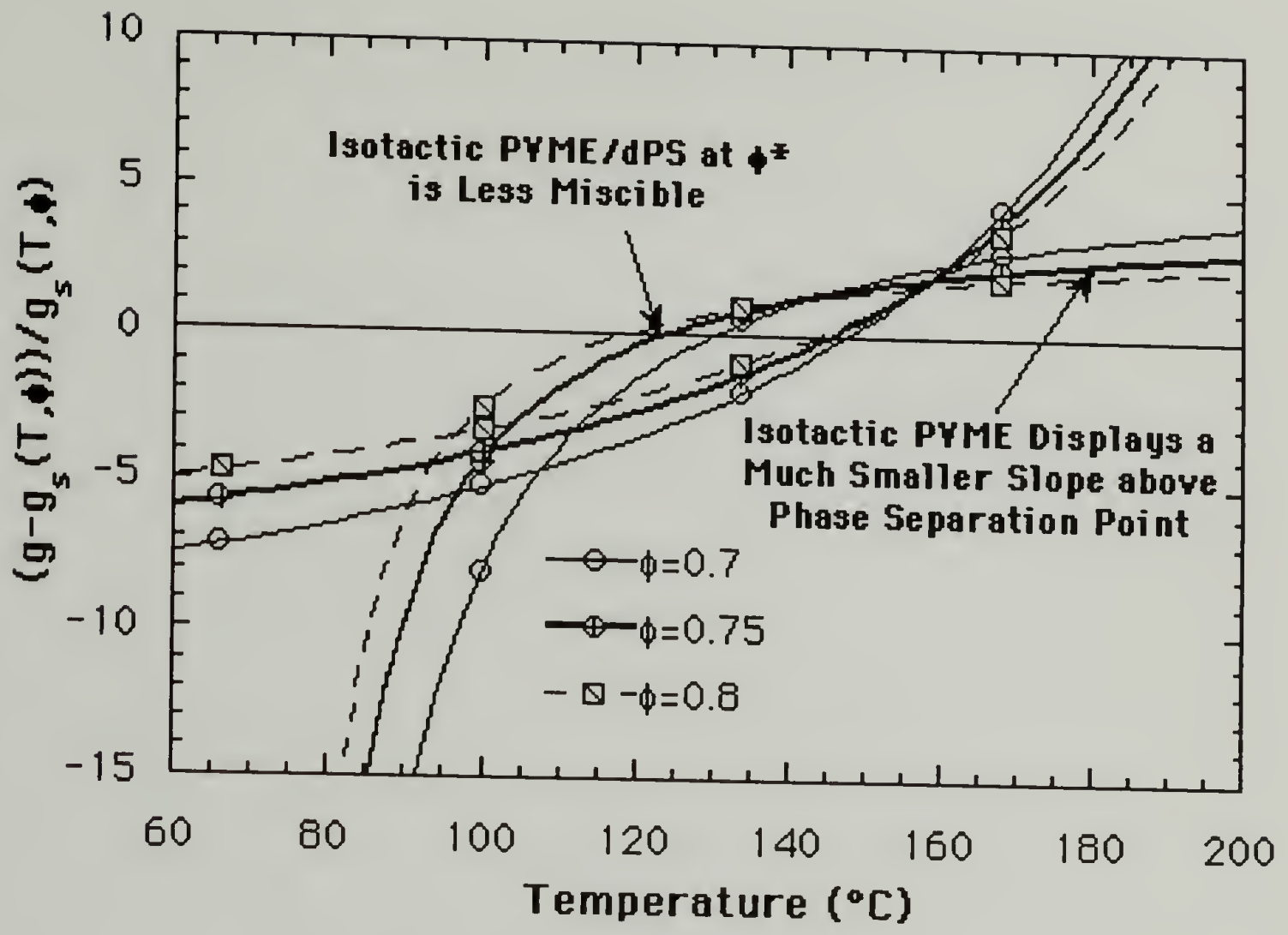

Figure 7.33 Plots of $(g - g_s)/g_s$ versus temperature for PVME/dPS blends near the critical point. The behavior is reminiscent of PVME/PS blends studied using light scattering in the immiscible regime. The light scattering data was successfully used to predict the kinetics of phase separation.

The essential features in the immiscible regime (above $(g - g_s)/g_s=0$) of Figure 7.33 are lower miscibility for the isotactic PVME blends and a drastically reduced slope above the phase separation temperature. These features are in total agreement with the light scattering work and were the salient point of that work. The miscible regime for the isotactic PVME is also illuminating. At temperatures below the critical point (if this can be assumed to be a critical blend) $(g - g_s)/g_s$ shows a precipitous drop and a discontinuity at 72°C. This, again, is a consequence of the proximity of the equilibrium melting point.

Another feature of the $(g - g_s)/g_s$ curves is that they show dramatically different behavior for off critical blends. Further work is necessary in understanding the ramifications of these differences and comparative light scattering studies to verify the predictions would be of use.

Q. Chapter Summary

The F-H-S equation has been used as a basis for modeling the tacticity effect in the PVME/PS blend system as observed using SANS. A simplified geometric approach has been developed which explains, to some extent the experimental results. It is helpful to consider the interacting group as the interaction between two conceptual geometric rods. It is believed that the length of an interacting group is governed by dPS in these blends. Since the dPS component is the same in the atactic and isotactic blends (except for molecular weight which has been accounted for) it is believed that the interacting group remains of constant length when comparing the two blend systems. Isotactic PVME shows an increase in the enthalpic portion of g which is believed to be caused by a more compact structure which can allow more interactions per interacting group. This can be related to a decreasing radius of the PVME rod (Figure 7.26). While the enthalpic component of g appears to be directly related to the surface area of an interacting group, the composition dependent entropic component appears to be more closely related to the volume of the interacting group. The change in this entropic component between the isotactic and atactic PVME is roughly twice that of the enthalpic component. This is analogous to comparing the relative change in volume and

surface area of a fixed length rod. The relationship between entropy and volume in this case may be due to internal (to the rod) ordering which can occur in the isotactic PVME's interaction unit but not in the atactic. Enthalpic interactions would be limited to the surface area of the rod.

An alternative explanation involves the ground states to which the blend is to be compared in determining the change in free energy on mixing. The ground state for the isotactic PVME, below the equilibrium melting point of 72°C, is the equilibrium crystalline state. Above the melting point the ground state is the amorphous state. A large difference between the entropy of the crystalline state and the blend leads to enhanced miscibility below the crystalline melting point. Above the melting point this difference is dramatically reduced.

Calculated statistical segment lengths for the isotactic PVME from the scattering data show a strong composition and temperature dependence which can be related to the melting point, a melting point depression and a composition dependent Staverman parameter, c. The statistical segment length for the atactic blends remains comparatively constant. A relationship between the temperature and composition dependence of the statistical segment length and the Staverman parameter, c, has been developed which has proven useful in explaining the behavior of g.

Trends evident in light scattering studies which predicted the observed slowed kinetics in the less miscible isotactic blends of critical composition, were mimicked in the calculated values for

$(g-g_s)/g_s$ from the neutron scattering data. These predictions into the immiscible regime from data taken well into the miscible regime support the usefulness of the F-H-S equation as a modeling tool. Dramatic changes in the behavior of $(g-g_s)/g_s$ below the miscibility limit ($(g-g_s)/g_s = 0$) explain large differences in a, b_0 and b_1 between light scattering cloud point calculations and SANS calculated values. Additionally, the deuteration effect is expected to shift the F-H-S parameters significantly.

References

1. P. G. de Gennes, *Scaling Concepts in Polymer Physics*, Cornell Univ. Press, London, 1979, Chapter IV.

2. H. Yang, Ph.D. Dissertation, University of Massachusetts, Amherst 1986.

3. J. M. Carpenter, W. B. Yelon, in *Neutron Scattering, Part A*, edited by K. Skold and D. L. Price, Academic Press Inc., NY, 1986, Chapter 2.

4. P. G. de Gennes, *Scaling Concepts in Polymer Physics*, Cornell Univ. Press, London, 1979, Chapter II.

5. J. F. Joanny, *C. R. Acad. Sci., Paris*, **286B**, 89 (1978).

6. V. F. Sears, in *Neutron Scattering, Part A*, edited by K. Skold and D. L. Price, Academic Press Inc., NY, 1986, Appendix.

7. G. Hadziioannou, J. Gilmer, R. S. Stein, *Polym. Bull.*, **9**, 563 (1983).

8. R. S. Stein, G. Hadziioannou, *Macromolecules*, **17**, 1059 (1984)

9. M. Shibiyama, H. Yang, R. S. Stein, University of Massachusetts, Amherst, Department of Polymer Science, Internal Report Prepared by M. Shibiyama, 1984.

10. See for example R. S. Stein, *Electro-optical Behavior of Polymers*, Univ. Mass. Video Instructional Program Lecture Notes, Amherst, MA, 1989.

11. J. Brandrup, E. H. Immergut, *Polymer Handbook*, John Wiley and Sons, N. Y., 1975, Chapter V.

12. C. T. Murray, Ph.D. Dissertation, University of Massachusetts, Amherst , 1985.

13. M. Shibayama, H. Yang, R. S. Stein, *Macromolecules*, **18**, 2179, (1985).

14. *Kaladigraph Version 2.0.2*, Abelbeck Software, 1989.

15. A. Kuhn, *Kolloidzschr.*, **68**, 2 (1934).

16. R. Koningsveld, A. J. Staverman, *Koll. Polym. Z.*, **218**, 114 (1968). See also references 1-5 Chapter 5.

17. R. Koningsveld, *Disc. Farad. Soc.*, **49**, 144 (1970). See also references 1-5 Chapter 5.

18. P. G. de Gennes, *Scaling Concepts in Polymer Physics*, Cornell Univ. Press, London, 1979, Chapter X.

19. J. Brandrup, E. H. Immergut, *Polymer Handbook*, John Wiley and Sons, N. Y., 1975, Chapter VI.

20. I. Sanchez, *Polymer*, **30**, 471 (1979).

21. T. Nishi and T. T. Wang, *Macromolecules*, **8**, 909 (1975).

22. T. K. Kwei, G. D. Patterson and T. Wang, *Macromolecules*, **9**, 780 (1976)

23. C. J. Ong, Ph.D. Dissertation, University of Massachusetts, Amherst, 1974.

24. L. Mandelkern, P. J. Flory, *J. Am. Chem. Soc.*, **73**, 3206 (1951).

25. S. Wolfram, *Mathamatica™ A System For Doing Mathamatics*, Wolfram Research Inc., Champaign, IL, 1989.

CHAPTER 8

T_g OF POLYSTYRENE AT INTERFACES

(ELLIPSOMETRIC STUDY)

A. Introduction

As was noted in Chapter 4, phase separated domains in a glassy polymer have been thought to alter the stress fields in the glassy matrix. Localized stress concentration has been thought to increase the free volume of the matrix phase and shift its glass transition temperature. A shift in the glass transition temperature has been thought to be related with a lower stress for onset of crazing and shear banding. Additionally, in the blends discussed in Chapter 4 differences in the thermal expansion and contraction of the intimately bound PVME phase on crystallization may be thought to induce strains in the plasticized interfacial zone. In this chapter, related work involving measurement of the glass transition temperature of thin films of polystyrene is discussed. In these films it is thought that thermal expansion differences between the substrate and the polystryene film may induce large strains in the film. Observation of the glass transition of these films using an ellipsometer indicates a strong shift to lower temperatures which is related to the thickness of the films and only occurs on heating the films from the glassy state. These observations give support to the concept that inherent strains in a glassy material lead to shifts in the glass transition. Such shifts

are of great importance to composite materials such as those discussed in Chapter 4.

B. Anomalies in Tg for Thin Films

The glass transition of thin polymer films cast on a surface may be affected by energetic interactions with the interface, molecular ordering at the interface and inherent stresses and/or strains which occurs on cooling a thin film due to differences in the coefficient of thermal expansion between film and substrate. Observation of these effects are of interest to applications in which polymers are subjected to confined geometries such as in the use of thin polymer layers in the electronics industry, in the study of filled polymer systems and in the study of immiscible polymer blends in which interface interactions are of importance. In this chapter a novel technique for the determination of the glass transition of thin polymer films is demonstrated and results are shown which indicate that strain induced shifts in T_g may play a dominant role in thin films and at interfaces.

The effect on T_g of increasing the surface to volume ratio $\left(\frac{S}{V}\right)$ was observed by Bares[1] for styrene-butadiene-styrene triblock copolymers. Bares expanded the Flory-Fox equation to include these effects,

$$T_g = T_{g,\infty} - \left(\frac{K_M}{M}\right) - K_S\left(\frac{S}{V}\right) \qquad (8.1),$$

where K_M and K_S are constants and $T_{g,\infty}$ is the glass transition temperature of a polymer of infinite molecular weight and negligible surface area. Bares noted a depression in T_g with increasing surface area of up to 20°C. Lipatov[2] observed an increase or decrease in T_g depending on interfacial conditions in filled polymeric systems. In these studies an increase in interfacial thickness was related to an increase in filler content. Natta and coworkers[3] looked at the glass transition of thin films through measurement of surface tension. Within the limits of resolution no shifts in T_g were reported. Confined geometries have also been reported to have effects on other thermodynamic properties of polymers such as phase separation. Reich and Cohen[4] noted effects of film thickness on the spinodal phase separation temperature in LCST blends. For films of less than one micron, shifts in the miscibility were observed with thickness.

C. Stress/Strain Effects

Shifts in T_g due to strain have been observed in the literature. The effect has generally been related to a dilatational increase in the free volume due to strain. Increases in the free volume would be expected to lower the glass transition (similar to the effect of a plasticizer).

Several groups have studied shifts in T_g for rubbery networks. Nose[5] noted an increase in T_g for chlorinated polyethylene vulcanizate with strain for sound velocity and shrinkage measurements and a decrease in T_g for tensile force measurements, thus shifts in T_g may be dependent on the measurement technique. J. E. Mark[6] noted a

slight increase in T_g for PVAC networks (about 3°C). Guzman[7] related strain effects on T_g to the free volume theory of the glass transition. It was noted that strain can alter both the activation volume and the activation entropy with opposite directions to the shift in T_g . Thus, a theoretical basis is provided for contradictory observations. For poly(neopentylglycol adipate) Guzman observed a -2°C shift in T_g for a strain of $\lambda = 1.88$. Tang[8] related shifts in the glass transition under stress conditions for elastomers to the Gibbs-Dimarzio theory.

Kovacs and Hobbs[9] used birefringence measurements on heating and cooling to determine the glass transition of strained polymer glasses including PS and PMMA. PMMA displayed an increase in T_g of 8°C under a constant strain. PS showed a decrease in T_g under strain of 13°C. These workers also studied various crystallizable polymers. Due to the experimental technique, a quantitative value for strain was not measurable.

Several investigators have looked at shifts in T_g for filled polymer composites. Empirical equations relating shifts in T_g to the strain have been developed for these materials based on continuum mechanics. Kajiyama[10] investigated the thermal expansion coefficient and glass transition of PSAN filled with glass fibers. They concluded that $\alpha_{composite}$ shifted from a rule of mixtures value due to thermally induced stresses. These thermal stresses were postulated to occur on cooling starting at $T_g + 20°K$. Alfthan[11] developed a continuum theory to model shifts in T_g for cellulose filled PS. For this system a decrease in T_g of 10°C is observed for a 50% cellulose composite. A

good fit with experimental results for ΔT_g versus volume fraction filler is obtained.

D. Use of the Index of Refraction to Characterize T_g:

The change in index of refraction with the glass transition for organic materials has been extensively documented. Parks[12],as early as 1928, showed such behavior for glucose glass. Wiley[13,14] in the 1940's, observed T_g for polyvinyl acetate and polystyrene among other polymers using an Abbe refractometer. More recently, Krause and coworkers[15] reported the use of refractive index data to determine T_g of low molecular weight PS.

In a series of papers Krause[16,17,18] studied T_g of PS-Polybutadiene-PS triblock copolymers of various morphologies using refractometry. Krause notes the effects of $\left(\frac{S}{V}\right)$ on T_g for the micro-phase separated system. C. Li has recently studied the glass transition of PS, poly(ethylene terephthalate), PMMA and PVC using the variation in the thermal coefficient of the refractive index.

Generally, plots of index of refraction, n, versus temperature exhibit a change in slope at T_g for organic glasses. This behavior is related to the expansion of free volume above T_g. Under the assumption of a spherical molecule, the density, ρ, can be related to the index of refraction, n, using the Lorentz-Lorenz equation,

$$\left(\frac{(n^2 - 1)}{(n^2 + 2)}\right) = \rho\, C \qquad (8.2),$$

where C is the specific refraction which depends on the polarizability of the molecules (temperature independent)[19]. Equation (8.2) results in a monotonically decreasing index of refraction with decreasing density.

Taking the derivative of the Lorentz-Lorenz Equation with respect to temperature, T,one obtains,

$$\frac{dn}{dT} = \left(\frac{(n^2+2)(n^2-1)}{6n}\right)\frac{1}{\rho}\frac{d\rho}{dT} = -\, q(n)\, \alpha \qquad (8.3).$$

Deviation from equation 8.3 reflects deviation from the assumptions used in the Lorentz-Lorenz derivation, chiefly the assumption of a spherical molecule.

E. Ellipsometry

The index of refraction, n, and thickness, t, of thin polymer films have been characterized using conventional ellipsometry[20,21], multiple-reflection ellipsometry, and by attenuated total internal reflection techniques.

Ellipsometry (Figure 8.1) allows for the noninvasive determination of the index of refraction and the thickness of a polymer film cast on a reflecting substrate.

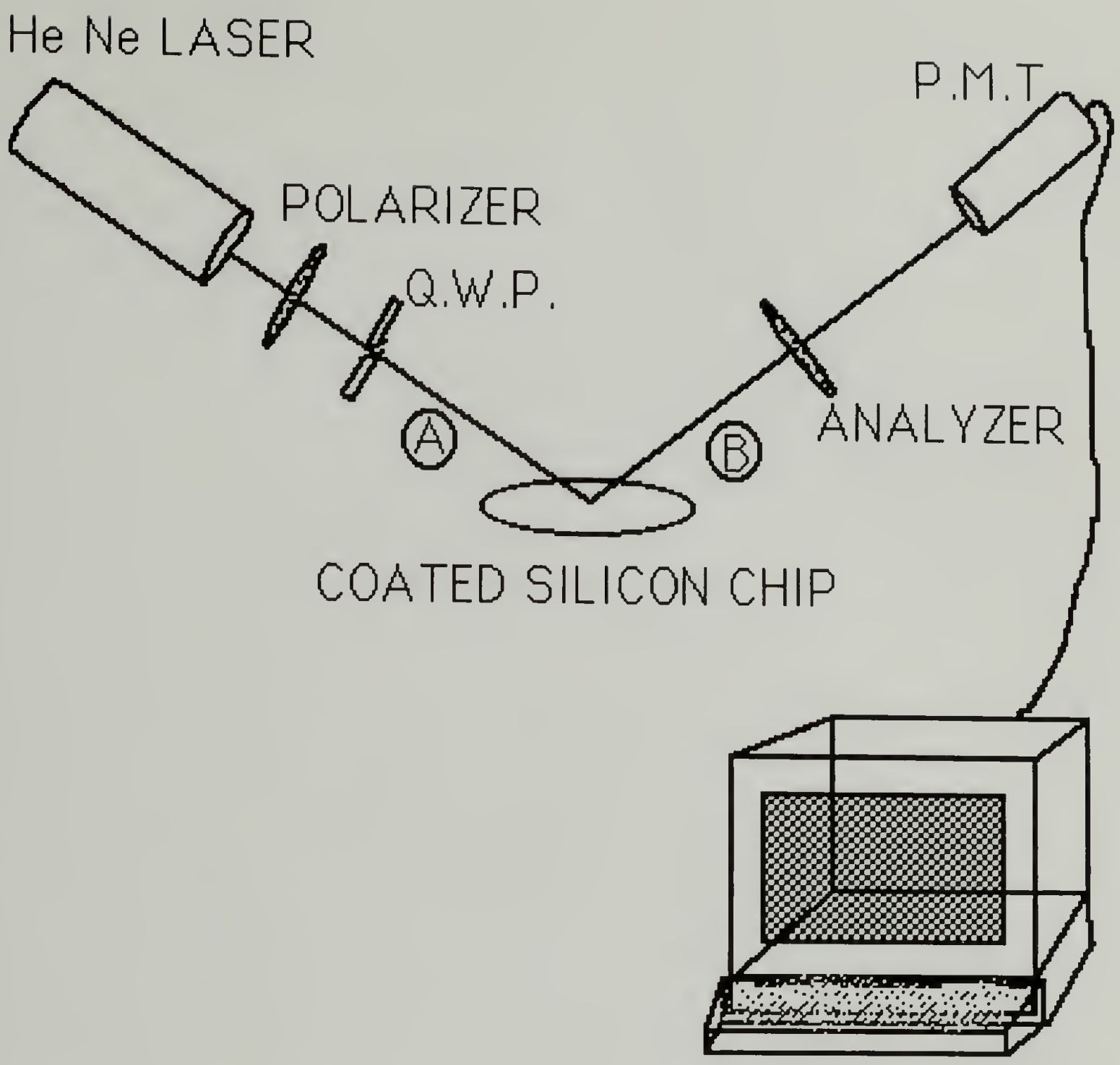

Figure 8.1 Experimental setup for an ellipsometer. Incident circularly polarized light becomes elliptically polarized after reflection. Index of refraction and thickness may be obtained.

Ellipsometry measures the reflection coefficients and the ratio of phase shifts of the parallel and perpendicular components of elliptically polarized light reflected from a surface. When a beam of circularly polarized light is reflected from a surface the amplitude and phase of the electro-magnetic (EM) waves are changed differently for the components of the EM waves parallel and perpendicular to the

surface. The circularly polarized EM waves become elliptically polarized due to the non-symmetric nature of the reflection. Generally, the amplitude of elliptically polarized EM waves can be broken down into orthogonal components,

$$E_x = a_x \cos (T + dx) \qquad (8.4),$$

$$E_y = a_y \cos (T + dy)$$

where a_x and a_y are the maximum amplitudes of the two components and (T + dx) and (T + dy) are the phases of the two components. The reference axes in ellipsometry are taken to be the axes parallel and perpendicular to the reflecting surface. In this case, the state of polarization of the light beam can be defined by the phase difference, Δ, between the two perpendicular components (parallel, p, and perpendicular, s, to the reflecting surface),

$$\Delta = dp - ds \qquad (8.5),$$

(where dp and ds are the phase angles of the parallel and perpendicular components) and by the amplitudes E_s and E_p of the perpendicular and parallel components.

For reflection of circularly polarized EM waves at a surface the phase difference, Δ, and amplitude ratio, tan ψ, are determined by the ellipsometer,

$$\tan \psi = \left(\frac{(E_s''/E_p'')}{(E_s'/E_p')} \right) \qquad (8.6),$$

where E_s and E_p are the amplitudes of the perpendicular and parallel components , " indicates the reflected beam and ' indicates the incident beam. A discussion of the relation of n and t to Δ and tan ψ is given in the literature[22] based on the governing equation for ellipsometry,

$$\rho = (\tan \psi)\ (e^{i\,\Delta}) \qquad (8.7),$$

where ρ is the reflection ratio,

$$\rho = \frac{R_p}{R_s} \qquad (8.8).$$

R_p and R_s are given by Drude's equations. Drude's equations use the index of refraction, n, and thickness, t, of the film and substrate to generate ρ.

A Rudolph Research® Ellipsometer (Auto EL2) was used in conjunction with a Koffler® hot stage (Figure 8.1). Δ and tan ψ values obtained using the ellipsometer were converted to n and t using an iterative Fortran program provided by the National Institute of

Standards and Technology[23]. Plots of n versus T were generated in order to observe a change in slope at T_g. Plots of t versus temperature were generated in order to determine the thermal expansion coefficient of the polystyrene films.

F. Sample Preparation

Toluene solutions of monodisperse PS (number average molecular weight 120,000 Polymer Laboratories, Amherst MA) of 10 weight percent were spun onto silicon chips. The spun samples were dried in a vacuum oven at 150°C for one week.

Two samples will be discussed. The first sample sample, having a thickness of about 3000 Å, was heated to 140°C in the apparatus and allowed to equilibrate for one hour. The temperature was then lowered at 2°/min to room temperature. The sample was equilibrated at room temperature for one hour followed by a heating run at 2°/min to 150°C. The second sample had a measured thickness of about 3500 Å and was cooled to room temperature from 150°C under ambient conditions. It was then heated in the ellipsometer to 150°C at 2°/min with measurements taken at about 1° increments.

G. Results/Discussion

Figure 8.2 shows a plot of refractive index (n) versus inverse temperature (1/°K) for cooling a 3000Å PS film (inverse temperature plots were found to show the shift in slope at T_g more clearly than

straight temperature plots, although the shift is clear in temperature plots as well).

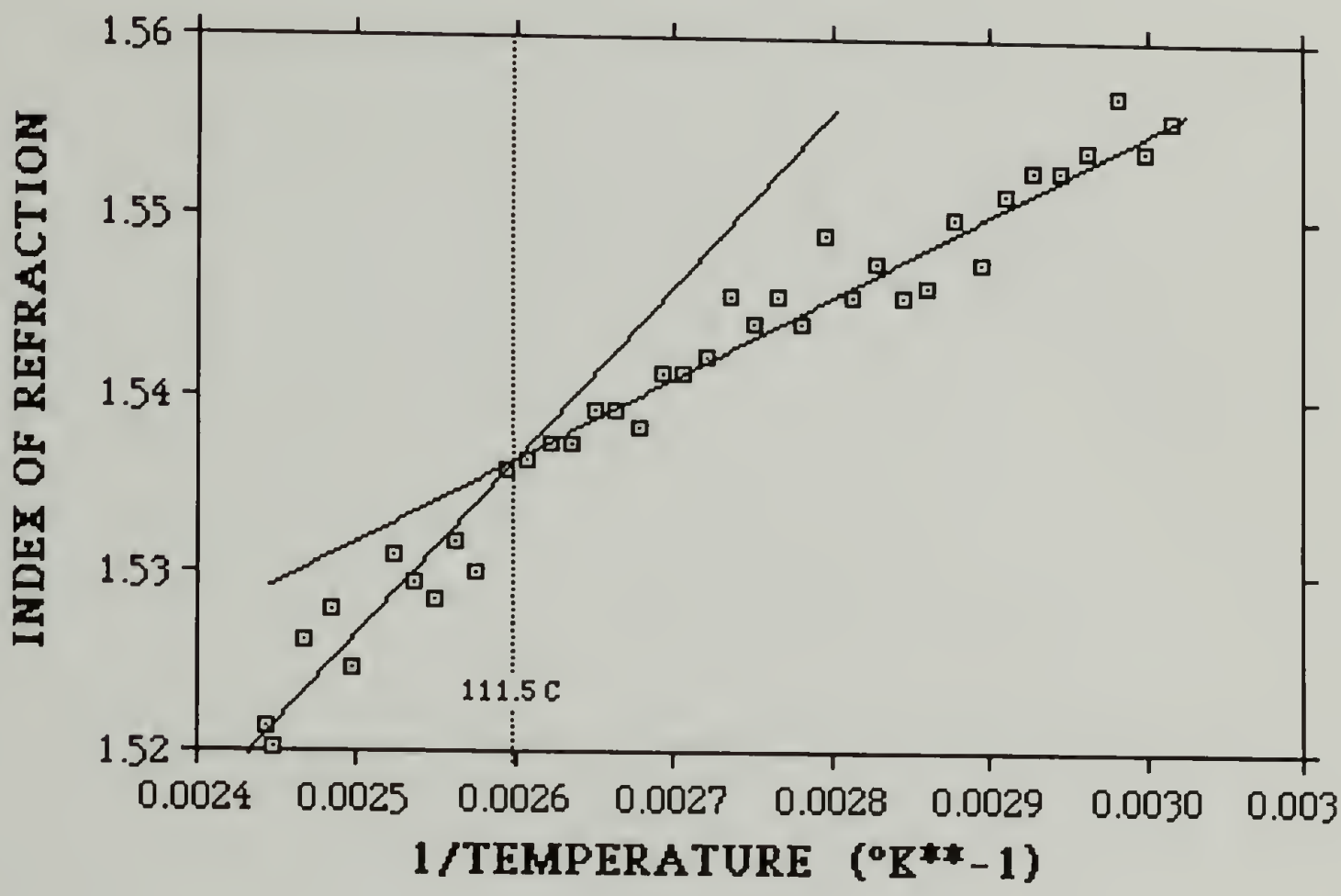

Figure 8.2 Index of refraction, n, versus 1/T ($°K^{-1}$) for 3000 Å film cooling from 140 °C. (Error is reflected in the scatter of the data.)

A shift in slope is observed at approximately 112°C (±2°C). This corresponds to the bulk glass transition temperature as measured by DSC using a heating rate of 10°/min. After the film had equilibrated at room temperature for one hour a heating run at 2°/min was conducted (Figure 8.3). The thickness of the film had not changed significantly during the room temperature equilbration.

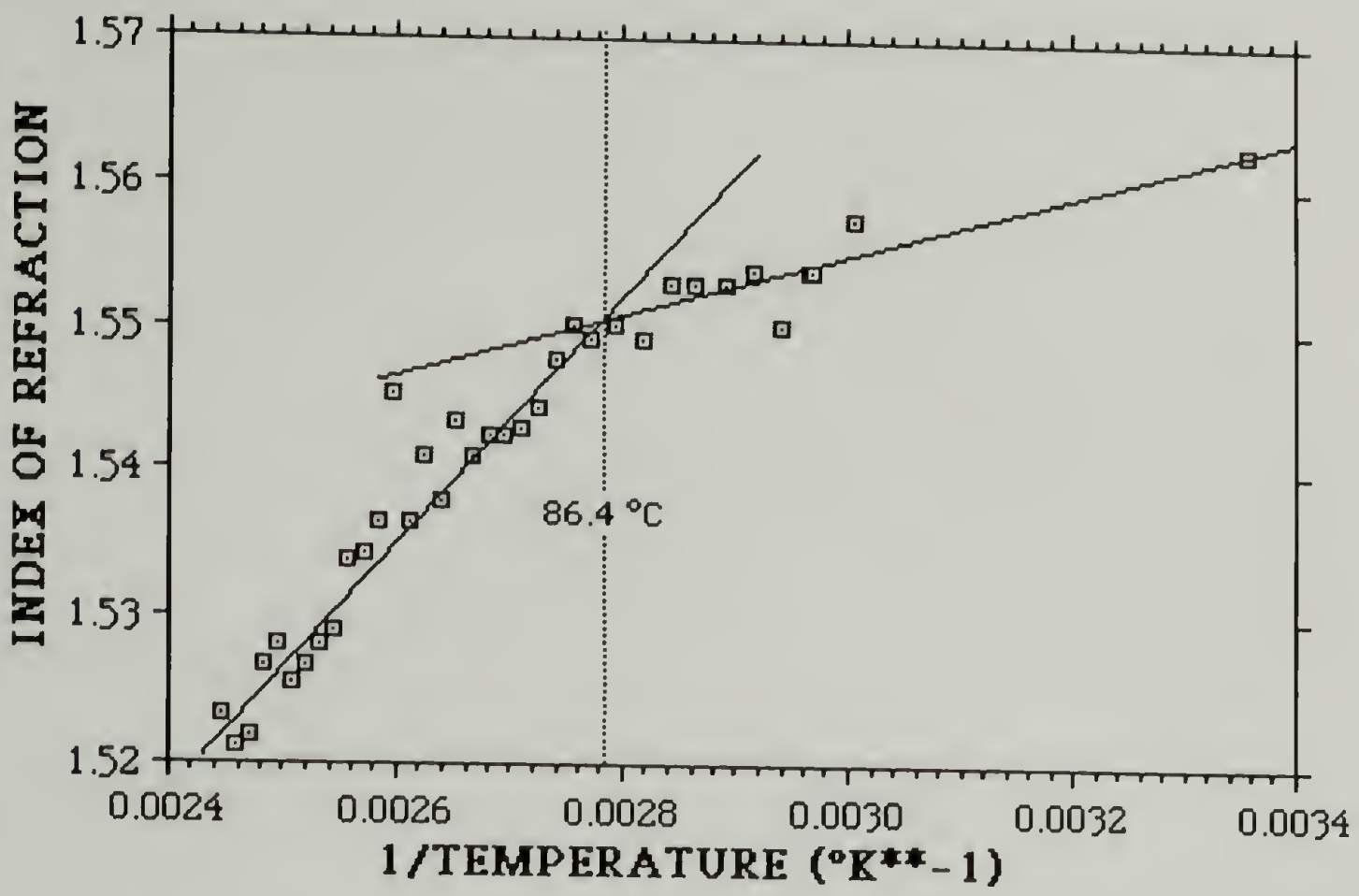

Figure 8.3 Index of refraction, n, versus 1/T ($^{\circ}K^{-1}$) for 3000 Å film heating from room temperature. (Error is reflected in the scatter of the data.)

For the heating run the change in slope of n vs T occurred at approximately 84°C (±2°C). The optically determined T_g agrees with the calorimetric T_g on cooling, but is shifted on melting the thin glassy film ($\Delta T_{g\ melting} \approx$ -25 C°).

Figure 8.4 shows a heating run for a thicker film, 3500Å. Again, on heating from a glass, the optical T_g is shifted $T_{g,3500Å,heating} \approx$ 92° C (±5°C).

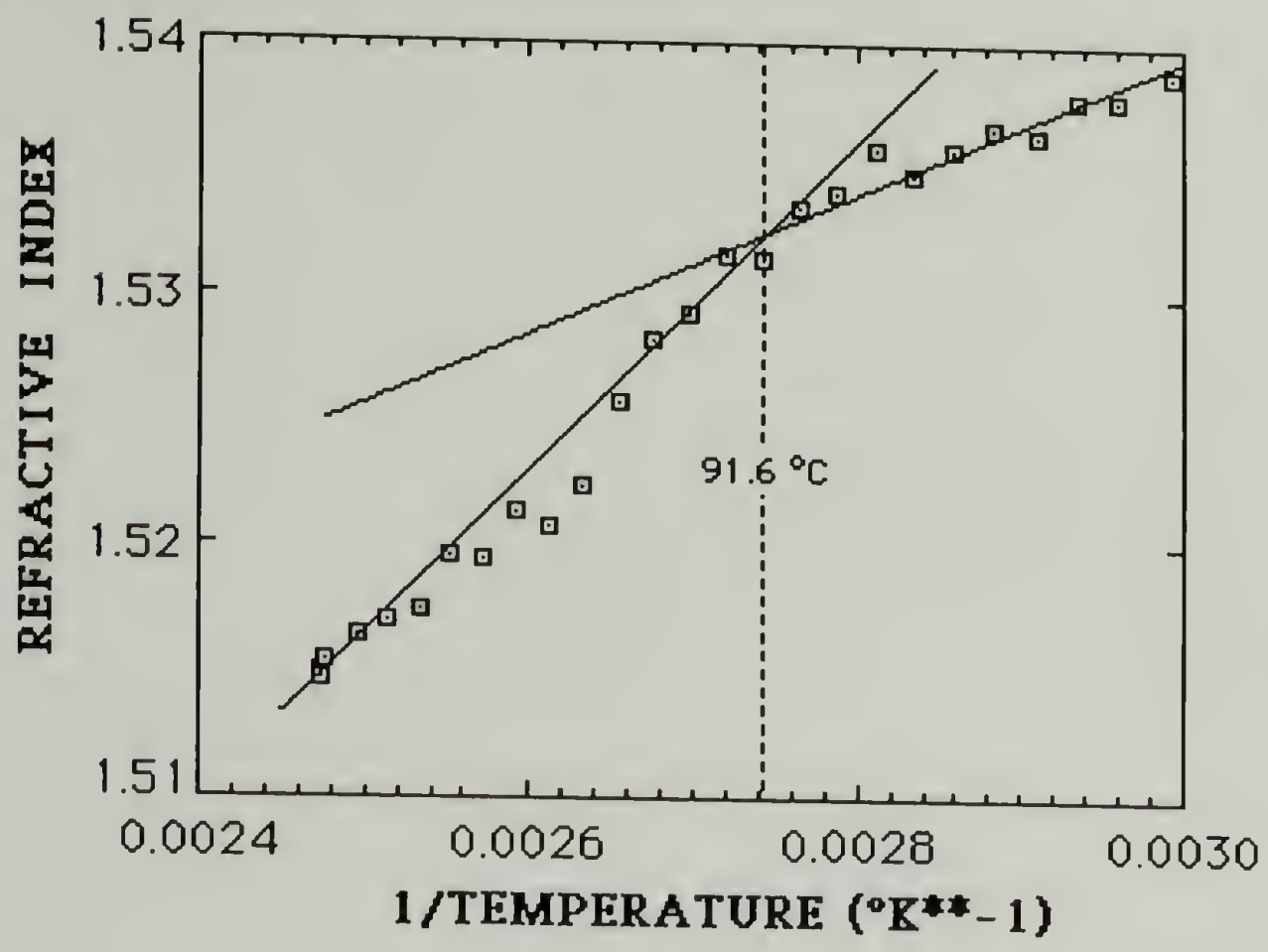

Figure 8.4 Index of refraction versus 1/T ($°K^{-1}$) for 3500 Å film heating from room temperature. (Error is reflected in the scatter of the data.)

The observed shift in optical T_g, about -18 C°, is smaller than was observed for the 3000Å film. (Error is reflected in the scatter of the data.)

The precision of the graphically determined T_gs are in the order of ±3 °C.

Figure 8.5, 8.6, and 8.7 show plots of thickness, t, versus temperature for the two polystyrene films and correspond to Figures 8.2, 8.3 and 8.4 respectively.

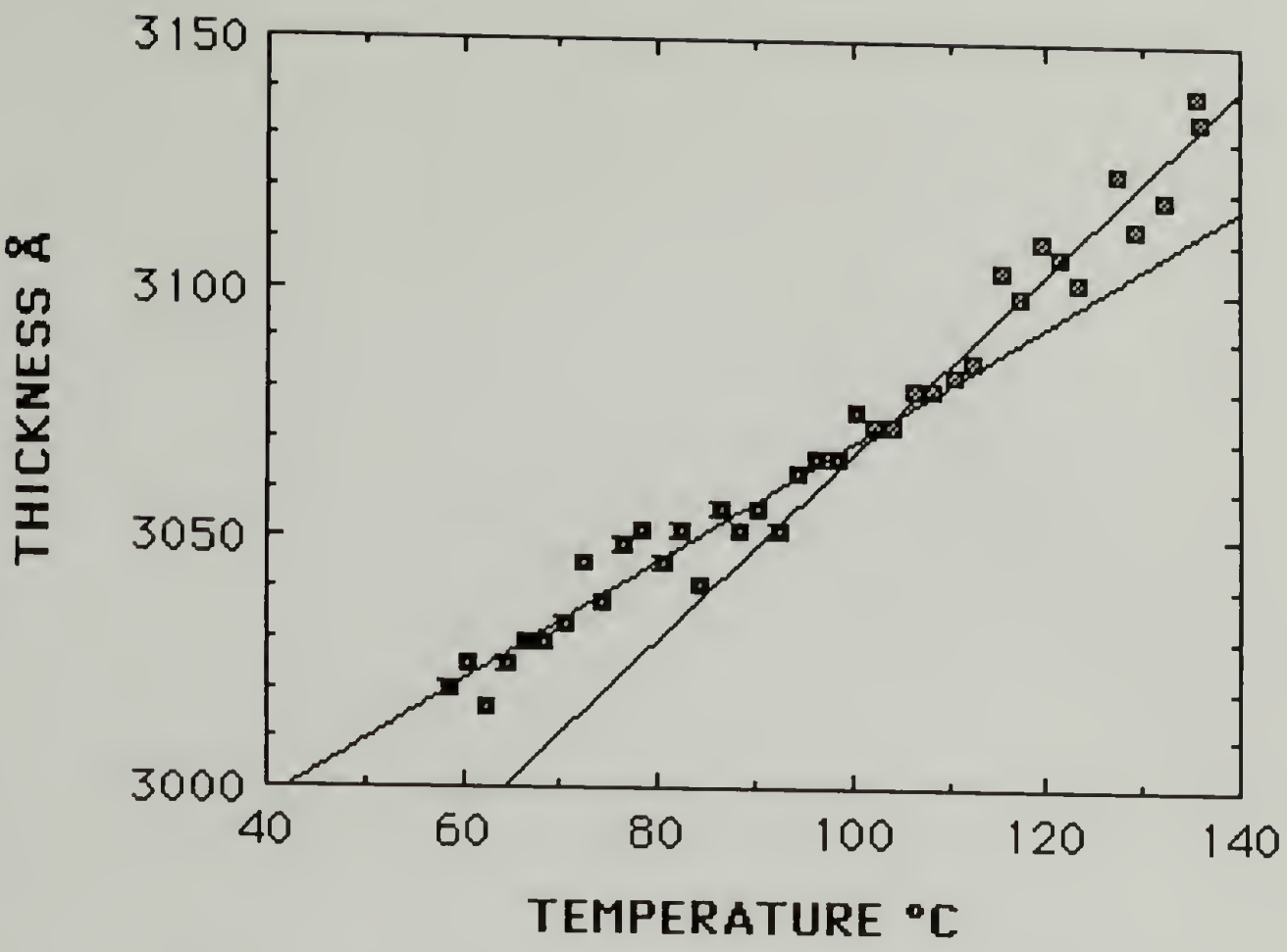

Figure 8.5 Thickness, t, versus temperature (°C) for the 3000 Å film of Figures 8.2 and 8.3 on cooling. Error is reflected in the data scatter.

A shift in the slope of the thickness versus temperature plots is observed close to the optical T_g for all runs.

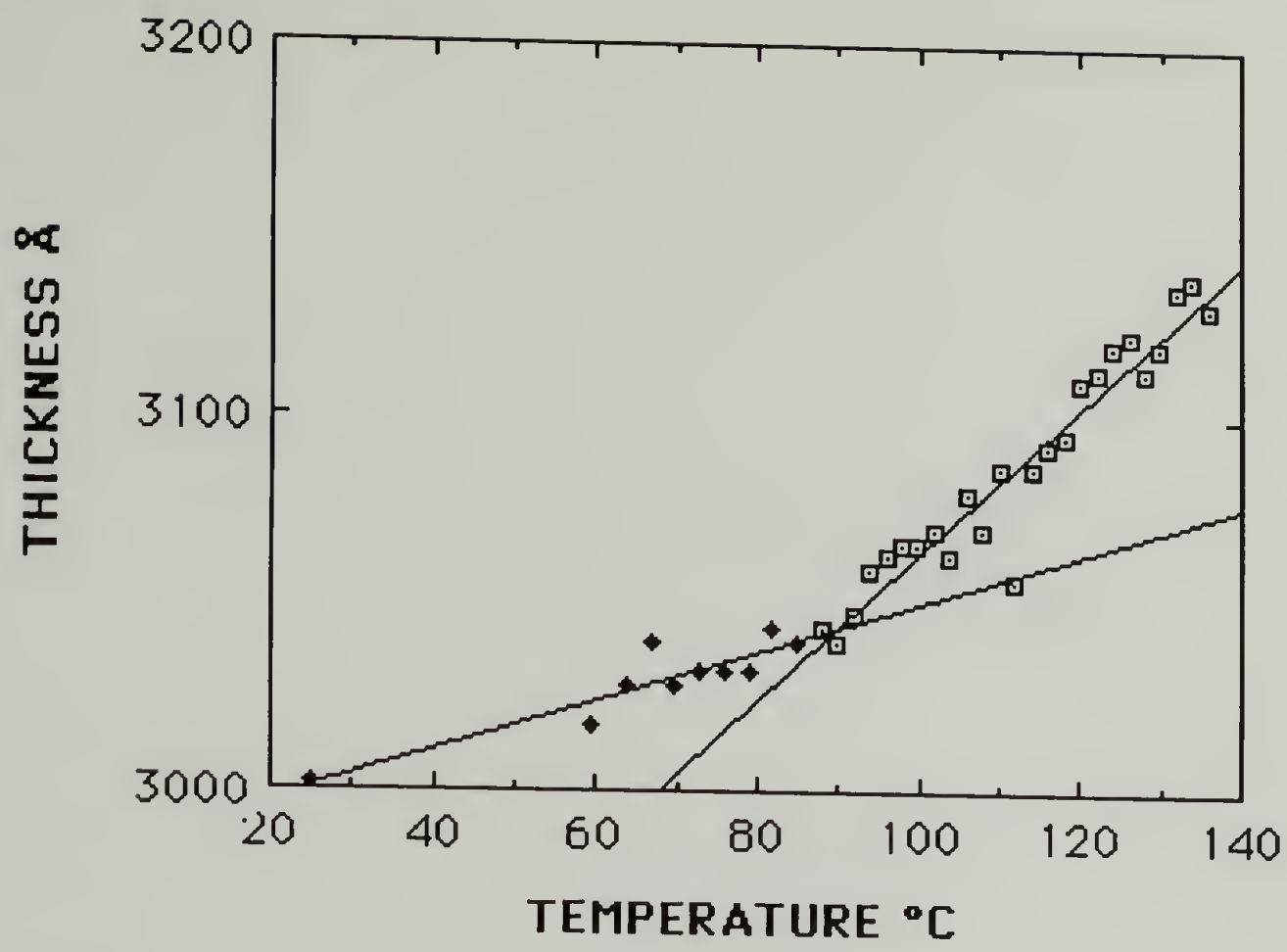

Figure 8.6 Thickness, t, versus temperature (°C) for the 3000 Å film of Figures 8.2 and 8.3 on heating from the glass. Error is reflected in the data scatter.

The difference in thickness and index of refraction measurements are believed to be due to stresses and strains which occur in the film on heating and cooling due to differences in thermal expansion coefficient between the film and the substrate. It is believed that geometric constraints on the thin film alter the thickness measurements.

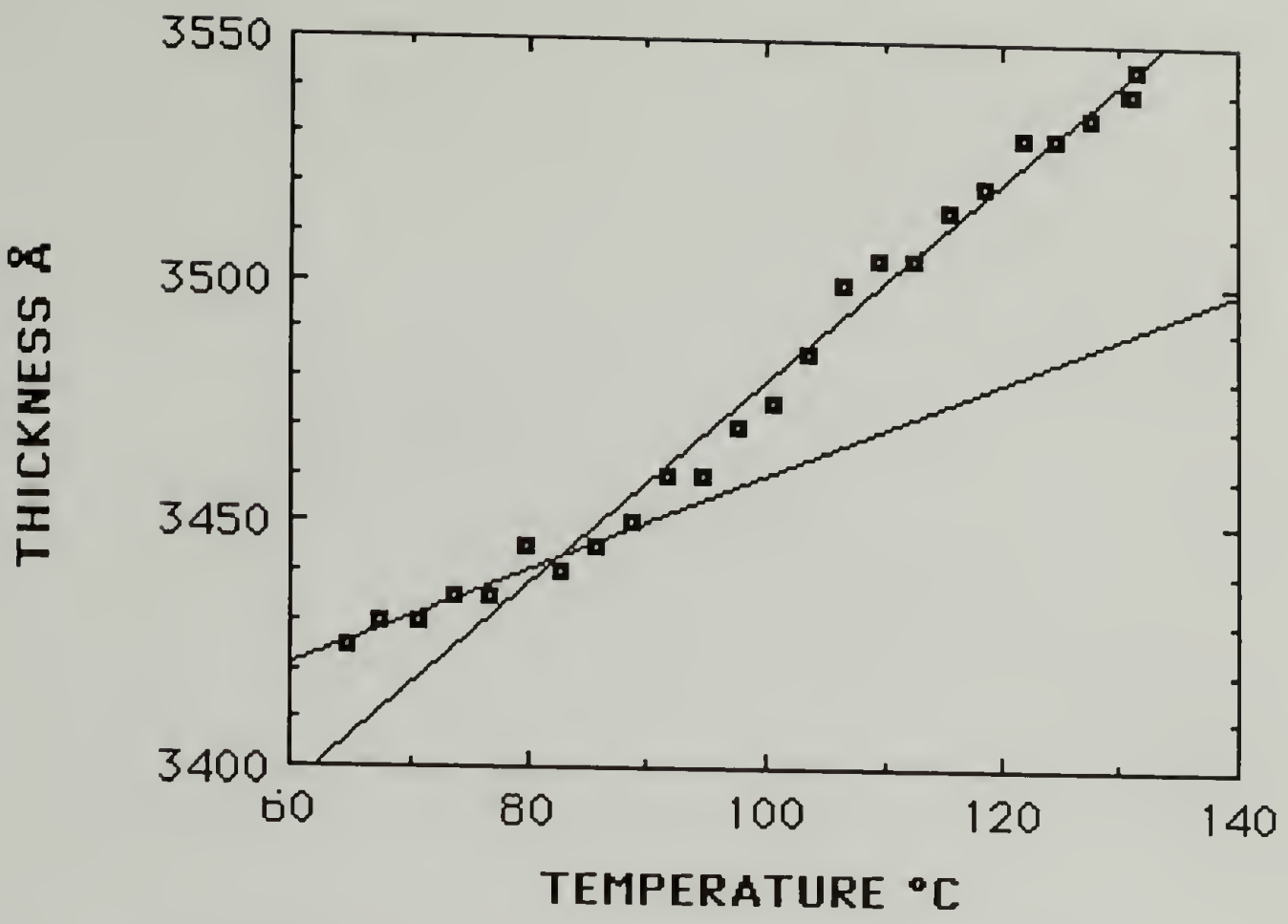

Figure 8.7 Thickness, t, versus temperature (°C) for the 3500 Å film of Figures 8.4 on heating from the glass. Error is reflected in the data scatter.

The volumetric thermal expansion coefficient is given by,

$$\alpha = -\frac{1}{\rho}\left(\frac{d\rho}{dT}\right) = -\frac{V_{avg}}{M}\left(\frac{d(M/V)}{dT}\right) \qquad (8.9),$$

where ρ is the density, and V is the volume of a mass of material M. If it is assumed that a given area of the substrate contains a fixed mass of polymer (due to lateral constraints), the thickness, t, can be used to determine the volume (M cancels out of equation 8.9). Thus,

$$\alpha \equiv - t_{avg} \left(\frac{d(1/t)}{dT} \right) \qquad (8.10).$$

Figure 8.8 is a typical plot of 1/t versus T for the films.

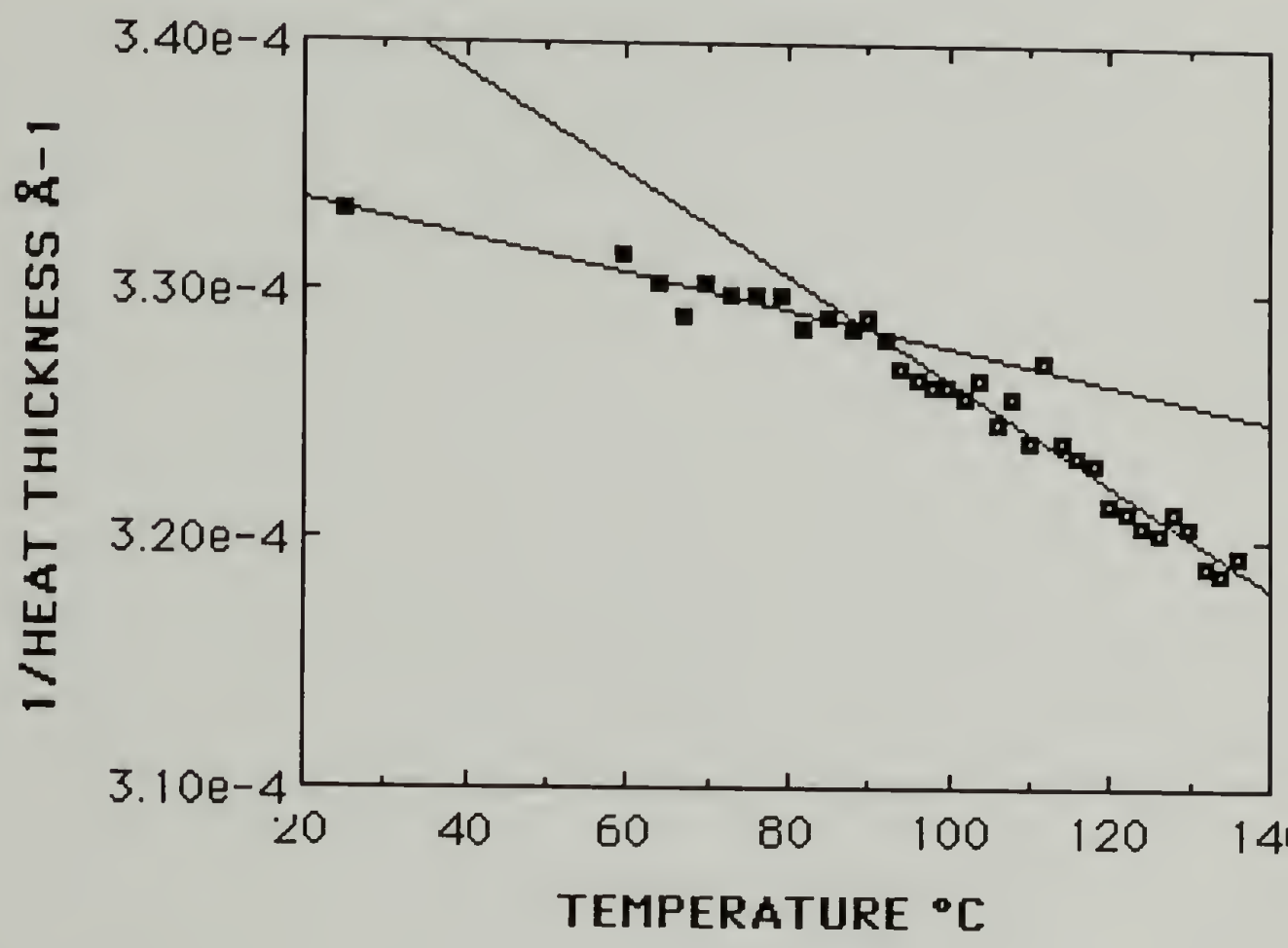

Figure 8.8 Inverse thickness, 1/t, versus temperature (°C) 3000 Å film on heating. (Error is reflected in the scatter of the data.)

Table 8.1 lists the calculated values of the parameters in equations 8.3, 8.9, and 8.10.

Table 8.1 Calculated values of the parameters in equations 8.3, 8.9, and 8.10.

		3500 Å FILM HEATING	3000 Å FILM COOLING	3000 Å FILM HEATING
GLASS	$\alpha \times 10^4$	2.725	3.966	2.194
	n_{avg}	1.536	1.546	1.553
	t_{avg} Å	3436	3051	3031
	$\frac{dn}{dT} \times 10^4$	-1.776	-3.709	-2.089
	$\frac{d(1/t)}{dT} \times 10^8$	-7.931	-13.00	-7.238
MELT	$\alpha \times 10^4$	6.164	5.943	6.441
	n_{avg}	1.521	1.529	1.535
	t_{avg} Å	3510	3110	3089
	$\frac{dn}{dT} \times 10^4$	-4.208	-5.196	-5.918
	$\frac{d(1/t)}{dT} \times 10^8$	-17.56	-19.11	-20.85

The Polymer Handbook[24] gives the volumetric thermal expansion coefficients for PS glass as 1.7-2.4 x 10^{-4} K° and for PS melt, 5.1-6.0 x 10^{-4} K°. Manabe[25] gives values of $\alpha_{glass} = 2.45 \times 10^{-4}$ K° and $\alpha_{melt} = 5.55 \times 10^{-4}$ K°. The α values measured in this experiment are of the same order of magnitude as the literature values but slightly higher. The coefficients of linear regression for the 1/t versus T plots was close to 0.95 for all runs.

Table 8.2 lists the values of $q(n)_{calc}$ obtained by dividing $\frac{dn}{dT}$ by -α and the calculated value of $q(n_{avg})$ using the average n values (from Table 8.1) in equation 8.3 for the melt and glassy states.

Table 8.2 $q(n_{avg})$ and $q(n)_{measured}$.

		3500 Å FILM HEATING	3000 Å FILM COOLING	3000 Å FILM HEATING
GLASS	$q(n_{avg})$	0.27	0.66	0.67
	$q(n)_{meas}$	0.65	0.94	0.95
MELT	$q(n_{avg})$	0.62	0.63	0.64
	$q(n)_{meas}$	0.68	0.87	0.92

Deviations of the two q(n) values indicate that the assumption of spherical molecules used in the Lorentz-Lorenz equation is not valid. The values of q(n) presented in Table 8.2 indicate that the thicker film in the melt is closest to the idealized spherical molecular shape. The thinner film in the melt displays a degree of molecular distortion to a greater extent on heating from the glass than on cooling from the annealed state. The glassy films deviated greatly from the spherical approximation. The thicker film in the glassy state, which was quenched from the melt at room temperature, showed the largest deviation form spherical behavior. The thinner film showed similar

deviation from spherical behavior on heating and on cooling in the glass, as would be expected.

The observed shift in the glass transition is most likely due to strain induced in the films on cooling through the glass transition. The film is free to thermally contract on cooling until the glass transition region is approached (Manabe[27] notes that strain effects in composite materials probably begin to occur at T_g + 20°C). At this point the material becomes rubbery to leathery and orientational creep is induced. The free surface may be able to continue it's contraction to a greater extent. In this regard a gradient of strain may be induced in the material. Similar effects may occur during solvent casting as the gelation point is passed through[26]. On heating, the oriented material shows a shift in glass transition.

For the thin film samples studied in this chapter, the modulus of the silicon substrate can be assumed to be infinite with respect to the polymer. Also, the thermal expansion coefficient of the substrate is negligible in comparison to that of the polymer. Using a continuum approach, the expected thermal stress can be related to the shift in T_g. Since the relaxation modulus E(T) and Poisson's ratio ν(T) for the material changes with temperature, temperature dependent data for E(T) and ν(T) must be used. Manabe[27] reports such data for PS in his study of T_g for phase separated polymer systems. Since the film is very thin in comparison to the dimensions of the chip, a equi-biaxial stress distribution can be used to model the film. For such a stress distribution under thermal stress conditions we have[28],

$$de_{zz} = -\beta \left(1 + \frac{2\,\nu(T)}{1 - \nu(T)}\right) dT = d\left(\frac{\Delta t}{t}\right) \qquad (8.11),$$

$$d\sigma_{xx} = d\sigma_{yy} = -\beta \left(\frac{E(T)}{1 - \nu(T)}\right) dT \qquad (8.12),$$

$$e_{xx} = e_{yy} = -\beta\, \Delta T \qquad (8.13),$$

where β is the linear thermal expansion coefficient, $\nu(T)$ is Poisson's ratio and $E(T)$ is the relaxation modulus. Table 8.3 lists values for use in equations 8.11-8.13. The $E(T)$ and $\nu(T)$ values are for a relaxation experiment at 120 seconds as reported by Tobolsky[29]. Figure 8.9 is a plot of $-\sigma_{xx}/\beta$ and $-e_{zz}/\beta$ versus temperature from Table 3.

Numerically integrating $\left(1 + \frac{2\,\nu(T)}{1 - \nu(T)}\right) dT$ from equation 8.11, and dividing by the experimental $\frac{\Delta t}{t}$ values yields the values for the linear thermal expansion coefficient, β, in Table 8.4. The values for σ_{xx} given in Table 8.4 are obtained using these β values in equation 8.12 and numerically integrating $d\sigma_{xx}$. The e_{xx} values are obtained from equation 8.13.

Table 8.3 Integration parameters for the determination of β, σ_{xx}, and e_{xx}.

Temp °C	Relaxation Modulus $E(T)^{27}$ dyn/cm^2	Poisson's Ratio $\nu(T)^{27}$	$\left(1 + \frac{2\,\nu(T)}{1 - \nu(T)}\right)$	$\left(\frac{E(T)}{1 - \nu(T)}\right)$ dyn/cm^2
75	2×10^{10}	0.36	2.13	3.1×10^{10}
80	1.7×10^{10}	0.37	2.18	3.2×10^{10}
85	9.8×10^{9}	0.39	2.28	1.6×10^{10}
90	3×10^{9}	0.46	2.70	5.6×10^{9}
95	1×10^{8}	0.497	2.98	2.0×10^{8}
100	1.5×10^{7}	0.4997	3.00	3.0×10^{7}
105	1.2×10^{7}	0.49981	3.00	2.4×10^{7}
110	9.45×10^{6}	0.49985	3.00	1.9×10^{7}

The stresses and strains reported in Table 8.4 are small. It should be noted however, that the thickness of the film is of the order of 15 diameters of the polymer molecule in the theta condition ($R_g \cong$ 86 Å for a 120,000 molecular weight PS). Thus, the continuum concepts used to obtain the values in Tables 8.3 and 8.4 must be drawn in to question. The q(n) data indicates that the orientation of

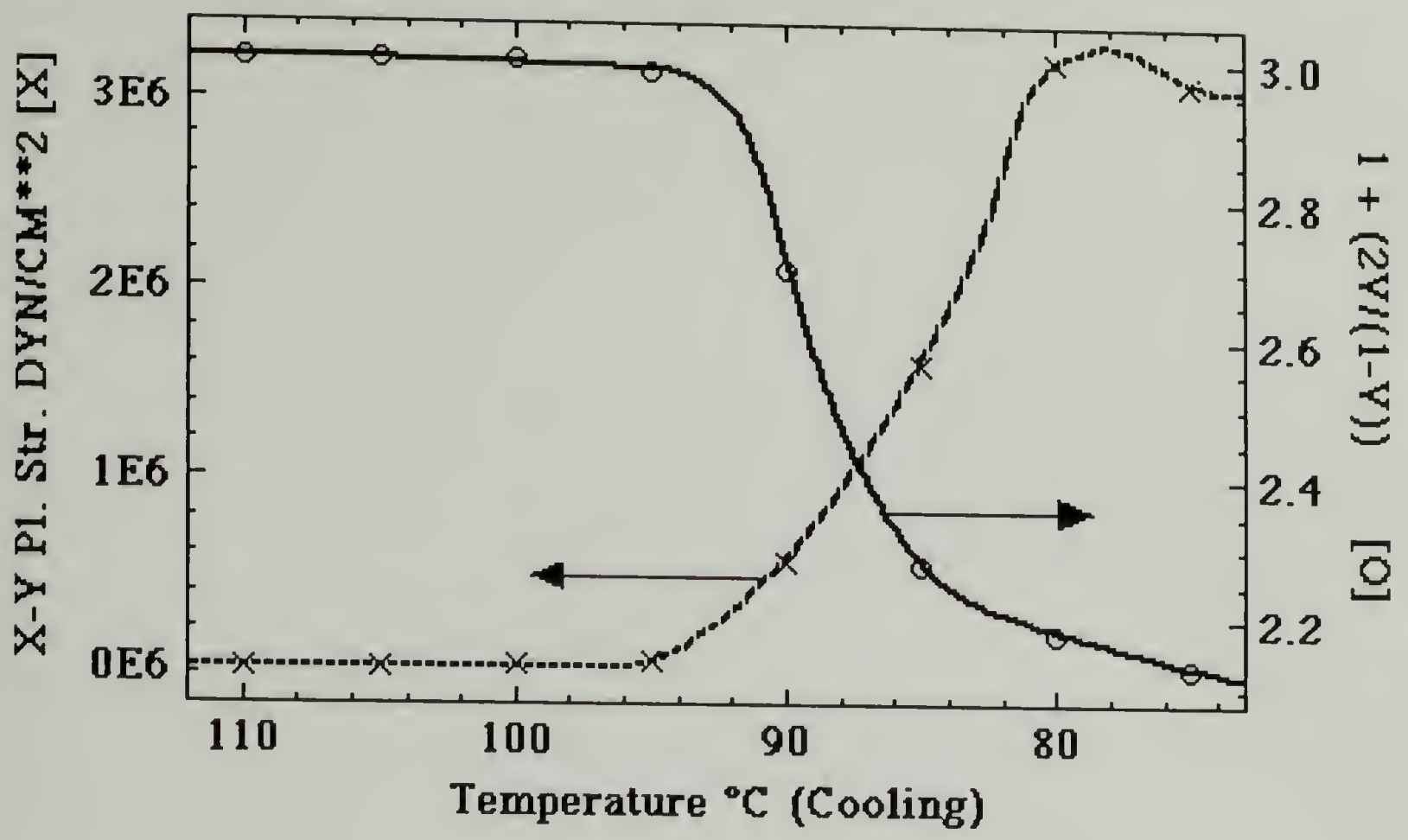

Figure 8.9 $-\sigma_{xx}/\beta$ (N C°/cm^2 x 10^{-4}) and $-e_{zz}/\beta$ (C°) versus temperature (°C) from Table 8.3.

individual chains in such a film may be much greater than in a bulk polymer under similar stress conditions.

Table 8.4 Calculated parameters for the glassy films.

	3500 Å FILM HEATING	3000 Å FILM COOLING	3000 Å FILM HEATING
β x 10^4	2.2	1.6	1.9
σ_{xx} (N/cm^2)	763	555	659
e_{xx} %	0.77	0.56	0.67

H. Conclusions

A novel technique for the determination of the glass transition of thin polymeric films has been demonstrated. In investigating this new technique it was observed that significant shifts in T_g occur on heating from the glass. This behavior may be explained by large molecular deformations which lead to a dilatational increase in the free volume of the polymer. The shift appears to decrease on increasing thickness.

Although only one polymer was investigated in these preliminary studies, there are several important implications to these observations. First, the thermal behavior of thin films, such as those used in the micro-electronics field, may be drastically different than that determined from bulk measurements. Secondly, mechanical models of composite materials such as phase separated blends and fiber reinforced composites which generally assume a constant modulus (related to T_g) of the matrix and suspended materials may be effected by shifts in T_g near the interfaces. Finally, this study lends support to the concepts that in polymer failure, local deformation and strain in polymeric materials leads to a shift in the local glass transition.

References

1. J. Bares, *Macromolecules* **8**, 244 (1975).

2. Y. S. Lipatov and L. M. Sergeeva, *Adsorption of Polymers*, Wiley and Sons, NY, 1979, Pages 140-59.

3. G. Natta, E. Fermi and G. Gabrielli, *La Chimica e L'Industrai*, **47**, 1 (1965).

4. S. Reich, Y. Cohen, *J. Polym. Sci., Polym. Phys. Ed.*, **19**, 1255 (1981).

5. M. Naoki and T. Nose, *Polymer J.*, **6**, 45 (1974).

6. M. A. Sharaf and J. E. Mark, *Rubber Chem. and Tech.*, **53**, 982 (1981).

7. R. Diaz-Calleja, E. Riande and J. Guzman, *Polymer*, **28**, 2190 (1979).

8. K. D. Pae, C. L. Tang and K. Vijayan, *J. Mat. Sci*, **21**, 2901 (1986).

9. A. J. Kovacs and S. Y. Hobbs, *J. App. Polym. Sci.*, **16**, 301 (1972).

10. T. Kajiyama, T. Yoshinaga and M. Takayanagi, *J. Polym. Sci.: Polym. Phys. Ed.* , **15**, 1557 (1977).

11. E. Alftan, A. de Ruvo and M. Rigdahl, *Intern. J. Polymeric Mater.*, **7**, 163 (1979).

12. G. S. Parks, H. M. Huffman, and F. R.Cattoir, *J. Phys. Chem.* **32**, 1366 (1928).

13. R. H. Wiley, *J. Polym. Sci.*, **2**, 10 (1947).

14. R. H. Wiley, and G. M. Brauer,*J. Polym. Sci.* **3**, 455 (1948).

15. S. Krause, and Z. Lee, *J. Polym. Phys. Ed.* **19**, 1925, (1981).

16. S. Krause, Z. Lu, and M. Iskandar, *Macromolecules* **15**, 105 (1982).

17. S. Krause, Z. Lu, and M. Iskandar, *Macromolecules* **15**, 112 (1982).

18. S. Krause, Z. Lu, and M. Iskandar, *Macromolecules* **15**, 1076 (1982).

19. See for example R. S. Stein, *Electro-optical Behavior of Polymers*, Univ. Mass. Video Instructional Program Lecture Notes, Amherst, MA, 1989.

20. R. R. Stromberg and F. McCrackin,in *Clean Surfaces*, G. Goldfinger ed., Decker Co., NY, 1970, Page 74.

21. F. L. McCrackin, E. Passaglia, R. R. Stromberg and H. L. Steinberg, *J. of Res. National Bureau of Standards, A. Phys. and Chem.* **67A**, 363 (1963).

22. F.L. McCrackin, E. Passaglia, R. R. Stromberg, H. L. Steinberg, *J. of Res. National Bureau of Standards, A. Phys. and Chem.* **67A**, 383 (1963).

23. Personnel communication with R. R. Stromberg.

24. J. Brandrup, E. H. Immergut, *Polymer Handbook*, John Wiley and Sons, N. Y., 1975, Chapter V ,Page 81.

25. S Manabe, R. Murakami, M. Takayanagi, and S. Uemura, *Intern. J. Polymeric Mater.*, **1**, 44 (1971).

26. T. S. Chow, C. A. Liu and R. C. Penwell, *J. Polym. Sci.: Polym. Phys Ed.* , **14**, 1311 (1976).

27. S Manabe, R. Murakami, M. Takayanagi, and S. Uemura, *Intern. J. Polymeric Mater.*, **1**, 44 (1971).

28. Y. C. Fung, *A First Course in Continuum Mechanics, 2'nd ed.*, Prentice-Hall, Englewood Cliffs NJ, 1977, Pages 312-3.

29. A. V. Tobolsky, *Properties and Structures of Polymers*, Wiley, NY 1960, Page 74.

CHAPTER 9.

CHAIN END SEGREGATION AT INTERFACES (NEUTRON REFLECTION STUDY)

A. Background

The surface tension of polymers tends to increase with molecular weight[1]. This behavior has been described by the empirical equation[2,3],

$$\gamma = \gamma_\infty - \frac{k}{M_n^{2/3}} \qquad (9.1).$$

γ_∞ is the surface tension at infinite molecular weight, k is a constant, and M_n is the number average molar mass. de Gennes[4] has theorized that this behavior can be explained as an attraction of terminal end groups to the surface. Powers of the molecular weight other than -2/3 are suggested by this analysis depending on the relative attraction of the end groups to the surface. Wu[1] noted that the empirical behavior described by equation 9.1 is followed by polystyrene. Bender and Gaines[5] reported that monodisperse polystyrene samples of molecular weights 1 to 100 kg/mole qualitatively follow equation 9.1.

In regard to the phase separated blends discussed in Chapter 1, end group segregation at the interface would be thought to have a deleterious effect on interfacial adhesion. Segregated end groups at

the interface of a composite material would be thought to promote interfacial failure. Such interfacial failure is observed in some of the well phase separated blends discussed in Chapter 4.

B. Experimental

It is the purpose of this chapter to determine the extent of end group segregation in polystyrene in an extreme case, that of the polystyrene/air and polystyrene/silicon surface. For this purpose monodisperse block-copolymers of deuterated and hydrogenous polystyrene were synthesizes by S. Smith at Procter and Gamble's Central Research Department in Cincinatti OH. The block copolymers were synthesized with either deuterated end groups and hydrogeneous main chains or hydrogenous end groups with deuterated main chains.

Working with R. J. Composto (U. Penn.), M. Satkowski (Procter and Gamble), T. Mansfield (U. Mass.), Bill Hamilton(Oak Ridge National Lab) and G. Smith (Los Alamos National Lab) neutron reflection measurements were made on thin films spun from dilute toluene solutions of the block copolymers onto silicon wafers. Samples were dried under vacuum without heating. (In such thin films spun from dilute solution solvent removal is not a serious problem.)

Measurements were made at Los Alamos National Lab's LANSCE facility. Figure 9.1 shows the experimental geometry used in the reflectivity experiment.

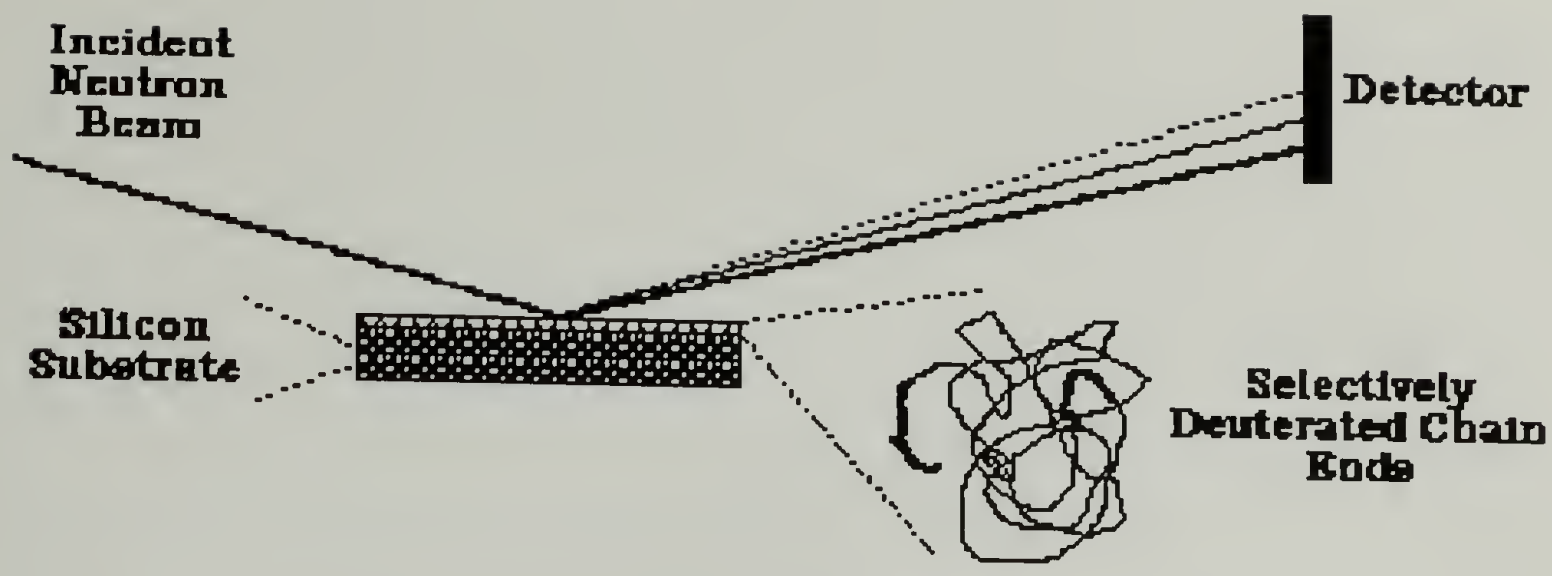

Figure 9.1 Experimental geometry for the neutron reflection experiment. The incident beam reflects from the sample at a grazing angle of about 0.5°.

Reflectivity measurements were made without annealing in order to obtain a background profile for comparison with annealed films. It was believed that the unannealed, spun films would show a reflectivity profile without segregation since solvent evaporation occurs very rapidly (less than one second), essentially locking in a fairly random distribution of the polymer chains. The films were then annealed above the glass transition temperature for an extended period and a comparative profile was measured. Segregation of the chain ends (if it occurred) would be observable in the annealed samples as a shift in the reflectivity pattern, especially at high q. Figure 9.2 shows the expected reflectivity results for the chain end segregation experiment.

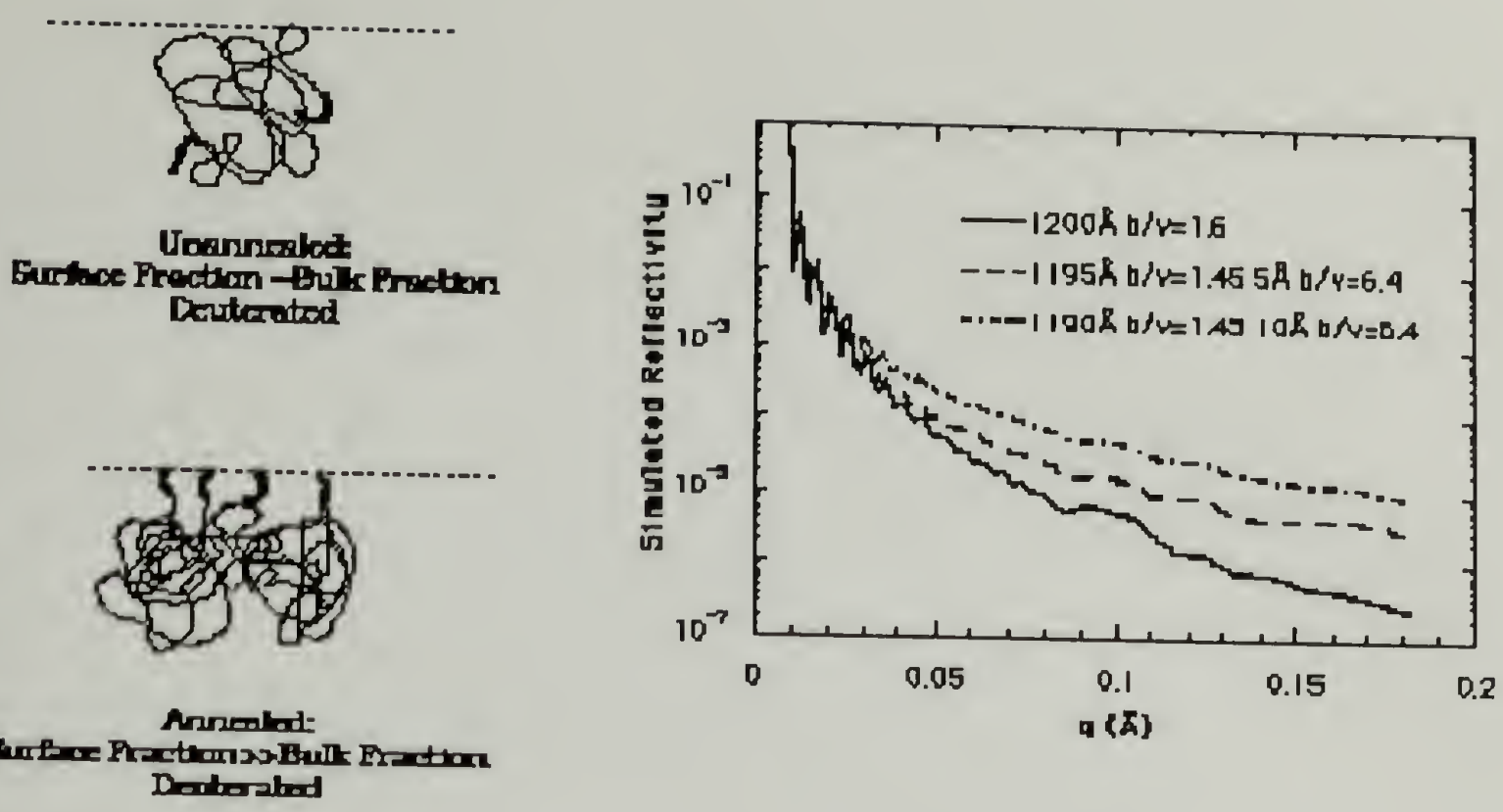

Figure 9.2 Simulation of the expected results for the chain end segregation experiment following the reasoning of de Gennes (reference 4). Simulated reflectivity profiles are for 1200Å films with a 10Å deuterated layer at the surface (top dashed curve), 5Å deuterated layer (middle dashed curve) and no deuterated layer (bottom solid curve).

C. Results and Discussion

Table 9.1 lists the samples which were run. Molecular weights are indicated in kg/mole for the blocks of deuterated and hydrogeneous PS. The annealing conditions are also listed. The last column gives the calculated value of the neutron scattering cross section, calculated using the molecular weights given in column 1. In all cases a simulation of a simple-block neutron-cross section profile yielded an equally good or better fit to the data than more complicated profiles which would indicate chain end segregation. The results of the block profile fits are given in columns 3 and 4. (These results are

in agreement with experiments done on polystyrene samples at Argonne National Lab by B. Sauer and D. Walsh[6] using lower molecular weight polystyrene than samples 1,2 and 3.)

Table 9.1 Experimental samples and results of simple block profile simulations.

Sample Block kg/mole d=Deuterated d	Annealing Temp/Time	Fit Thickness Å	Fit b/v x 10^6	Stoichio-metric b/v x 10^6
#1 2/1d/2	Unannealed	830	2.36	2.36
	-----	-----	-----	
#2 0.5d/4/0.5d	Unannealed	1100	2.20	2.36
	130°C 300 min	1000	2.36	
#3 4/1d	Unannealed	1080	2.30	2.36
	130°C 300 min	950	2.40	
#4 34/3d/34	Unannealed	1510	1.50	1.60
	160°C 400 min	1510	1.50	
#5 1.3d/63/1.3d	Unannealed	1490	1.52	1.52
	160°C 400 min	1510	1.52	
#6 60/1.2d	Unannealed	950	1.49	1.49
	160°C 400 min	870	1.49	

Figures 9.3 and 9.4 are plots of reflectivity versus q for

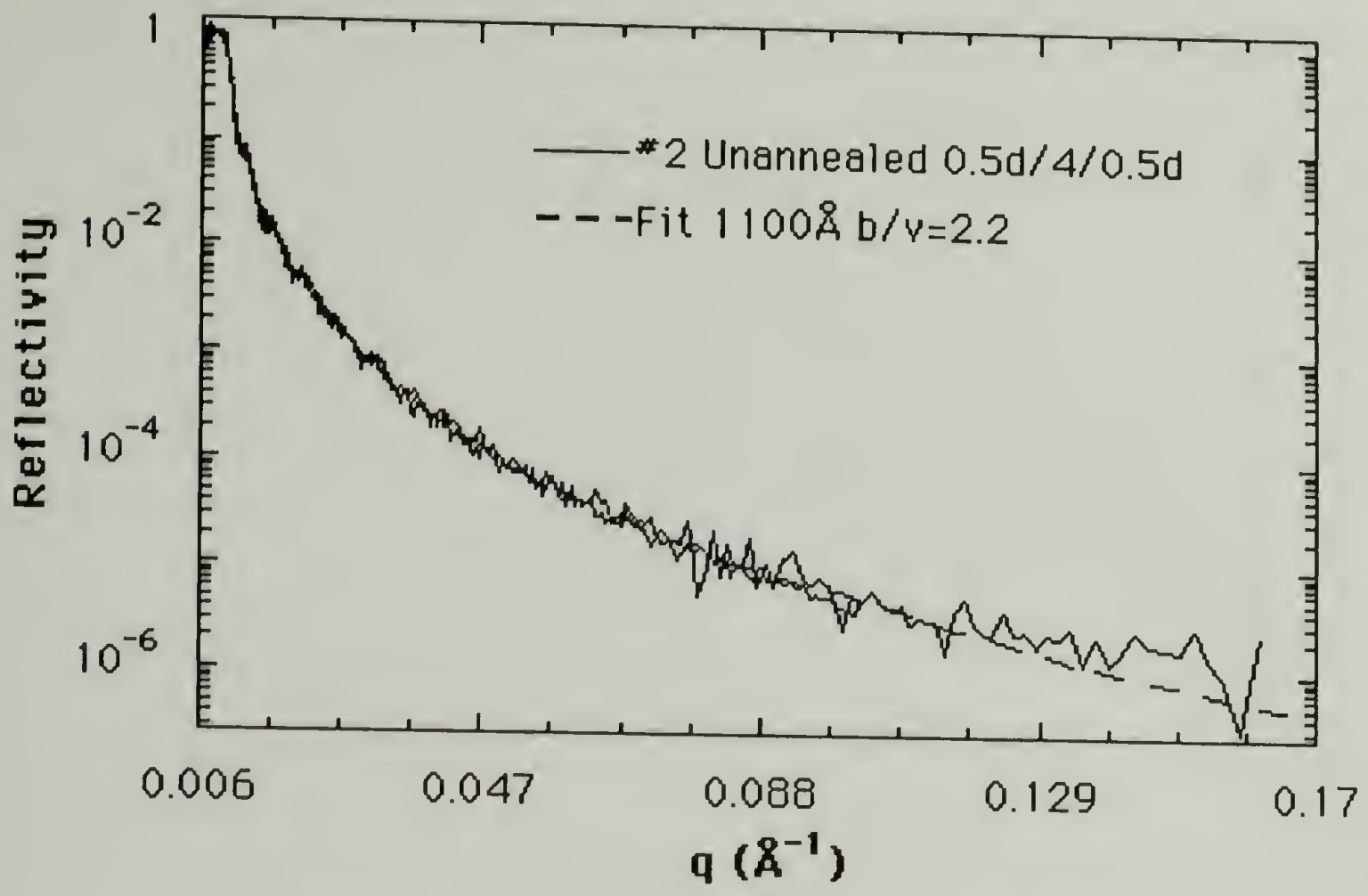

Figure 9.3 Unannealed Sample #2 (0.5d/4/0.5d). The dark dashed curve is a simulation using a 1100Å film of neutron cross section b/v=2.20.

Sample #2. Figure 9.3 shows the unannealed run with a block profile fit. Figure 9.4 shows the same film after being annealed at 130°C for 300 minutes. Some degree of densification as indicated by an increase in the neutron cross section may occur on annealing.

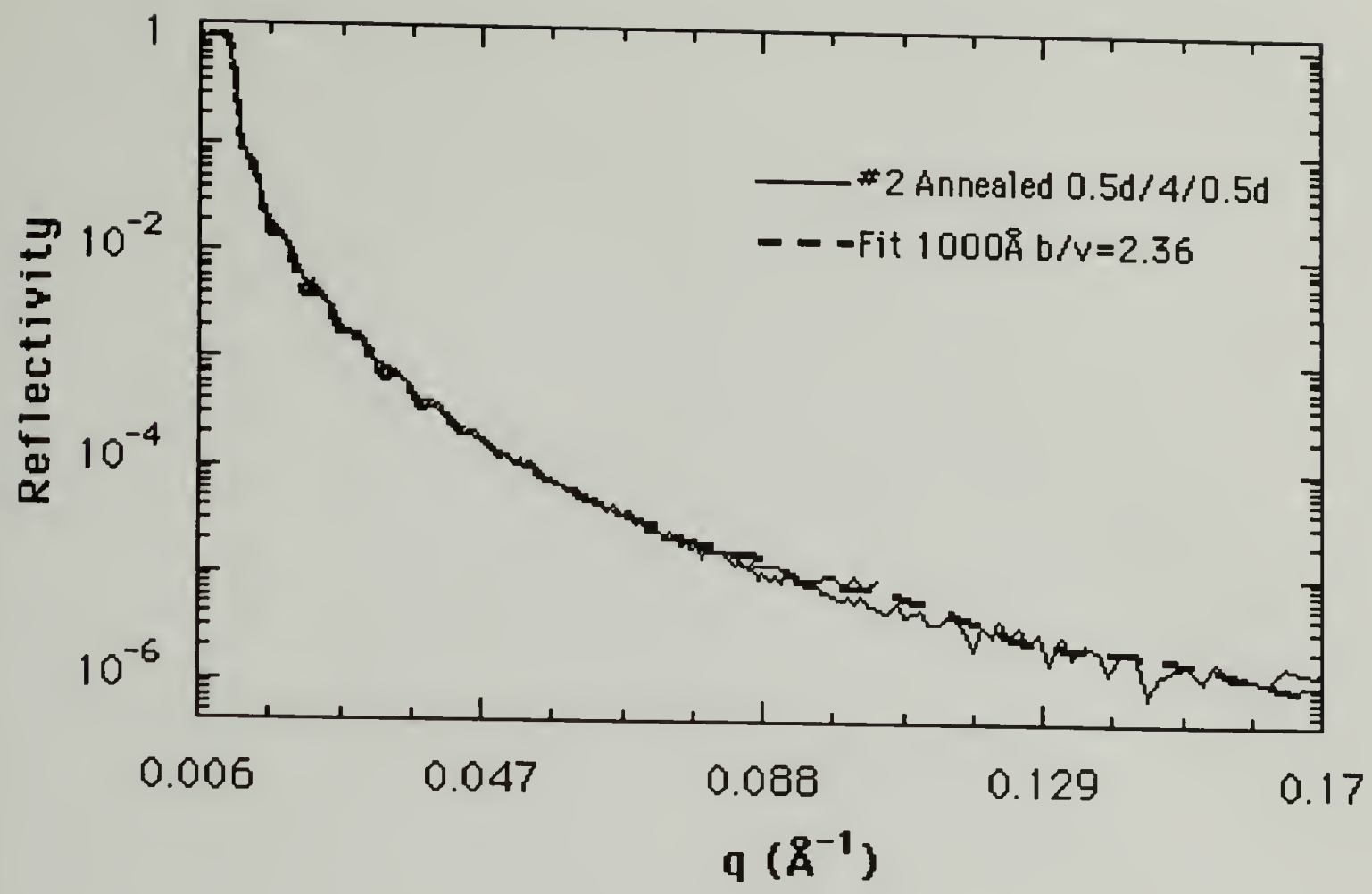

Figure 9.4 Annealed Sample #2 (0.5d/4/0.5d). Annealing time and temperatures are given in Table 9.1. The dark dashed curve is a simulation using a 1000Å film of neutron cross section b/v=2.36 indicating some degree of densification of the film.

Figures 9.5 and 9.6 are similar plots to 9.3 and 9.4 in which a higher molecular weight sample is run. Figure 9.5 is the unannealed run.

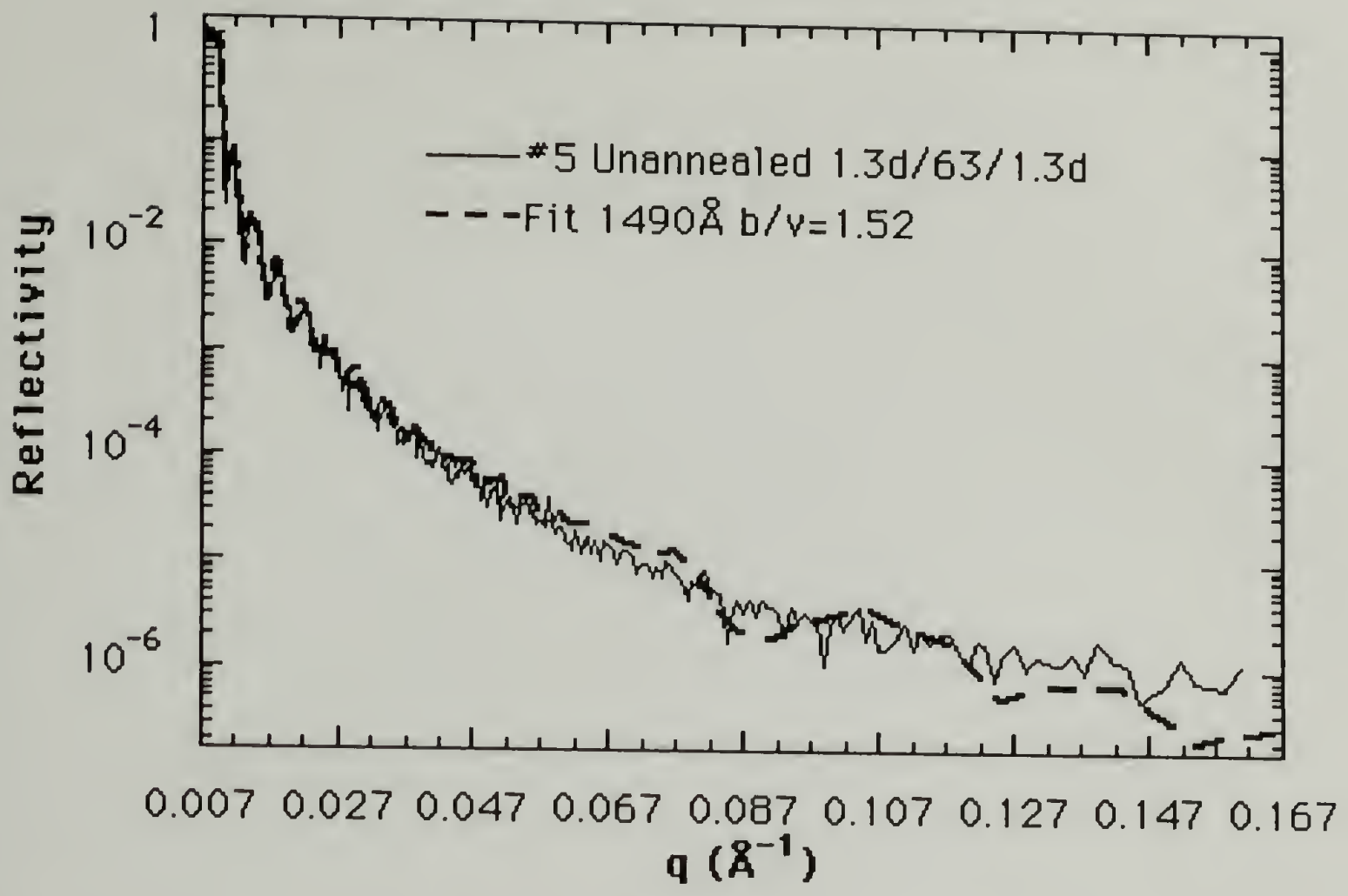

Figure 9.5 Unannealed Sample #5 (1.3d/63/1.3d). The dark dashed curve is a simulation using a 1490Å film of neutron cross section b/v=1.52.

Figure 9.6 is the annealed run for sample #5.

From the reflectivity results it can be said that, for the molecular weight samples investigated, chain end segregation does not appear to be a significant phenomenon in thin films of polystyrene. These

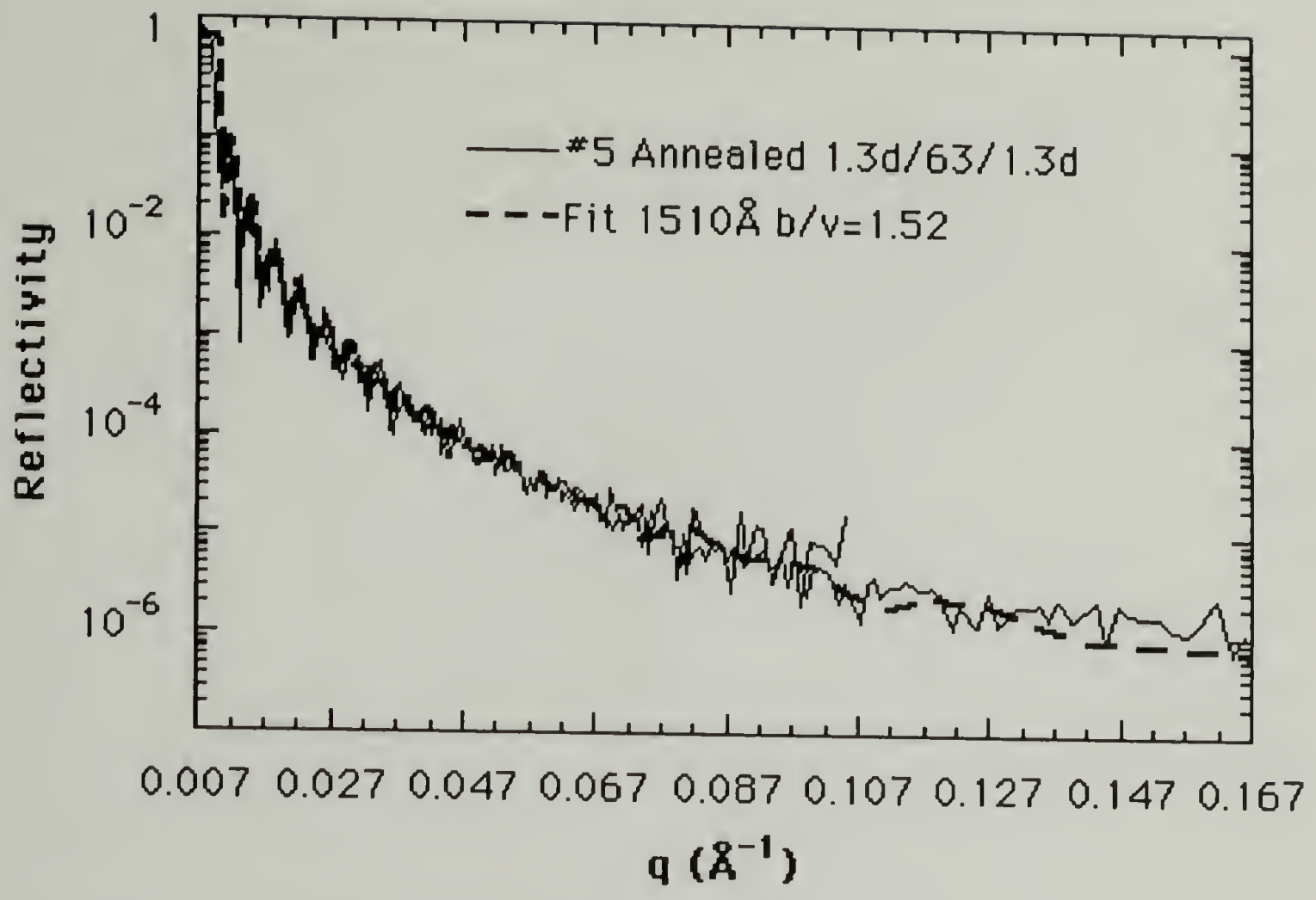

Figure 9.6 Unannealed Sample #5 (1.3d/63/1.3d). The dark dashed curve is a simulation using a 1510Å film of neutron cross section b/v=1.52.

results agree with unpublished results of B. Sauer and D. Walsh at DuPont using lower molecular weight samples of polystyrene as was mentioned above. (The DuPont group performed essentially identical experiments at Argonne National Lab.) In the next section an alternative approach to the molecular weight dependence of surface tension in polymers is presented.

D. Proposed Physics of the Molecular Weight Dependence of Surface Tension in Polymers

Figure 9.7 shows the behavior of surface tension as the molecular weight of polystyrene samples (in the melt) is varied (at several temperatures).

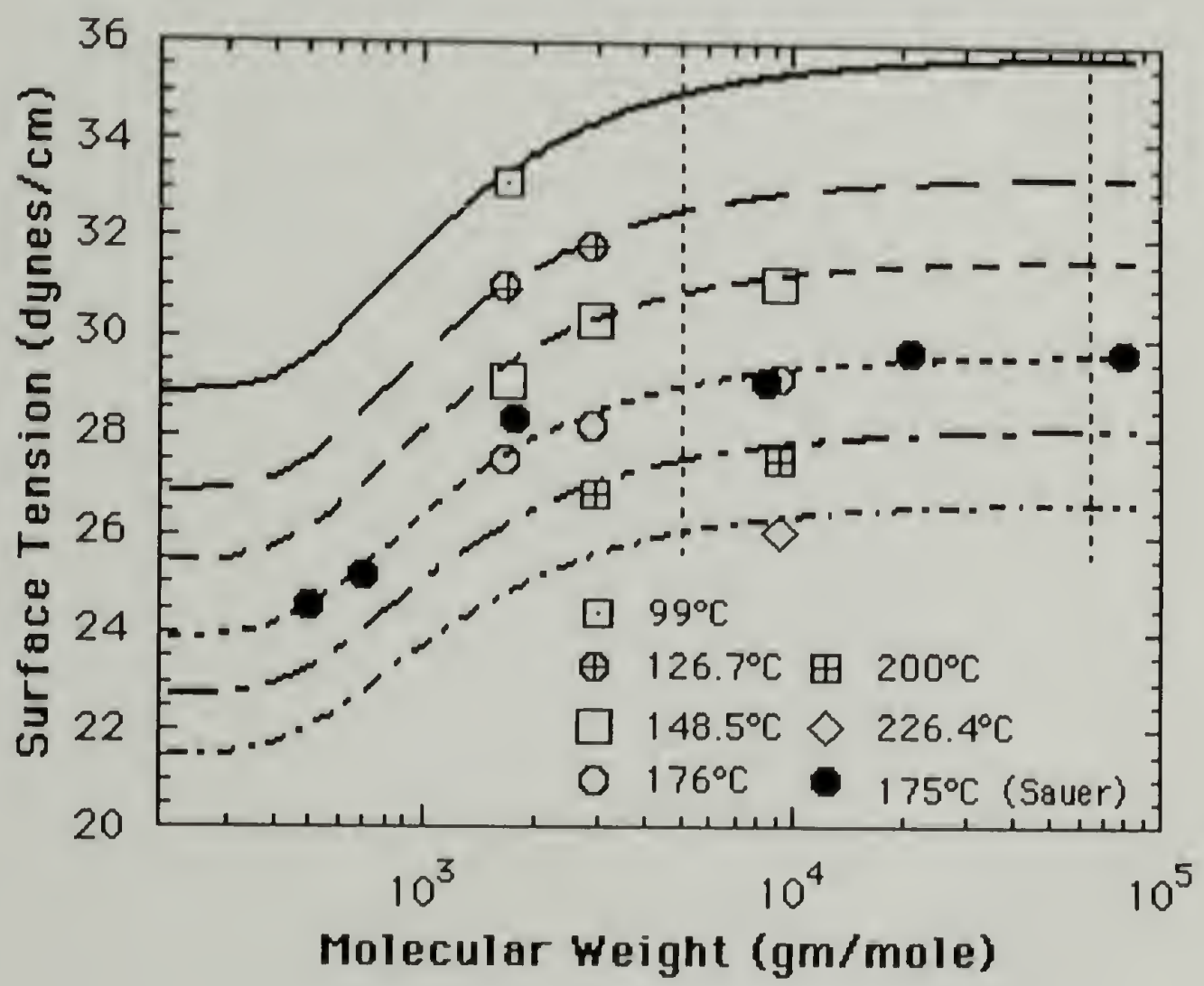

Figure 9.7 Surface tension versus molecular weight for polystyrene melts. (All data is from Gaines and Le Grand[7,8] except where indicated[9].) Vertical dashed lines indicate the two molecular weights used in the neutron reflectivity experiments of this chapter. Equation 9.2 was used to generate the fits shown. A single set of constants was used to fit all of the data in Figures 9.7 and 9.8.

The vertieal dashed lines indieate the two moleeular weights used in the neutron refleetivity experiments of this ehapter. It should be noted that the lower moleeular weight sample studied is just at the beginning of the molecular weight range where chain end segregation would be expected to be observed. The data of Sauer and Walsh (mentioned above) in whieh lower molecular weight PS films were used also failed to display observable ehain end segregation. Figure 9.8 shows additional data taken as a function of temperature for surfaee tension of various moleeular weight polystyrenes in the melt.

Under the assumption that ehain end segregation is not the source of the moleeular weight dependence of surfaee tension (supported by the neutron reflectivity simulations shown above), one may consider if alternative explanations for this dependenee are feasible. Sauer and Dee[10] have reeently proposed a tenable relationship between the bulk thermodynamie properties of the polymer and the surfaee tension based on equation of state theories and pressure-volume temperature data. An alternative approaeh based on a shift in the modulus of a single chain (estimated using rubber elasticity theory[11]) is also possible and will be presented below.

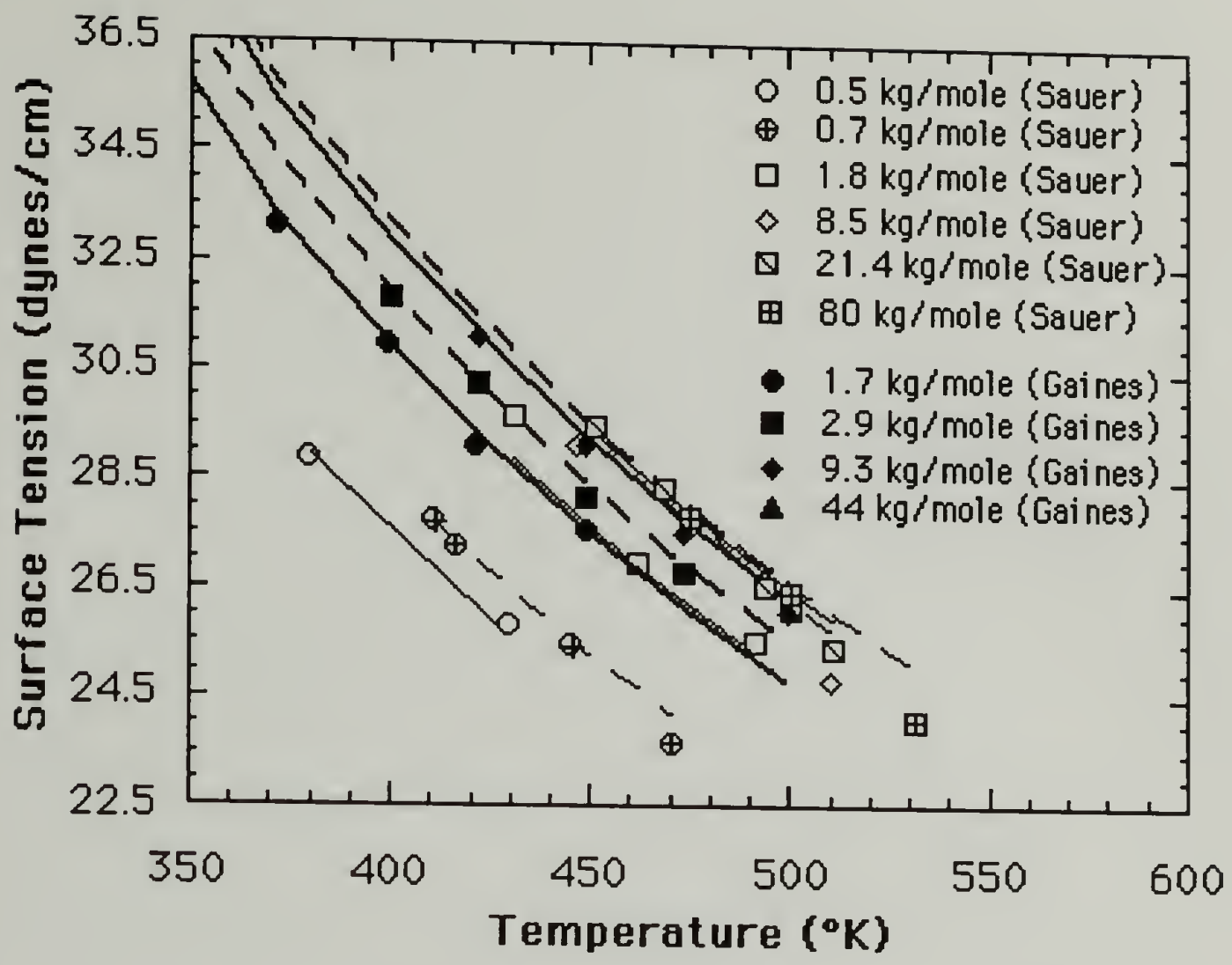

Figure 9.8 Surface tension versus temperature for polystyrene in the melt. The data labeled Sauer is from reference 9 and that labeled Gaines is from references 7 and 8. Equation 9.2 was used to generate the fits shown. A single set of constants was used to fit all of the data in Figures 9.7 and 9.8.

Figure 9.9 shows a schematic of a single polymer chain in the vicinity of an interface. On can consider two simplified geometric conditions for various sections of the chain at the interface. The chain may have sections in the plane of the interface, and secondly, at the chain edges of these in-plane sections, there may be sections which bend away from the interface (expanded in Figure 9.9). The

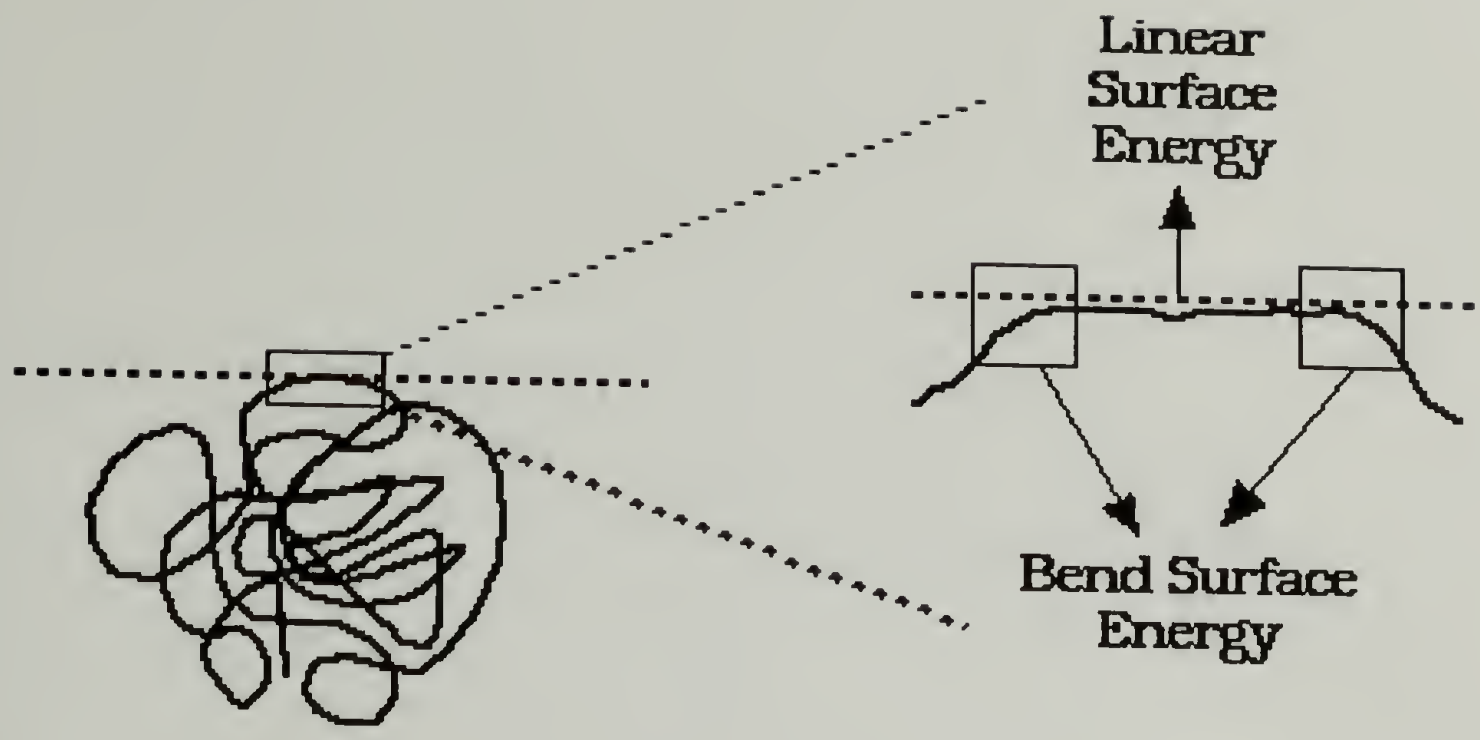

Figure 9.9 Schematic diagram of a single polymer chain selected from a melt sample in the vicinity of an interface.

surface energy for the bent region might be expected to be quite higher than that of the in-plane section. (In analogy the surface energy for a chain fold in a polyethylene crystal has been estimated to be an order of magnitude higher than that of the linear chain in a crystalline lamellae.)

These two general geometric orientations of chain sections at the interface could be thought of as comprising a certain fraction of the interfacial area. In this scenario one would expect increasing entropy (with molecular weight) to increase the bent fraction and decreasing enthalpy to favor chains aligned with the interface (both of these effects leading to a minimization of the chain free energy). A fully aligned chain could be though of as having a minimum surface energy (and surface tension). Increasing the bent fraction would have the effect of increasing the surface tension.

The balance between entropy (which favors a high fraction of bent regions) and enthalpy (which favors a high fraction of in-plane regions) is governed by the ability of the chain to deform in the interfacial region (Figure 9.10).

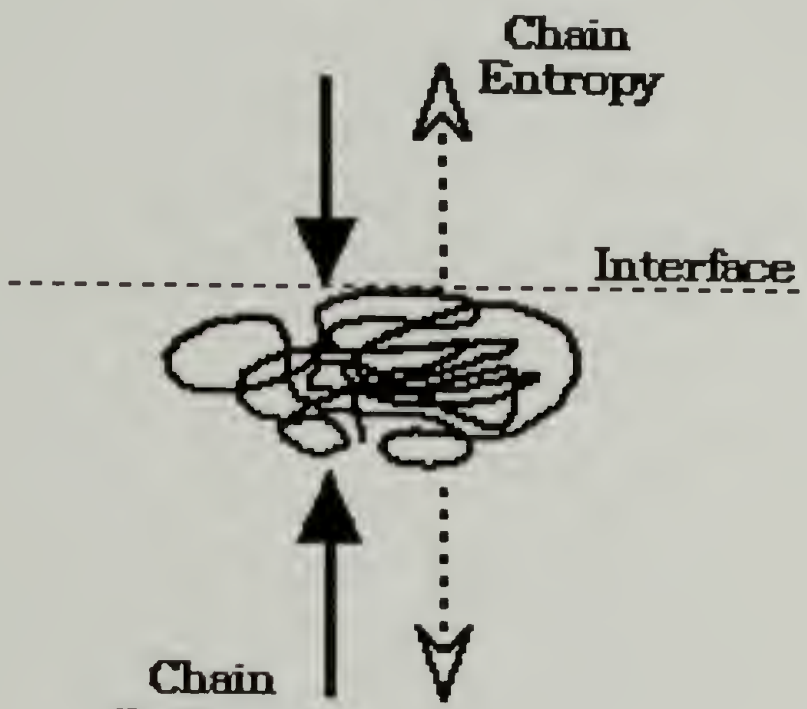

Figure 9.10 Ethalpy/entropy balance at the interface. Enthalpy favors alignment of chains with the interface, entropy favors an increased number of folds at the interface.

The modulus of a chain, as given by rubber elasticity[11], is proportional to the inverse of the chain molecular weight. In this way one might expect the surface tension to be functionally related to the inverse of the molecular weight, lower molecular weight chains having a large modulus (and smaller entropy) would be expected to have a lower fraction of chain bends (and a lower surface tension).

Given this analysis of the interfacial physics one can define a aligned surface tension, γ_0, and an average bend surface tension, $(\gamma_0+\Delta\gamma)$. The total surface tension can be thought of as a sum of the aligned surface tension, γ_0, times the fraction of aligned sections at the interface and the average bend surface tension times a fraction of bends at the interface. The fraction of bends at the interface might be expected to follow a probabilistic functional form in $1/M_n$. This functional form is expected to show a critical $1/M_n$ above which deformation at the interface due to enthalpic considerations becomes possible (with respect to entropy), $1/M_{n\ crit}$. Additionally, this deformation is expected to occur over a range of $1/M_n$'s beyond which a constant low molecular weight surface tension is expected, $1/M_{n\ range}$.

Equation 9.2 reflects the above discussion together with and inverse temperature dependence which empirically follows the data (and is suggested by thermodynamic considerations in regard to the surface energy),

$$g = \left(\frac{T^*}{T}\right)\left(\gamma_0 + \Delta\gamma\left(1 - \mathrm{erf}\left(\frac{1/M_n - 1/M_{n\ crit}}{1/M_{n\ range}}\right)\right)\right) \qquad (9.2).$$

Equation 9.2 has been used to fit the data of Figures 9.7 and 9.8. In all of the fits T^*=474.8 °K, γ_0 = 22.6 dynes/cm (linear surface tension), $\Delta\gamma$ = 5.05 dynes/cm (increase in surface tension due to bends), $M_{n\ crit}$ = 8 kg/mole and $M_{n\ range}$ = 0.6 kg/mole. These fits give a satisfactory description of the behavior of polymeric surface tension with molecular weight.

E. Conclusions

From data obtained using neutron reflec
the molecular weight range studied, chain en
significant phenomenon. Additionally, from d
weights obtained by workers at DuPont, chai
not appear to be justified as a basis for the m
dependence of surface tension in polymers. A
explanations of the molar mass dependence o
possible. In this chapter a new approach was
deformation of polymer chains at the interfac
the chain free energy under interfacial constr
capable of fitting the available data on surface
It remains to test this approach with other po
possible to test the proposed physics by selec

References

1. S. Wu, *Polymer Surface and Adhesion*, Marcel Dekker, inc. NY, 1982 Pages 72 and 169.

2. D. G. LeGrand and G. L. Gaines, Jr., *J. Colloid Interface Sci.*, **31**, 162 (1969).

3. D. G. LeGrand and G. L. Gaines, Jr., *J. Colloid Interface Sci.*, **42**, 181 (1973).

4. P. de Gennes, *C. R. Acad. Sci. Paris, t. 307*, **II** 1841 (1988).

5. G. W. Bender and G. L. Gaines. Jr., *Macromolecules*, **3**,128 (1970).

6. B. Sauer and D. Walsh, Personnel Communication 10/90.

7. D. G. Le Grand and G. L. Gaines, Jr., *J. Colloid Interface Sci.*, **31**, 162 (1969).

8. D. G. Le Grand and G. L. Gaines, Jr., *J. Colloid Interface Sci.*, **42**, 181 (1973).

9. B. Sauer, D. Walsh, DuPont Central Research, Experimental Station, Wilmington, DE.

10. B. B. Sauer and G. T. Dee, *Macromolecules* (in press).

11. L. R. G. Treloar, *The Physics of Rubber Elasticity*, Clarendon Press, Oxford, U. K. , 1975.

CHAPTER 10.

CONCLUSIONS AND FUTURE WORK

A. Results and Conclusions

A novel approach to the production of a toughened glassy polymer was introduced in Chapter 1 (Figure 1.1). It was hoped that a miscible blend of a glassy polymer and a rubbery polymer which exhibited partial miscibility (with a temperature dependence) would exhibit strongly bound interfaces between phases after phase separation and quenching. Strong interfacial adhesion has been considered a prerequisite for the production of a mechanically improved composite material[1]. Additionally, a slight plasticization of the matrix glassy polymer was anticipated.

The system isotactic PVME/PS was chosen for this study since it exhibited the phase behavior described in Figure 1.1 and because isotactic PVME, which has a glass transition temperature at about -30°C, was capable of forming physical crosslinks via crystallization thereby forming a rubbery phase (at a degree of crystallinity of about 5 to 10%). For this purpose isotactic PVME, which is not commercially available, was synthesized (by the author) first on a lab scale and second on a larger scale (10 pounds were produced) at Polysar's Sarnia Ontario pilot plant.

Phase diagrams were determined for the isotactic PVME/PS blend (for a variety of molecular weights) and were compared with those of atactic PVME. The phase diagrams were determined by optical cloud point measurements using the internal reflection from glass microscope cover slips to obtain an integrated intensity at wide angles. This integrated intensity behaved in a predictable manner when compared with discrete angular scattering data from the same system obtained using a 500 channel detector. It is believed that the integrated data, although very simply and inexpensively obtained, may yield kinetics data comparable to discrete angular data. The integrated data was also found to be very useful in the observation of liquid crystalline transitions, melting points, glass transitions, and other polymer blend system phase separations which previously could not be experimentally observed due to low contrast. Cloud points obtained using the integrated intensity were comparable to data obtained using a single detector, wide angle setup by Hashimoto at Kyoto University.

In solution cast blends the isotactic PVME crystallized. On heating a clearing point was observed which corresponded to the melting point in the blend at high PVME weight fractions and to the glass transition of the blend at high PS weight fractions. A miscible regime could be obtained in which the samples were annealed for the determination of the cloud point. At the critical composition, a reduction in the miscibility of the isotactic blends of about 10°C for similar molecular weights was observed. For higher percentages of PS this difference appeared to become smaller. The wide range of molecular weights for the isotactic PVME, atactic PVME and PS

samples was used to crudely determine the temperature dependence of the χ-parameter for the blends. It was found that the tacticity effect was grounded principally in the non-combinatorial entropic part of the χ-parameter (Figure 3.11). This entropic difference was similar to entropic changes in miscibility observed for polyolefin blends mentioned in Chapter 3, section F which have been related to "correlations of molecular orientation above the crystalline melting point" [2,3].

Solution cast films of the isotactic blends, which were phase separated due to crystallization of the isotactic PVME in the casting process, showed shear banding whose presence correlated with a large increase in the strain at failure and energy absorbed. A reduction in the modulus for the isotactic blends indicated plasticization of the matrix. Atactic blends which were not phase separated showed a reduction in modulus in comparison with PS produced under identical conditions but no increase in strain at failure or energy absorbed. It is believed that the presence of rubbery domains of about 5μ in addition to the plasticization of the matrix are necessary for the production of shear bands and the improved energy absorption.

Samples melt blended in the miscible regime and phase separated by LCST behavior in a melt press failed to show drastically improved mechanical properties for either the isotactic or atactic blends. Crystallinity was not present in the LCST samples and an attempt was made to induce crystallization using nucleating agents and various annealing schemes. These efforts were unsuccessful.

In Chapter 5, F-H-S theory was used to analyze the cloud point curves for two of the samples in the hope that the poor mechanical properties of the melt blended samples could be elucidated. Account was made of the polydispersity of the PVME in the blends which lead to a predicted shift in the composition of the coexisting rubbery phase. The polydispersity of the PVME resulted in a predicted fractionation of the higher molecular weight PVME into the rubbery phase which would serve to inhibit crystallization since high molar mass PVME fails to crystallize. (Fractionation in regard to tacticity of the PVME was not addressed but may also be a factor in the LCST blends).

In Chapter 5 account was made of the composition dependence of the χ-parameter using the F-H-S analysis. Values for the two entropic, enthalpic and surface area fitting parameters were determined from the cloud point curves. Figure 5.5 graphically illustrates the behavior of these parameters in composition at 120°C. As was the case in the variable molecular weight analysis discussed above, the enthalpic term showed a small comparative change between the isotactic and atactic blends. The entropic differences between the isotactic and atactic blends dominated the tacticity effect. A shift in the surface area term, the Staverman parameter, was also necessary in order to fit the high and low composition regions of the phase diagram for the isotactic blend. Simple molecular models presented in Chapter 5 (Figures 5.8 to 5.10) give an indication of the type of molecular ordering which might lead to shifts in the entropic component of the χ-parameter and to the observed shift in the

Staverman parameter. These effects occur on the 3-15 mer unit length scale indicating that the unit cell of real polymer blends may be composed of more than one mer unit and may not be symmetric as was assummed in the F-H theory. The F-H-S theory is an attempt to account for these types of lattices using a semi-empirical approach. This approach is the best practical approach available, however, newer theories, specifically the Curro-Schweitzer RISM theory show promise in accounting for such factors

Also in Chapter 5, predictions were made as to the phase separation kinetics from the cloud point data. Generally, one does not expect to directly relate shifts in the cloud point curve to the kinetics of phase separation so this prediction is a test of the usefulness of the F-H-S analysis in predicting values of the χ-parameter out of the range of measurement. (One might expect that less miscible blends might show the same or increased phase separation kinetics for similar quenches into the immiscible regime.) The F-H-S analysis predicted a dramatic decrease in the driving force for phase separation in the early stages for immiscible blends of the isotactic PVME when compared with the atactic blends. As was noted above this prediction was strikingly different from what one might expect since these two blends are chemically identical (i.e. the interaction energy between the methoxy group and the aromatic group of PS for isotactic and atactic PVME would be expected to be identical). An analysis of the relative changes in the driving force for phase separation with changes in the F-H-S parameters (Chapter 5 section J.) indicated that changes in the composition dependent entropic component of χ dominate this

slowing of the kinetics. That is to say, that some type of ordering of the PVME component which is strongly effected by the composition of the blend is leading to a large reduction in the kinetics of phase separation. The type of ordering which occurs is believed to be related to the ordering observed in the molecular models shown in Chapter 5. The monotonic increase in this ordering in the blend with PVME composition, above the melting point is believed to indicate that it is driven by i-PVME/i-PVME interactions which can occur in the presence of PS above the melting point of the i-PVME.

In any case, the dramatic decrease in the rate of phase separation for the isotactic blends in comparison with the atactic blends was clearly confirmed by experiment. Linear Cahn-Hillard theory was used to analyze the apparent diffusion constant for early stages of phase separation. The apparent diffusion constant (Figure 6.8) is the product of a translational diffusion constant and the thermodynamic driving force for phase separation, the latter having been predicted in the F-H-S analysis. It is expected that the translational diffusion constant will be close to identical for the two blends since the glass transition temperature is the same for the two PVMEs ,and the PS used was identical. When the F-H-S prediction was fit to the experimentally determined values for the apparent diffusion constant versus temperature using a one parameter fit (the translational diffusion constant times temperature), the theory fit the experimental results (Figure 6.8). Further, K_c was found to be essentially identical for the two blends. Finally, the value for the translational diffusion constant for the PVME/PS blend (at critical

composition and 100°C) was found to agree very well with values determined using an unrelated technique (NMR). Thus, the predictive ability of the semi-empirical F-H-S analysis was demonstrated.

Finally, in Chapter 5 a new approach to the analysis of early- and mid-stage phase separation based on a modified Cahn-Hillard approach was outlined. This approach is based on the concept of self-similarity in structure of the early and mid-stage decomposition leading to a spinodal and a pseudo-spinodal structure respectively. Further work is needed in this regard. Hashimoto in a personnel communication has reported that the pseudo-spinodal structure has been observed experimentally for diene based blends using microscopy and a wide range of scattering techniques (SALS, SAXS and SANS). The modified Cahn-Hillard approach was shown to predict the behavior observed in the light scattering data well beyond the linear Cahn-Hillard regime (Figure 6.11).

Neutron scattering was used to determine the average statistical segment length and the scattering χ_{sc} modified Zimm approach of Stein and coworkers (correlation length approach) and the RPA theory of de Gennes. A strong composition and temperature dependence for the average statistical segment length above the equilibrium melting point was found (Figure 7.19). Since this did not occur in the atactic blends it was assumed that the dPS statistical segment length was not the cause of the dependencies. A determination of the PVME statistical segment length based on this assumption yielded dependencies on composition and temperature which could be fit

with a binary chemieal kinetics model (equation 7.28) or, alternatively, by a relationship to the PVME/PVME eorrelation funetion (equation 7.26). Both approaehes yielded the same functional form. Using the chemieal kineties model it was found that the change in enthalpy and entropy of formation (of an oriented PVME pair) were elose to literature values for the ehange in enthalpy and entropy of similar polymer crystals. This was not expeeted sinee measurements were made in the melt blend in whieh erystallization is essentially impossible and above the melting point for the i-PVME. The correlation function analysis indicated an interaction distance of from 2 to 20 Å.

The seattering χ was analyzed using Sanchez's seeond derivative (with respeet to eomposition) approaeh and values for the F-H-S parameters (a, b_0, b_1 and e) were determined for the ataetie (using the data of Yang) and the isotactie PVME/PS blends. The fit to the data over a wide range of composition and temperature data is fairly good (Figures 7.24 to 7.27). Changes in the enthalpic parameter, b_1, are direetly proportional to the surface area ratio of the two eomponents. This proportionality was explained using a geometrie argument. It was proposed that the interaeting region of the PVME and PS ean be thought of as two rod like structures interaeting (referenee to the molecular models in Figures 5.8 to 5.10 is helpful in visualizing this interacting region). The length of the interacting region is defined by the PS rod which is the same in the two blends. The tighter paeking of the i-PVME ean be thought of as deereasing the radius of the PVME rod thereby decreasing the surfaee area of the rod. At the same time a

byproduct of this increased packing is the presence of more methoxy interacting units within the same length of rod (defined by the PS rod). Thus, a proportionality between the surface areas and b_1 (which is taken as the change in enthaply on mixing for one interacting region, i.e. the two rods) can be explained. The change in the composition dependent entropic term is roughly twice that of the enthalpic term. The volume for a rod of fixed length and changing radius changes as twice the relative amount as the surface area. Further, one would expect changes in the entropy of an interacting region to scale like the volume of the rods since ordering throughout the volume occurs for the PVME (Figures 5.8 to 5.10). The composition dependent entropic parameter, b_0, was determined to change twice as much as the enthalpic parameter, b_1, in agreement with the geometric analysis.

It is important to note that the scaling behavior of the entropy with volume and the enthalpy with surface area defines the tacticity effect. That is, the reduction in miscibility which occurs in tactic PVME blends is directly related to an entropic term, b_0, which scales with volume changes on changing tacticity, being relatively larger than an enthalpic term,b_1 , which scales with surface area changes on changing tacticity. Thus, the difference between surface area and volume of the interacting components is vital to understanding the tacticity effect. This is a phenomena completely ignored by the F-H theory and empirically addressed as far as surface area changes in the F-H-S theory.

The change in the composition and temperature independent entropic term, "a", is explained in terms of the ground states for the two components at low temperatures. This term reflects the negative (since $\Delta G/T = \Delta H/T - \Delta S$) of the change in entropy between the blend components in their ground state and the blend components in the blend. The ground state for dPS is an amorphous melt and does not change for the two tacticities. The ground state for the atactic PVME is also an amorphous melt. The ground state for the isotactic PVME is an equilibrium crystal whose melting point is about 72°C. Thus, the change in entropy on taking a ground state PVME into a blend might be expected to be a large positive value (large negative "a") since the i-PVME is mueh more randomly ordered in the blend than in an equilibrium crystal, while the change in entropy for the atactic PVME might be expeeted to be a comparatively smaller negative value (small positive "a") since the interactions which occur in the blend might be expected to lead to a small decrease in the randomness of the system. This is what is observed in Table 7.3. Thus, a crystalline ground state which is impossible to attain in the melt blends and which does not exist at the temperatures for whieh the χ_{sc} measurements were made, may govern the eomposition and temperature independent eomponent of χ.

The ground state analysis proves useful in understanding the overall behavior predicted for χ by the F-H-S analysis. Generally, the temperature and eomposition dependenee of $\chi_{i\text{-PVME/dPS}}$ is dominated by the ground erystalline state for the i-PVME across the temperature and composition speetra (Figure 7.28). This is strikingly

demonstrated by essentially equal values for χ at the equilibrium melting point of 72°C where the enthalpy of crystallization and the entropy of crystallization balance ($\Delta H_m = T_m \infty \Delta S_m$) as predicted by the F-H-S fits to the experimental data. Further, below the equilibrium melting point a large change in entropy of mixing between a crystal and the blend is expected to drive the higher compositions of the ground state crystalline component to be more miscible than lower concentrations. Above the crystalline melting point this large entropic change vanishes, since the ground state is amorphous, and the "a" parameter governs a reduction in miscibility for the higher concentrations of the better ordered material. This is exactly the behavior that the F-H-S analysis gives.

In view of the χ analysis given above, the temperature and composition dependence of the i-PVME statistical segment length was further investigated (Figure 7.29). In this analysis it was assumed that points of discontinuity in the temperature dependence predicted by the modeled form of $b_{i\text{-PVME}}$ correlated with the equilibrium melting point of very high concentration i-PVME blends ($\phi_{i\text{-PVME}}$=0.8 to 1.0). The discontinuity temperatures were found to fit the Nishi-Wang prediction for melting point depression if a composition dependent χ was used. The prediction for the $\phi_{i\text{-PVME}}$=1.0 blend, i.e. for pure i-PVME, agreed with the expected equilibrium melting point for this material from DSC, x-ray, and index of refraction measurements. (The blend compositions and temperatures used for this melting point depression analysis were beyond the ranges measured in this work either for cloud point, SALS or SANS experiments.)

Finally, the immiscible regime phase separation kinetics predictions made for hydrogenous PS blends from cloud point measurements using the F-H-S analysis could be qualitatively reproduced using the SANS analysis on dPS. This prediction is not expected to qualitatively agree since the dPS blends are known to be more miscible by about 10°C due to the deuteration effect which was studied by Yang[4].

Finally, two related studies were reported in which shifts in the glass transition of thin films of PS were investigated and in which the segregation of chain ends in thin films of dPS to interfacial regions were studied (Chapters 8 and 9 respectively). Large shifts in the glass transition for thin films of PS are believed to be due to large inherent interfacial strains in the films caused by differences between thermal expansion between the substrate and the polymer. These localized strains might be thought to increase the free volume of the films and thereby lower the glass transition. This type of behavior is important to the toughened blends since inherent strains may be present in the plasticized matrix PS phase due to contraction of the i-PVME domains on crystallization. In the confined geometry of the polymer blend this type of strain might induce local shifts in the glass transition which could lead to a change in the yield criterion for shear banding and crazing.

A neutron reflection experiment was also performed which showed that chain end segregation at interfaces is probably not an important factor at blend interfaces. The increase in surface tension with molecular weight was related to chain deformation at the

interface and an equation was derived on this basis which accounts for the available surface tension data on polystyrene.

B. Future Work (General)

In continuation of the Polysar supported work we have turned our attention to other polymer blend systems of greater commercial potential which may show mechanical improvement in the phase separated state. Blends of bisphenol-A-polycarbonate were chosen.

Polycarbonate (PC) is widely used due to its toughness in comparison to other glassy, commodity polymers such as polystyrene. It has been noted[5] that improvements in notch-sensitivity, thick-section impact properties (plane-strain conditions) and low temperature toughness are desirable. Pure PC absorbs energy via shear banding in contrast to PS and fails ductally in fairly thin specimens (plane stress conditions) at ambient temperatures. In thicker samples, at low temperatures (below 0°C) or in the presence of a sharp notch, PC toughness is reduced. It should be noted that it is yet to be determined whether rubber modification can be effective in a material which absorbs energy chiefly via shear banding. Two candidates for the PC blend study were initially selected chiefly from a survey of the literature. PC blended with various polyesters, and PC/PMMA blends.

C. Polycarbonate/Poly(methyl methacrylate)-PC/PMMA

This system reportedly exhibits a LCST and shows improvement in mechanical properties relative to those of pure PC[6]. Kyu has demonstrated that the mechanism of phase separation plays a dominant role in controlling the blend properties. Furthermore, tacticity is known to have a profound effect on the miscibility and consequently the modes and kinetics of phase separation. Since this work has been previously addressed by Kyu and coworkers with a similar approach it was rejected as a candidate.

D. PC/Polyester Blends

Barlow, Paul and coworkers[7] have demonstrated the miscibility of PC/Polyester blends in the absence of crystallinity. The T_g for a PC miscible polyester such as Poly(ethylene adipate) is -70°C. This is well within the range desirable for the production of a conventional rubber toughening additive such as polybutadiene. Generally, these systems do not show phase separation below the degradation temperature and above the respective T_gs and T_ms. The thermal behavior of a series of polyesters with different -(CH_2)- group lengths has been documented[8]. We have further investigated the phase behavior of these blends in the hope of finding a PC/polyester blend with a polyester T_g below -60°C which displays LCST behavior and in which a degree of crystallinity of about 10% can be induced in the phase separated polyester domains. Several polycarbonate/polyester blends were prepared with various blending procedures including solution

casting, melt blending, and solution blending followed by precipitation. It was found that solution casting yielded highly crystalline polycarbonate which resulted from solution induced crystallization and was thus unsuitable for this study. Melt blending seemed promising, however, concerns as to blend homogeneity for thermodynamic studies were raised. Solution blending followed by precipitation yielded highly homogeneous materials suitable for light scattering studies with polycarbonate crystallization almost completely suppressed. This method consisted of dissolving the two polymers in a common solvent (chloroform) and precipitating in a non-solvent (methanol).

Table10.1 shows the polyesters examined to date (for comparison, PC has been included). Preliminary investigations under a continuation of this project have been conducted by W. Cheung. Differential scanning calorimetry (DSC) was used to investigate the phase behavior of the blends. Melting point depression and glass transition temperature depression were used as criteria for miscibility. The 70PC/30PEA blend was found to be miscible however did not show an LCST. Due to PEA's relatively "high" Tg and lack of an LCST, efforts were directed to other systems with lower Tgs which should yield better impact modification (especially at cryogenic temperatures). Polycarbonate was found to readily undergo crystallization in the presence of PCL even when the blend was prepared from solution blending followed by precipitation. The PC/PHS system was found to be partially miscible, that is, the 50PC/50PHS blend is not miscible while the 70PC/30PHS is miscible

(by DSC). An interesting feature in this system is that PHS readily undergoes crystallization even in a quenched 70PC/30PHS sample. Other polyesters crystallized much slower in the presence of PC. This rapid crystallization of PHS may be exploited as means to induce phase separation which may render a rubber reinforced polycarbonate.

Table 10.1 Polyester candidates for the continuation of the Polysar sponsored blends study.

POLYESTER	T_m, C	T_g, C	ABBR.
poly(ethylene adipate)	52.3	-47	PEA
poly(1,4-butylene adipate)		60.0	-68 PBA
Poly(caprolactone)	65.7	-68	PCL
poly(hexamethylene sebacate)		67.4	-60 PHS
(polycarbonate	217	151	PC)

The PC/PBA system was found to be completely miscible, that is, the two polymers seem to be miscible in all compositions by DSC. Preliminary optical studies indicate that this system exhibits a lower critical solution temperature (LCST). This finding is yet to be confirmed with more precise light scattering studies. It should be noted that transesterification may be a significant problem with the

PC/polyester blends which could result in the formation of a copolymer via ester exchange reaction. Chemical techniques for suppressing transesterfication have been noted in the literature, for instance addition of an organo-phosphite to the PC/PET system has been shown to be effective in eliminating the trans-reaction.

Although the findings noted above, especially the LCST behavior of the PC/PBA blends are encouraging, much work remains to be done:

1) Determine the phase diagram of PC/PBA system;

2) Investigate the phase separation kinetics of PC/PBA blend and the crystallization kinetics of PBA.with an aim at controlling the morphology and degree of crystallinity of phase separated PBA domains;

3) Investigate the mechanical properties and phase morphologies of the following systems:

Partially miscible blend of PC and poly(hexamethylene sebacate), and

Miscible blend of PC and poly(1,4-butylene adipate); and

4) Examine transesterification behavior.

It is hoped that these studies will lead to important principles which may be used by Polysar as a guide as to which types of polymer blends will be useful in products involving polycarbonates. Specifically, the universality of the rubber toughening phenomena in the polystyrene system will be tested in a non-crazing matrix polymer.

Our experience in the polymer miscibility field as studied by various scattering techniques is the cornerstone of our approach. A novel light scattering apparatus built under Polysar sponsorship is capable of sensitive measurements concerning phase separation point, and kinetics as well as crystallization and glass transition behavior (in conjunction with DSC data). The PC/Polyester blends are excellent candidates for study using this apparatus since a myriad of phase separation, crystallization and T_g phenomena have been observed in our lab. It is believed that through careful control of this behavior, mechanical properties of the final thermally treated blend will be optimized. Additionally, our expertise in x-ray diffraction and small angle x-ray scattering will be of use in this study. It is believed that the final degree of crystallinity for the phase separated domains of polyester will govern their ability to toughen polycarbonate. X-ray diffraction is the most sensitive technique for the determination of degree of crystallinity and type of crystal. SAXS and SALS are useful in determining the larger scale crystalline structure and growth rate. Finally, a determination of the thermodynamic parameters governing phase separation in PC/polyester blends has not been conducted. Neutron scattering may be used in this regard if a source of deuterated polycarbonate can be found.

E. Future Work with the i-PVME/PS System

Clearly, more data is needed in order to fully determine the temperature and composition dependence of the χ-parameter so as to provide a better basis for the F-H-S model. The abstract for continued

work involving SANS studies on the i-PVME/PS system is presented below.

"In a continuation of studies of the tacticity dependence of the Flory-Huggins interaction parameter (χ) for blends of deutero–polystyrene (dPS) with isotactic poly(vinylmethylether) (i-PVME) a wider range of temperature and composition scans will be investigated in order to test the predicted composition and temperature dependences of the statistical segment length and χ determined using Flory-Huggins-Staverman theory."

Work remains to be done on the modified Cahn-Hillard analysis presented at the end of Chapter 6. Determination of the local composition changes which occur in a phase separated blend might be studied using neutron reflection techniques. The experiment would essentially consist of spinning a bilayer of dPS and PVME on a silicon wafer and calculating the interfacial composition (between the dPS and PVME) at temperatures above the phase separation temperature. This data might be used to estimate the time dependence of the interfacial composition in a phase separating blend. A better understanding of this behavior is of primary importance in the modified Cahn-Hilliard approach.

In regard to the mechanical properties of the LCST produced isotactic PVME/PS blends, the F-H-S analysis has indicated several approaches to producing the desired phase compositions. Of primary importance is reducing the polydispersity of the blend components. One way of doing this for PVME is to take advantage of its solubility in

water. In biological polymers it is common to use membrane filtration to separate aqueous solutions of molecules with very close molecular weights. Membrane filtration could easily be applied to the PVME system (e.g. membranes are commercially available which would allow for the selection of a monodisperse 100 kg/mole fraction). Use of lower molecular weight isotactic PVME would be desirable since it appears that the higher molecular weight material does not crystallize as readily. Use of too low of a molecular weight might lead to too large of an increase in miscibility; however, from the data presented in Chapter 3 it is clear that monodisperse molecular weights of about 30 kg/mole are acceptable. Annealing of the phase separated blends above the glass transition temperature but below the phase separation temperature for extended periods showed the greatest promise in Chapter 4 and further pursuit of this might prove fruitful. Finally, a full study of the solution cast samples including an observation of the effects of phase size on the mechanical properties was not conducted due to time constraints and redirecting of attention to melt blends when large quantities of the isotacitic materials were synthesized. A study along these lines might prove to be of value.

The author hopes to further analyze the tacticity effect using Curro-Schweitzer RISM theory which does not rely on the limitations of a symmetric and uniform lattice cell. It is hoped that surface area and volume changes with tacticity can be accounted for in this analysis yielding a broader understanding of the tacticity effect.

References

1. D. Hull, *Cambridge Solid State Sci. Ser.: An Intro. to Composite Materials*, Cambridge U. Press, N.Y. 1981.

2. G. Charlet, G. Delmas, *Polymer*, **22**, 1181 (1981).

3. A. Barbalata, T. Bohossian, K. Prochazka, G. Delmas, *Macromolecules*, **21**, 3286 (1988).

4. H. Yang, Ph.D. Dissertation, University of Massachusetts, Amherst, 1985.

5. D. W. Gilmore, M. J. Modic, *Plastics Engineering*, **4**, 51 (1989).

6. J.M. Saldanha, and T. Kyu, *Macromolecules*, **20**, 2840 (1987).

7. A. C. Fernandes, J. W. Barlow and D. R. Paul, *Polymer*, **27**, 1799 (1986).

8. F. Schultze-Gebhardt, *Acta Polymerica* **38**, 36 (1987).

BIBLIOGRAPHY

Aoki, O.; "The Phase Separation Behavior of Poly(vinyl methyl ether)/Polystyrene Semi-IPN", Ph.D. Dissertation, University of Massachusetts, Amherst, 1990.

Bates, F. S.; "Small-Angle Neutron Scattering from Amorphous Polymers", *J. Appl. Cryst.*, **21**, 681-691 (1988).

Beaucage, G., Stein,R. S. , Koningsveld,R. , Berard, M. T. ; "Polymer Blend Miscibility and Phase Separation Kinetics Analyzed uning Flory-Huggins-Staverman Theory"; *Polymer Preprints*, **32**(1), 475-6, 1991.

Beaucage, G.; Stein, R. S.; Hashimoto, T.; Hasagawa, H.; "Tacticity Effect in Polymer Blend Miscibility", *Macromolecules* (in press).

Beaucage, G.; Stein, R. S.; *Impact Modification of Glassy Polymers via LCST-Type Phase Separation*, U.S. Patent Application Filed 9/1988.

Beckman, E. J.; Porter, R. S.; R. Koningsveld; "Mean-Field Lattice Equations of State. 2. The Role of the Segmental Contact Surface Area in the Unification of Recent Lattice Models", *J. Phys. Chem.*, **91**, 6429-39, 1987.

Berard, M. T.; *The Poly(alpha methyl styrene)/Polystyrene Polymer BLend System.* Ph.D. Dissertation University of Massachusetts, Amherst, 1991.

Bevington, P. R.; *Data Reduction and Error Analysis for the Physical Sciences*, McGraw-Hill, New York, 1969.

Bondi, A.; "Estimation of Surface Area for Various Organic Compounds", *J. Phys. Chem.*, **68**, 441, 1964.

Bruins, P. F.; *Polyblends and Composites*, Wiley-Interscience, New York, 1981.

Bucknall, C. B.; *Toughened Plastics*; Applied Science Publishers LTD, London, 1977.

Burkert, U.; Allinger, N. L.; *Molecular Mechanics, ACS Monograph 177*, Amer. Chem. Soc., Washington D.C. 1982.

de Gennes, P. G.; *Scaling Concepts in Polymer Physics*, Cornell Univ. Press, London, 1979.

de Gennes, P.; "Tension superficielle des polymeres fondus",*C. R. Acad. Sci. Paris, t. 307, Serie II*, 1841-6, 1988.

Flory, P. J.; *Principles of Polymer Chemistry*, Cornell University Press, London, 1953.

Glatter, O.; Kratky, O.; *Small-Angle X-ray Scattering*, Academic Press, New York, 1982.

Hashimoto, T.; Kumaki, J.; Kawai, H.; "Time-Resolved Light Scattering Studies on Kinetics of Phase Separation and Phase Dissolution of Polymer Blends. 1. Kinetics of Phase Separation of a Binary Mixture of Polystyrene and Poly(vinyl methyl ether)", *Macromolecules*, **16**, 641-8, 1983.

Herman, W.; "Miscibility of the PMMA/PVF_2 Polymer Blend System", Ph.D. Dissertation, University of Massachusetts, Amherst, 1987.

Higgins, J. S.; Stein, R. S.; "Recent Developments in Polymer Applications of Small-Angle Neutron, X-ray, and Light Scattering", *J. Appl. Cryst.*, **11**, 346-75, 1978.

Hull, D.; *Cambridge Solid State Sci. Ser.: An Intro. to Composite Materials*, Cambridge U. Press, N.Y. 1981.

Karasz, F. E.; MacKnight, W. J.; "Dependence of the Glass Transition Temperature on Tacticity", *Macromolecules*, **1**(6), 229-31, 1963.

Ketley, A. D.; *The Stereochemistry of Macromolecules, Volume 2*, Marcel Dekker, New York, 1967.

Kinloch, A. J.; Young, R. J.; *Fracture Behavior of Polymers*, Elsevier Applied Science Publishers, New York, 1983.

Koningsveld, R.; Kleintjens, L. A. ; Leblans-Vinck, A. M.; "Mean-Field Lattice Equations of State. 1. Possible Molecular Basis for Empirical Parameters", *J. Phys. Chem.*, **91**, 6423-8, 1987.

Kostorz, G.; *Treatise on Material Science and Technology*, **15**, Academic Press, New York, 1979.

Langer, J. S.; Bar-on, M.; Miller, H. D.; "New computational method in the theory of spinodal decomposition", *Phys. Rev. A* , **11**(4), 1417-29, 1975.

Lenz, R. W. ; *Organic Chemistry of Synthetic High Polymers*, Interscience Publishers, New York, 1967.

Lipatov,Y. S.; Sergeeva, L. M.; *Adsorption of Polymers*, Wiley and Sons, NY, 1979, Pages 140-59.

Murray, C. T.; "Neutron Scattering Investigations of Amorphous, Miscible Polymer Blends", Ph.D. Dissertation, University of Massachusetts, Amherst , 1985.

Olabisi, O.; Robeson, L. M.; Shaw, M. T.; *Polymer-Polymer Miscibility*, Academic Press, New York, 1979.

Paul, D. R.; Newman, S.; *Polymer-Polymer Misciblity*, Academic Press, N. Y., 1979.

Prigogine, I.; *The Molecular Theory of Solutions*, North Holland Publishing Co., Amsterdam, 1957.

Schweitzer, K. S.; Curro, J. G.; "Integral equation theory of the structure and thermodyanmics of polymer blends", *J. Chem. Phys.*, **91**(8), 5059-81, 1989.

Shibayama, M.; Yang, Y.; Stein, R. S.; Han, C. C.; "Study of Miscibility and Critical Phenomena of Deuterated Polystyrene and Hydrogenated Poly(vinyl Methyl ether) by Small-Angle Neutron Scattering", *Macromolecules*, **18**, 2179-87, 1985.

Skold, K.; Price, D. L.; *Neutron Scattering, Part A*, Academic Press Inc., NY, 1986

Stein, R. S.; *Electro-optical Behavior of Polymers*, Univ. Mass. Video Instructional Program Lecture Notes, Amherst, MA, 1989.

Stein, R. S.; Hadziioannou, G.; "Generalization of the Zimm Equation for Scattering from Concentrated Solutions", *Macromolecules*, **17**, 1059-62, 1984.

Stromberg, R. R.; McCrackin, F.; "Optical Techniques for Investigating Surfaces", in *Clean Surfaces*, G. Goldfinger ed., Decker Co., NY, 1970, Page 74.

Tobolsky, A. V.; *Properties and Structures of Polymers*, Wiley, NY 1960.

Tompa, H.; *Polymer Solutions*, Butterworth, London, 1956.

Treloar, L. R. G.; *The Physics of Rubber Elasticity*, Clarendon Press, Oxford, U. K. , 1975.

Walsh, D. J.; Higgins, J. S. ;Moconnachie, A.; *Polymer Blends and Mixtures*, NATO ASI Series E: Applied Sciences-No. 89, Martinus Nijhoff Publishers, Boston, 1985.

Wu, S.; *Polymer Interface and Adhesion*, Marcel Dekker Inc., New York, 1982.

Yang, H.; "Misciblity and Phase Separation Behavior of Amorphous/Amorphous Polymer Blends", Ph.D. Dissertation University of Massachusetts, Amherst, 1985.

Yang, H.; Shibayama, M.; Stein, R. S.; Shimizu, N.; Hashimoto, T.; "Deuteration Effects on the Miscibility and Phase Separation Kinetics of Polymer Blends", *Macromolecules*, **19**, 1667-74, 1986.

Yang,H. ; Hadziioannou, G.; Stein,R. S.; The Effect of Deuteration on the Phase Equilibrium of the Polystyrene/Poly(vinyl methyl ether) Blend System", J. Polym. Sci., Polym. Phys. Ed. , **21**, 159, 1988.